FATIGUE/FRACTURE MECHANICS ANALYSIS OF THREADED TETHER CONNECTIONS

by

David Anthony Topp B.Sc., M.Sc.

A Thesis Submitted for the Degree of
DOCTOR OF PHILOSOPHY
in the
Faculty of Engineering
University of London
November 1990

Department of Mechanical Engineering
University College London
Torrington Place
London WC1E 7JE

ABSTRACT

The use of threaded connections for joining tubes and pipes is widespread within the oil and gas drilling industry. Such connections have more recently been employed for the joining of tethering elements for a new generation of offshore platform, the Tension Leg Platform (TLP). The platform design depends totally on the integrity of the tethering system and the threaded connection between tether elements has been identified as a critical structural component. The hostile environment of the North Sea leads to severe cyclic loading on the tethering system and fatigue is the most likely in-service damage mechanism.

This study involves an analysis of the fatigue behaviour of large threaded connections of the type proposed for tethering applications and considers the implications for subsequent in-service inspection and integrity assessment.

A simplified model for the prediction of the non-uniform load distribution within the connection is proposed and this is validated using finite element (FE) modelling of a complete connection. A methodology for the use of this model, in conjunction with simple FE sub models, for the prediction of dynamic stresses in preloaded and unpreloaded connections is presented.

Fatigue initiation and fracture mechanics based crack growth models are proposed for this application and large scale tests, to provide experimental data for validation of these models, have been conducted. An inspection system was developed to enable fatigue crack growth to be measured during the test. It is likely that this system will be suitable for integrity monitoring of large scale threaded connections removed from service. The requirements for integrity monitoring during service, based on a knowledge of the likely fatigue behaviour, are considered for a tethering system and a methodology for defining service inspection intervals as discussed.

ACKNOWLEDGEMENTS

I would like to thank all those who offered advice and assistance throughout this project. Special thanks go to my supervisor, Professor Bill Dover, for his guidance and encouragement. Thanks also to my wife Lucy for her enthusiastic support and to Brisia Perry for her patient efforts in the typing of this thesis.

Finally, I wish to acknowledge the financial support of the Science and Engineering Research Council and the Industrial Sponsors of the Cohesive Fatigue Programme.

Table of Contents

Chapter 3: Finite Element Analysis of Threaded Connections

Chapter 4: Model for the Prediction of Tooth Loads in Threaded Connections

Chapter 5: Experimental Work

Chapter 6: Fatigue and Fracture Mechanics Modelling of Crack Growth in Threaded Connections

Chapter 7: The Use of Controlled Inspection for Maintaining Component Integrity

Chapter 8: Conclusions and Recommendations

Appendices

Appendix A: Sopwith's Analysis of Load Distribution in Threads

Appendix B: Stress and Deflection of A Stubby Cantilever

Appendix C: Use of Inspection Trials for the Evaluation of Inspection Performance

Appendix D: Fortran Programme for Tooth Load Distribution

References

NOMENCLATURE

319

Table of Tables

Chapter 3

Chapter 4

Chapter 5

Chapter 6

Appendix A

Table of Figures

Chapter 1

Chapter 2

Chapter 3

Chapter 4

Chapter 5

Chapter 6

Chapter 7

Appendix A

Appendix B

Appendix C

CHAPTER 1

THREADED TETHER CONNECTIONS

1.1 INTRODUCTION

As the demand for Offshore hydrocarbons increases, so it becomes necessary to explore into deeper waters. Conventional production platforms are large steel structures supported from the sea bed, which in turn support the working platform above the waves. As exploration moves to deeper waters, the weight of a conventional fixed "jacket" structure increases considerably due not only to the increase in structure height but also due to the stiffness requirements to resist environmental forces due to wind, waves and current. The increase in weight leads to a high construction cost and poses considerable problems of transportation from the construction site and deployment on station.

It is currently considered that these constraints make a conventional jacket design unsuitable for water depths much greater than 1000 feet in hostile environments such as the North Sea. In order to recover hydrocarbons from greater depths, new platform designs are required. A number of conceptual designs have been investigated including floating production platforms, guyed towers and sub-sea systems. Of these the floating platforms appear to be the most attractive at the present time.

Floating semi-submersible platforms have been successfully used for drilling and accommodation platforms. These are conventionally held on station by catenary mooring lines whilst some employ dynamic positioning systems for improved station keeping. In bad weather however the station keeping capabilities of such platforms are poor due to the low stiffness of the mooring system. This type of platform is therefore unsuitable for production in deep water since excessive platform motions in bad weather can lead to extreme problems with marine risers and seabed links.

The fundamental principle of a floating platform for deep water applications is sound. This essentially leads to a platform size that is independent of water depth. It is then the mooring system that reflects the water depth and it is this which ultimately dictates the station keeping capabilities. This was recognised some years ago and led to the Tension Leg Platform (TLP) concept.

1.2 TENSION LEG CONCEPT

This concept was conceived in the late 1970's and represents a major change from conventional jacket design. The TLP system comprises a floating hull supporting the deck structure, tethered to the seabed using vertical mooring lines. Figure 1.1 shows a typical TLP arrangement. The use of vertical mooring lines provides a very stiff mooring

system leading to much smaller platform motions than those for a conventional catenary moored platform. The mooring system is deployed by first ballasting the hull and then fixing the mooring lines between the hull and seabed. The hull is then deballasted, thus preloading the mooring against the natural buoyancy of the hull. With the mooring lines preloaded, heave motion is restrained by the axial stiffness of the mooring line. Surge, sway, roll and pitch motions are restrained by the hull buoyancy and mooring tension. The platform behaves in much the same way as an inverted pendulum, with mooring always tending to the vertical.

1.2.1 Design Requirements

In broad terms the design requirements for a TLP are the same as for a conventional jacket structure, that is the structure should perform safely for the duration of the design life. In order to ensure that any structure is performing as expected, periodic inspection of key components must be carried out. It is important to note one major difference between a jacket structure and a TLP, that is the redundancy of the structure. The conventional fixed jacked design leads to a highly redundant structure with multiple load paths. This is not the case for the mooring system of a TLP. The platform shown in Figure 1.1, which is now in place and operational, has essentially 4 moorings, one at each corner. The loss of mooring on any corner would be catastrophic. Each corner mooring is made up of four mooring lines, all working in parallel. Whilst the moorings have been designed such that three lines are adequate a fourth has been included. It could be considered that this results in an element of redundancy since theoretically, one could fail and still leave three lines - the design number. This is not a redundant system however because there is not a secondary load path. Since all four lines act in a parallel, they experience near identical load histories. It is likely therefore that if one line had accumulated enough damage to cause a failure, the remaining three, having experienced the same loading history and environmental influences, cannot be assumed to be intact. It is also likely that a failed line would inflict damage on the remaining lines, due to their close proximity, as it became detached from the structure. It is clear from this discussion that even one mooring line failure should be avoided at all costs. This puts heavy emphasis both on the design and subsequent inspection of the mooring system on which the integrity of the whole structure depends.

1.2.2 Service Conditions For A TLP Mooring System

As previously mentioned, the predominant loading on the mooring will be axial loading. With the platform at rest, the mooring experiences a high static load as a reaction to the buoyancy of the hull. Environmental loading on the hull and deck lead to fluctuating

mooring loads. The high static load with fluctuating loads about this mean, makes fatigue an important consideration for the mooring. Loading of the mooring by direct wave and current forces may be important as could vortex shedding which could occur as the whole structure moves laterally through the water.

The mooring must perform in a corrosive environment and must therefore be adequately protected and designed against corrosion fatigue, stress corrosion cracking and general corrosive degradation. The use of low alloy high strength steels in a corrosive environment with cathodic protection can lead to problems with hydrogen embrittlement and stress corrosion cracking.

As previously stated, the integrity of the complete structure is totally dependent on the integrity of the mooring. The mooring must therefore be regularly inspected. Moreover, if defects are found, assessments must be made to determine the integrity of the mooring system.

1.2.3 Types Of Mooring Line

So far, the mooring system has been described as consisting of a number of mooring lines. The primary mode of loading in the mooring line is tension, with bending and torsional loads being of secondary importance, providing the bend stiffness of the line is low compared to the axial stiffness. In the event of a problem developing in one of the mooring lines, it may become necessary to remove the line and replace it. If these platforms are deployed in deep waters, each mooring line could be several thousand feet long. The suitability of handling therefore must be considered when selecting a mooring system. Various types of mooring line have been considered. The most important ones will be discussed here.

1.2.3.1 Chain

Chains have been extensively used for many types of mooring and anchoring systems. Extremely large chains are now available and it is likely that chains of sufficient strength could be produced for use with a TLP. Despite obvious weight problems, chain mooring lines could be removed at intervals and could be deployed as a number of lengths connected by removable links.

The major problem with chains is the inspection. Load transfer between links is crude and a chain mooring system cannot be adequately inspected in situ. The periodic

removal of a line for routine inspection would probably be unsatisfactory from an operational standpoint. Even with the line removed, the inspection of each link would be extremely difficult to carry out other than visually.

The performance of a chain under in-service fatigue loading in a marine environment is complex. The numerous contacting surfaces prohibit the use of coatings for corrosion protection. Cathodic protection using either impressed current or sacrificial anodes would be difficult, not least due to the variable electrical contact between loaded surfaces on each link. The load transfer mechanism between links results in the possibility of fretting fatigue between contacting surfaces which are themselves not inspectable in service. A further problem with chain is that of damage during handling and deployment. Large chains are difficult to handle and surface damage could lead to fatigue initiation.

A further disadvantage when considering the use of chain lines in parallel is that of differential elongation. This would tend to result in a single line taking a greater proportion of the total load.

It is seen from the above discussion that a conventional chain mooring solution is not adequate for a TLP.

1.2.3.2 Ropes

Wire ropes are widely used for mooring and tethering. These are available in sizes up to 125mm diameter and could be made to suit TLP moorings. Wire ropes are made up of many individual wire strands woven and wound together. Figure 1.2 shows some typical wire rope constructions, some of which may be suitable for offshore applications. It is seen from Figure 1.2 that there is a wide range of different constructions. These are discussed in Reference [44]. Ideally wire ropes should be used in one continuous length. Whilst it is possible to effect joins, the most common failure site is at a join or terminator. Problems also occur where ropes are fed around hausers but this is not relevant to the TLP application. Clearly a handling problem exists with continuous lengths of large diameter wire rope.

Again a major problem is that of inspection. The integrity of a wire rope is extremely difficult to assess using Non-Destructive Testing (NDT) techniques. The construction of the rope can tolerate a number of breaks in individual wire strands but an "acceptable" number is hard to quantify. This coupled with very little understanding

of the mechanisms by which wire ropes fail under fatigue loading, and uncertainties in corrosion behaviour makes their use for key components such as TLP mooring lines unlikely.

Synthetic ropes have become more popular in recent years and are certainly being used for mooring applications. One feature of synthetic rope is the ability to withstand shock loading, which has led to their use in composite wire/synthetic rope catenary mooring systems as a shock absorber. This benefit cannot be usefully employed in a TLP mooring since the design relies on the tether being constantly under tension. Snatch loads would only occur if the tether were to go slack and this would be considered a major design failure.

Inspection and subsequent integrity assessment is still a major problem and it is unlikely that such ropes could be employed for any TLP applications.

1.2.3.3 Steel Tubes

Conventional mooring systems usually demand that the mooring lines be capable of assuming a curved (catenary) shape and that they should be capable of running around hausers and blocks. The demands of a TLP mooring in this context are less stringent in that the mooring remains essentially straight. This opens up the possibility of using straight steel elements as mooring lines.

The terminology has changed with the consideration of heavy steel elements, for which the description "mooring line" seems inadequate. This type of mooring is now termed a tether, with the individual components being called tether elements. The use of steel tubes as a tension element again leads to problems of handling. This is overcome by making up the required length by joining a number of identical elements. The method of joining is clearly most important since it may be necessary to remove a tether during service. By providing a threaded connection on each end of each element, the tether can be broken down and removed if necessary and it is also possible to replace an individual element.

The use of steel tethers satisfies most of the design requirements in that they could be made removable, they exhibit high axial stiffness and they can also be made hollow to overcome platform weight problems. However, the in-service inspection of such a component is difficult, especially at the critical point, ie the threaded section. Some inspection groups claim to be able to inspect threaded components in-service using ultrasonics techniques, although this ability has not been demonstrated to date.

The use of steel tethers offers a number of possibilities covering solid and hollow sections. Ultimately there must be sufficient material to sustain the service loading. The final geometry will depend on other factors. A solid section provides the minimum presented area to direct wave and current loading. A hollow section attracts higher environmental loads but offers dead weight benefits. These points are discussed in further detail later.

Two types of steel tether have been considered for TLP applications, one being a thick walled forging, the other a thin walled tube. These are shown in Figure 1.3 and 1.4 respectively. Both types employ tapered threaded connections at each end and, due to weight considerations, are manufactured from high strength steels.

i) Forged Tether

Conoco have used a forged tether for the Hutton TLP (Fig. 1.4). This is essentially a thick walled tube with large diameter forged ends, on which the threads are cut. The use of a thick walled tube results in lower outside diameter than a corresponding thin walled design of the same static strength. This results in a lower bend stiffness and lower environmental loading from waves and currents.

ii) Thin Walled Tether

High strength thin walled tubes, connected by threaded connections have been employed extensively in the oil industry for well casing and risers. The industry therefore has considerable experience in this type of component and the material and manufacturing processes, unlike the forged tether which is a novel design although there are similarities with drill strings. However, it should be noted that the service conditions for a tether are vastly different from those experienced by other threaded tube designs. The tether loading is predominantly fluctuating tensile loading whereas casings usually experience relatively small fatigue loads. Also the integrity requirements for a tether are the most important factor. Designs for casing and risers usually call for pressure tightness from the inside of the component and a smooth internal bore, neither of which are high priorities for a tethering system. Drillstrings have axial, bending and torsional loads and also have the requirement for regular make and break as part of routine drilling operations. These parameters feature strongly in the connection design for drillstrings. It should be noted therefore that although the offshore industry has a lot of experience with threaded tubulars, these components have been designed and developed for different situations.

iii) Welded Steel Tethers

Another variation in tether design being considered is again based on steel tubes, but this time with welded connections. It is doubtful whether welding is a practical solution to the problem if high strength steels are likely to be used. In addition, problems associated with deployment and being unable to readily break down the tether for removal or replacement suggest this may be an impractical solution. It must also be questioned whether the use of welding, and the associated fatigue and metallurgical problems, would be prudent considering the inspection and integrity requirements. However, the development of automated ultrasonic scanning techniques for the inspection of girth welds [1] suggest the requirements for inspection could be soon met. However, the fact remains that the installation and removal in deep water would be a fundamental problem.

1.3 INTEGRITY ASSESSMENT OF TETHERS

Providing corrosion can be controlled by conventional means, the major in-service damage mechanism is that of fatigue cracking. In service inspection must be conducted at regular intervals to determine whether fatigue damage is occurring. The most critical region on any threaded element will be the threaded section itself or geometric changes in section. Design & quality control of plain sections should be adequate to ensure that the plain section does not become more critical than a highly stressed area at the thread.

The minimum requirement of the in- service inspection system is that it is capable of detecting and locating defects in critical areas before they reach a critical size. The definition of critical size depends on the way in which fatigue cracks propagate in such a component under service loading and the subsequent way in which the component fails. The rate of crack growth also dictates the inspection interval.

The rate at which fatigue cracks grow in a component is the key to defining inspection requirements. All inspection techniques have threshold detection levels where defects of a size lower than the threshold can exist but not be detected. Assuming that a defect is present but just below the inspection threshold size when an inspection is conducted, the defect will not be found. An analysis of the growth of such a defect must be conducted to determine the remaining life of the component. From this analysis, the next inspection would be scheduled to ensure that the defect was found and that remedial action would be taken in time to prevent a failure.

The analysis of crack growth in a component is conducted using a Fracture Mechanics approach. This requires a fracture mechanics model of crack growth in the component, which could be either a theoretical model or an empirical one based on experimental results. In either case the model requires two sets of information to enable the remaining life to be calculated. The first is the stress history likely to be experienced in service. The second is the size of the defect.

The stress history depends on environmental loading (global loading) and the local geometry (stress concentrations). The defect size can only be provided from the in-service inspection. The quality of the information coming from the in-service inspection determines the validity of the integrity calculation and must therefore be determined.

1.4 SUMMARY

From the above discussion it is seen that, when considering the design of threaded tether connections, there are a number of factors to be considered:-

1) The design of tether to withstand fatigue loading and environmental effects.

2) The system must be inspectable and the reliability of the data collected must be known.

3) Fracture mechanics models are required to describe the behaviour of the component if fatigue cracks are present. These can be experimentally or theoretically derived.

This study reviews the use of threaded connections and highlights some of the problems associated with the design and analysis of such components. The stress analysis of threaded components is complex due to the non-uniform load distribution that exists across the component.

A novel technique for the determination of the load distribution in threads is presented in Chapter 4 and is integrated with modern Finite Element techniques to provide a tool for the stress analysis of threaded connections. Large scale fatigue tests have been conducted to provide information on the crack growth behaviour in such components and these are described in Chapter 5.

A Fracture Mechanics analysis has been conducted and is described in Chapter 6 where theoretically derived results are compared.

Finally, the inspection philosophy for such tethers in-service is discussed, in Chapter 7, with particular reference to the need for full validation of the performance of the inspection techniques used in order that the inspection and Fracture Mechanics capabilities can be integrated to enable a Structural Integrity Assessment of the tether to be made.

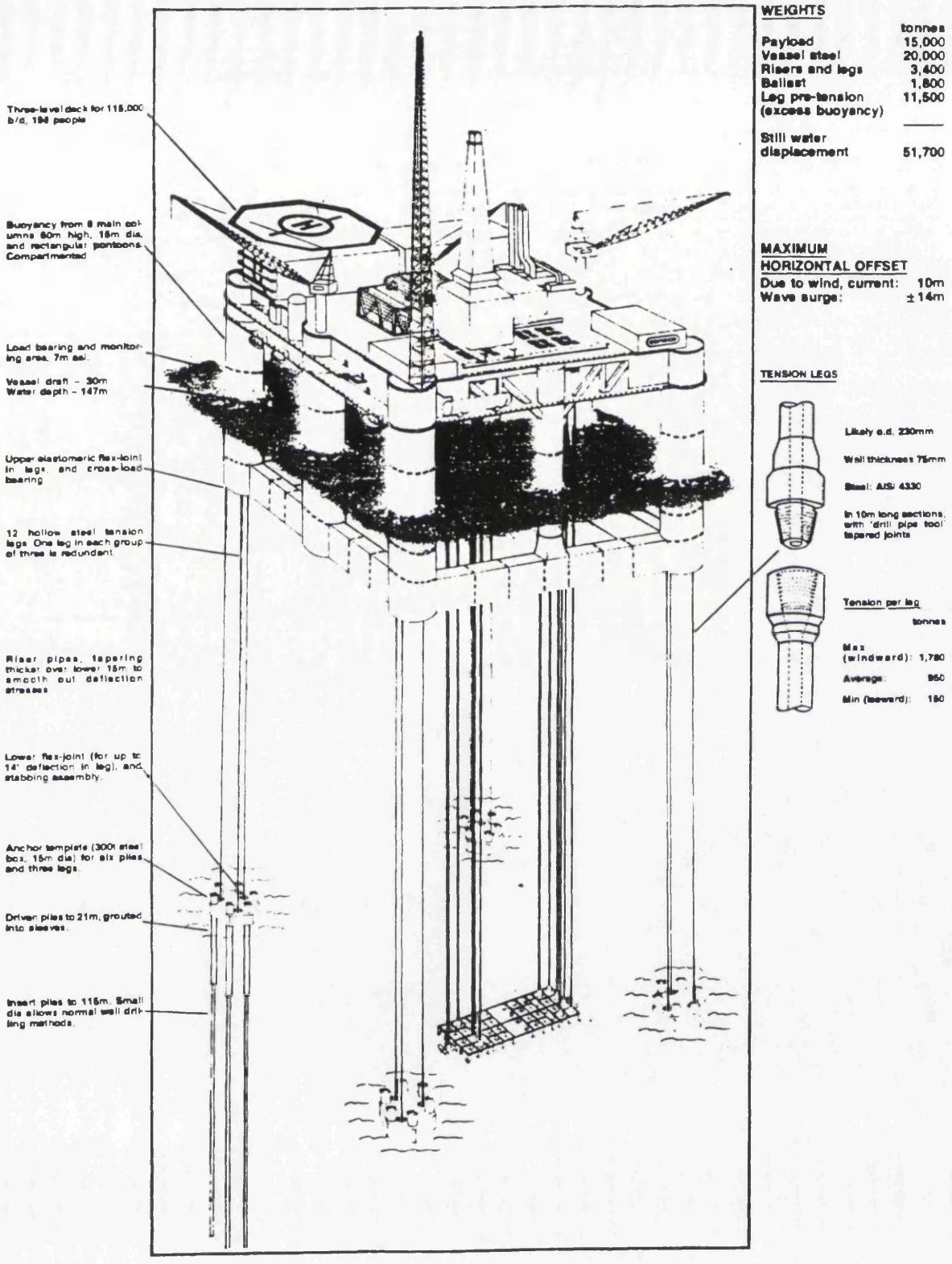

Fig. 1.1 General arrangement of Conoco Hutton Tension Leg Platform (TLP)
(Reproduced from Ref. 42)

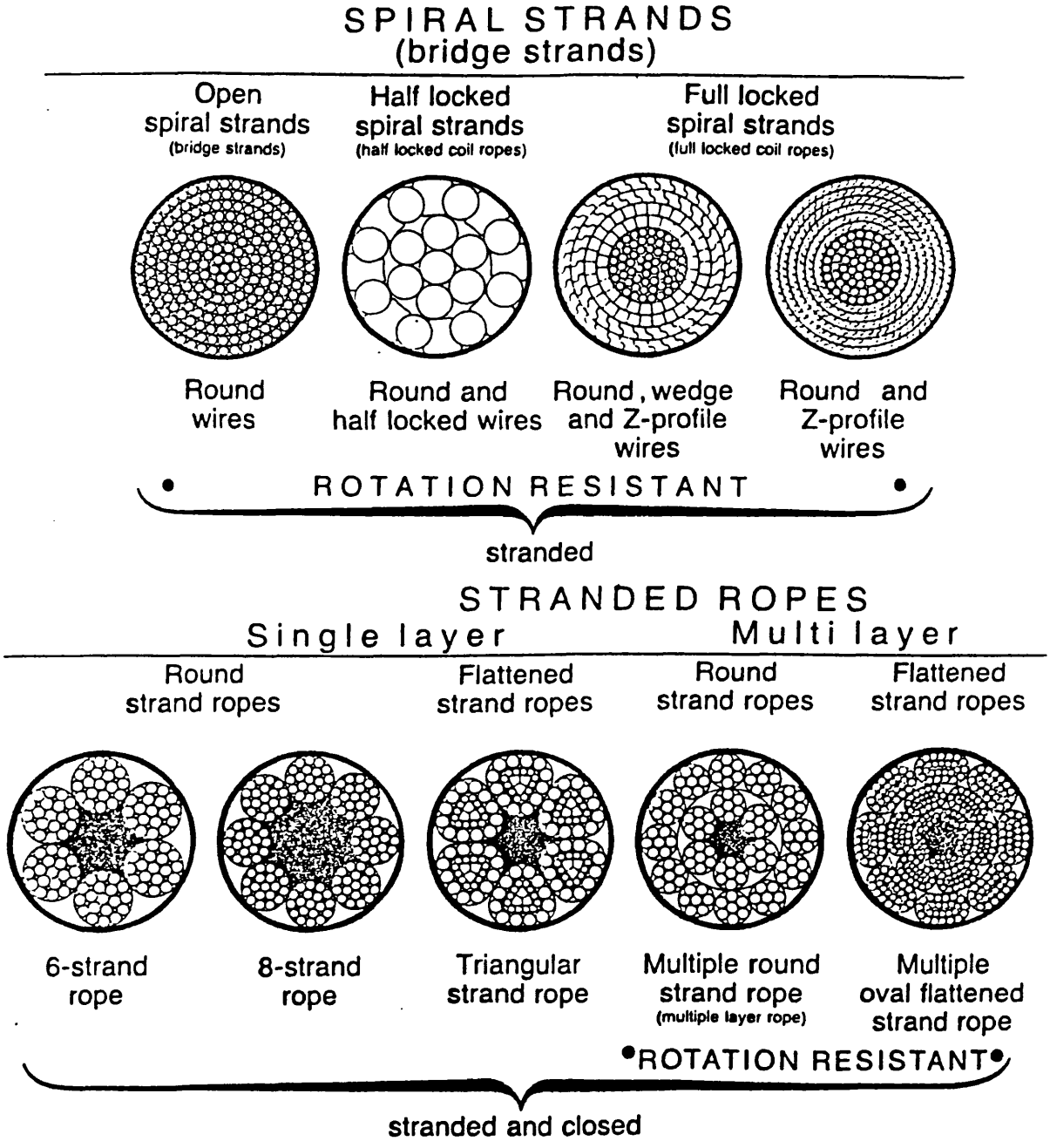

Fig. 1.2 Typical wire rope constructions. (Reproduced from Ref. 42)

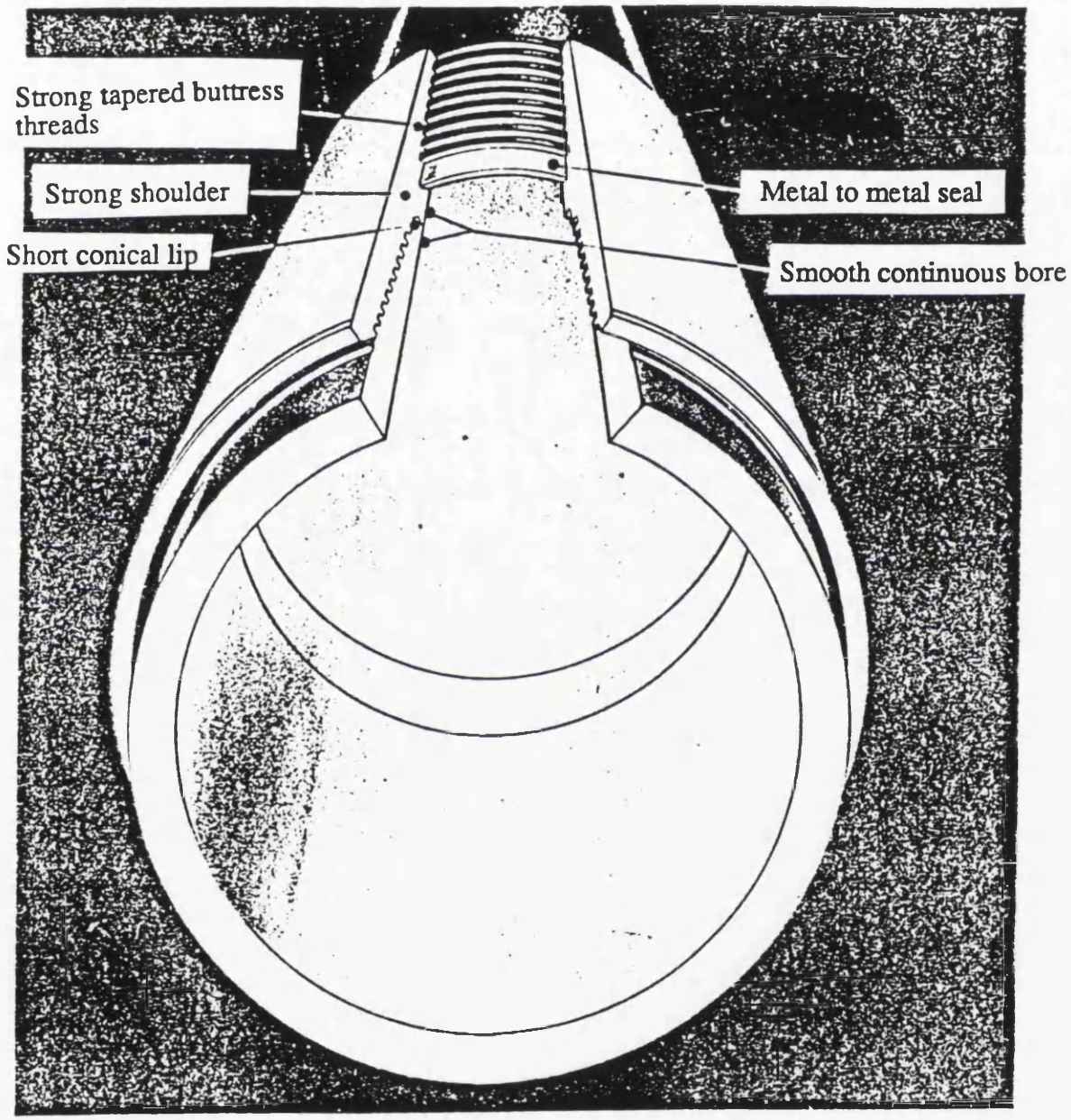

Fig. 1.3 Schematic view of thin walled tether.

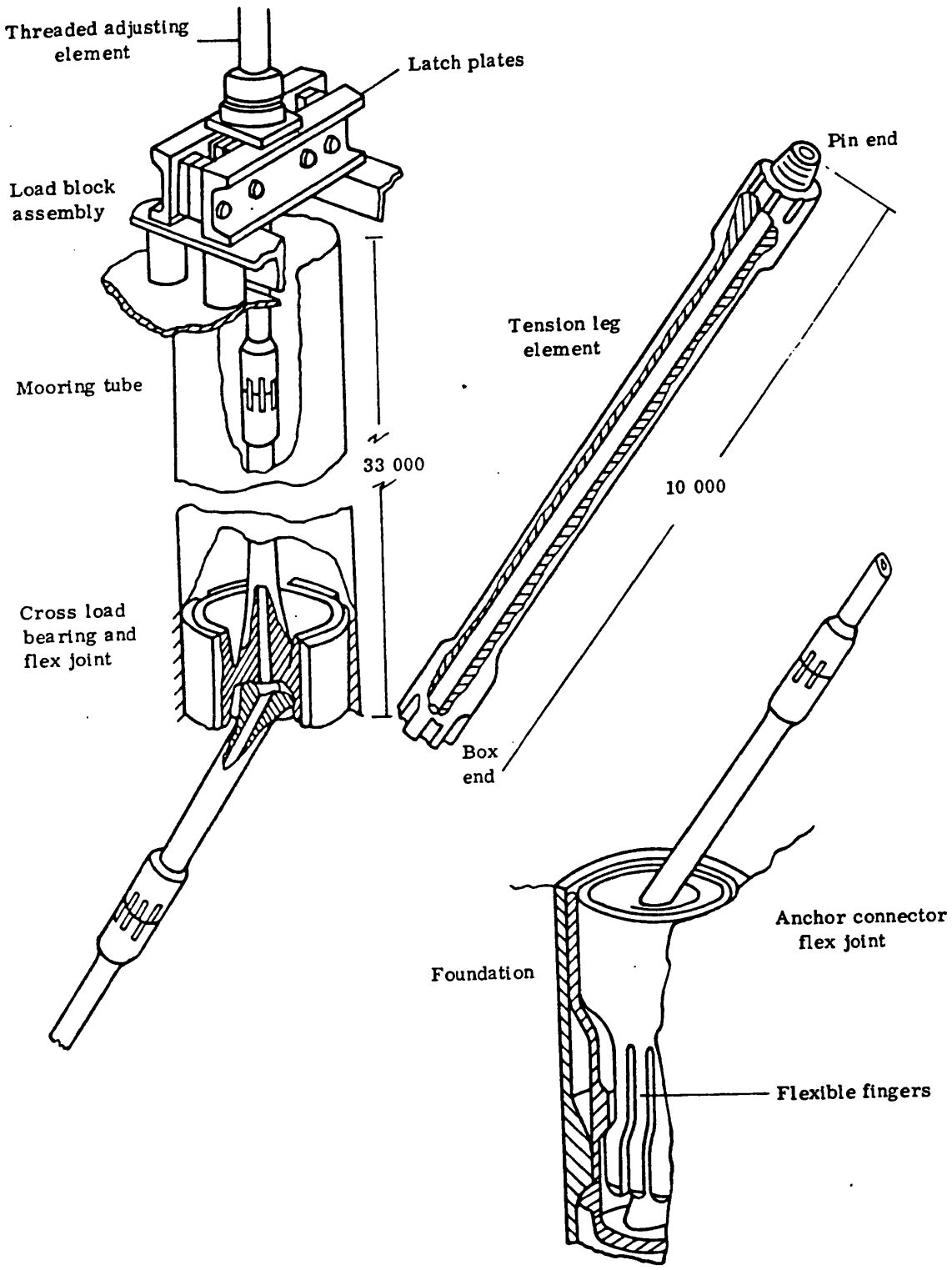

Fig. 1.4 Schematic view of forged tether element. (Reproduced from Ref. 42)

CHAPTER 2

SCREW THREADS

and

THREADED CONNECTIONS

2.1 INTRODUCTION

The discussion in the previous Chapter outlines the requirements for a TLP tether and suggests that a mooring formed of steel tubes joined together by threaded connections is the favoured solution. Threads have been used for centuries in many engineering applications, yet it is surprising that the analysis of threaded connections and in particular their performance under dynamic loading is still not well documented.

The first spiral screw was developed by Archimedes and this was used for raising irrigation water around 250 BC. The first documented use of screw threads for the transmission of loads was by Gutenburg when he produced a screw-driven printing press in the 15th Century. From that time up to the present day, Engineers have been designing and developing screw threads for use in all fields of engineering. Indeed after the common nail, screw products are the most widely used fasteners.

The success of the threaded connection throughout Industry has tended to obscure the complexity of the design problems associated with screw threads. The most common screwed fastener is the nut and bolt. This has successfully been used for many years to sustain static tensile and shear loads. It is only relatively recently in the Aerospace Industry that attention has been given to the problems associated with bolted connections in situations where fatigue could be a problem.

In any threaded connector the main area of interest is the threaded portion. Design to take account of all other areas should not be a problem. The complexity of the load and stress distribution in the threaded portion of the connector makes detailed analysis extremely difficult.

It has been recognised by a number of investigations [eg. 2, 3, 4] that the tooth load distribution in a threaded member is highly non-uniform and invariably leads to high tooth loads on the first loaded teeth.

This can be best understood by considering a simple nut and bolt assembly as shown in Figure 2.1. Assuming the threads to all be in contact but unloaded, when a load is applied to the bolt the load is transferred into the nut via teeth loads. The first tooth becomes loaded and deflects. Due to the uniform pitching, only then can subsequent teeth be loaded. The

resulting differential strains in the threaded section leads to a load distribution with loading on each tooth with the first tooth being the most highly loaded and subsequent teeth taking a reducing percentage of the total load. A typical tooth load distribution for both nut and bolt assembly and for a threaded connection are shown in Figure 2.3[34]. This highly non-linear load distribution is very important and is the primary unknown facing the engineer.

In order to determine the stresses acting in the joint, the tooth load distribution must first be found. Knowing this, a stress analysis can be carried out. It is important to note at this stage that there are two primary contributions to the high SCF typically found in threaded components. The first is the effect of the tooth loading and the second is the notch effect that arises due to that portion of the load in the thread core, Figure 2.2.

One of the most comprehensive piece of work carried out to investigate the load distribution was carried out by Sopwith in 1947 [2]. It is interesting to note that this is still the most definitive piece of work available today, despite the fact that this was carried out some fifty years ago. The work of Sopwith concentrated primarily on bolt threads with a 'V' profile. The work is highly mathematical and for engineers, the complexity of the analysis could be prohibitive. Since Sopwith, a number of researchers [eg. 3, 4] have used finite element analysis and photo-elasticity methods to determine the stress and load distribution in screw threads for both bolts and threaded couplings.

Before discussing the load distribution in detail, it is important to recognise the types of threaded connections available and their relative merits:

2.2 THREAD FORMS

2.2.1 'V' Thread

The most common thread form for general engineering application is the 'V' thread. There are a number of standard forms and the most common of these are shown in Figure 2.4. The 'V' thread form is easy to produce and can be produced in many cases using tap and die techniques. The important feature is that the amount of material to be removed in the manufacturing reduces towards the root of the thread which is ideal for manufacturing consideration. It is the ease of manufacture that has led to this being such a popular form of thread. The requirement for mass produced threaded components has led to the development of new techniques for producing threads. The most common now in use is the thread rolling technique. This technique results in no material removal with the threads

simply being created by plastic deformation. The variability in thread forms shown in Figure 2.4 have been developed to aid manufacture assembly and to a lesser extent, strength. The fact that the screw thread has successfully been used in this form for the last 100 years is reason enough not to change it for general applications.

The load carrying mode of a 'V' thread is complex due to the varying stiffness of the tooth section. Sopwith [2] shows the deformed shape of the tooth as in Figure 2.5. It is seen that the inclined face of the tooth will lead to a tendency for separation of the male and female components with high frictional forces being developed on the mating faces.

From the fatigue consideration, the geometric stress concentration factors at the thread root are not excessive due to the generous radius at the thread root. However, the sharp crown of the thread makes it susceptible to mechanical damage due to impact or abrasion.

2.2.2 Buttress Thread

In contrast to the triangular cross section of the 'V' thread, the buttress thread is essentially a rectangular thread form and like the 'V' thread these are produced in a number of forms. Some common forms are shown in Figure 2.6. The production of buttress threads is more difficult than a 'V' thread. The rectangular cross-section means that this type of thread cannot be produced using taps and dies, due to the large amount of material to be removed at the root of the thread. The manufacture, therefore, dictates the use of turning tools to produce the thread. This is commonly carried out using specially profiled single tip tools. It follows, therefore, that it would be extremely difficult to produce a buttress thread in a small diameter, especially in the female component due to difficulty of access for the turning tool. For this reason, the use of buttress thread is generally restricted to components of diameters greater than 70 mm.

It is seen immediately that the buttress form is a more robust section and is, therefore, more resistant to accidental damage. Another interesting feature is the loading face which is cut approximately normal to the axis of the thread. This results in a large mating area and greatly reduced radial separation forces between male and female components. One obvious drawback to this design is the relatively small root radius which can lead to high geometric stress concentrations locally at the thread root.

2.3 LOAD DISTRIBUTION

2.3.1 General

As briefly mentioned earlier, a screwed connection exhibits a highly non-uniform load distribution along it's length, as illustrated in Figure 2.3b. Figure 2.7 shows an idealised section of a threaded assembly. Consider the effect of loading the assembly. Section 'A' and 'B' carry the full applied load and since all teeth are in contact in the unloaded condition i.e. the teeth are equally pitched, tooth 1 starts to attract load and deflects, thus loading tooth 2 etc. until all forces are balanced. Absolute deflection of each tooth is dictated not only by the stiffness of the tooth but also by the stiffness of the overall section on which the tooth is formed. This is an important point and is covered in detail in Chapter 4.

At this stage it can be seen that the tooth load distribution depends on both the tooth stiffness and the stiffness of the section. With this in mind, a number of attempts have been made to physically alter the cross-section of the threaded coupling to improve this distribution. Whilst this is covered in detail later, it is important at this stage to appreciate the reasoning behind some of the designs that will be considered.

2.3.2 Tapered Section

Considering the joint shown in Figure 2.7, if the tooth was be made less stiff, the load would be more readily transferred to subsequent teeth. One way of achieving this would be to reduce the stiffness of the section at the teeth, Figure 2.8 shows one way in which this can be done. It is seen that the threads are still produced parallel with the axis. Another way of achieving the same thing is to form the teeth inclined to the axis as shown in Figure 2.9. This has an additional benefit which makes the solution particularly attractive. That is the speed of make-up. With the threads inclined to the axis, it is no longer necessary to make-up the joint starting at thread No 1. For a parallel thread, the number of revolutions to full engagement equals the number of teeth i.e. 25 teeth require 25 full revolutions to engage fully. A tapered thread enables the joint to be partially engaged by "stabbing" as shown in Figure 2.9. The joint then requires only a minimal number of revolutions to fully engage all the teeth.

Thus assembly time is considerably less than for a parallel thread. For this reason, taper threads of the form shown in Fig: 2.9 are widely used in applications where repeated make and break is important.

Tapered connections of the type shown are used extensively with the buttress thread profile. The buttress form is robust enough and insensitive to minor damage to withstand the "stabbing" operation. A 'V' thread form with fine thread crowns could be easily damaged, which prohibits its use for some heavy engineering applications. However, the drilling industry have developed 'V' thread forms which are used extensively in make and break situations. The thread geometries are produced to an API standard [7] and generally have truncated thread crowns. It is common however to see significant damage on the thread crown apparently due to the make up operation and it is not clear whether this damage contributes significantly to the number of failures experienced by that industry.

2.3.3 Differential Pitching

The term "differential pitching" can have two distinct meanings when referred to threaded connection design. Basically the two types of differential pitching are used for entirely different reasons, one type being used to modify the tooth load distribution directly, the other was designed for a specific application where the technique is used to develop high preloads which, in turn modify the tooth load and amplitude of dynamic loading. The preload principle is discussed in the next section and the principle of differential pitching will be discussed here.

Type 1 - Direct modification of load distribution.

Hunting Oilfield Services [5] have developed a patented design based around differential pitching. Figure 2.10 shows the basic principle of this design. This threaded design, known as the "Fox" thread has a small pitch reduction towards the free end of the box. The result is that when the coupling is made up, the teeth in the centre are in contact whilst those at either end are not. As the coupling is then loaded, the teeth towards both ends of the coupling progressively mate and take up load, resulting in a more uniform tooth load distribution and hence more uniform stress distribution. The manufacturing tolerances of such a design are stringent and the analysis of the coupling is more complex than for a conventional design.

Type 2 - Preloading System

Chen and Williams [6] describe a differential thread connector for use in situation where the connector needs to sustain torque in both directions during service. In this technique, two male members are connected using a female connector. At one end, male and female are threaded at 5 t.p.i., on the other they have 4 t.p.i. The ends of the male components are provided with interlocking tongue and grooves and the coupling is rotated back to engage

the 4 t.p.i. threads. The coupling is then turned to engage onto the 5 t.p.i. pin resulting in effectively a 20 t.p.i. action as the tubes are drawn together and preloaded across their ends. This system has the benefit of the effect of a fine thread whilst using coarse robust threads to achieve this and is shown in Figure 2.11.

2.4 PRELOAD

Preloading a threaded member by torquing has long been accepted as standard practice in engineering. One reason for this is to achieve a tight joint and to overcome any "slack" in the thread. The action of tightening a threaded component applies static forces to the joint which induce high frictional forces on the teeth and prevent loosening of the connection due to vibration. However, a less known benefit is that the preloading of the threaded component relieves the thread of a proportion of any subsequently applied load and hence is beneficial in fatigue applications by reducing the amplitude of the fatigue loading. This can be demonstrated by considering a simple bolted joint as indicated in Figure 2.12.

As the bolt is tightened, a tension is applied in the bolt and the shank stretches. The overall stiffness of the nut and bolt is represented by the line "AD". Similarly the plate compresses under the applied load. The compression stiffness, in the region of the bolt, is represented by the line "CD". It is seen that there is equilibrium with the tensile load in the bolt equal to the compression on the plate. The load in each component is represented by line "BD". When an external load is applied to the bolt, the bolt stretches by δ due to the applied load P. However, the stretching of the bolt relieves compression on the plate and hence the reaction force in the bolt reduces. The net result is that the load in the bolt, and hence the threaded component increases by only a proportion of the applied load. The remainder results in a reduction in the compression (preload) of the joint.

Referring to Figure 2.12, and denoting the axial stiffness of the fastener as K_{Bo} and the compressive stiffness of the plate as K_{Pl}, the effect of an axially applied load can be derived as :-

$$\Delta P_{bolt} = P\left(\frac{K_{Bo}}{K_{Bo}+K_{Pl}}\right)$$

and

$$\Delta P_{plate} = P\left(\frac{K_{Pl}}{K_{Bo}+K_{Pl}}\right)$$

A similar concept applies to a threaded coupling as shown in Figure 2.13. In this case, however, the compressive loads are developed over a shoulder at the end of the thread. Here the critical sections are the end of the pin and the preloaded end of the box. Using a similar approach to that for the bolted joint, the effect on the load in a preloaded pin is again found to be

$$\Delta P = P\left(\frac{K_{PB}}{K_{BB}+K_{PB}}\right)$$

where K_{PB} = Bulk stiffness of the pin and K_{BB} = Bulk stiffness of the box.
(Note that bulk stiffness refers to the total stiffness of the component including the bulk section and the threaded section).

These derivations and the modelling of this effect are given in Chapter 4.

It is seen that with suitable design and correctly applied preloads, significant benefits can be achieved due to the reduction of fatigue loading amplitudes. This is at the expense of high mean loads, and is therefore a compromise situation.
High mean loads necessitate heavier sections to satisfy the applied stresses. The "R" ratio (ratio of minimum to maximum applied loads) is increased and this can lead to adverse fatigue properties for high strength steels which tend to be far more sensitive to "R" ratio effects than ordinary mild steels. High mean loads also increase the susceptibility to stress corrosion cracking.

It will be seen in Chapter 4 that the significant reduction in fatigue loading makes the option highly attractive and preload is generally adopted. In addition to the fatigue benefits, high make up torques provide good sealing forces and can be utilised to prevent the ingress of corrosive products into the highly stressed regions of the thread.

Theoretically, therefore, the use of preload is ideal for most aspects. However, in practical terms, preload is difficult to apply and almost impossible to measure in the field.

In general engineering, bolted assemblies are tightened by known torque. The act of tightening induces high loads between the threads on the male and female components leading to high frictional forces. Similarly the frictional force on the preloading surfaces,

since one is moving relative to the other, must also be overcome. Both components of frictional resistance depend upon the quality of machining i.e. surface finish, the tolerance of machining and the degree of lubrication applied.

Haviland [4] reviews the mechanisms of torquing a simple bolted connection and gives some interesting results. In an analysis of the torque effort applied to two different bolt designs (UNC and UNF), it was found that only 10 - 15% of the torque contributed to bolt pretensions with approximately 40% used to overcome thread friction and the remainder being used to overcome friction under the head. It is interesting to note that only 70% of the tightening torque was necessary to loosen the joint. Haviland also investigated the scatter on the pretension achieved on notionally identical bolts with the same lubrication and produces a scatter envelope in which it is seen that the pretension achieved can vary by a factor of almost 2.

When one considers a typical offshore casing type tapered threaded connection which is machined to create radial interference, between male and female components, any relationship between torque and preload is complex.

Whilst discussing preload, it is necessary to appreciate that the torquing of large threaded joints is physically difficult since they are produced on round pipes. The torque applied needs to be transferred into the thread which is extremely difficult without damaging the tube. Conoco found it necessary to provide lugs machined on to the end of the forging to allow the torque to be applied. This then introduces stress raisers due to the geometry which in itself can lead to problems. The torquing operation also would damage any corrosion resistant coatings that are applied to the tether.

The act of preloading a threaded joint by torquing necessitates the relative rotation of the two components to induce high loads across the teeth and one effect of this is the possibility of galling. Damage due to galling can occur during the torque tightening and this can cause problems with re-make if the component is designed for successive make and break operations such as required for drill pipe. Specialist coatings can be applied to alleviate such problems but galling must be seriously considered at the design stage for certain applications. One of the major problems is that the preload is concentrated on the first few

threads of a conventional joint. The Hunting Fox [5] connector is claimed to minimise galling problems by distributing preload over a larger number of teeth and hence reducing the frictional load on the teeth.

One final consideration is that the high torque loads can lead to sufficiently high tooth loads to cause local plastic deformation. When this occurs, it is unlikely that the joint could be broken down for inspection and then reassembled to the same condition.

It is the practice in some industries not to specify torque loads but to define an angular displacement for make up. The American Petroleum Institute API [7] recommend the technique for linepipe connections. This does overcome the main problem, that of uncertainties due to friction, by effectively applying a fixed displacement. This requires careful control of make up to define the start point from which angular rotation measurement commences. "Hand Tight" is not sufficient for a tether element weighing a few tonnes.

From the above discussion, it is clear that preload is in principle beneficial but in practice difficult to control. Any design relying on preload must ensure that the required preload can be achieved and, more importantly, that it is maintained throughout the life of the component. Initial preload can be lost due to a number of factors. Bickford [8] lists some factors that can lead to loss of preload on bolted connections. The threaded coupling for offshore application could lose preload due to corrosion attack of the preloaded surfaces, or indeed due to a change in stiffness due to corrosion or fatigue damage. This must always be considered when evaluating the integrity of the components during service.

2.5 ANALYSIS TECHNIQUES

The foregoing section details some of the factors that must be considered before embarking on the design of a threaded component. So far it has been stated that the load distribution in threaded connections is non-linear. For fatigue analysis, it is not load but stresses that are required. The analysis of a thread depends on knowing the loads acting on each tooth and secondly the effect the tooth load has on the stresses in the component.

One of the earliest studies of the distribution of stress in threaded connections was conducted by Stromeyer in 1918 [3]. This work cites the observed failure of a number of threaded components and attempts an analysis to describe the stress distribution in a nut and bolt connection. Stromeyer recognised the effect of differential strains on the stress distribution

along the nut and produced a mathematical analysis based on this which predicted the non-uniform stress which is characteristic of this type of joint. The paper is significant in the fact that, it identifies some of the fundamental characteristics of the threaded connection.

Firstly, it identifies the non-uniform stress distribution associated with the bolted connection and indeed suggests that differential pitching between the nut and bolt would alleviate this, a feature patented by Hunting Oilfield Services [5] some 65 years later. Stromeyer also refers to early experimental work by Coker [22] on loaded projections. This was based on an early photoelasticity process and, whilst not able to quantify the results at that time, Stromeyer suggested that the studies confirmed qualitatively his findings. Stromeyer also raised the question of manufacturing tolerances, discussing how accidental mismatch of pitch may influence the performance of the joint and also commenting on the problem of manufacturing tolerances for the 2D photoelasticity models, a problem which is reported by Broadbent in 1986 [15].

Immediately two analysis methods have been introduced, the mathematical analysis and the photoelasticity experimental method. The various analysis techniques, together with reviews on previous work are given below.

It should of course be recognised that much of the early work has been conducted on bolted connections, that is the analysis of the behaviour of a nut and bolt. The tethering application using threaded connectors does represent a different situation since both male and female components are subjected to applied tension, unlike the nut and bolt in which the bolt load is tensile whilst the nut is compressive. However, the fundamental principle of load transfer is the same and it is important to consider how the various analysis techniques have developed and how similar techniques have been used later for the analysis of threaded connections for offshore applications.

2.5.1 Mathematical Analysis

The mathematical analysis depends solely on the mathematical solution to an engineering problem based on a basic engineering theory. Following from the early work of Stromeyer [3] the most rigourous piece of mathematical modelling to be reported to date is that by Sopwith in 1948 [2].

Sopwith analysed the strains in the bolt and nut components in order to determine the distribution of tooth load around the thread. The study is directed towards the determination of load rather than stress distribution, although it is considered that the stresses may be readily derived once the tooth loading and hence the joint loading is known.

The analysis is extremely complex to apply and is based on the 'V' form although Sopwith does claim it can be equally applied to a buttress thread. The threads are modelled as contacting cantilevers, their relative displacements being due to tooth bending, axial strains in the body (nut and bolt) and axial recession, as defined earlier by Goodier [12].

There is a fundamental difference between the analysis of bolted connections and the threaded coupling. Sopwith recognised this and presented results that were applicable to a turnbuckle type of connection. These are investigated in Appendix A, modified for a buttress thread. It is seen that the analysis is complex and it was found that it is not applicable to large numbers of teeth.

The full 3D approach to mathematical analysis does result in an extremely complex solution. This combined with the problems described in Appendix A do rather preclude its use for applications employing threaded connections rather than nuts and bolts. In addition, the analysis as presented, cannot take preload into account which is a serious drawback when considering threaded couplings.

No other workers have attempted such a rigourous mathematical approach to the load or stress distribution in threads. There are a number of likely reasons for this:

i) It is unlikely that the Sopwith analysis for bolted connections could be improved.

ii) The advent of experimental techniques involving photoelasticity allowed empirical solutions to be investigated.

iii) The number of influencing variables leads to such a complex analysis that the results are difficult to use for general engineering applications.

iv) The advent of finite element techniques allow complex numerical modelling from which empirical solutions can be derived.

It is however considered that an engineering mathematical solution could provide a valuable tool if it could be simplified. Chapter 4 details a new approach that is proposed for the analysis of tooth load and stress distribution in threaded connections.

This employs a simplified mathematical model integrated with modern Finite Element techniques to provide a powerful analytical tool, which is capable of modelling preloaded joints.

2.5.2 Experimental Techniques

Experimental techniques can provide valuable insight into the behaviour of threaded connections. Two experimental methods are discussed here.

2.5.2.1 Photoelastic Methods

Stromeyer [3] described some early experiments conducted using stressed celluloid plates illuminated with polarised light in which "stress patterns" were observed. These were conducted in 1911. This study involved the observation of stress patterns during loading.

The photoelasticity method of stress analysis as we know it today, involving stress freezing, was developed in the 1930's and is well documented [9, 10]. Early work on threads [9, 10,] was conducted using 2D photoelastic models, basically modelling the teeth as loaded projections. The results from these studies were at best inconclusive and on occasions contradictive. Strain measurements made on bolted joints by Goodier [12] suggested that some of the strains that contribute to the load distribution are 3-dimensional in nature and thus the 2D models do not properly represent the real situation. In particular Goodier identifies the failure to model hoop restraint and nut wall bending as possible reasons for the poor results.

Hetenyi [13] also attributes some of the problems with the early 2D photoelastic studies to the inability to produce models to sufficient tolerances, as indicated by Stromeyer [3] much earlier. Hetenyi [13] investigated different nut designs using 3D models and concluded that in all cases, the peak stress occurred at the first full thread of the bolt. He also confirmed the benefit of using tapered threads although reported that in the nut

and bolt case, high applied loads reduced the benefits of the tapers investigated. The results of these studies, as for all photoelasticity works are presented as maximum stresses at the thread root.

Heywood [17] analysed the stresses at the roots of loaded projections using the photoelasticity method and compared the results for various tooth profiles. This comprehensive review covers the performance of both thread and gear teeth and concludes that a "stub shaped" thread gives the greatest strength. However, of the "general purpose" threads, he suggests the Whitworth form is remarkably close to an optimum in terms of strength. It must be recognised however, that this comprehensive study does not address the load distribution in the threaded connection and as such, cannot be used unless the distribution of tooth load is known. The earlier work described above suggests that this can only be derived, by photoelastic studies, using full 3D models.

Fessler has conducted a great deal of photoelastic work on 3D threaded joints. Whilst some address specific problems associated with the use of bolts [18, 19], much work has been conducted recently on threaded connections for offshore applications. Modern fringe measurement techniques [25] have been used by Broadbent and Fessler [15, 24] to measure stress distribution in 3D models of threaded connections, as proposed for tethering applications. These studies were combined with 2D studies of the local stress at the root of different thread forms, as described by Heywood [17] in order to select a suitable thread prior to investigating the overall stress distribution in the joint.

Marino [16] has also investigated threaded couplings for pressure vessels using photoelasticity methods. The work was conducted to optimise thread root contours but went beyond that, in that the stress distribution in the whole joint was studied using 3D models. This work is interesting in that 2D models were compared. Whilst this had not gained favour by other workers as discussed above, Marino considered that the use of buttress type threads would not lead to the tendency of large radial forces as a 'V' thread form would. It may therefore be possible to use the 2D model since the hoop stress would be small and therefore could possibly be ignored. The result for the 2D model certainly showed similar trends to the 3D results with the peak stresses at each end agreeing within approximately 20% of the 3D analysis.

Allison [26] has compared the results from a 3D analysis of a threaded turnbuckle type coupling and showed reasonable agreement with predictions using a modified Sopwith analysis. He concludes however, that there is no advantage in introducing tapered section to the coupling either in terms of load sharing or maximum fillet stresses at the thread root.

It is interesting to note that the majority of F.E. work is quite old with the notable exception of that of Fessler and Broadbent [15, 18, 19, 24] who have conducted full studies of an offshore threaded connector, proposed by them as suitable for tethering applications. The use of photoelastic techniques demands sophisticated models and extremely specialised analysis equipment and techniques which are rarely available to the designer.

The development of advanced computing capabilities have led to the development of sophisticated mathematical modelling tools, notably the Finite element technique. The F.E. technique has been used by a number of workers and this previous work is discussed in Section 2.5.3.

2.5.2.2 Strain Measurement Methods

Conventional experimental stress analysis methods usually employ strain measuring devices to physically measure the strains occurring as a component is loaded. Stresses are then usually deduced from the strain measurement using elastic theory [46].

In the case of threaded joints, the nature of the joint dictates that it is not possible to directly measure strains at the critical regions i.e. on the teeth and at the thread roots. Thus it is not possible to predict stresses directly. However, strain measurements have been used by other workers to enable global behaviour predictions to be made.

Goodier [12] measured the strains on a loaded nut in a bolted joint using extensometers. He deduced that the load distribution is governed by axial strains in the nut and bolt and that tooth bending tended to relieve the load concentrations due to axial strains. Goodier attempted to derive values for tooth loads from the measured deformations.

Wooley [21] used more modern strain gauging techniques to confirm the results of mathematical modelling of a casing type of threaded joint loaded to static failure and found there to be good agreement. However, this work did not attempt to predict loading from measured strains.

2.5.3 Finite Element Method

The abundance of computers and commercial software packages has inevitably led to the widespread use of numerical modelling techniques. The Finite Element Method is well established as a technique for the solution of many engineering problems. Techniques for stress analysis in particular are well developed.

The advantage of the FE approach is that stress, displacement and loads are usually produced from a single analysis. This "one shot" approach is obviously attractive. The degree of sophistication of the FE analysis ultimately depends on the mesh used to model the thread. In almost every case, previous workers have adopted an axisymmetric 2D analysis since a full 3D analysis of a complete joint, modelling the thread helix, would demand massive computing power.

The fineness of the FE mesh dictates the resolution, in terms of stress, that can be achieved. Crose et al [20] used a non-linear FE method to determine the failure mechanism of a casing connection. The teeth were modelled quite crudely, the root radius being ignored but this was considered adequate to determine global displacements. The failure mechanism was by thread jumping and hence a high resolution of stress was not important, the main feature requiring modelling being the plastic deformation due to high static loads. Similarly Wooley [21] used such an approach to determine the strain limit state of casing. Again the accuracy on stress was not required as the analysis did not rely on accurate tooth stress predictions, but simply the comparison of strain on the outside of the casing with experimentally measured strain using strain gauged models. The analysis by Wooley above details the use of interface elements between the mating components, these allow the modelling of separation and tooth friction. A similar approach is described in this work in Chapter 3.

The work by Crose [20] and Wooley [21] do not actually represent the tether problem since the subject of this study is fatigue failure and hence static load failure by thread jumping is not considered. Instead, an analysis to produce load and stress distributions is required.

Pick [28] described such a study conducted for the analysis of threaded end closures for pressure vessels. This was a detailed axisymmetric elastic plastic analysis and it is reported that the results for load distribution were in agreement with an analysis conducted by Warnke [29] using the photoelastic method plus an extension of Sopwith's analysis. Pick's work demonstrated that a "one shot" analysis of threaded connections was possible using the FE technique and that the results of both stress and load distribution were in agreement with previous work.

Subsequent studies by Gray [30] have identified the shortcomings of a "one shot" analysis particularly in the time required to prepare data. For this reason, due consideration of the agreement with results using the Sopwith analysis [2], as reported by Pick [28], has been made and Gray uses a combined analysis using that of Sopwith to predict the tooth load distribution and an FE analysis to determine the tooth stresses.

2.6 DISCUSSION OF EARLIER WORK

It has already been seen that many workers have addressed the problem of the nut and bolt connection. It has already been stated that the threaded connection represents a different problem to the nut and bolt analysis, although some of the analysis methods are common.

In particular it is agreed by all previous workers on threads that the load distribution in threaded connections is non-uniform and that concentrations of load occur generally at the first loaded tooth for a nut and bolt, Figure 3a and at the first and last loaded teeth in a threaded coupling Figure 3b.

It is important to make the distinction between load distribution and stress distribution.

The stress at the root of a thread depends not only on the tooth loading, creating bending and shear stress at the thread root but also the notch effect of the thread on the load carrying body of the component. For this reason, it is likely that early attempts to use the load distribution of Sopwith [2] to predict stresses were in error.

It is considered that notwithstanding the complexity of the analysis, the Sopwith approach for load distribution is sound in principle in that it investigates tooth deflections by modelling

as cantilevers and considers axial and radial separation. Indeed the use of Sopwith's analysis for threaded couplings is documented by Allison [26] and Gray [30] and is considered to be acceptable but difficult to apply due to the complexity of the analysis.

The photoelastic methods have attracted a lot of attention and have advanced considerably since the early work by Hetenyi [13]. The photoelastic analysis only provides stresses although Gray [32] is reported to have integrated the contact stresses on the thread teeth, from a photoelastic analysis, to derive tooth load distributions. Whilst many workers have investigated the bolted connection, Broadbent [15] and Allison [26] have conducted studies on the type of threaded connector suitable for offshore use. It is interesting to note that the 2D analysis was considered unsuitable for tooth load distribution but that the effect of local stress due to tooth loading was successfully derived by Gray [30] and Heywood [17] using 2D models.

Marino [16] is the only worker that appeared to obtain reasonable results for load distribution using 2D modelling. The reason for this is the fact that the majority of other workers investigated 'V' threads whereas Marino investigated the buttress thread. The difference being the 'V' threads tend to radially separate when loaded, whereas the buttress thread loading flank is perpendicular to the loading axis, resulting in minimal radial separation and hence is more suited to 2D modelling.

One major drawback of the photoelastic technique is the sophistication of the models required. A full 3D stress freezing photoelastic study is extremely time consuming and labour intensive. The nature of the modelling also demands extremely accurate model making since pitching errors are of fundamental importance to the tooth load distribution [2,33].

The FE technique allows stresses and loads to be derived in one analysis. However, the demands of accurate modelling dictates that full 3D modelling is not practical. Indeed an axisymmetric 2D model can be extremely time consuming to prepare. The major problem is in the development of a suitable mesh and ensuring that the correct mode of loading across the teeth is developed (See Chapter 3).

Strain measurement techniques are impractical for the determination of tooth loads and stresses since it is not possible to measure strains at the point of interest, i.e. at the threads.

The discussion of techniques has been based on their suitability for stress analysis. For threaded connectors subjected to cyclic loading, where fatigue in the primary design consideration, the important parameter is the fluctuating or dynamic stress. This is an extremely important point since a preloaded connection has the "mean" preload plus an applied dynamic load and the dynamic component needs to be extracted from the combined effect. Since Photoelastic methods can only look at a single loading, only the combined effect can be studied. If the effect of applied load needs to be determined, the only method for achieving this is to test a second model with preload only and subtract the results. This is not a recommended route since it assumes that the preload applied to both models, and its effects are identical. Considering the sensitivity of the photoelastic techniques to manufacturing tolerances for the model and the difficulty in applying known preload to any threaded connection, it is unlikely that the preload condition could be repeated on two models, hence introducing errors in any predicted dynamic stress in the preloaded sections.

Thus there are basically three techniques all with their own relative merit. For a full 3D analysis, photoelastic methods are available. However the requirement for extremely accurate modelling makes such a technique expensive and time consuming and allows only one geometry and loading to be investigated and gives only stresses. The full FE technique is only really practical in 2D axisymmetric cases and is again time consuming but gives stresses plus tooth loading for a range of applied loadings. Again only one geometry can be investigated, small changes often requiring complete remodelling.

For the designer, the need to look at various parameters such as pitch, tooth height, tooth shape and overall geometry dictate a requirement for an analysis package that enables parametric studies to be conducted. It is for this reason that "hybrid" techniques have been developed, making use of the best features and versatility of the various techniques.

Warnke [29] describes the way in which Sopwith's [2] work can be used together with photoelastic techniques to consider various design options. Gray [30] describes how the tooth loading, derived from Sopwith's work [2] can be integrated with Finite element models to predict tooth stresses.

It is considered that the mathematical approach combined with Finite element modelling is a suitable compromise to allow parametric studies to be conducted. A novel technique is described in Chapter 4 where a mathematical model, based on the accepted feature of tooth

load being directly related to the relative displacement of the male and female components, is used to predict load distribution and a simplified Finite element technique is used to convert the tooth loads into tooth stresses.

The model has significant advantages over the existing methods of analysis. It is simpler to use than the Sopwith approach and most importantly, accounts for the effect of preload and taper, a major weakness of the Sopwith model which precludes its use from the anlaysis of the offshore type of threaded couplings. Indeed the inclusion of preload in all other techniques poses a major problem and this is a real weakness when analysing threaded connections which depend on preload. The stress analysis part of the model takes due account of not only tooth flank loading but also the notch effect due to load in the core of the connector. It is seen that the new proposed model allows parametric studies to be conducted easily and cheaply and it is proposed here as an analysis tool at the design stage to determine the effect of various geometric parameters on the joint behaviour.

It is of course recommended that any final design be fully investigated using a different analysis technique and for this, the 3D photoelastic technique or full FE modelling are available.

2.7 SUMMARY

The complexity of the mathematical modelling used by Sopwith [2] to determine the load distribution is threads has generally precluded the widespread use of that technique. However some of the benefits of such a technique are still attractive in that the mathematics and hence the solution can be verified - not an easy task with FE techniques. The modelling of the tooth as a cantilever seems reasonable and it was considered that such an approach could prove usable if the analysis could account for preload and taper and was also easier to use. The FE approach dictates that only 2D analyses are feasible due to modelling constraints. If that assumption is adequate for a FE analyses, it could also be adequate for a mathematical approach, reducing the variables considerably. Another simplification arises from the use of buttress type threads which act approximately normal to the thread axis. This minimises radial separation and simplifies the analysis considerably. These considerations were taken into account when developing the new mathematical model described in Chapter 4.

2.8 ANALYSIS FOR A TLP

The previous sections have highlighted some of the key points to be considered when analysing a threaded connection for offshore application. These are now summarised:

1. *Service Loading*

The global loading on the tethering system due to environmental forces.

2. *Local Loading*

A local stress analysis of the threaded connection is required. This must take into account the non-uniform load distribution along the coupling and must take into account preload effects if necessary. This will then provide a local stress history at critical points in the connection derived from the global loading.

3. *Fatigue Behaviour*

A study of the effects of a fatigue crack growing in the connection. This could be a theoretical or empirical study employing fracture mechanics techniques to predict the behaviour of the coupling once cracked.

4. *Design against the environment*

Analysis of corrosion protective system employed and also any sealing mechanism. Corrosion fatigue studies of relevant area.

5. *Practical Implications*

Convenience of installation, inspectability and maintenance required.

Of the five points, Items 2 and 3, the stress analysis and fatigue analysis are considered in detail in the following Chapters.

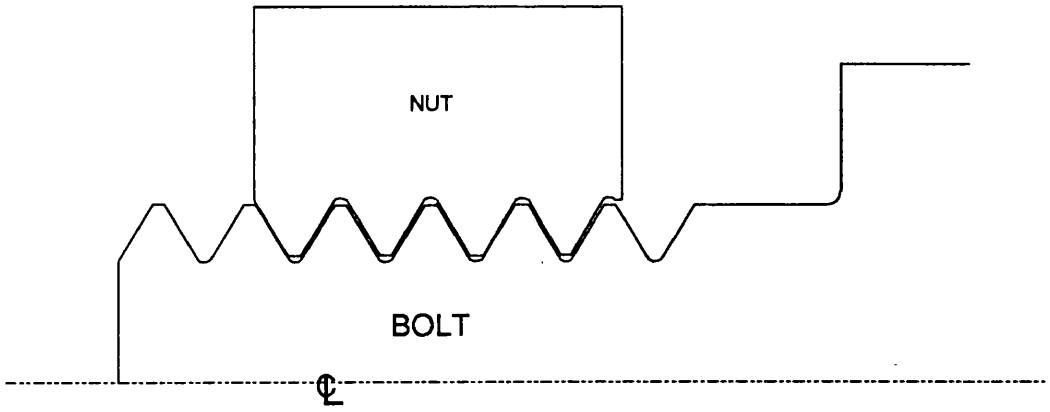

Fig. 2.1 Nut & Bolt Assembly

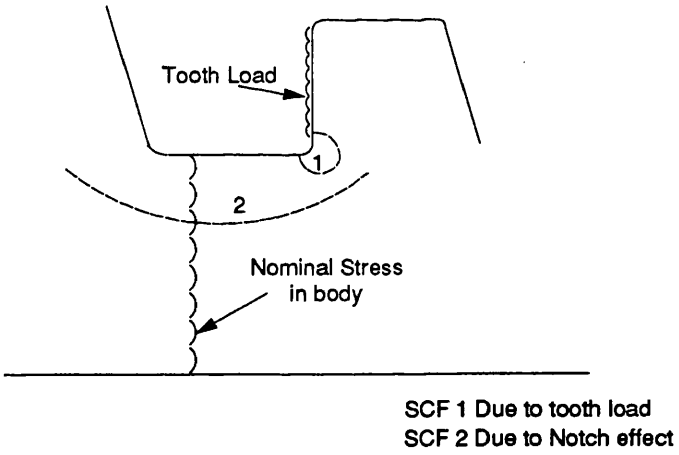

Fig. 2.2 SCFs Associated with threads

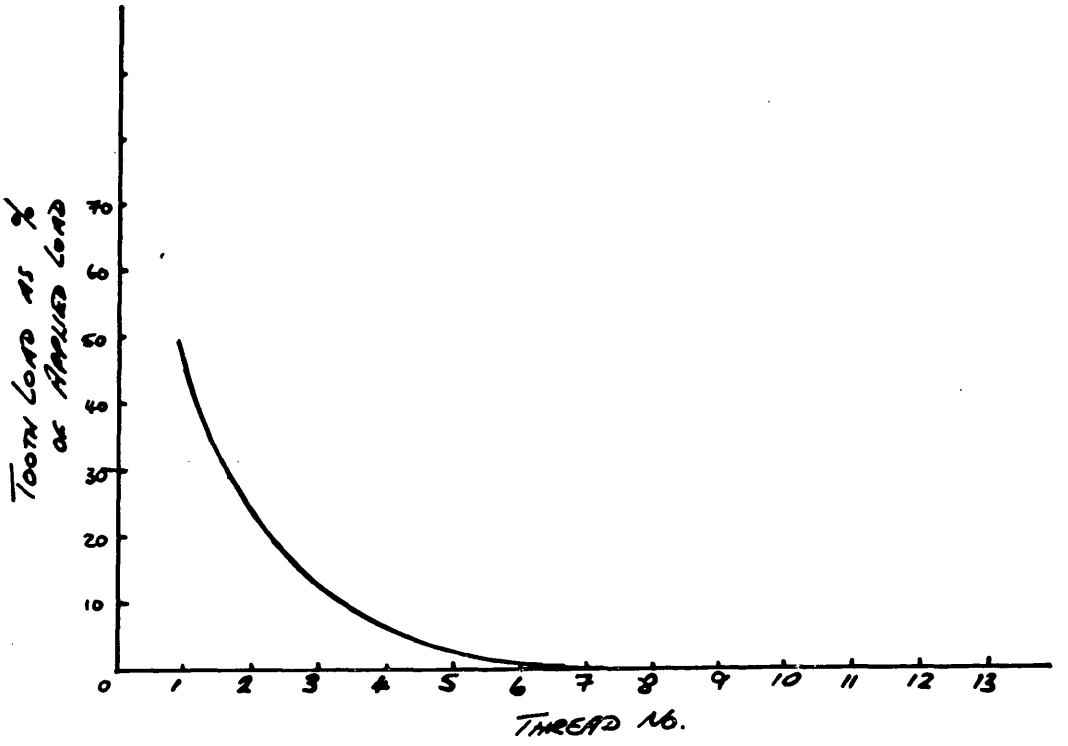

Fig2.3a Load distribution in nut and bolt assembly.

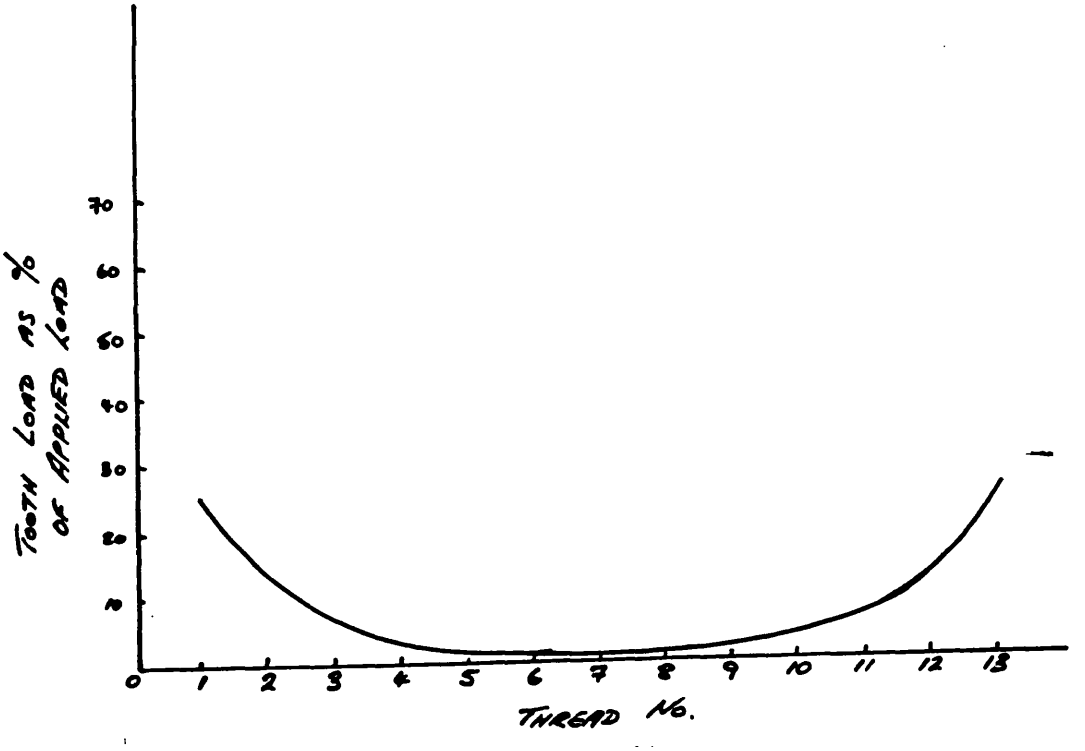

Fig 2.3b Variation in tooth load along a threaded connection.

Fig. 2.3 Tooth load distributions for bolted joints and threaded connections. [34]

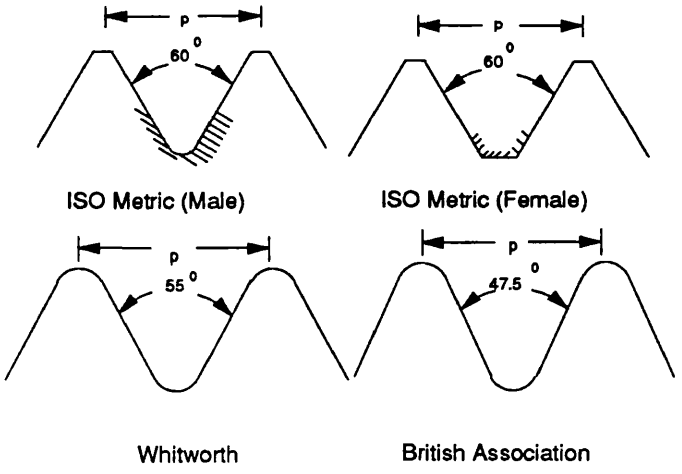

Fig. 2.4 Common V Thread Forms

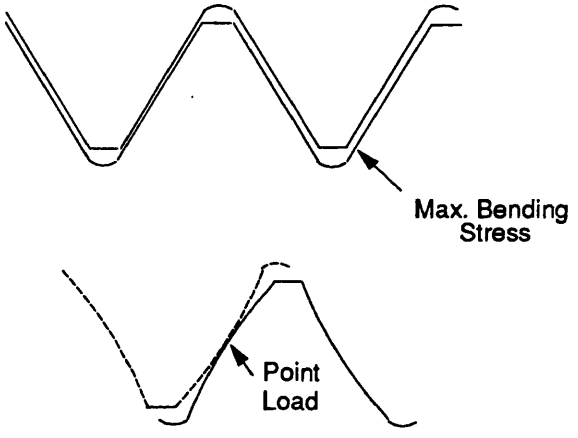

Fig 2.5 Location of Max Stress and resulting Deflected Shape

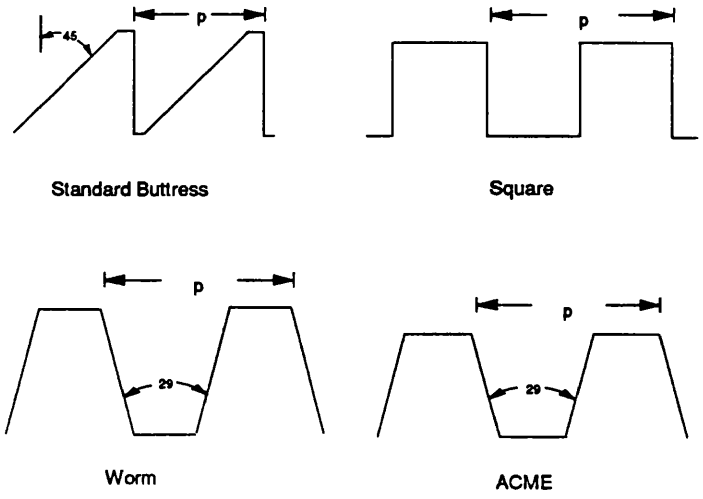

Fig. 2.6 Common Non-V Thread Forms

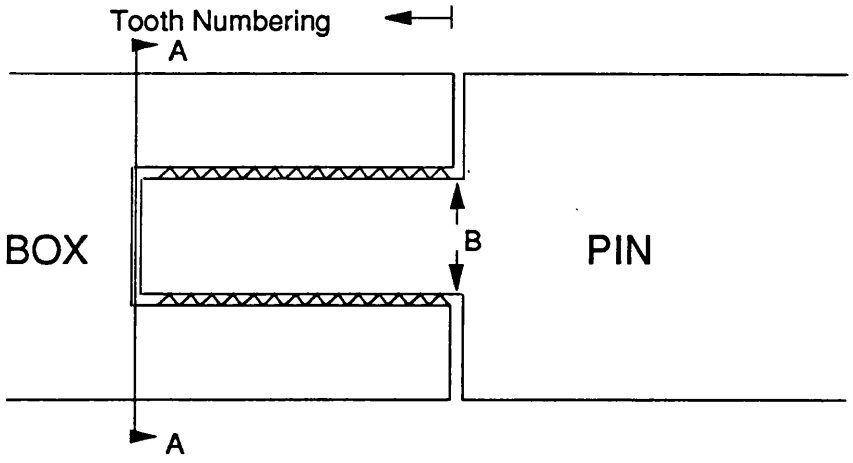

Fig. 2.7 Idealised Threaded Connection

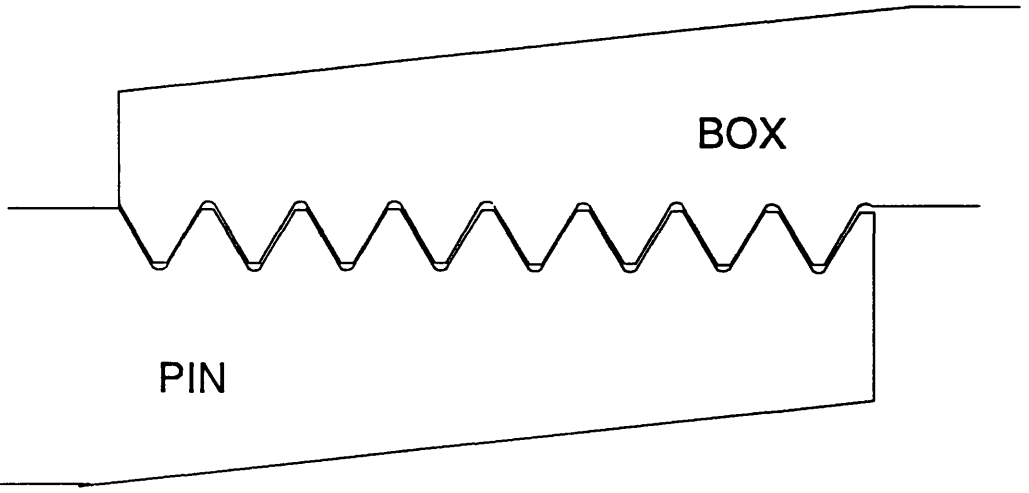

Fig. 2.8 Example of Tapered Threaded Connection (Parallel Thread)

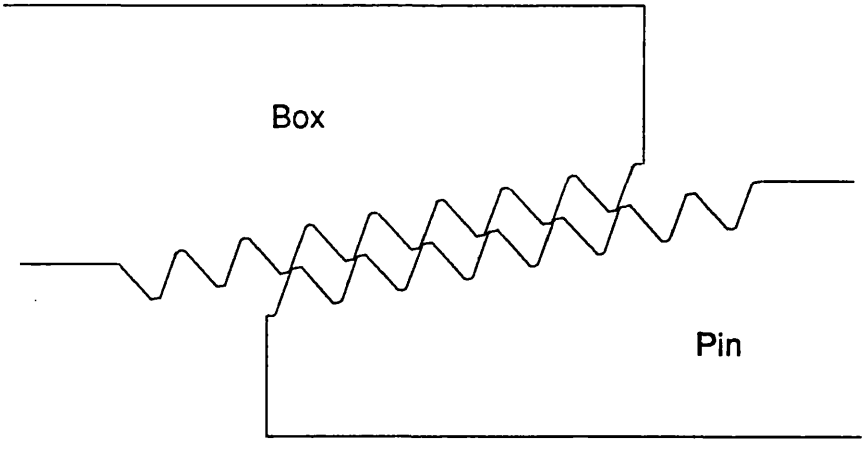

Fig 2.9 Stabbing of Tapered Threads for easy makeup

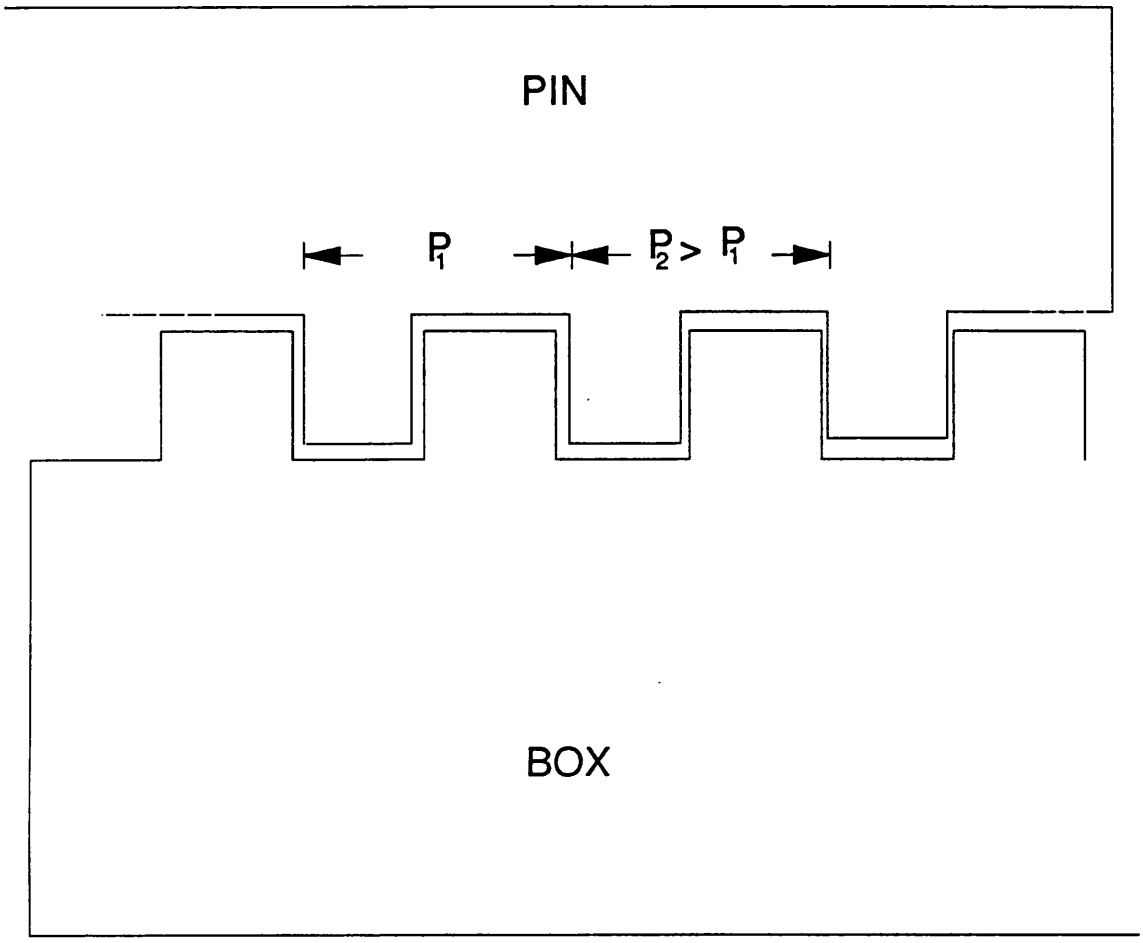

Fig. 2.10 Principle of differential pitching

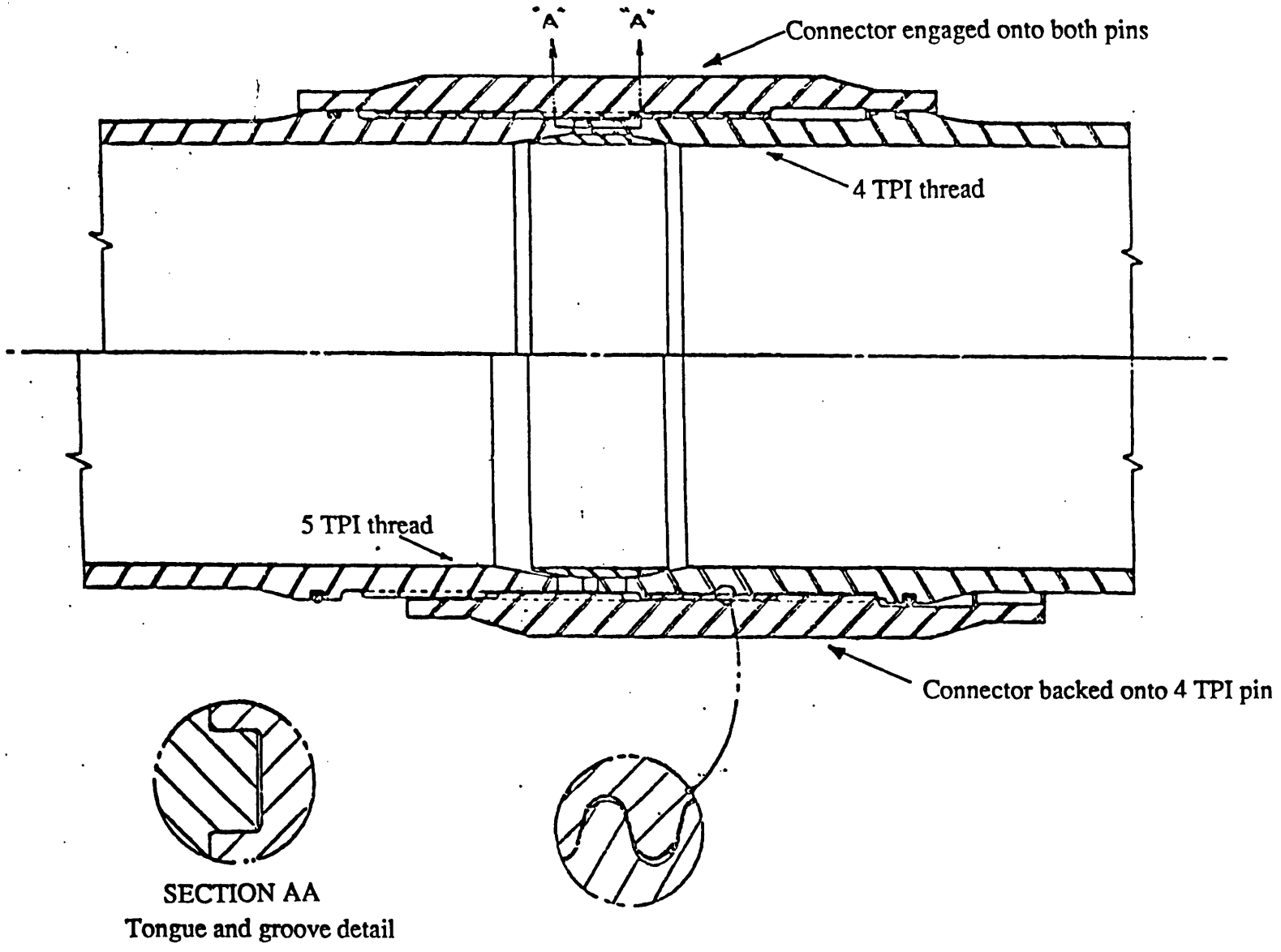

Fig. 2.11 Differential pitch connection.

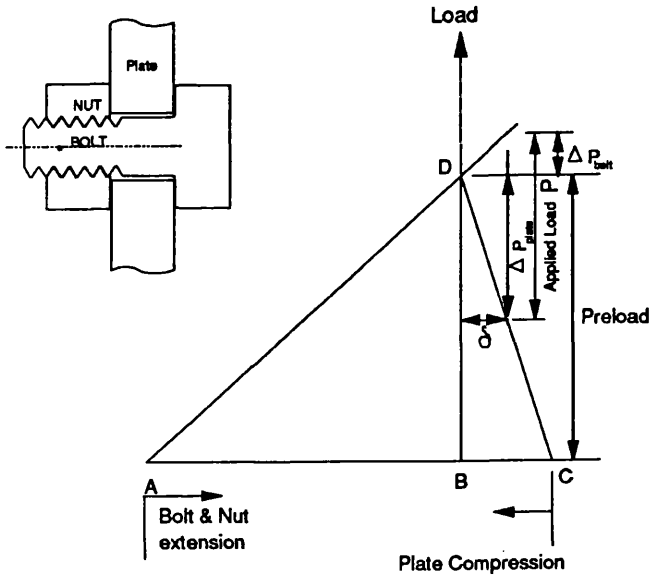

Fig. 2.12 Preload Mechanism in a Bolted Connection

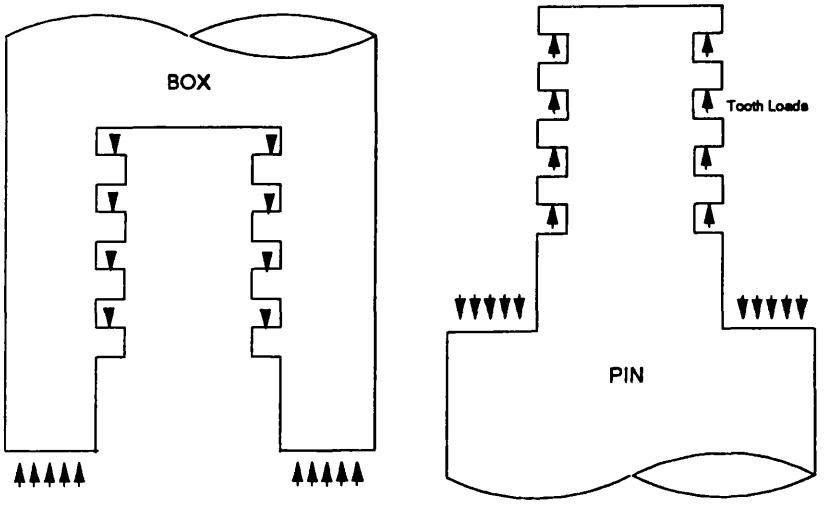

Fig. 2.13 Preload Mechanism for a threaded connection

CHAPTER 3

FINITE ELEMENT ANALYSIS

of

THREADED CONNECTORS

3.1 INTRODUCTION

Stress analysis using the Finite Element (FE) method is common in many fields of engineering and many commercial software packages are now available. The F.E. method was used to analyse a number of threaded connections in order to provide information on both stresses and tooth load distribution. The geometric complexity of a threaded connection means that a number of compromises must be made when using the F.E. method. The F.E. method necessitates the handling of large arrays and the size of the task is usually limited to the size of the computer being used. The F.E. package used in this study was PAFEC, a general purpose commercial package developed originally at Nottingham University. The programmes were run on the SERC Prime computer at UCL.

The use of finite element analysis to solve structural problems is becoming increasingly popular. The following discussion shows that finite elements by no means solve all our problems and their use, particularly in the analysis of threaded connections, is subject to many assumptions and constraints. This does not mean that they do not have an important part to play but, when using finite elements, it is important to understand the limitations and the assumptions relative to the particular task.

3.2 THE FINITE ELEMENT AXISYMMETRIC ELASTIC ANALYSIS

A threaded connection exhibits no symmetry and thus a full 3D F.E. model is necessary to fully describe the geometry. However, the complexity of this type of analysis, plus physical computing limitations make the task virtually impossible for a full connection. However, it is doubtful whether this approach is really necessary. Fessler [18, 19] however does show significant variations in stress around the thread circumference which suggests this may be important and this will be discussed later. The alternative to a 3D model is an axisymmetric model in which the thread is modelled as axisymmetric about the axis of the connection. The choice of axisymmetry means that the connection can be modelled as a plane two dimensional section which is then rotated about the axis to form a solid. This results in the threads being modelled as parallel annular projections instead of a helix. For the thread modelling in this study, plain isoparametric eight noded rectangular and six noded triangular elements were used with two degrees of freedoms at each node. These are curvilinear elements and are shown in Figure 3.1. The elements can only carry loads in their plane which is acceptable for an axisymmetric analysis. Hoop stresses are of course considered.

3.2.1 Elastic Analysis Of Axial Loading

All F.E. models in this study assume fully elastic behaviour. This will be discussed in Section 3.3. The target thread form on which modelling is based is shown in Fig. 3.3. The following discussion is based on the thread form and connection geometry shown in Figure 3.3 with various internal and external diameter configurations.

3.2.2 Load Transfer Across Teeth

When modelling meshing teeth, it should be remembered that the teeth are individual components and that the only possible modes of load transfer between the teeth of the male and female components is via frictional forces on the faces or compressive forces across the face. It should also be noted that radial separation of the male and female teeth must be permitted. It is necessary to give special attention to the modelling of the teeth. PAFEC has a facility called GAPS which was used for this purpose. The GAPS facility enables the bearing surfaces of the teeth to separate should the conditions dictate this.

Initially the teeth are modelled as fully meshed as shown in Figure 3.2. When the load is applied to the model, load is transferred between the male and female components via compressive tooth loading. This loading results in deformation of the teeth due to bending and shear. Should the tooth deflection become such that the teeth try to separate, under normal modelling the teeth would experience a tensile load across the interface. The GAPS model senses this and allows the teeth to separate at that particular node and then reiterates the tooth load over the remaining joined nodes. If the tooth deflections of the mating teeth cause the teeth to interfere, this introduces a force across the tooth faces. This modelling accounts for loading normal to the teeth. Friction loads can be introduced on the tooth interface. This was not done in this study (i.e. coefficient of friction was taken as zero) for two reasons. Firstly, the friction state in the mated joint is extremely difficult to assess and therefore it is difficult to input a coefficient of friction that would properly represent the real situation. Secondly, the model without friction shows very little radial movement of one tooth relative to the other and therefore it is considered that frictional loads are small, due to a combination of the high restraint of the joint due to hoop stress and the loading on the buttress thread being perpendicular to the loading axis. Reactions are given at each GAP node and these can be summed to provide loads on individual teeth and hence the tooth load distribution.

3.2.3 Loading

One important result from the FE model is the tooth load distribution. In order to obtain the complete load distribution, it is obviously necessary to model the complete joint and to apply the loads remote from the joint. The loading and restraints applied to a typical FE model are shown in Figure 3.4.

3.3 DISCUSSION OF ASSUMPTIONS

One criticism of axisymmetric modelling is that it gives results for both tooth loading and stress which are in fact averaged over one circumference. Broadbent [15] has carried out 3D photoelastic investigations into this type of connector and found that there are considerable variations in tooth loading, especially around the first loaded thread. These variations are partly due to thread lead in and run out. Thread lead in is usually introduced during manufacture and results in a varying tooth width as the first tooth increases from nothing to fully developed tooth profile at the start of the second thread. These variations lead to local "hot spots" which are not obtained using the 2D axisymmetric FE method. This suggests that the axisymmetric analysis gives results that are non-conservative due to the averaging implicit in the axisymmetric assumption. However, in practice it is not usual to include the thread runout in the loaded portion of the thread and hence the results of Broadbent [15] can be considered conservative.

Another feature is that frictional effects due to the helix angle are neglected in the FE analysis. For a typical offshore threaded connection the helix angle is in the order of 1^0 and this effect is therefore minimal.

As stated earlier, the analysis is carried out assuming fully elastic behaviour. It is considered that for most applications this is adequate. In general, for buttress threads the highly stressed regions are extremely localised at the thread root. The effect on the stiffness of the tooth of a small plastic zone, in this region, would be extremely small. Since the load distribution is determined by the stiffness of each section, the tooth load distribution is therefore unlikely to be affected to any great degree by this small zone. However, one should note that, should the geometry be such that gross plasticity results, then it is likely that the load distribution could be affected by this assumption. Such a design, however, should not be seriously considered, since the presence of gross plasticity would not be tolerated from static strength consideration, nor for situations where make and break are required.

Local plasticity would have a more marked effect on the local stress analysis at the thread root. Since these areas are small, they are important only from a fatigue initiation viewpoint. This can adequately be accounted for by using analysis such as that of Neuber [35] and are discussed in Chapter 6.

3.3.1 Initial Joint Make-Up

The Finite Element analysis conducted here have all assumed that the teeth on the male and female components are initially in contact but unloaded. This assumes a perfect matching of pitch between the male and female components. The validity of this assumption depends on the quality of manufacture. Any mismatch between the pitching will lead to concentration of loading on those teeth initially in contact. If this should occur at a critical region, the FE stress analysis would be non conservative. These points have been recognised by other workers and have been discussed in Chapter 2.

3.4 FINITE ELEMENT MODELLING

Obviously with a limit on the number of elements that can be handled, even in the 2D analysis, a compromise must be reached between modelling the whole structure with a fairly coarse mesh, or modelling only a small part of the structure with a much more refined mesh, or a combination of the two.

3.4.1 Full Analysis

The whole structure can be modelled in as much detail as possible, the constraints on detail are likely to be dictated by the computing facilities. Ultimately the restriction is on the number of degrees of freedom, i.e. number of elements. By carrying out this type of "one shot" analysis, one obtains the best estimate of both load distribution and stress analysis from one run, albeit a very large run. Obviously the convergence of the analysis can be checked to ensure that the mesh is sufficiently refined to prevent large rounding errors on the stress. The advantage of this analysis is that the best estimate of load distribution is obtained.

3.4.2 Two Part Analysis

A common practice in engineering is to model a whole structure using a coarse mesh to obtain displacements, the primary unknown in an FE analysis. The displacements thus obtained are then used as "loads" on a refined model of the particular areas of interest. In

this way the stresses, which are a secondary unknown in the analysis and derived from displacements, are obtained. Since stresses are obtained by differentiating the displacements, it follows that a finer mesh results in a more exact solution of stress. This approach is widely accepted in structural analyses. However, the thread analysis is rather unique in that it is highly sensitive to relative stiffness. In order to obtain a tooth load distribution, the whole joint must be properly modelled. If a very coarse mesh is used, i.e. if the thread stiffness is not modelled accurately, the resulting load distribution will be in error. It should be noted that, due to the non-uniformity of the load distribution, changes in stiffness not only affect the magnitude of load on each tooth but affect the total load distribution in the joint. It is therefore necessary to carry out as detailed an analysis as possible for the whole joint. If this is ignored, the displacements from a coarse mesh when fed into a refined mesh will lead to misleading results, however, the stresses will converge and thus there is no indication of any problems.

3.4.3 Modelling of Preload

As previously discussed, preload is extremely important to the performance of a threaded connector and must be included in a full FE model. The modelling of preload cannot be done by simply applying an additional force to the area of interest. In an FE analysis, applied forces remain constant throughout the analysis, that is to say that, even if the face to which the force is being applied is deformed, the force remains acting on that face. This is not the case for preload. A preload force reduces as the joint is loaded, that is to say, the initial compression across the preloaded section decreases with applied tensile load.

In order to determine the stresses resulting from external loads only, for a joint with preload, two FE runs are necessary, one with lack of fit and a second with both lack of fit and external load. The difference between the two gives the desired stresses.

One way to model preload is by a "lack of fit" modelling method. In this study the technique was applied by heating a "ring" at the preloaded section in the model such that it expands, thus reacting against the remaining section which is unheated. This is shown schematically in Figure 3.5. The required preload is obtained by adjusting the temperature and thus the expansion or "lack of fit". Other FE packages allow displacements to be applied to the interface thus inducing a lack of fit.

In practice this method is quite difficult to apply to the FE model.

1) Care must be taken that the heat is contained in the section you require and that the model does not apply temperature gradients to the remaining section to dissipate the heat. This can be achieved by applying thermal isolation at the heated element boundaries.

2) The expansion of the sections heated are greater in the radial direction than in the axial direction. Care must be taken in the modelling to ensure that the radial expansion does not result in radial forces being applied to the section. This can be achieved by releasing radial degrees of freedom at the interface of the heated zone.

3) If displacements are applied, the notional differences in stiffness across the interface boundary must be considered to ensure the correct "release" of preload across the boundary. The exact method by which this can be achieved depends on the modelling facilities available in each proprietory FE package.

These difficulties can be overcome by careful modelling but care must be taken when using these "secondary" techniques to ensure that the loads being applied are those required.

In some cases it is not necessary to consider the full effects of preload. If the behaviour of the joint is required at various external loading levels, these can be investigated separately and the results added to the effect of the static preload. In this alternative approach it is necessary to model the preload section as an integral part of the joint. The preloaded face can in effect be considered as welded. In this way the correct stiffness will be modelled. The simple coupling shown in Fig. 3.5 was investigated using a preload plus external load and external load only using a welded interface merely to confirm that the alternative approach was satisfactory. A study of a full threaded connection has also been carried out [40] using FE methods to validate the approach adopted here and it has been confirmed that the superposition method gave near identical results to those from a single combined analysis.

The use of a fixed (welded) preload shoulder to simulate the additional load path available in a preloaded connection in fact offers significant benefits over a "full" analysis using lack of fit techniques. In cases where the dynamic load is required, the cyclic stress for a fatigue analysis, the results are produced in a single run. In order to consider this significant advantage, one must look at the alternative. If a "lack of fit" analysis is used, the resulting stresses are due to a combination of preload and applied load (just as they are with a photoelastic study). In order to obtain the effect of applied load only, a second run is needed

to obtain the effect due to the lack of fit only. At the critical section for the pin, the magnitude of the preload is possibly two orders of magnitude greater than that of the applied load and hence the result required is obtained by subtracting two large numbers to give a small number. Any naturally occurring errors in the two runs could lead to the possibility of significant errors in the result. Thus any technique that is capable of predicting the dynamic and static stress independently then combining to give a static and dynamic stress is preferable from a theory of errors stand point.

3.5 MODELLING DETAILS

In order to validate and compare the modelling techniques developed in this study it was necessary to conduct at least one full 2D axisymmetric FE analysis of a threaded connection. The connection chosen was that used in the experimental work and represented a thick walled forged connection.

3.5.1 Description of Model

The threaded coupling modelled was geometrically similar to the thick walled specimen used in the experimental work described in Section 5. The model configuration is shown in Fig 3.3. Fig 3.3 shows the geometry for the primary model, Model 1, and it is this model that has yielded the majority of results presented below.

The FE model for the pin is shown in Figure 3.6 and it is seen that the threaded portion of the joint is tapering, as is the internal part of the pin. The connection has 25 teeth and these were fully modelled. Details of the tooth modelling are shown in Figure 3.2. The GAPS facility was introduced at all nodes where the teeth contacted, including mid side nodes. The basic elements used for the modelling are shown in Figure 3.1. The majority of modelling was done using rectangular elements although triangular infill elements were used where necessary.

No automatic mesh generation facility was available for modelling threads and thus all modelling was done manually with the aid of small self written routines, the difficulties being to ensure that the tooth interfaces were correctly matched and that the GAPS elements were fully implemented. The mesh development was an enormous task and extremely time consuming. It is recommended that such an analysis should only be considered if automated, interactive mesh generation facilities exist. To develop such a tool was beyond the scope of this study.

The model used was the maximum that could be handled on the computer with each run taking around 25 hours. The model was developed using 1400 elements resulting in around 5000 node points and 10000 degrees of freedom.

3.6 FINITE ELEMENT RESULTS

The full FE analysis described earlier yielded results both in terms of load distribution along the joint and the complete stress distributions throughout the connection. The results for this analysis are summarised in Table 3.1. Results for a second model, which was identical in all respects except the outside diameter of the model was reduced to 120mm and the pin bore was increased to 70mm, are given in Table 3.2. All other results quoted are for model 1 unless otherwise noted.

3.6.1 Discussion of Table 3.1 and 3.2

Column 1 gives the tooth number, where tooth 1 is at the fixed end of the pin.
Column 2 shows the individual tooth loads for each tooth. These have been derived from the summation of loadings on each individual node making up the loaded face of the tooth. PAFEC provides the load carried by each GAP element and thus loads are obtained directly from the model. Note that the tooth loading is equal for corresponding teeth on pin and box.
Column 3 gives the % of load being taken by each individual tooth and Column 4 gives the cumulative tooth loading. Note that this represents the % of load transferred to the box at that point.
Columns 5 and 7 give the stress concentration factor SCF for the tooth root in the pin and box respectively. The value of SCF has been calculated using the maximum principal stress at the thread and the nominal stress applied to the pin remote from the threads. Fig 3.6 gives the dimensions of the joint used to calculate this. Thus, the values of SCF are all calculated using the same value of nominal stress. This is important since a different approach is used in Chapter 4. The values of SCF are seen to differ at matching teeth of the pin and box and, since the tooth load and tooth form are the same, the difference is due to the different level of stress acting in the member (notch effect of the teeth).
The last column shows the SCF (taken from a separate FE run) due to an axial tensile load on just the pin, that is, with no box present and loads applied at each end of the pin. These results show the effect of a tensile load in the body of the pin with no tooth loading and allow an investigation into the relative effect of the two contributions to total SCF.

3.6.2 Effect of tooth loading and notch stress at thread root.

Figure 2.2 showed how the high stress at the thread root was due to contributions from tooth loading and notch stresses. The results from the FE analysis demonstrate this effect:

Consider tooth 1:

(Nominal stress = 100 MPa)

Box load = 0% Pin load = 100 %

Box SCF = 8.03 Pin SCF = 11.80

σ_{Box} = 803 MPa σ_{pin} = 1180 MPa

Since there is no load in the box, all of the stress at the thread root can be considered to be due to tooth loading.

Using the principle of superposition, the stress due to the notch is estimated as:

σ notch = 1180 - 803 = 377 MPa

From the analysis of the pin only, i.e. no box modelled and hence no tooth loading, a stress of 357 MPa was found. Thus it is seen that the principle of superposition for the stress is justified and that at the first loaded tooth, approximately 30% of the stress is due to the axial load in the pin (notch effect).

A similar calculation for tooth 25 confirms this approach.

3.6.3 Stress distribution

The most highly stressed tooth is tooth No.1 on the pin. Figure 3.7c shows how the max. principal stress varied through the section of the pin on the plane of the most highly stressed part of the thread root. This is drawn as a section normal to the axis of the connection passing through the most highly stressed node. Figs.3.7a and 3.7b show the position of the nodes near the area of interest and Table 3.3 gives the stress values at each node.

It is immediately seen that the high SCF is extremely local to the surface and rapidly diminishes with depth into the section.

Further results for tooth 1 are shown in Figure 3.8 as a developed section. Again it is seen that the stress reduces dramatically with depth into the section. Figure 3.8 also shows the transition into compression at the loaded tooth flank. Figure 3.9 shows a similar trend for teeth 1, 2 and 3.

3.6.4 Tooth deflections

The FE results allow the tooth loading and tooth deflection to be investigated. Figure 3.10 shows the distribution of load at various nodes on the loaded flank of the teeth whilst Figure 3.11 shows the tooth deflections.

It is seen from Figure 3.10 that the tooth load is not uniform over the tooth flank although the displacements are approximately linear as show in Figure 3.11. This indicates a number of important features. The displaced shape of the loaded flank of the tooth indicates that bending is not an important consideration. Instead, the tooth appears to undergo shear deformation. This is predicted from the modelling using Stress Functions described in Appendix B, Figure 3.12 shows the predicted deflections using this approach. The distribution of tooth loading shown in Figure 3.10 is unusual in that it is seen to concentrate at the top and bottom of the tooth. This situation has been observed by other workers [20] but no explanation was given. It is considered that the feature may be due to the tooth deformation attempting to assume a slight concave shape, as shown in Figure 3.12, due to classic shear loading, and that the contacting teeth maintain contact by forcing the tooth into a uniform shape as evidenced by Figure 3.11.

Figures 3.13 and 3.14 show the overall displacement of teeth 1 and 5 plus the immediate section of the pin onto which the tooth is attached. It is seen that there is a significant shear deflection at the root of the thread. The loads acting on the teeth have been applied to the beam model described in Appendix B and the results from this comparison are also shown. Whilst these are discussed in detail in the next Chapter, it is seen that the deflections from the FE analysis are quite consistent with those obtained from a theoretical analysis taking into consideration shear deformation.

3.6.5 Effect of joint geometry on load and stress distribution

One of the major drawbacks of the FE technique is that even small modifications to the geometry, especially the thread form, can necessitate complete re-modelling. The easiest parameters to adjust are the outside diameter of the box and the internal diameter of the pin. This has the effect of reducing the axial stiffness of the box and thus modifying the load distribution. The results for the primary model (Model 1) are given in Table 3.1 and are presented graphically in Figure 3.15. The results for the smaller model, Model 2, are given

in Table 3.2 and are plotted in Figure 3.16. By comparing the load distribution for the two models and it is seen that changing the pin and box stiffness has modified the load concentrations at the two ends of the connection. In the FE analysis, the nominal stress has remained constant although the area of the model has changed, hence the total load applied has reduced in Model 2 to 68% of that used in the original model (Model 1).

Looking at tooth No.1 for Model 1 (Table 3.1), it is seen that at the box, the SCF is 8.03 whereas from Model 2, the corresponding SCF is only 6.33 (Table 3.2) even though the load concentration (% of total load carried by that tooth) has increased. This apparent contradiction highlights the problem with relating SCF's to a nominal stress at a particular section. This is perfectly acceptable for comparison of results from one particular analysis, however, when comparing results from different analyses, one must be extremely cautious to ensure that comparisons are like with like.

Comparing tooth loads shows that for each model, the SCF is directly proportional to the absolute tooth load for Tooth 1 of the box. This is of course as expected since the box carries no load at that point and therefore the SCF is due totally to tooth bending.

This does demonstrate the difficulties in comparing tooth load/stress behaviour and that caution is needed to ensure that the SCF quoted in results is a direct measure of the important parameters. This question is discussed further in the next Chapter and a revised definition of SCF is described.

3.7 DISCUSSION OF FE RESULTS

The FE modelling has indicated some important aspects of threaded connection behaviour. The one shot analysis was extremely complex to model and literally took hundreds of man hours for mesh development. This immediately highlights one major difficulty with such complex analysis, that of modifications to the geometry of the connector. Any changes in thread form would necessitate complete remodelling each time. The size of the computer runs and sheer volume of paper produced again made checking and validation of the results an extremely tedious task. (Each computer run on a new model produced 820 pages of output!)

However, despite these difficulties, the analyses give valuable insight into the load distribution in these components and provide information on the mode of load transfer across the teeth. This information has proved invaluable in the validation of new models for predicting load and stress distribution described later.

The assumptions for 2D elastic analysis have already been discussed but must be taken into account when analysing the results.

In summary, the analysis of screwed connections using the FE technique has been demonstrated to be possible and has yielded valuable information. The complexity of the modelling would preclude this technique from being used for parametric studies at the design stage but the technique would be extremely useful for the full analysis of a final connection design.

The FE modelling carried out here concentrated on axial loading on unpreloaded connections. The techniques for modelling the behaviour of preloaded connections were established and tested on smaller FE models. The FE analysis provided a benchmark for evaluating the suitability of the mathematical models developed and it is these simplified models that have been used to provide comparisons of preloaded and unpreloaded behaviour.

The 2D axisymmetric model cannot be used for loadings other than axial but, modelling techniques are available which allow approximations to pure bending loads to be applied. However these techniques will not accomodate the use of GAP elements at the tooth interfaces.

Table 3.3 and Figs. 3.7a and 3.7b show how the stresses vary at each node in the critical region of tooth 1. The mesh density in this case was limited by the computer system. The convergence was tested by comparing the stresses at the most highly stressed node, as determined from adjoining elements. The results showed that the difference in stresses (compared on the basis of a percentage of the maximum stress in the component) to be 7.9%. According to PAFEC, values less than 10% are considered acceptable.

3.8 TABLES

Outside dia= 140mm Run Ref SCR 1 Total Applied Load 589.8kN

				PIN		BOX		SCF
Tooth No	Tooth Load x10^4N	% Total Load	ΣP %	Node Ref	SCF	Node Ref	SCF	Axial Load Pin Only
1	7.94	13.5	13.5	19	11.80	2140	8.03	3.57
2	5.19	8.8	22.3	62	7.57	2097	6.12	3.26
3	3.90	6.6	28.9	105	5.89	2054	5.11	3.14
4	3.18	5.4	34.3	148	4.99	2011	4.49	3.10
5	2.71	4.6	38.9	191	4.42	1968	4.07	3.06
6	2.41	4.1	43.0	234	4.05	1925	3.78	3.04
7	2.18	3.7	46.7	277	3.76	1882	3.52	3.03
8	2.02	3.4	50.1	320	3.55	1839	3.34	3.03
9	1.86	3.2	53.3	363	3.35	1796	3.15	3.05
10	1.76	3.0	56.3	406	3.22	1753	3.02	3.09
11	1.65	2.8	59.1	449	3.07	1710	2.89	3.15
12	1.54	2.6	61.7	492	2.92	1667	2.75	3.22
13	1.46	2.5	64.2	535	2.81	1624	2.66	3.31
14	1.37	2.3	66.5	575	2.70	1581	2.56	3.42
15	1.33	2.3	68.8	621	2.60	1538	2.50	3.52
16	1.28	2.2	71.0	664	2.55	1495	2.45	3.63
17	1.27	2.1	73.1	707	2.52	1452	2.43	3.75
18	1.30	2.2	75.3	750	2.54	1409	2.47	3.85
19	1.32	2.2	77.5	793	2.55	1366	2.50	3.96
20	1.42	2.4	79.9	836	2.66	1323	2.63	4.05
21	1.52	2.6	82.5	879	2.71	1280	2.78	4.14
22	1.72	2.9	85.4	922	2.98	1237	3.05	4.23
23	2.02	3.4	88.8	965	3.26	1194	3.47	4.34
24	2.62	4.4	93.2	1008	3.73	1151	4.32	4.51
25	4.00	6.8	100.0	1051	4.74	1108	6.59	4.84

Total Tooth Load 589·8kN

Note 1. σnom = 100 MPa (Applied remote from threads)

Note 2. $SCF = \frac{Max\,stress}{\sigma_{nom}}$

Table 3.1 Finite Element Results from 140mm OD Connection

Outside dia. = 120mm

			PIN		BOX	
Tooth No	**Tooth Load x10^{4}N**	**Tooth Load %**	**Node Ref**	**SCF**	**Node Ref**	**SCF**
1	6.13	15.3	19	9.82	2140	6.33
2	3.57	8.9	62	5.96	2097	4.65
3	2.50	6.2	105	4.52	2054	3.88
4	2.01	5.0	148	3.86	2011	3.48
5	1.74	4.3	191	3.48	1968	3.21
6	1.55	3.9	234	3.24	1925	3.01
7	1.37	3.4	277	3.02	1882	2.79
8	1.22	3.0	320	2.84	1839	2.63
9	1.06	2.6	363	2.65	1796	2.47
10	0.95	2.4	406	2.53	1753	2.36
11	0.85	2.1	449	2.39	1710	2.25
12	0.76	1.9	492	2.27	1667	2.15
13	0.71	1.8	535	2.19	1624	2.10
14	0.66	1.6	578	2.11	1581	2.04
15	0.66	1.6	621	2.08	1538	2.03
16	0.66	1.7	664	2.06	1495	2.03
17	0.70	1.7	707	2.07	1452	2.04
18	0.78	1.9	750	2.13	1409	2.12
19	0.84	2.1	793	2.18	1366	2.19
20	0.98	2.4	836	2.32	1323	2.34
21	1.10	2.8	879	2.46	1280	2.52
22	1.33	3.3	922	2.72	1237	2.83
23	1.67	4.2	965	3.05	1194	3.32
24	2.34	5.8	1008	3.60	1151	4.28
25	3.96	9.9	1051	4.75	1108	6.88

Total Load 401·1kN= 100%

Table 3.2 Finite Element results from 120mm OD Connection

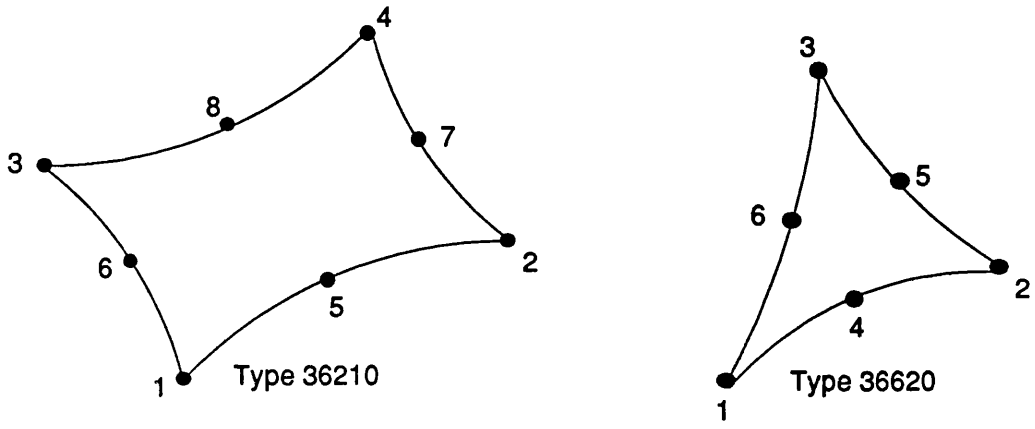

Fig 3.1 Isoparametric Curvilinear Elements used in PAFEC

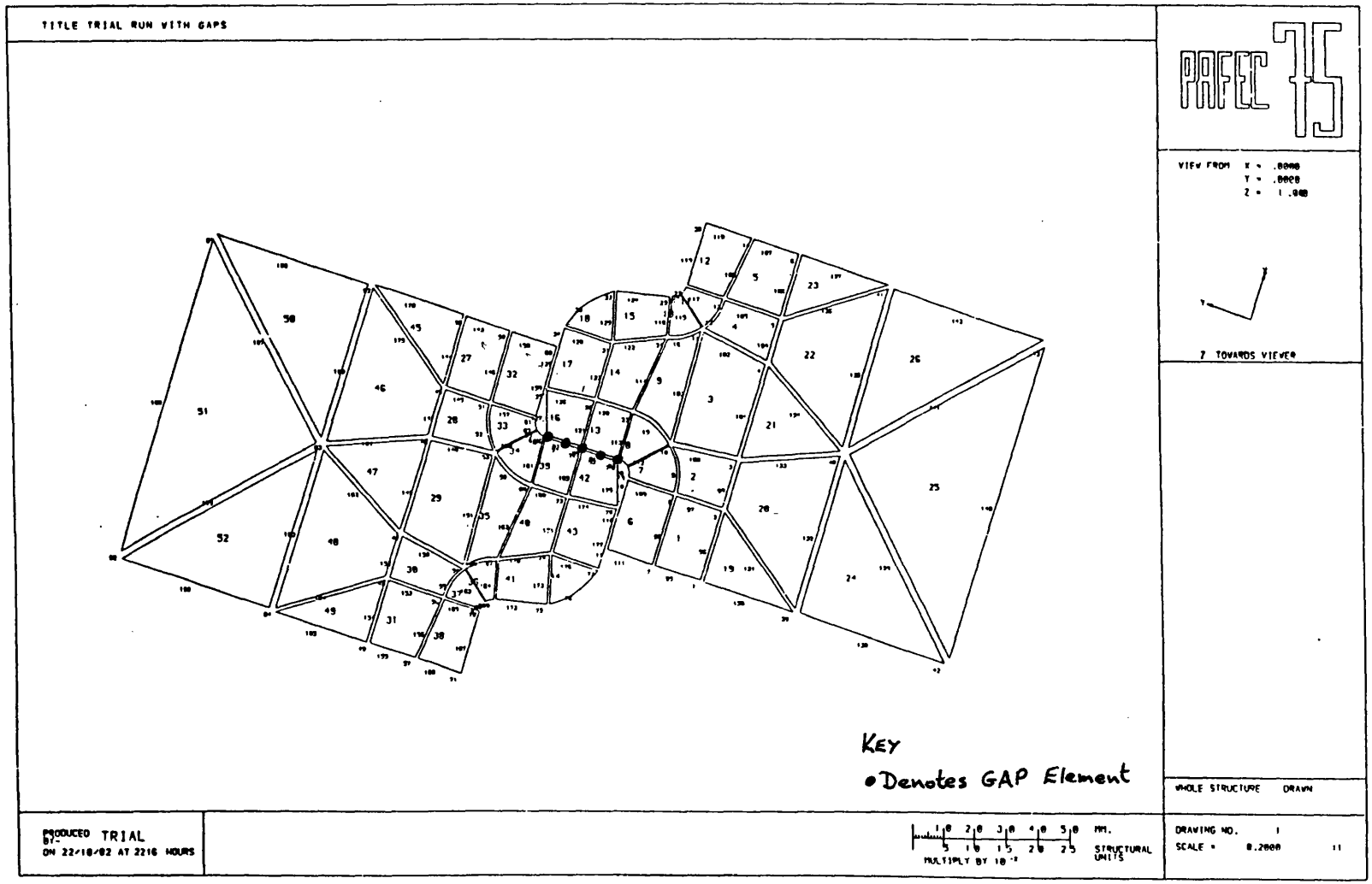

Fig. 3.2a Example of a single tooth showing meshing.

Fig. 3.2b Example of a fully meshed connection model.

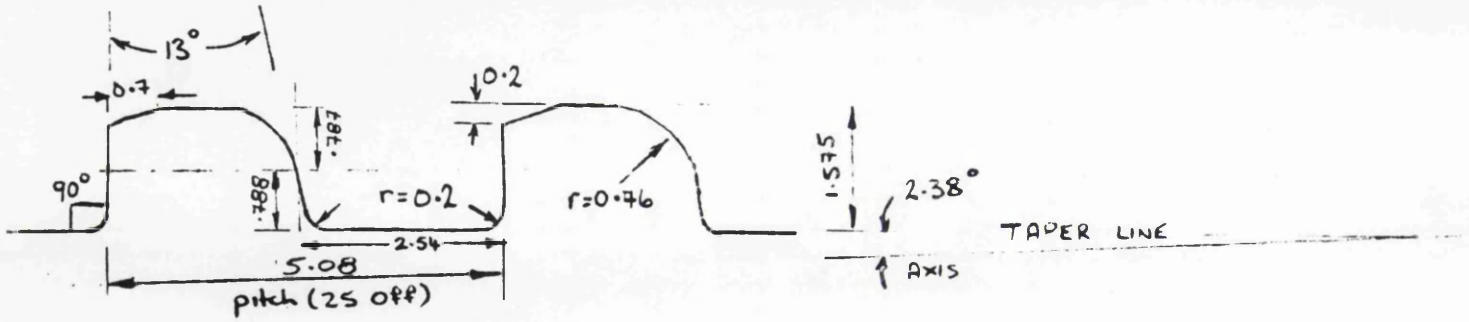

THREAD FORM (PIN & BOX)

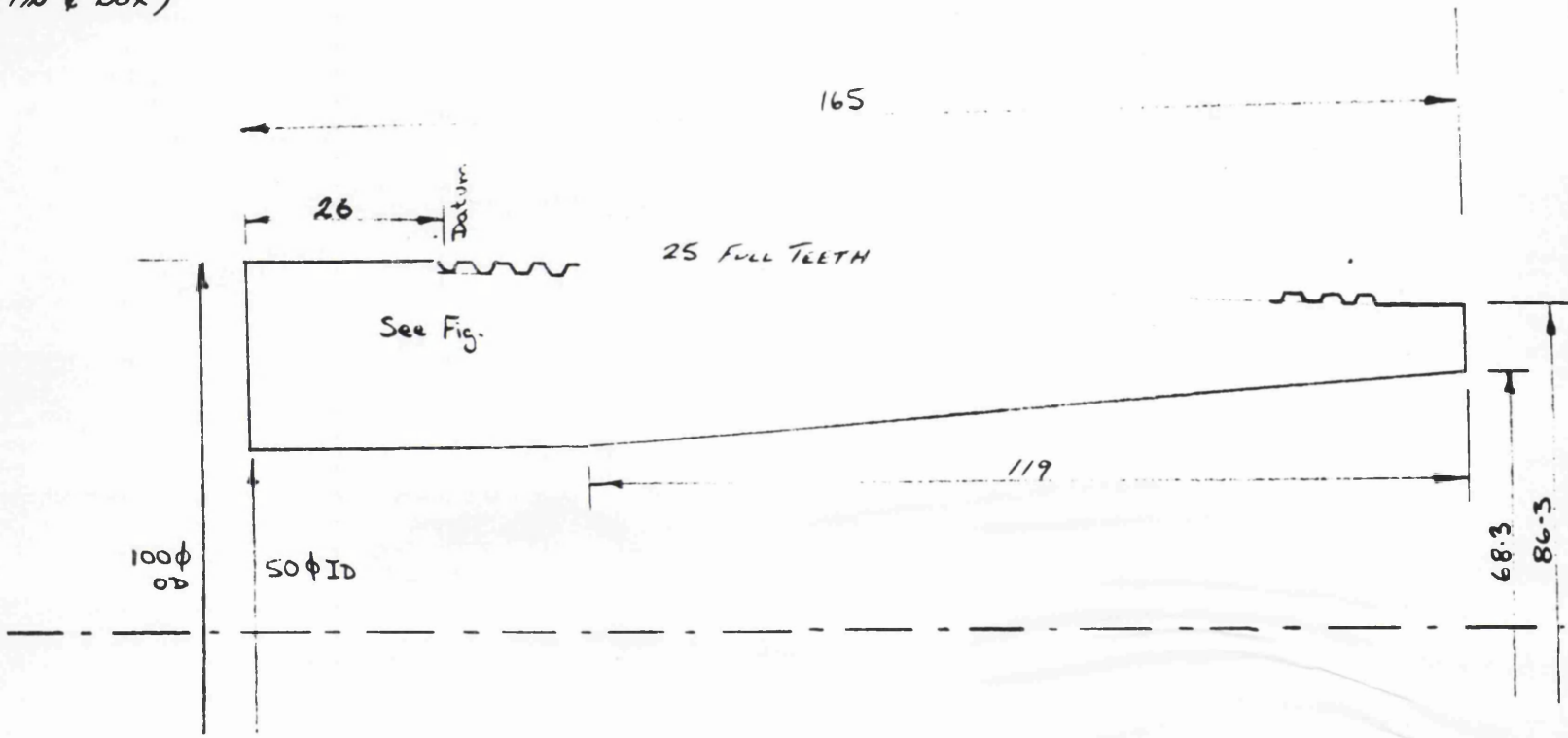

DIMENSIONS IN

FIG. 3.3a PIN DETAILS FOR F.E. MODEL 1

See also Figs. 3.3b, 3.3c &

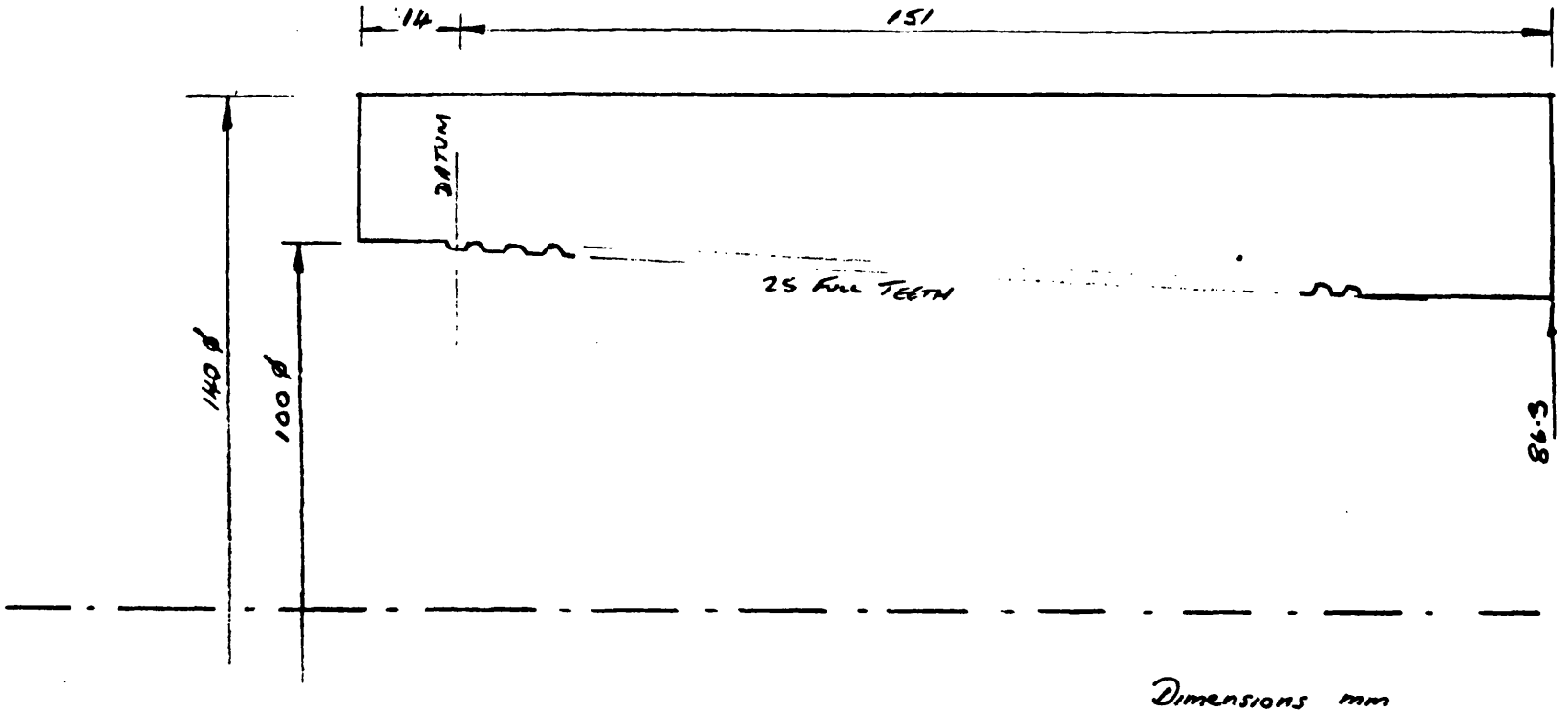

FIG. 3.3b BOX GEOMETRY FOR MODEL 1

See also Figs. 3.3a, 3.3c & 3.6

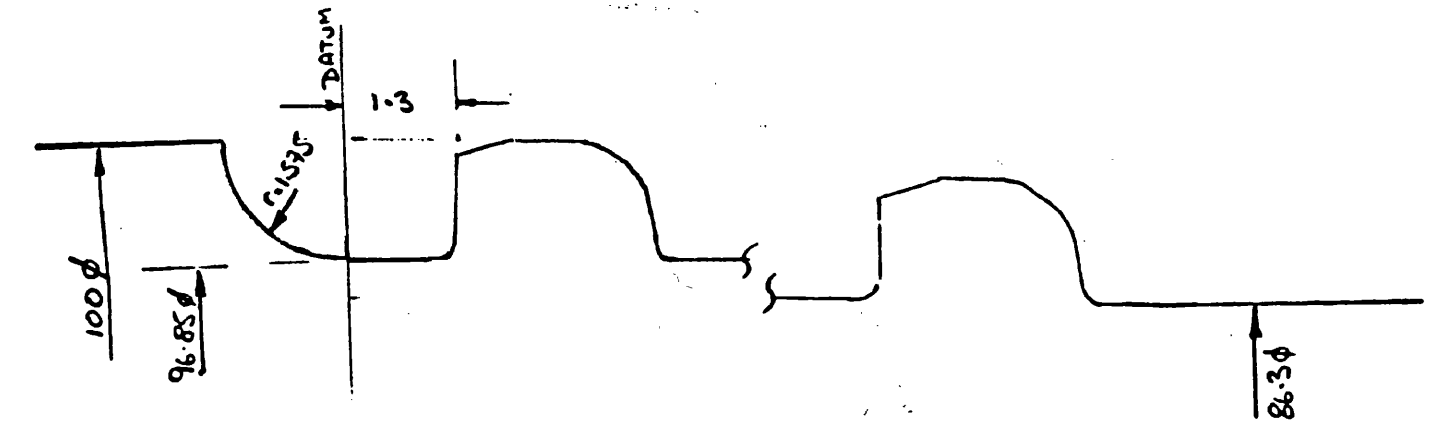

PIN

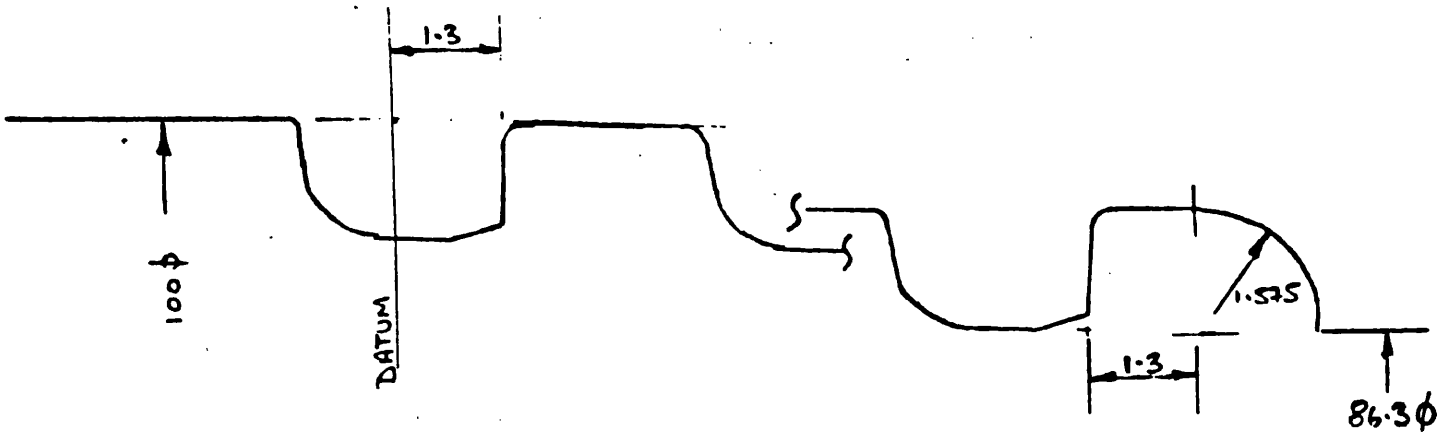

BOX

DIMENSIONS mm.

FIG. 3.3c TOOTH DETAILS FOR FIRST AND LAST TEETH.

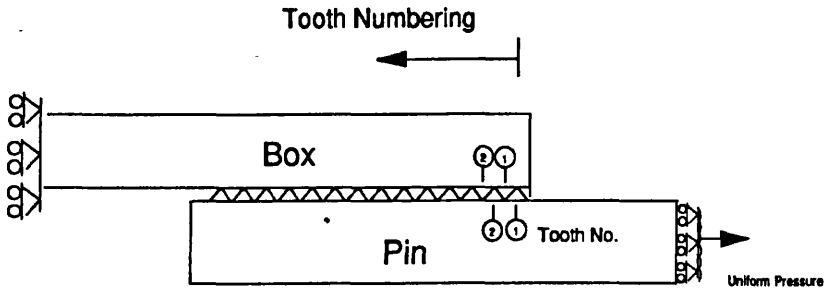

Fig. 3.4 Details of Constraints and loads applied to FE Model

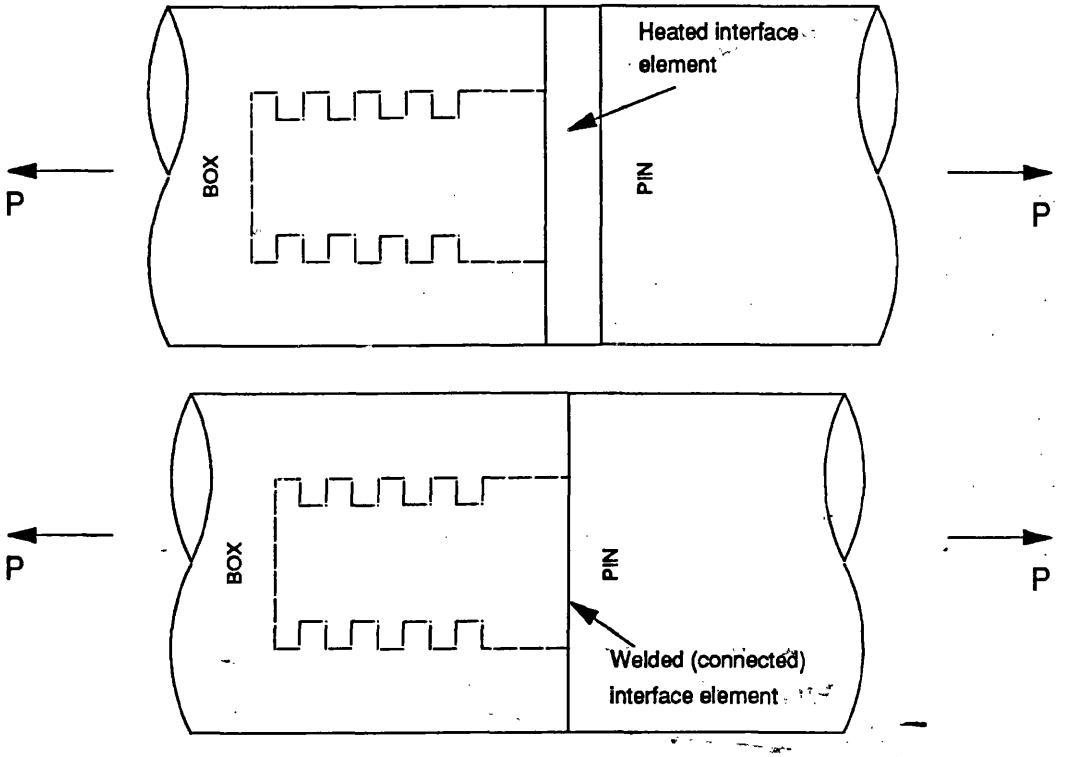

Fig.3.5 Preload modelling using welded interface and lack of fit

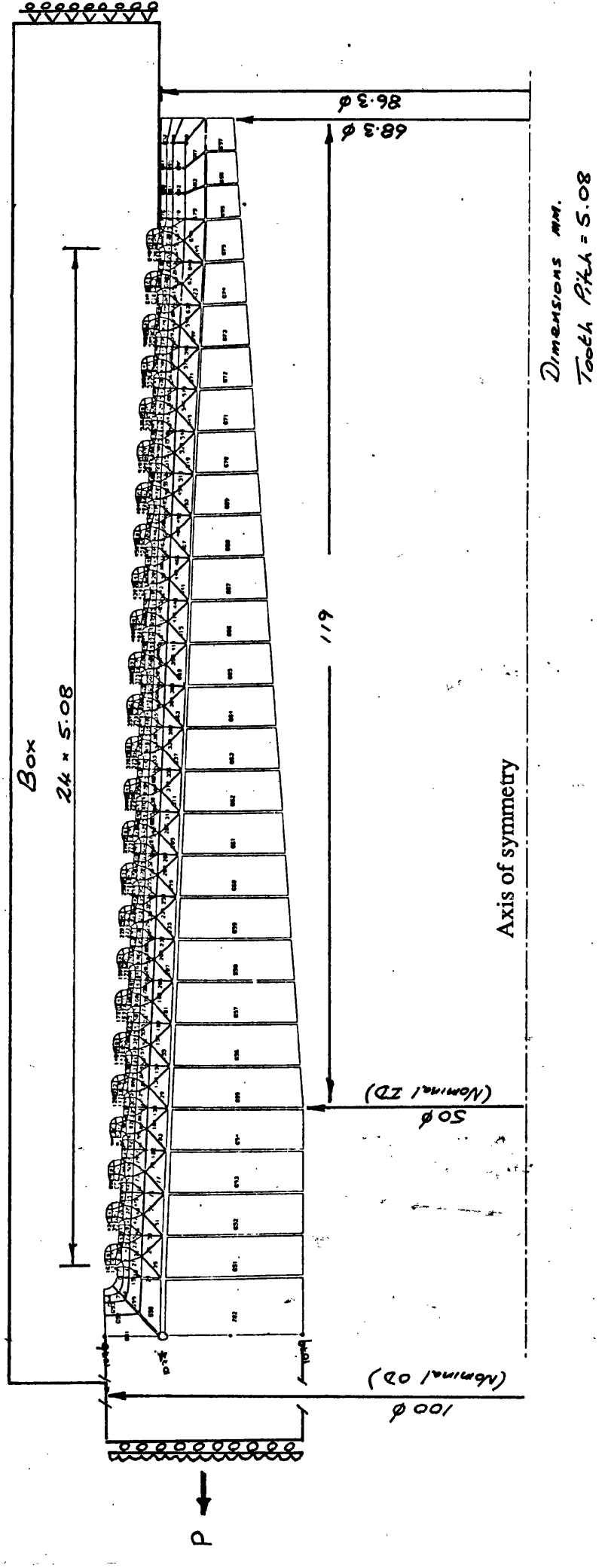

Fig.3.6 Full mesh for the pin member of the model.

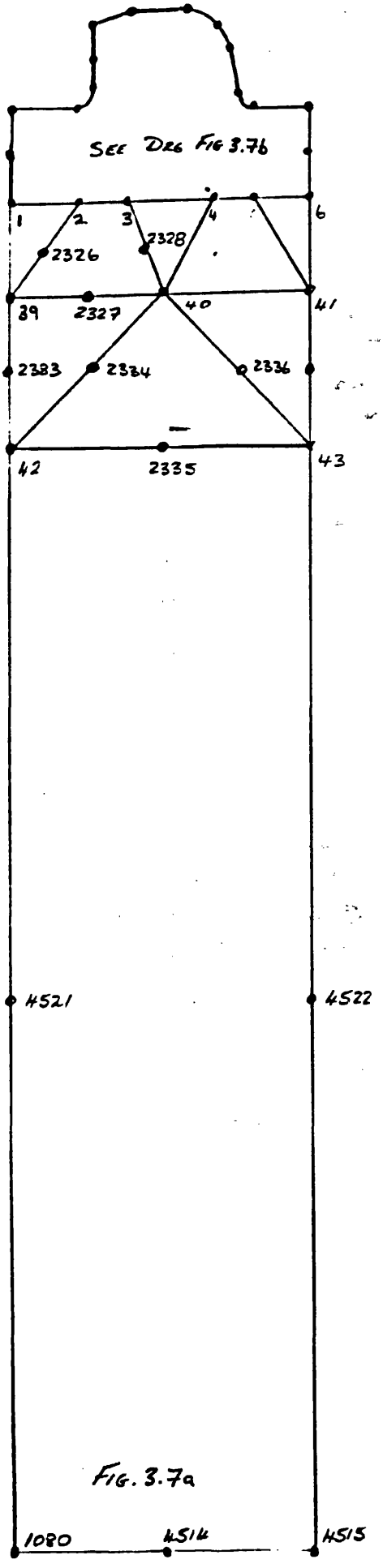

FIG. 3.7a

TABLE 3.3 Stress Results from FE Model 1.
Stresses in MPa

NODE	SCF	Dist from surface (mm)	sigma 1	hoop stress	Sigma2
19	11.8	0	1180	466	435
21	10.2	0.8	1020	334	147
20	9.33	-0.1	933	352	296
18	6.65	0	665	206	81.4
2305	3.54	0	354	84.5	-8.71
17	3.09	0	309	73.5	0.267
2304	2.89	0.4	289	85	52.6
8	2.24	0.8	224	78.6	97.6
2292	1.54	1.1	154	49.8	72.9
2	1.47	1.5	147	47	71.6
2326	1.29	2.2	129	35.1	49.6
2328	1.24	2.3	124	20.2	9.84
40	1.23	3.1	123	19	7.51
39	1.23	3	123	27.8	34.7
2327	1.2	3	120	27.4	34.8
2334	1.13	4.3	113	21.9	24
2333	1.13	4.2	113	22.5	24.7
2336	1.11	4.4	111	11.6	-2.68
42	1.07	5.5	107	19.1	20.2
2335	1.06	5.6	106	15.7	12.7
43	1.02	5.7	102	9.39	-0.138
4521	0.863	14.6	86.3	4.38	-1.3
1080	0.846	23.4	84.6	9.97	0.535
4522	0.83	14.8	83	1.23	-2.41
4514	0.813	23.4	81.3	6.94	1.85
4515	0.812	23.4	81.2	5.53	1.67

Note Nominal stress = 100 MPa

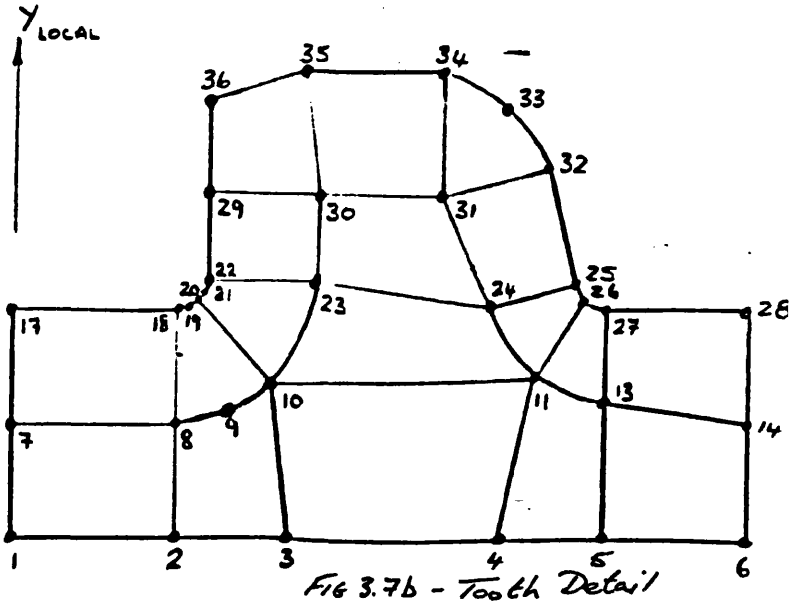

FIG 3.7b - Tooth Detail

FIG. 3.7a,b NODE DETAILS AROUND CRITICAL PIN TOOTH

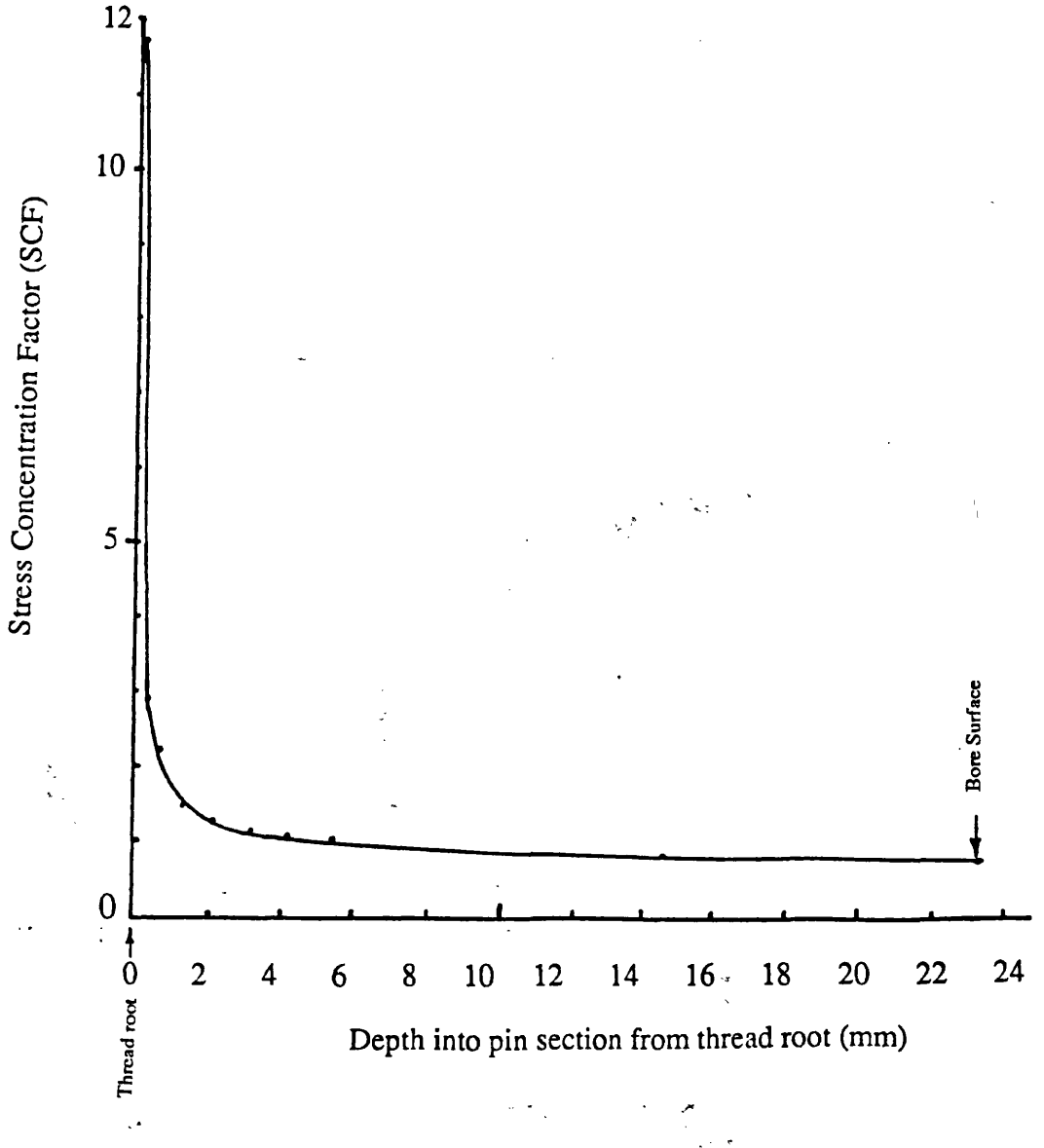

Fig 3.7c Through thickness SCF Distribution at thread root of thread No.1

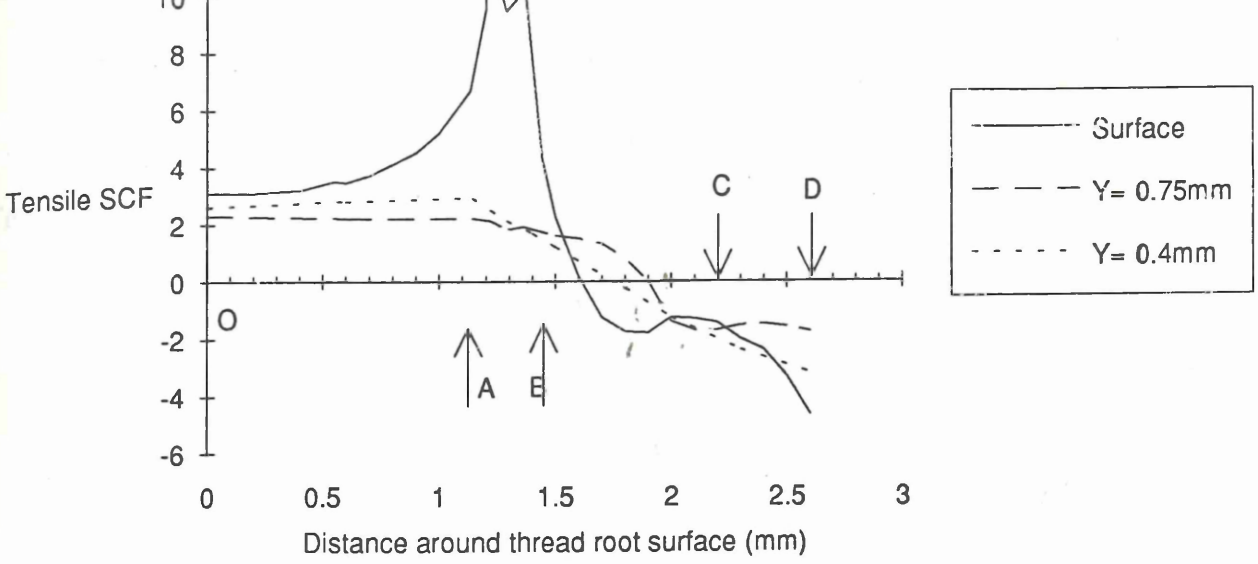

Fig 3.8 SCF Distribution as developed Section - Tooth No. 1

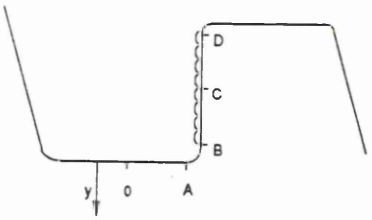

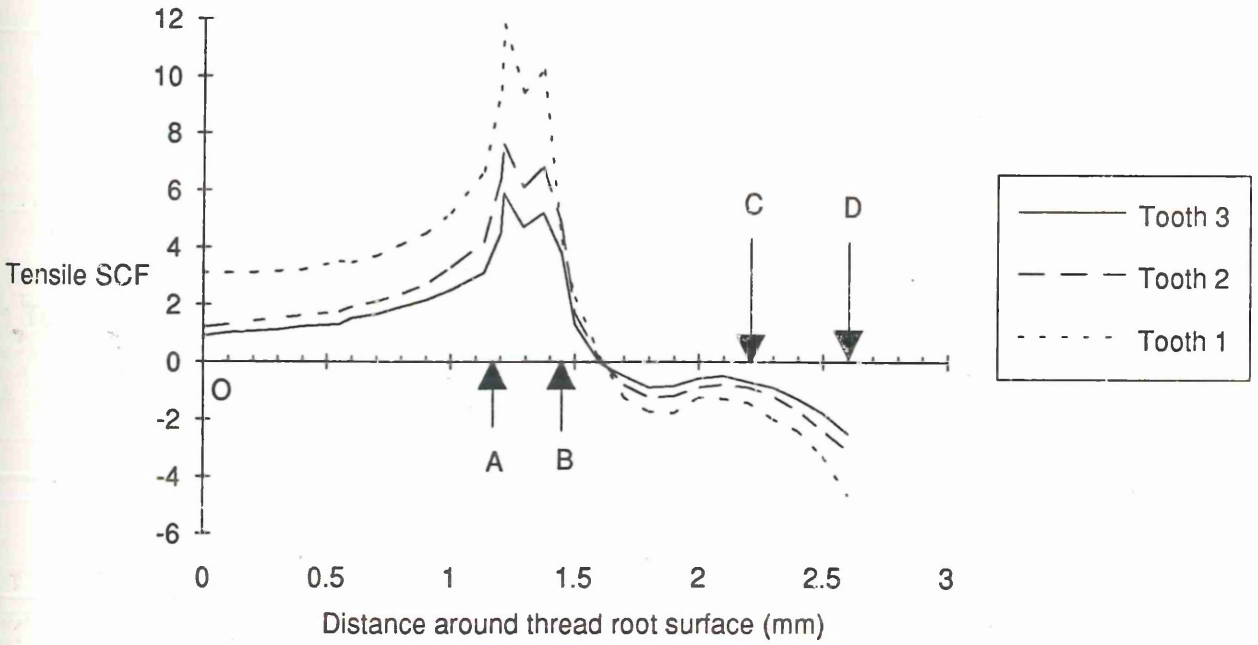

Fig 3.9 SCF Distribution for pin as developed section

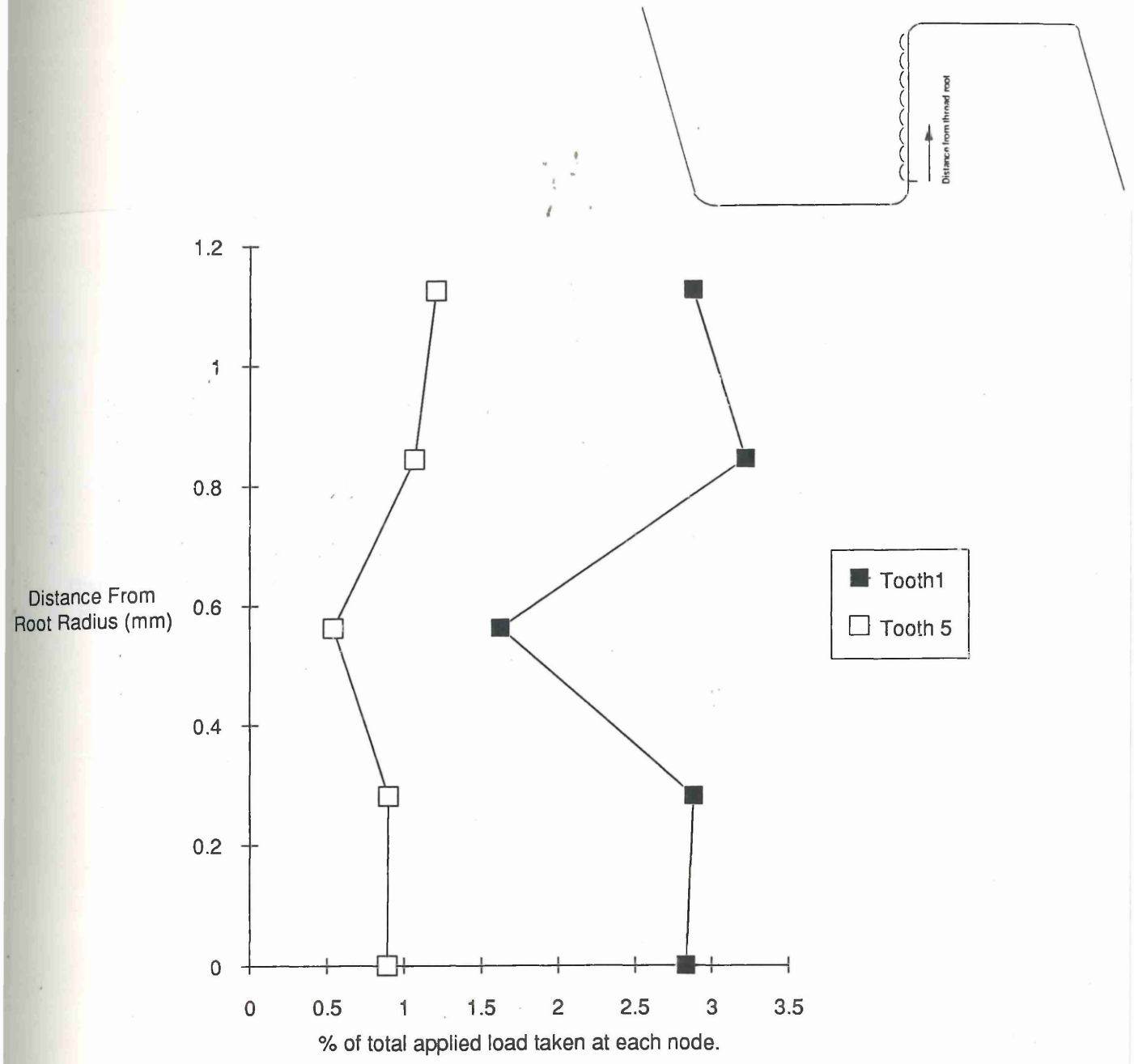

Fig. 3.10 Comparison of load distribution on loaded face

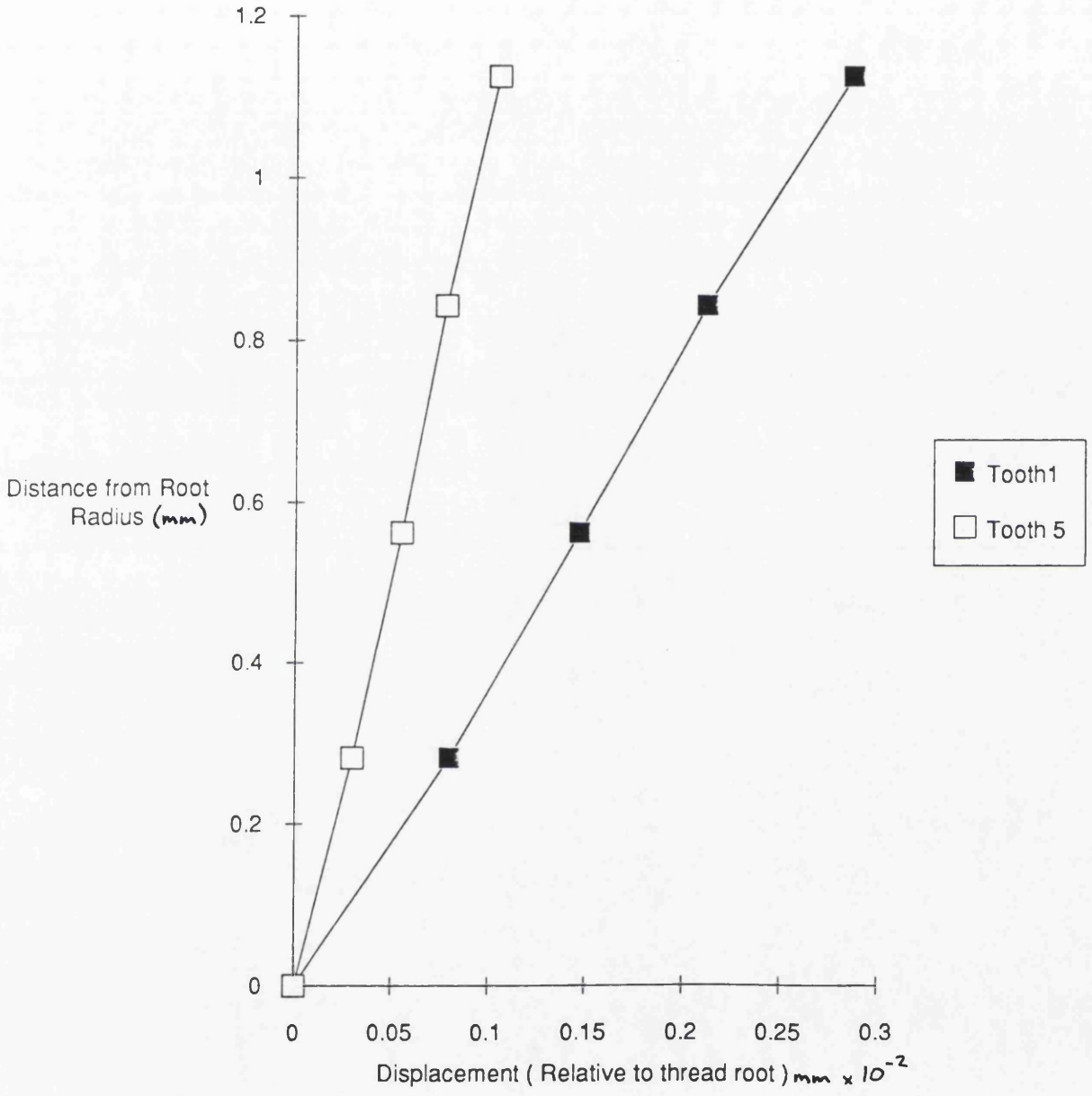

Fig 3.11 Comparison of Tooth Deflections

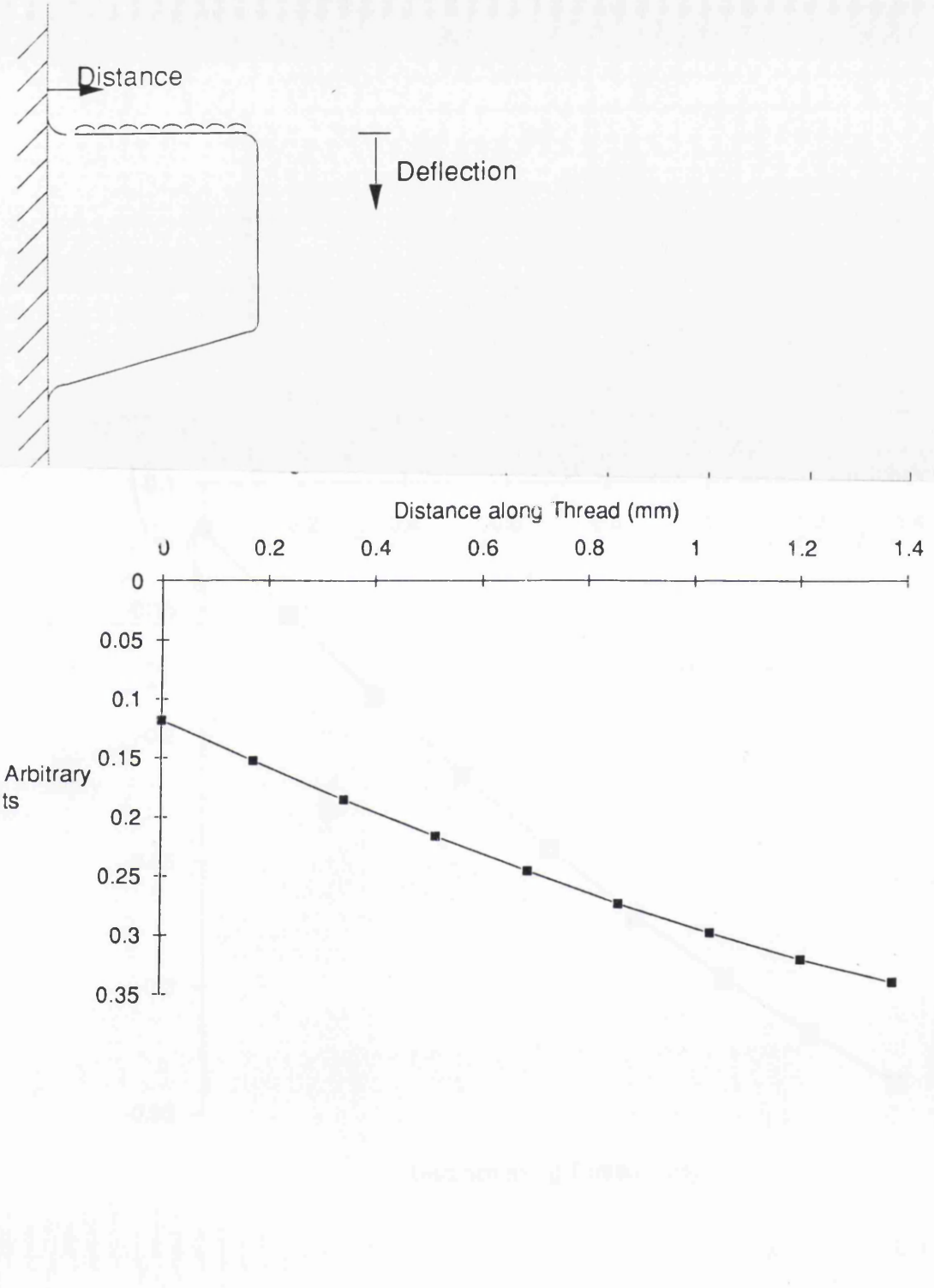

Fig3.12 Theoretical Deflection of Cantilever under udl

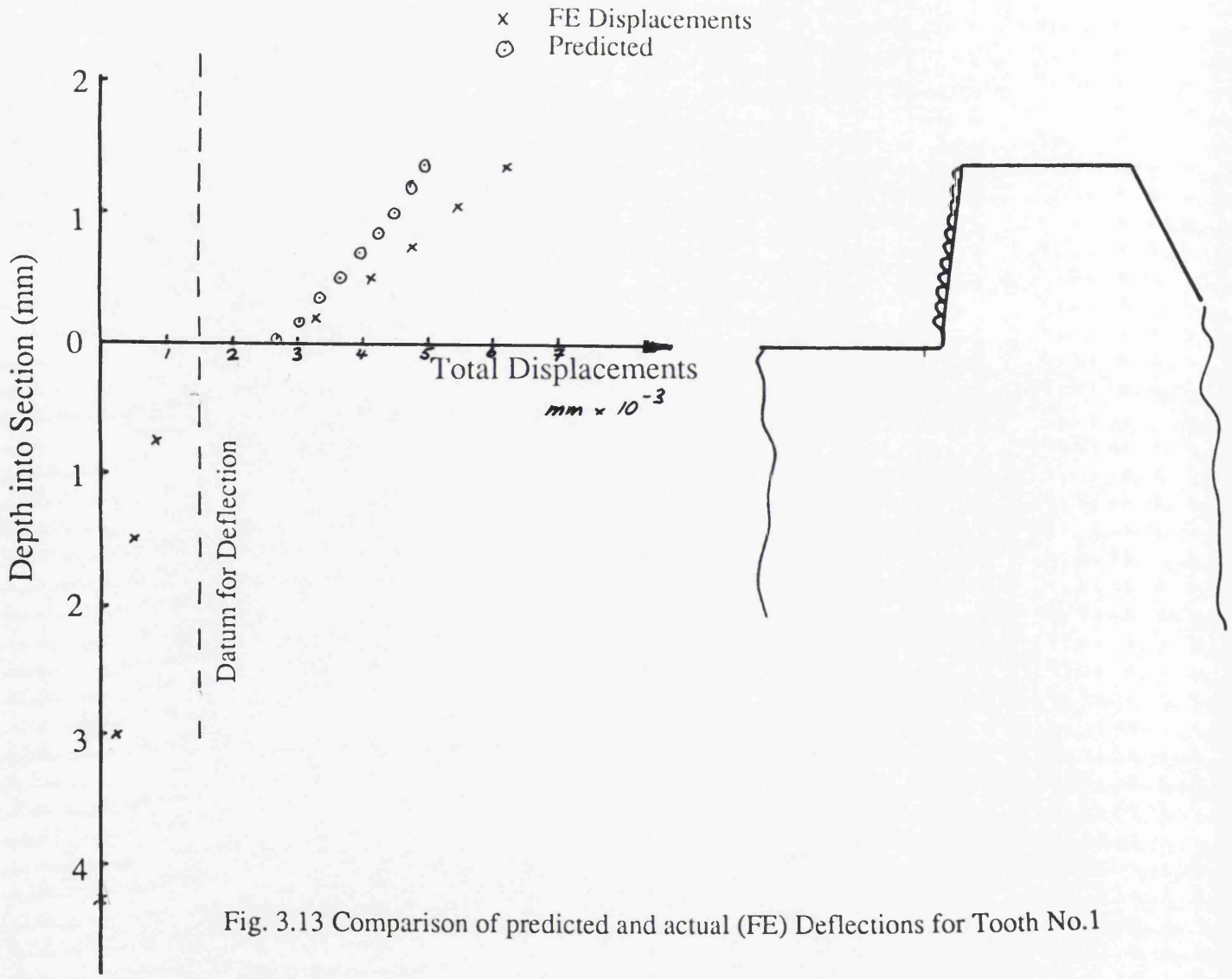

Fig. 3.13 Comparison of predicted and actual (FE) Deflections for Tooth No.1

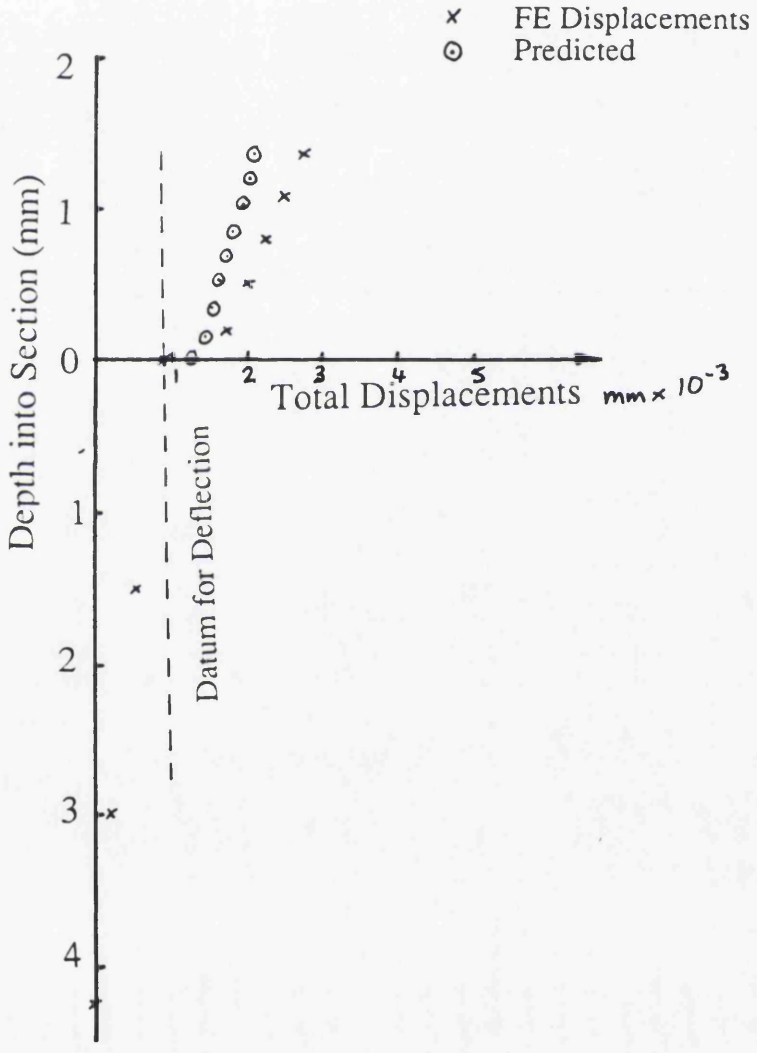

Fig. 3.14 Comparison of predicted and actual (FE) Deflections for Tooth No.5

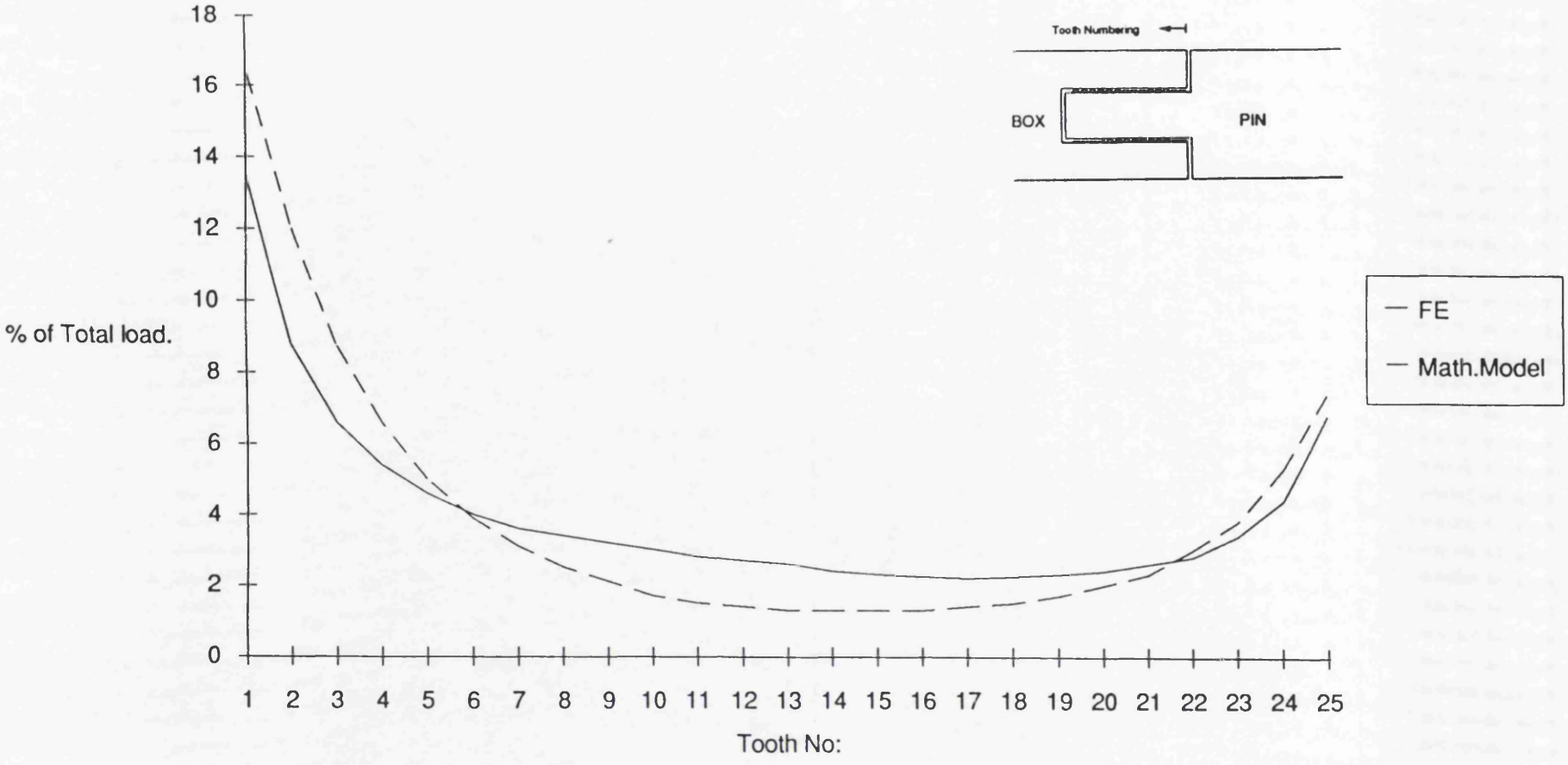

Fig 3.15 Comparison of predicted load distribution for 140 OD Connection. (Model 1)

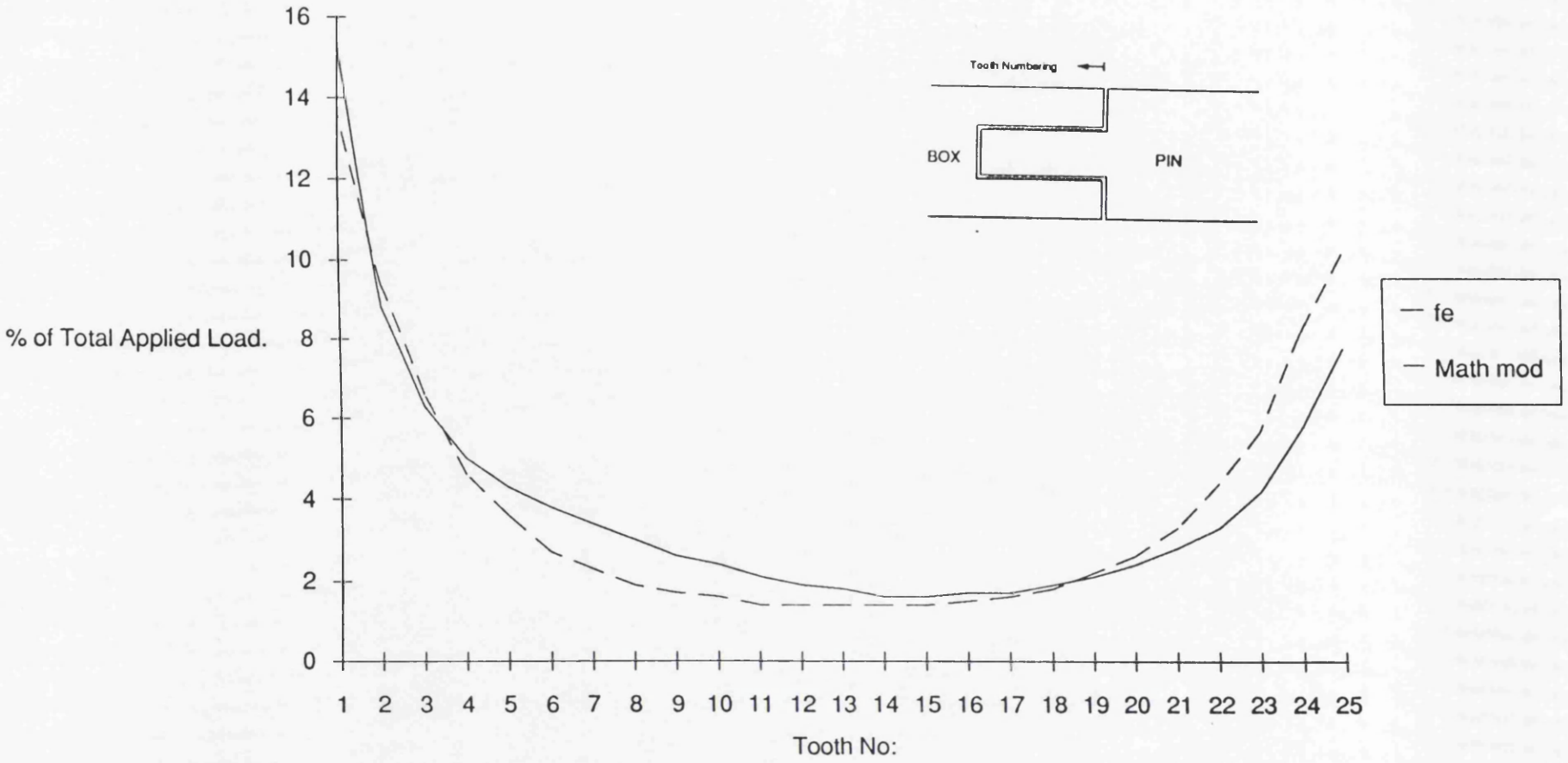

Fig 3.16 Comparison of Predicted Load Distribution for 120mm OD Connector (Model 2)

CHAPTER 4

MODEL FOR THE PREDICTION

of

TOOTH LOADS IN THREADED CONNECTIONS

4.1 INTRODUCTION

It has already been seen that the analysis of threaded connection can be extremely complex and that the only technique readily available for obtaining the full 3D solution for a threaded connection is the Photo-elasticity Method as described by Broadbent [15].

The modelling of meshing teeth using a full 3D FE analysis is prohibitive and the application of preload to FE models is extremely difficult. The final technique is that of complete mathematical modelling using basic Engineering theory as proposed by Sopwith [2]. This method results in a complex mathematical solution to the 3D problem but does appear to give good results (Appendix A) for simple situations. The major drawback of this technique is that it cannot cope with complex geometries (tapers etc.) and does not account for preload.

It is considered that none of the techniques as described provide a convenient tool for the analysis of threaded connections by the design engineer. At the design stage, flexibility of analysis is paramount. The designer needs to be able to compare the performance of various design concepts quickly and easily, effectively conducting initially a parametric study in order to optimise the design for the specific application. At the start of a design procedure, the following parameters must be established:-

1. Number of teeth
2. Tooth size
3. Pitch
4. Thread Form
5. Preload requirement
6. Degree of taper of box and pin etc.

If any attempt to optimise the design is to be made, the effect of all of the parameters must be investigated. It follows that the analysis technique must be flexible enough to enable these parameters to be varied in the modelling and the effects defined.

From the discussion in Chapter 2, it is seen immediately that none of the common techniques allow such flexibility. The Photoelasticity Method requires far too sophisticated models to enable it to be used for parametric studies. In addition, the specialist equipment necessary [15] and the expertise required precludes this as a design tool suitable for use in the design

office. The FE modelling is so complex that modifications to accommodate a parametric type study are prohibitive. The mathematical modelling cannot accommodate preload and hence is not suitable for such a task. Table 4.1 summarises the capability of the various techniques.

For this reason, a new analytical model is proposed here which enables such a design procedure to be conducted and which provides the flexibility necessary at the design stage.

4.2 DESCRIPTION OF MODEL

The proposed model is in fact a hybrid model which combines mathematical modelling with FE methods. The approach adapted is a logical one, first solving the tooth load distribution in the connection using a mathematical technique to derive the stresses due to that load distribution.

4.2.1 Model for Determination of Tooth Load

Many earlier workers [e.g. 2, 3, 4] recognised that the non-uniform tooth load distribution characteristic in threaded connections, is due to differential strains between the male and female components. The full 3D analysis by Sopwith [2] attempts to model these strains around the helix. For designs where the tooth form is essentially a buttress type, i.e. where the loaded flank is perpendicular to the loading axis, radial separation of the teeth is small compared to those in a 'V' thread. Thus, the initial displacements are due to axial stretch of the body of the threaded coupling and tooth deflection. Both can be adequately modelled using a 2D analysis. In the proposed model, which is developed specifically for the analysis of offshore type components where the thread form is a buttress type and where both the male and female components of the coupling experience tensile loads as the joint takes load, a 2D analysis is adopted.

4.2.1.1 Modelling of the Connection as a Series of Springs

The 2D analysis results in the threads being modelled as annular rings which may considered as annular cantilever beams. The beams are connected by the body of the male and female components, with which are associated axial stiffnesses. Thus the thread may be considered as a purely mechanical system represented by rigid levers connected by springs, whose stiffness represent the axial stiffness of the male and female components and the stiffness of the thread. Denoting the male member as the pin, and the female member as the box, a simple threaded connection can be represented by Figure 4.1.

Note that Figure 4.1 is drawn for the axisymmetric case, where the connection could be considered as rotated around the axis of symmetry. However, the model as denoted in Figure 4.1 is adequate to describe the behaviour of the coupling even if it is difficult to visualise as a mechanical system. In the modelling, three stiffness parameters are used:-

K_M Stiffness of Male Member (Pin)

Knowing the area of the pin at the section of interest, A_p, the axial stiffness K_M is defined as EA_p/p where E = Modulus of elasticity and p = tooth pitch.

KF Stiffness of Female Member (Box)

Similarly, the axial stiffness of the box is defined as:

K_F is defined as $\frac{EA_B}{p}$ where A_B is the box cross sectional area.

KB Tooth Stiffness

The tooth stiffness K_B is referred to as the bending stiffness. However, this is a slight misnomer since the shape of the tooth is such that the deflections are often more related to shear than to bending due to the ratio of tooth height to length (half pitch). This prohibits the use of simple beam theory to describe the behaviour of the loaded tooth and instead a solution using stress functions is used. This is described in detail in Appendix B.

The method used is to investigate the deflection of a stubby cantilever due to a uniform distributed load (representing the tooth load around the annulus). Figure 4.2 shows the representation of the tooth as an annular ring. A typical tooth deflection is shown in Figure 3.12.

The tip deflection is calculated in terms of the tooth loading pressure on the flank of the tooth, p^1. For the thread as a whole, i.e. around a full circumference, the total tooth load acting is P. The model stiffness is defined as:-

$$K_B = \frac{P}{\delta}$$

Taking the pressure as acting over the tooth depth, d,

$$K_B = \frac{\pi D d p'}{\delta}$$

The load transfer between teeth can then be investigated using this simple model. Figure 4.3 shows the model for the first two teeth of the connection (that is, the two teeth nearest to the free end of the pin). From Figure 4.3, it is seen that the load in the final section of the Pin, denoted P_1, is transferred into the box across the first tooth. Similarly, tooth 2 transfers a load from the pin to the box, denoted P_3. Note that in this modelling, tooth numbering starts from the tooth closest to the free end of the pin.

Denoting in general terms the loads in each section as P_n and the deflections as δ_n

we have $\delta_1 = \frac{P_1}{K_B}, \delta_2 = \frac{P_2}{K_F}, \delta_3 = \delta_1 + \frac{P_1}{K_M}$

Noting that tooth loads must be compressive

$$\delta_3 > \delta_2 \text{ and } P_3 = K_B(\delta_3 - \delta_2)$$

$$\delta_3 = P_1\left(\frac{1}{K_B} + \frac{1}{K_M}\right)$$

$$P_3 = K_B\left[P_1\left(\frac{1}{K_M} + \frac{1}{K_B}\right) - \frac{P_2}{K_F}\right]$$

writing $\frac{K_B}{K_M} = \theta, \frac{K_B}{K_F} = \alpha$

we get $P_3 = P_1(1+\theta) - P_2\alpha$

This analysis can then be extended to the next branch of the network. However, the deflections at subsequent teeth become difficult to visualise. A simpler way to consider the problem is to now model the system of springs as an electrical resistance network. This method was adopted by Bluhm [34] who solved the problem using an electrical circuit. In this study, the solution is obtained mathematically.

4.2.1.2 Electrical Analogy

Figure 4.1 may be redrawn as a network, Figure 4.4.

As a spring network (Figure 4.1) this is very difficult to conceive physically, indeed since the axisymmetry is not shown the model is incomplete, however, if this is considered as an electrical circuit, the axisymmetry is implicit since an electrical current does not behave as a vector. Consider now an electrical analogy to the spring model

For Loads	**For Electricity**
P=Kδ	$V = IR$ or
	$I = V x \frac{1}{R}$

In this case, which is a static analysis, it is easier to visualise a current as being analogous to a load and a voltage drop across a resistance being analogous to a deflection of a spring. The stiffness of the spring is therefore analogous to the inverse of resistance. If we now consider Figure 4.3, can be considered as an electrical network as shown in Figure 4.5.

using Kirchoff's Laws

$$I_1(R_M + R_B) = R_F I_2 + R_B I_3$$

$$I_3 = I_1\left(1 + \frac{R_M}{R_B}\right) - I_2\frac{R_F}{R_B}$$

we also have that $R_M \equiv \frac{1}{K_M}$ and $R_F \equiv \frac{1}{K_F}$ etc.

hence $\theta = \frac{R_M}{R_B}$ and $\alpha = \frac{R_F}{R_B}$

$$I_3 = I_1(1+\theta) - I_2(\alpha)$$

i.e. the solution is identical to the equivalent one for the mechanical model. However, the ease by which the system is modelled favours the electrical analogy.

For this reason an electrical analogy was chosen. This simple example is for a parallel thread with no preload. Before considering the solution for a general case it is necessary to look at the effect of preload.

4.2.2 Modelling of Preload

The mechanism by which preloading works is complex and was discussed in Section 2.4. This effect can be demonstrated by first considering what happens when a thread is preloaded.

Essentially the thread is forced against a shoulder which becomes in compression. For equilibrium the core of the thread must be under an equal tensile load. Figure 4.6 shows the connection under preload.

After preloading, the forces are in equilibrium and we see that there are equal loads in the two components. The magnitude of the load being equal to the preload value. Denoting the stiffness of the pin at the preloaded section as K_p and the corresponding stiffness of the box as K_c, the preload condition can be summarised in Figure 4.7

If a load is now applied to the system, causing a deflection of the connection, δ, as shown in Figure 4.8, it is seen that the compressive load in the coupling has reduced and that the tensile load in the pin has increased.

However, for load equilibrium

$$P_r + K_p\delta - P_r + K_c\delta = P$$

$$K_p\delta + K_c\delta = P$$

$$\delta = \frac{P}{K_p + K_c}$$

Hence the increase in load in the pin is found as

$$\delta P_p = P\left(\frac{K_p}{K_p + K_c}\right)$$

It is seen therefore that a load of P applied to the system results in an increase in pin load of only a proportion of P and this can have great benefits in fatigue applications. One interesting point here is that providing the preload is never released, i.e. providing the joint remains closed, this benefit occurs. However, if the joint opens the join behaves as if it were not preloaded. This means that once the critical preload level has been reached there is no benefit in tightening the joint further. Indeed the additional tightening could be to the detriment of the joint due to the high mean stresses induced.

This model also shows that it is possible to use superposition when considering preload. In this way, the load distribution due to preload can be determined separately. When determining the load distribution due to an applied load, the stiffness of the pin and coupling must be included. The model will give a tensile load in the "compression" part of the coupling. It must be remembered that this result must be interpreted as a reduction in the

initial preload. It is therefore necessary to ensure that the reduction in preload calculated from the model is less than the applied preload, otherwise the model will be modelling load transfer across a free surface which is incorrect.

Having established a simple model of the preload mechanism, a general model can now be constructed which will take into account preload at both ends of the joint plus tapered sections and variable tooth stiffness. This model will take preload into account in as much as it includes the additional load path effect, due to preload. However, the results from a second model must be included by superposition to take into account the initial load in the teeth due to the preload. The model for pure preload will follow the general model for applied loads.

4.2.3 General Model of Tooth Load Distribution

In order to develop a fully generalised model for threaded connections it is necessary to consider preload at both ends of the connection. This would not be attempted in a design since the lack of control of preload at each end means the preload benefit could not be relied upon. However, some designs preload the free end of the pin only and some rely on the preload applied at the free end of the box only. The Conoco design for the Hutton TLP required preload at the free end of the box whereas the VAM connector relies on preload at the end of the pin only.

Figure 4.9 shows the generalised model allowing for preload to be applied at either end or both.

It is seen that the first and last branch are the same regardless of the number of teeth. Increasing the number of teeth simply increases the number of "branches" in the system.

Consider the general case of the middle section of the model. For the i^{th} tooth we have the situation in Figure 4.10.

For equilibrium at each connection:-

$$I_{1_{i+1}} = I_{1_i} + I_{3_{i+3}}$$

$$I_{2_{i+1}} = I_{2_i} - I_{3_{i+1}}$$

$$I_{3_i} R_{B_i} + I_{1_c} R_{M_i} = I_{2_i} R_{F_i} + I_{3_{i+1}} R_{B_{i+1}}$$

$$I_{3_{i+1}} = I_{1_i}\left(\frac{R_{M_i}}{R_{B_{i+1}}}\right) - I_{2_i}\left(\frac{R_{F_i}}{R_{B_{i+1}}}\right) + I_{3_i}\left(\frac{R_{B_i}}{R_{B_{i+1}}}\right) \qquad 4.1$$

$$I_{2_{i+1}} = -I_{1_c}\left(\frac{R_{M_i}}{R_{B_{i+1}}}\right) + I_{2_i}\left(1 + \frac{R_{F_i}}{R_{B_{i+1}}}\right) - I_{3_i}\left(\frac{R_{B_i}}{R_{B_{i+1}}}\right) \qquad 4.2$$

$$I_{1_{i+1}} = I_{1_c}\left(1 + \frac{R_{M_i}}{R_{B_{i+1}}}\right) - I_{2_i}\left(\frac{R_{F_i}}{R_{B_{i+1}}}\right) + I_{3_i}\left(\frac{R_{B_i}}{R_{B_{i+1}}}\right) \qquad 4.3$$

Defining

$$\theta_i = \frac{R_{M_i}}{R_{B_{i+1}}}, \quad \alpha_i = \frac{R_{F_i}}{R_{B_{i+1}}}, \quad \tau_i = \frac{R_{B_i}}{R_{B_{i+1}}}$$

Equations 4.1, 4.2 and 4.3 can be expressed as:-

$$\begin{pmatrix} (1+\theta_i) & -\alpha_i & \tau_i \\ -\theta_i & (1+\alpha_i) & -\tau_i \\ \theta_i & -\alpha_i & \tau_i \end{pmatrix} \begin{pmatrix} I_{1_i} \\ I_{2_i} \\ I_{3_i} \end{pmatrix} = \begin{pmatrix} I_{1_{i+1}} \\ I_{2_{i+1}} \\ I_{3_{i+1}} \end{pmatrix} \qquad 4.4$$

or in general terms,

$$[A_i] \times [I_i] = [I_{i+1}] \qquad 4.5$$

Note that all components of the A matrix are dimensionless.

In terms of **stiffness**

$$\theta_i = \frac{K_{B_{i+1}}}{K_{M_i}}$$

$$\alpha_i = \frac{K_{B_{i+1}}}{K_{F_i}}$$

$$\tau_i = \frac{K_{B_{i+1}}}{K_{B_i}}$$

The A matrix can then be formed for teeth from 1 to n-1 since the "stiffness" matrix for the $(n-1)^{th}$ tooth gives the values of current in the n^{th} tooth.

The first and last branches of the network can now be investigated.

First Tooth

The first tooth is shown in Figure 4.11

$$I_{1_1} = I_A + I_{3_1}$$

$$I_{2_1} = I_B - I_{3_1}$$

$$I_A R_{P_1} = I_B R_{C_1} + I_{3_1} R_{B_1}$$

which can be re-arranged as

$$I_{3_1} = I_A \frac{R_{P_1}}{R_{B_1}} - I_B \frac{R_{C_1}}{R_{B_1}} \qquad 4.6$$

$$I_{2_1} = I_B \left(1 + \frac{R_{C_1}}{R_{B_1}} \right) - I_A \frac{R_{P_1}}{R_{B_1}} \qquad 4.7$$

$$I_{1_1} = I_A \left(1 + \frac{R_{P_1}}{R_{B_1}} \right) - I_B \frac{R_{C_1}}{R_{B_1}} \qquad 4.8$$

Equations 4.5, 4.6 and 4.7 can then be expressed as

$$\begin{pmatrix} 1 + \frac{R_{P_1}}{R_{B_1}} & -\frac{R_{C_1}}{R_{B_1}} \\ -\frac{R_{P_1}}{R_{B_1}} & 1 + \frac{R_{C_1}}{R_{B_1}} \\ \frac{R_{P_1}}{R_{B_1}} & -\frac{R_{C_1}}{R_{B_1}} \end{pmatrix} \begin{pmatrix} I_A \\ I_B \end{pmatrix} = \begin{pmatrix} I_{1_1} \\ I_{2_1} \\ I_{3_1} \end{pmatrix} \qquad 4.9$$

or, $[AI]\,[I] = [I_1]$

By combining equations 4.10 and 4.5 we have a solution for the n^{th} tooth in terms of I_A and I_B.

$[I]_n = [A]_{n-1}\ [A]_{n-2}....[A]_2\ [A]_1 \begin{pmatrix} I_A \\ I_B \end{pmatrix}$

$[AI]$

or,

$$[I]_n = [A_{Final}] \begin{pmatrix} I_A \\ I_B \end{pmatrix} \qquad 4.10$$

Now consider the last tooth as shown in Figure 4.12

$$I_{3_n} R_{B_n} + I_{1_n} R_{P_2} = I_{2_n} R_{C_2}$$

$$I_{3_n} = -I_{1_n} \frac{R_{PC}}{R_{B_n}} + I_{2_n} \frac{R_{C_2}}{R_{B_n}}$$

$$I_{3_n} = \left[-\frac{R_{P_2}}{R_{B_n}} \quad \frac{R_{C_2}}{R_{B_n}} \right] \begin{pmatrix} I_{1_n} \\ I_{2_n} \end{pmatrix} \qquad 4.11$$

Equation 4.10 gives

$$\begin{pmatrix} I_1 \\ I_2 \\ I_3 \end{pmatrix}_n = [A_{Final}] \begin{pmatrix} I_A \\ I_B \end{pmatrix}$$

Equation 4.11 gives

$$I_{3_n} = \left[-\frac{R_{P_2}}{R_{B_n}} \quad \frac{R_{C_2}}{R_{B_n}} \right] \begin{pmatrix} I_A \\ I_B \end{pmatrix}$$

Equations 4.10 and 4.11 can then be solved to give I_A in terms of I_B

Denoting $\frac{I_A}{I_B} = \gamma$

These values are then back substituted to give the value of load in each branch. This is done as follows:-

$$\begin{pmatrix} I_A \\ I_B \end{pmatrix} = \begin{pmatrix} \gamma \\ 1 \end{pmatrix} [I_B] \quad \text{or} \quad [I] = [Q]\,[I_B]$$

$$[I_1] = [AI]\,[Q]$$

$$[I_2] = [A_1]\,[I_1]$$

$$[I_3] = [A_2]\,[I_2]$$

$$[I_n] = [A]_{n-1}\,[I]_{n-1}$$

Hence the loads in all sections of the model are known relative to load in the first section. If the total applied load is known the individual tooth loads can then be found.

This solution is general and allows preload to be applied at both ends of the coupling. If the preload condition is not required, the value of preload stiffness is input as zero. It must be noted however, that if preload is not required at the free end of the pin K_{p1} is set to zero. If preload is not required at the free end of the box K_{c2} is set to zero.

It is now necessary to consider the case where the joint is under preload only, that is, there is no externally applied load.

Preload applied at the free end of the pin only

Preload is an "internal" effect, that is, there is no external load on a preloaded joint. For a joint with preload at the free end of the pin only, the joint can be modelled as shown in Figure 4.13.

This can be represented electrically as shown in Figure 4.14.

Around the last branch

$$I_{2_{n-1}} = I_{1_{n-1}}$$

$$I_{3_{n-1}}(R_{B_{n-1}}) = I_{1_{n-1}}(R_{M_{n-1}} + R_{B_n} + R_{F_{n-1}})$$

$$I_{3_{n-1}} = I_{1_{n-1}}\left(\frac{R_{M_{n-1}}}{R_{B_{n-1}}} + \frac{R_{B_n}}{R_{B_{n-1}}} + \frac{R_{F_{n-1}}}{R_{B_{n-1}}}\right)$$

in general $I_{1_i} = I_{2_i}$

The i[th] tooth can now be considered, Figure 4.15.

$$I_{1_i}(R_{M_i} + R_{F_i}) + I_{3_{i+1}} R_{B_{i+1}} = I_{3_i}(R_{B_i})$$

$$I_{3_i} = I_{1_i}\left(\frac{R_{M_i}}{R_{B_i}} + \frac{R_{F_i}}{R_{B_i}}\right) + I_{3_{i+1}} \frac{R_{B_{i+1}}}{R_{B_i}}$$

also $I_{1_i} = I_{3_{i+1}} + I_{1_{i+1}}$

Hence knowing $I_{1_{n-1}}$ all loads can be expressed in terms of this load.

Similarly the effect of preload at the coupling can be determined.

Preload applied at free end of the box only

This is a similar problem to preloading at the pin end. The electrical model is shown in Figure 4.16.

The general case is shown in Figure 4.17.

$$I_{1_i}(R_{M_i} + R_{F_i}) + I_{3_i}(R_{B_i}) = I_{3_{i+1}}(R_{B_{i+1}})$$

$$I_{3_{i+1}} = I_{3_i}\left(\frac{R_{B_i}}{R_{B_{i+1}}}\right) + I_{1_i}\left(\frac{R_{M_i}}{R_{B_{i+1}}} + \frac{R_{F_i}}{R_{B_{i+1}}}\right)$$

also $I_{1_{i+1}} = I_{1_i} + I_{3_{i+1}}$

from the first branch, Figure 4.18.

$$I_{3_2} = I_{1_1}\left(\frac{R_{M_1}}{R_{B_2}} + \frac{R_{B_1}}{R_{B_2}} + \frac{R_{F_1}}{R_{B_2}}\right)$$

Hence all loads are found with respect to I_1

4.2.4 Principle of Superposition

For dynamic applications, providing the joint remains closed, it is not necessary to know the value of the initial preload since this does not affect the stress amplitude in the threads. This is an important point, as is the way the principle of superposition can be applied, since the principle of superposition implies that the initial preload condition can be applied purely as a static offset to the dynamic load. If the general model is considered, the analysis effectively shows a transfer of load across the bearing faces of the preload shoulder. In fact identical results are obtained if the joint were considered as welded at the bearing face (it is interesting to note that if the joint is assumed welded, an estimate of the effect of the applied preload on the dynamic load in either component can be obtained by simply assuming that the load distributes according to the relative cross sectional areas of the pin and box at that point).

Whilst the model allows transfer of load across the bearing face, (a free surface) physically this cannot occur. Let us consider now what actually happens in a preload joint. Assuming an initial preload of P, and an applied load of T, the applied load of T must go through the pin, since tensile loads cannot pass across a free face, Figure 4.19. However, the increased load in the pin causes the pin to extend, thus reducing the preload on the shoulders. The preload reaction on the pin reduces to maintain equilibrium and hence there is an apparent load transfer across the compression face of the joint.

The situation shown in Figure 4.19 can be represented by superposition of the 2 cases shown in Figs 4.20 and 4.21

4.3 DISCUSSION OF TOOTH LOAD MODEL

The model just described has been computerised and runs on a mini or micro computer. The code has been developed in Fortran and a listing is given in Appendix D from the model, it is seen that the tooth load is derived by considering stiffness ratios. This means that providing the material of the box and pin are the same (or have the same elastic modulus) no knowledge of the modulus of elasticity (Young's modulus) is necessary. The relative stiffness of the box and pin members are calculated directly from the geometry. However, the tooth stiffness is not obtained directly from the geometry. It has already been stated that the teeth act as short beams and that Engineering Beams Theory will not apply since the ratio of bending to shear is small due the low length/depth ratio. It is therefore necessary to determine the tooth deflection by another method. The method adopted is the use of Airey Stress Functions.

The use of stress functions is well documented for the solution of stress analysis problems. This method depends on the choice of a suitable Stress Function Ψ which is then used to define the basic stress state of that structure in terms of the chosen function. In this case, the solution is used to determine the deflection, rather than the stress. The solution for the analysis of a cantilever is given in detail in Appendix B where it is seen that for low values of length/depth (i.e. tooth height/half pitch), the deflection is dominated by shear rather than bending.

The tip deflection solution as detailed in Appendix B is included in the computer model to allow tooth stiffness to be calculated directly. However, the option to input tooth deflection directly is also given. These could be derived from simple FE models. Note that the requirement here is for the tooth deflection due to a unit load and hence no modelling of meshing teeth is necessary. This option to use results from FE modelling allows the use of teeth with non rectangular cross sections where the stress function approach as developed here is inapplicable.

4.3.1 Tooth Stiffness Derivation

Appendix B gives the solutions for the deflection of a cantilever. It is important to define the stiffness carefully and for the model developed here, the tooth stiffness is calculated as follows:-

Consider a section of an infinite rectangular beam loaded under uniform unit pressure as shown in Figure 4.22

The tip deflection can be calculated using the stress function approach and is denoted δ. Now consider the above section as being part of an annular ring as shown in Figure 4.23. Again, a unit pressure will lead to a tip deflection of δ.

$$\text{Load on tooth} = \pi D d$$

$$\text{Therefore tooth stiffness} = \frac{Load}{Deflection} = \frac{\pi D d}{\delta}$$

In the modelling, all stiffnesses are normalised with respect to Youngs Modulus and hence the stiffness co-efficient used as input to the model, denoted as K″ is given by

$$K'' = \frac{Stiffness}{E} = \frac{\pi Dd}{\delta E}$$

It is important to note that the stiffness K and stiffness coefficient K″ vary with mean tooth diameter due to the influence of the changing area on the applied load. This means that for a tapering connection, the tooth stiffness reduces as the diameter reduces.

In order to explain this apparent anomaly whereby the teeth with identical cross sections have different stiffness according to their diameter, consider two teeth of identical cross section on different diameters both loaded under unit pressure.

Tooth No.	Mean Diameter	Pressure	Deflection	Load
1	D_1	1	δ	πdD_1
2	D_2	1	δ	πdD_2

It is seen that the calculated stiffness will be

Tooth 1 $K = \frac{\pi dD_1}{\delta}$

Tooth 2 $K = \frac{\pi dD_2}{\delta}$

Particular care is needed when considering results from FE analysis to provide tooth stiffness input. This is discussed in the next section.

4.3.2 Discussion of Assumptions

The tooth load model makes a number of assumptions and these are listed below

i) 2D Analysis

This was discussed in Section 2.6 and it is considered that at the initial design stage this is a reasonable approach. The primary effect of the 2D symmetric assumption is that the tooth loads are averaged around the circumference. This was discussed earlier and it was stated that this could lead to a non conservative result if the variation of tooth load around the circumference is significant. This effect was investigated using the Sopwith [2] analysis

detailed in Appendix A. The results show that, as expected, the first loaded tooth of the unpreloaded joint experiences the maximum tooth load variation. By consideration of the tooth load distribution, as discussed in Appendix A, it is possible to produce a correction factor to account for the variation in tooth load around the helix, thus improving the 2D axisymmetric analysis. However, this is only valid where the joint is un-preloaded since the Sopwith [2] solution is applicable only to this case.

One consideration is the fact that this model does not consider radial stiffness and all loads are calculated with respect to axial displacements due to nominal elastic axial stiffnesses. The FE analysis described in Chapter 3 considered hoop stresses but did not show significant radial deformation and this confirmed that the relative displacement between pin and box were predominantly axial. However, the most important consideration is that the model here is dealing with ***load*** prediction. Providing therefore that displacements in the body are predominantly axial the model will predict the load distribution. It is discussed later that the calculation of ***stress*** does need to consider hoop stresses and this is of course accommodated.

For the buttress type threads, the loaded tooth faces are approximately perpendicular to the thread axis which again leads to axial deflection and hence the model is applicable. However, it must be considered that for 'V. thread forms which lead to loaded faces inclined significantly to the loading axis that the loading action could lead to displacements with a radial component and this leads to a number of important considerations. Firstly if the components deflect radially in opposite directions, the tooth load could be relieved. However it is noted that in this situation, a secondary effect is that the loading point moves toward the tip of the thread thus increasing the bending moment for a given load. Whilst 'V' threads were not considered significantly in this study, these are important factors which merit further attention.

ii) Linear Elastic Behaviour

This assumption was also made in the FE analysis. Providing large scale plasticity does not occur at the thread root, the joint strains will be dominated by elastic effects. Should the design be such that localised plastic strains are experienced for example at the small thread root radius, the effect of these, in terms of the overall joint stiffness would be small and therefore the load distribution obtained assuming Linear Elastic behaviour is acceptable.

Should large scale plasticity be found to result from the root loads so found, the design should be rejected since the plasticity will be unacceptable from considerations of break and remake of the joint.

iii) Tooth Geometry

The model as described has been derived for teeth of approximately rectangular cross section where the loaded flank is roughly perpendicular to the thread loading axis. Non-rectangular thread forms can also be accommodated with caution. In this case however, the stress function solution for beam deflection would not apply. To allow for this, a facility to input the tooth stiffness into the model, rather than to calculate it theoretically has been incorporated. This necessitates the use of a simple FE model to determine the tip deflection of a beam whose cross section is that of the thread. This needs only to be a simple model as shown in Figure 4.24 and does not require meshing teeth since the tip deflection under a unit uniformly distributed load is used to determine the stiffness. The use of the model for tooth sections where the loaded flank is not perpendicular to the thread axis is discussed above in (i).

4.4 COMPARISON OF RESULTS WITH THOSE FROM OTHER MODELS

The full FE model allows a comparison of results between the two methods. Prior to comparing the absolute tooth loadings, it is necessary to compare the tooth deflection obtained from the two methods since these are fundamental to the modelling.

4.4.1 Comparison of Tooth Deflection from FE and theoretical analysis

Figure 3.13 showed the tooth deflection for tooth No.1 from the FE analysis. By using the tooth load from the FE analysis, the average pressure loading on the loaded flank can be determined. This pressure was then used as input into the analysis described in Appendix B to determine the deflected shape of the beam (tooth) theoretically.

The results from theory (Appendix B) and FE analysis for tooth 1 are compared in Figure 3.13. It is seen that both analyses show a similar shear deflection at the thread root. However, the deflection of the thread tip is underestimated by the theoretical model. A similar result is shown in Figure 3.14 for tooth No.5.

Further examination of the FE results in Figs 3.13 and 3.14 show the body of the coupling to be "rotated" at the point of tooth attachment. This is not unreasonable since the tooth load is applied at the extreme surface of the coupling and the strains would be expected to decay into the body of the coupling from that point.

The results show that the absolute tip deflection of the tooth are a combination of tooth load effects plus a slight rotational effect. When this is accounted for, the results from the theoretical analysis in Appendix B are seen to be in good agreement with the FE analysis. It is also observed that the "rotation" effect is approximately proportional to the magnitude of tooth loading. For this reason, an empirical correction factor has been applied to the theoretical tip deflection to account for this effect. For the geometries investigated here, an empirical multiplier of 1.8 was applied to the tooth deflection calculated theoretically to account for these local effects.

This was another consideration when incorporating the facility to input tooth stiffness co-efficients directly into the model. By investigating the deflection of the particular tooth geometry under an applied tooth load, using a simple FE model, the tooth stiffness can be obtained directly and input into the model, thus improving the result by eliminating the effects of the assumptions implicit in the theoretical modelling of tooth deflection.

4.4.2 Comparison of Load Distribution from FE analysis and Mathematical Model

Two full FE analyses were conducted and the load distribution from these are compared with those obtained using the tooth load model. The comparison is shown in Figs 4.25 & 4.26. It is seen that the load distribution in the joint is modelled well using the simple model. The individual tooth loads for the two cases are compared in detail in Figs. 3.15 and 3.16.

4.4.3 Comparison of Load Distribution from Sopwith [2] and Mathematical Model

The load distribution obtained from the model assumes 2D axisymmetric analysis. The analysis by Sopwith, given in detail in Appendix A allows the calculation of tooth loading around the helix. By integrating the tooth load along the thread, the load distribution can be determined both around a portion of the thread helix for an individual tooth or around each circumference to compare with a 2D analysis.

The model in Appendix A after Sopwith requires a knowledge of the tooth deflection. By using the same tooth stiffness in both Sopwith and the mathematical model, the two analyses can be compared. The Sopwith analysis predicts the tooth loading around the helix in 3D form which can be integrated around the helix to allow comparison with the 2D model proposed here. The result of such a comparison are given in Figure A5 and it is seen that there is excellent agreement for the 2D case. The results for the tooth load distribution around the first two teeth are shown in Figs. A6 and A7 and this shows the variation in tooth load around the helix. The result from the 2D analysis is also shown as the mean load. This indicates the effect of the 2D modelling and the load averaging implicit in the model. It is seen that for the thread geometry investigated, this effect represents an underestimate for the most highly loaded tooth of around 15% when the 2D analysis is used.

4.4.4 Modelling Preload Effects

All of the above comparisons are for un-preloaded models simply because the modelling of preload with other techniques is difficult (for FE) or impossible (for Sopwith). One of the major benefits of the modelling proposed here is that preload can be easily accounted for. The effect of preload is demonstrated by using the same geometry as for the previous comparison with Sopwith. Figure 4.27 shows the effect of a preload at the free end of the box. It is seen that the majority of the preload is taken on the first few teeth. Figure 4.28 shows the effect now of applying a tensile load to the coupling. It is seen that the combined effect of preload plus tension results in only a small increase in the tooth load distribution at the preloaded end. Figure 4.29 shows the net effect of the tensile load when applied to both a preloaded and unpreloaded joints of identical geometry. This clearly demonstrates the preload benefit in terms of the result of applied dynamic loads. Note however that this benefit in reduced dynamic loading is at the expense of a high mean load (due to the preload alone).

These results show the way in which the preload effect is local to the end at which it is applied, the opposite end of the coupling receiving no benefit. Ideally preload should be applied to both ends simultaneously although the practicalities of achieving this and, probably more important, knowing that this has been achieved, has precluded its use from any commercial designs.

Preload is the most important mechanism for reducing dynamic stresses in threaded connections and for this reason it is important to consider very carefully how the preload mechanism works and how the benefits are derived. The model described above is ideal for such a study of the fundamentals of threaded connection behaviour.

Consider firstly the joint under preload only, the results for which are shown in Figure 4.27. It is noted that the peak load is at the tooth nearest the preloaded face and that the preload dies away to almost zero at the free end of the pin. Figure 4.30 shows the load distribution under preload and it is noted that all forces are balanced and that the net force across any section is zero.

As a load is applied, it is noted that the tooth load increases as shown in Figure 4.28. The combined effect is that the end of the box is still in compression and that the forces across any section have now changed, the magnitude of the change being the applied load. Note that in this case, the ratio of ***applied*** load in pin is 45.6%. Note that the cross section of the pin as a % of the total section is 48%. The preload therefore makes the joint behave similarly to as if it were a solid section. Using this simple model it is then seen that the load being transferred from pin to box is reduced and hence the effect of the applied (dynamic) load on the teeth is reduced.

4.5 HYBRID APPROACH TO STRESS ANALYSIS OF THREADED CONNECTIONS

The purpose of the tooth load model was to provide loadings that could then be applied to a second model to give stresses. It has already been seen that the stress acting at the thread roots are a combination of stresses due to tooth loading and notch effects (Chapter 3 Section 3.6.2).

Having derived the load distribution in the connection, simple FE models can be used to derive the stresses. In actual fact, the same FE model can be used to define the tooth stiffness to enable this to be applied directly into the tooth load model. This analysis technique is applicable to both the pin and box.

4.5.1 Method of Analysis

A small part of the coupling is modelled using the FE technique. For this, three teeth are modelled to represent three of the teeth in the complete coupling. Since this mesh is used solely for the calculation of stresses, it is not necessary to model the pin and box as meshing.

Consider the analysis of the pin member. A typical mesh is shown in Figure 4.31 where it is seen that only one tooth is modelled in great detail, in order to obtain good results for stress. The other teeth are used to provide the geometry to enable a multiple notch effect to be modelled and in order to simulate correctly the transfer of tooth loading into the pin body. Note that this is an axisymmetric analysis.

The tooth stiffness is derived by applying a uniformly distributed load to the contacting portion of centre tooth and observing the deflection of the root due to that tooth load. Only the deflection due to tooth load must be considered since the absolute tooth deflection would incorporate the axial stiffness of the pin between the tooth and support which is not required. Having determined the tooth stiffness using the FE model as described in Section 4.4.1., this can be directly input to the tooth load model to establish the load distribution in the whole connection.

The load distribution gives not only the tooth loads but also the load in the pin (or box) at any tooth. It follows that this information can then be input into the FE model to determine the stress acting at the thread root due to both tooth local and notch effects (due to stresses in the body of the pin).

For a tapered connection, the pin section area is reducing from the fixed to free end and hence the pin area at any tooth is different. Obviously one method of analysis would be to choose the tooth of interest and then model the exact geometry of the pin at that point using the simple FE model. However, this would necessitate the modelling of a different geometry at each tooth section. Since the aim of this work was to produce a simplified analysis, this approach was considered inappropriate. An alternative approach adopted was a parametric study of the combined stress effect for all teeth.

The maximum stress acting at any tooth can be defined as

Th $\sigma_i = K_{t_i} \times S_i$

$\sigma_i = K_{t_i} \times S_i$

Where K_{t_i} = SCF for that tooth

S_i = local nominal stress acting at the tooth section

$_i$ = tooth number

Note that in this case, the nominal stress acting at each section is different and hence the definition of SCF used here is the local SCF and is different to that used in Chapter 3. The use of K_{ti} allows a general expression for any tooth to be derived and it is considered that such an approach would be advantageous for a parametric study. However, it must be noted that the tooth with a highest value of K_{ti} is not necessarily the most highly stressed tooth since S_i for that tooth may be low.

Referring to Figure 4.32, the load in the pin at the i^{th} tooth is given by

Pin Load = ΣP_i where

P_i = Load on tooth $_i$

S_i = $\left(\sum_{i=1}^{i} P_i \right) / A_i$

Figure 4.33 shows load case 1 for the simple FE model and is used to obtain the effect of the notch effect due to an applied axial load on the pin body. Note that the SCF at the centre tooth only is considered. The other 2 teeth introduce a multiple notch feature to simulate adjacent teeth in the coupling. Figure 4.36 shows a qualitative example of the stress distribution due to an axial load, the results are plotted as stress contours. It is seen that the stress in the body of the model is uniform remote from the centre tooth, confirming the modelling is satisfactory. The notch SCF at the thread roots is clearly evident. Stresses local to the loaded end can be ignored. Figure 4.34 shows load case 2. This is used to determine the effect of tooth loading on the stress at the thread root.

Note in all cases that only the centre tooth is considered, the adjacent teeth simple being included to represent the effect of local notches. Note also that it is important to ensure that the coupling body is modelled at an appropriate thickness to ensure free surface effects are properly incorporated.

By using the principle of superposition, the effect of the ratio of tooth load to axial load ($P_i/\Sigma P_i$) can be established from load Cases 1 and 2.

Note that for the tooth nearest the free end of the pin or box, $\Sigma P_j/P_i = 1$.
Using this approach, since the analysis is linear elastic, it is possible to deduce the way in which the stress concentration factor at the thread root varies with the ratio $\Sigma P_j/P_i$. Figure 4.35 shows this effect for the geometry used in the FE analysis. This shows the way in which the value of K_{ti} varies with the ratio of tooth load. When compared with the FE results given in Chapter 3, there is a discrepancy at the teeth nearest to the fixed end of the pin (Tooth 25) where the stress predicted from this model is lower than that from the FE analysis.

However, the results from the remainder of the joints are in good agreement. This agreement exists despite the fact that the tooth load was overpredicted compared to the FE analysis. A similar situation was found when this approach was used for the analysis of a connection with 'V' threads [40]. The results are given in Table 4.2.

An analysis was conducted to investigate the effect of thread root radius on the calculated stresses. As would be expected, the effect of root on the tooth stiffness was small, resulting in only a small change in load distribution as shown in Figure 4.37. However, the effect on the SCF was significant as evidenced in Figure 4.38. Figure 4.39 compares the tooth load distribution obtained from the model by using the stiffness calculated from the FE model and that calculated theoretically. It can be seen there is very little difference, confirming the suitability of the two approaches.

The above situations have indicated the applicability of the technique to situations where the wall thickness is large compared to the tooth height. In these situations, the nominal section stress is not affected significantly by minor changes to the tooth geometry since the radius is remote from the opposite face of the coupling. This situation applies to the thick walled forged type of tether.

The situation for the thin walled connection is however different in that the wall thickness can in some cases be similar to the tooth depth. In this case, the same approach can be used except the effect of the back wall must be accounted for. Such a joint has been analysed by Broadbent (15) using photo- elastic techniques. The model described here can be used to compare the photo- elastic results with those from this model. Before detailing the analysis, it is interesting to compare the thin walled case to that of the thick walled connection.

For a thick wall, the notch due to the tooth is small compared to the wall thickness and hence changing the radius at the notch root affects the notch depth and hence the nominal stress at that point by only a small amount. However, increasing the root radius would be expected to reduce the SCF at that point. This effect is seen in Figure 4.38.

For a thin walled connection, increasing the root radius, whilst maintaining the same loaded tooth area results in an increase in effective tooth depth. The result would be a net increase in the nominal stress acting at that point, since the net section area reduces whilst the improved root radius will decrease the SCF.

Thus the effect is one of conflicting situations with local SCF reducing whilst increasing the nominal stress. This effect can be investigated using the proposed model and is being studied by Newport [39] as an extension of this study to investigate the optimisation possible of threaded connection design.

However, the effect of back wall proximity is important when analysing taper in thin walled connections. This will be demonstrated by comparing the result of Broadbent [15]. The connection modelled is shown in Figure 4.40 and it is seen that the connection is a thin walled joint with taper.

The simple FE model was used to investigate the effect of wall thickness on the value of K_{ti} and the results are shown in Figure 4.41 for the maximum wall thickness, minimum wall thickness and an intermediate value. These results are used to allow interpolation for the specific wall thickness at the point of interest, thus allowing the stress at any point, knowing the tooth load and wall thickness.

The results so obtained are given in Figure 4.42 where they are compared with those of Broadbent. It is seen that there is good agreement for most of the coupling but with a discrepancy in the stresses predicted at the two extremes.

Close examination of the geometry studies by Broadbent shows that half of the first tooth has been machined to form a thread run out, thus the tooth section is decreasing resulting in high stresses at the last half pitch. For the last tooth, a full tooth has been included whereas

in the photo-elastic model only half a pitch was present. This is likely to account for the discrepancy although it must be noted that it is unusual to have partial teeth or thread run outs in the load carrying portion of a connection.

Recent studies [40] on drillpipe connections have compared the stresses predicted by the simple model to those predicted from axisymmetric full meshing models.

A range of geometries and loading levels were investigated and the results are summarised below. Two thread forms studied were 6$_{5/8}$" REG threads and 4$_{1/2}$" NC50 threads, both of which have 60° V forms. Table 4.2 compares the maximum thread root stress calculated from a full 2D FE model and from the Hybrid Approach developed here. It is seen that for both preloaded and unpreloaded connections, the results compare extremely well.

4.5.2 Discussion of the Model Proposed

The proposed hybrid model allows a rapid assessment of any threaded connection to be made. The model was developed to allow parametric studies of threads to be conducted in order to allow optimisation to be carried out. The possibilities for thread optimisation are vast and only with such a model could these be considered. A follow on study by Newport [41] will use the tools developed here to study the optimisation of thread design for threaded connections.

The work so far has concentrated on the establishment of procedures to determine the stresses acting due to applied tensile loads in complex threaded geometrics (tapering connections) with buttress or modified buttress thread forms.

The tooth load distribution obtained from the model has been compared with the results from full 2D FE analyses and with 3D mathematical modelling and the model is seen to compare well with such techniques. The model benefits in that preload can be easily incorporated into the analysis, a major shortcoming of the other methods.

The stress distribution obtained from the model have been compared with full 2D axisymmetric FE analysis and with the results from a photo-elastic study. Where direct comparisons are possible, the results have been extremely encouraging.

The accuracy of the modelling is difficult to assess due to the lack of results from other techniques with which to compare. However, it does appear that, compared to the FE analysis, underestimates of the stresses may occur at high tooth loads. This effect is at first difficult to explain since the agreement for 24 out of 25 teeth were good. It is considered that the underestimate may be due to assumption of a uniform through thickness (nominal) stress at each tooth. It is likely that this could be non-conservative since at the extremes of the connection, where the tooth load is increasing rapidly, the loads from preceding tooth do not have a chance to disperse into the section resulting in a non-uniform stress distribution with higher than average stresses at the thread root, resulting in greater peak stresses than predicted using the mean section stress. The reason this occurs only at the ends is that the percentage load taken by the teeth is greater at the extremes leading to a greater percentage error. Notwithstanding this, it is considered that the model provides a powerful tool for the comparison of alternative designs and is considered to be a major contribution to the analysis of threaded connection. It is unlikely that full design optimisation could be achieved without such a tool.

By using such a model, a study has been conducted into the stresses acting at the thread roots of drillpipe [40]which represents a thick walled threaded connection. The results of this have been plotted as load capacity, defined as the inverse of the maximum local root stress per unit load. An example of the results obtainable is given in Figs. 4.43 and 4.44 where it is seen that the modelling technique allows for comparison of the stresses in different connection sizes and types.

The complexity of analysis of a threaded connection does however present a problem to the designer, that of verification of analysis. For a critical component such as a tether, on which the integrity of the whole structure depends, it would be wrong to suggest that the analysis from a simple model such as that proposed would be adequate. It is therefore recommended that a final design be fully evaluated using at least one other analysis technique. Having finalised a design, the most appropriate analysis would probably be a full 3D photoelastic study to obtain detailed stress information. Alternatively a 2D axisymmetric full FE analysis could be conducted, taking due account of preload and a "correction" factor applied to take into account any underestimate of stress around the first tooth probably adopting a modified Sopwith analysis as detailed in Appendix A.

4.6 PREDICTION OF CYCLIC STRESSES FOR FATIGUE ANALYSIS

The modelling conducted here under axial loading indicates that the most highly loaded teeth are those at the extremes of the threaded connection. Considering now the load at any section of the connection, the highest combination of body load and tooth load occurs for the box at the root of the thread nearest the fixed end of the box and for the pin at the root of the first thread nearest the fixed end of the pin. It is therefore clear that for an unpreloaded section, there are two potentially critical locations from a cyclic stress standpoint.

4.6.1 Loads in Unpreloaded Joints

For an applied load, the tooth load prediction from the analog model allows the load distribution due to that applied load to be predicted. For a cyclic applied load, the cyclic load distribution is again predicted directly. Consider a connection loaded under a mean load of 500 kN and a cyclic load of ±300 kN. The effect of the static mean load only can be predicted using an input load of 500 kN, the situation at the minimum load of Mean -300 can be investigated and the situation at a load of mean +300 can be investigated. The cyclic load effect can then be deduced. However, since the system is elastic, there is no need to go through these steps since, providing the load is always tensile, a reasonable assumption for a tethering system, an input of the load range gives an immediate result for the dynamic load range in the joint. Thus the results so calculated will automatically give dynamic stresses and SCF's, which are the ones which affect fatigue and growth behaviour.

4.6.2 Loads in Preloaded Joints

For the preloaded connection, the situation is rather different in that the absolute tooth loading on any given tooth is not directly proportional to the applied load. There is therefore an apparent non linearity in the system as indicated in Figure 4.45 where it is seen that as the applied load is doubled from 40 to 80, the total tooth load on tooth changes by only 68%. This is easily explained however by considering the change in load, from the preload condition due to the two applied loads. This is shown in Figure 4.46 where it is now observed that the effect is in fact linear and it is observed that the preload acts as a static offset and thus the tooth load due to preload should not be considered in any fatigue crack growth calculations.

To summarise, the model can be used to predict fatigue loads due to applied cyclic stresses by considering only the dynamic (reduced) tooth loading attributable to the applied load and ignoring the effect of the static preload.

4.6.3 Calculation of Stress

It is seen therefore that for preloaded and unpreloaded models, the system behaves totally linearly with a doubling of the applied load resulting in a doubling of all tooth loads associated with that applied load, although care must be taken when assessing preloaded joints.

The derivation of a single SCF value for any thread root therefore holds for both the preloaded and unpreloaded cases but the SCF for the two cases is not necessarily the same. It is important to consider again how SCF is defined. The requirement for dynamic stresses due to externally applied cyclic loads enables the concept of dynamic SCF to be employed and this will be defined here as follows:-

$$\text{Dynamic SCF} = \frac{\text{Thread root stress due to applied load}}{\text{Nominal stress away from the thread due to that applied load}}$$

See Figure 4.47

Note that for such a definition, one will expect very low SCF values for preloaded connections where the site studied is benefiting from the preload effect. Note also that this definition of dynamic SCF means that a comparison of SFC's provides a comparison of local stresses ie high SCF's means high local stress. For preload at the free end of the box, the tooth load on the pin at the preloaded end is low as is the nominal load in the pin since part of the load is transferred directly to the box. Hence $SCF_{DYNAMIC}$ is low on two counts. It is particularly interesting to note that in actual fact, SCF dynamic = SCF_{LOCAL} (as defined in Section 4.6.1). This is due to the fact that, since the load is shared across pin and box due to the preload, the nominal stress remote from the thread is identical to the nominal stress at the critical section.

It is also interesting to note that for the preloaded box end, the other end of the box has a similar SCF for preload or no preload. (Since there is little benefit to the box under this preload configuration.)

4.6.4 Effect of Geometry

One major benefit of the tooth load model is that one is able to investigate the effect of geometry very easily. In order to do this, a number of geometries have been modelled to investigate the effect of:-

1. Bore Diameter (Pin ID)
2. Outside Diameter (Box OD)
3. Tooth Height
4. Pitch
5. Taper
6. Number of Teeth

on both preloaded and unpreloaded joints.

4.7 RESULTS

The analog model developed can be used to conduct studies into the effect of various design parameters on the behaviour of threaded connections. The following sections give details of an investigation into the effect of various geometric parameters. The choice of basic joint geometry is arbitrary, Figure 4.48 and Table 4.3 give details of the geometries investigated. In all cases, the geometry of the joint denoted Case 1a is a reference.

The effect of six parameters were studies. Both preloaded and unpreloaded joints are considered. The 6 general cases are shown in Table 4.4

4.7.1 Unpreloaded Connections

4.7.1.1 Case 1 - Pin Bore of Unpreloaded Joint

The internal diameter of the connection influences the axial stiffness of the pin in the threaded area. For an unpreloaded connection an increase in bore diameter results in a decrease in pin stiffness. There is therefore an expected increase in the tooth loadings on the first loaded teeth of the pin as the load transfers to the stiffer section. This is matched by a decrease in the tooth loading at the first loaded tooth of the box (Tooth 1) since the load is concentrated away from the less stiff section. This effect is shown in Figure 4.49.

It is seen that as the pin ID reduces, that is, the section area increases, so the tooth loading becomes more symmetrical. When these results are plotted in terms of the sectional areas Figure 4.50 it is seen that as the sectional areas of pin and box become equal, so the tooth

load distribution becomes symmetric with the tooth at the critical section of the pin and box taking identical loads. Note that this will also result in identical thread root stresses since the nominal axial stresses at each section are also identical.

4.7.1.2 Case 2 - Outside Diameter - Unpreloaded Section

As would be expected from the discussion above, the effect of changing the OD of the connection has a similar effect to changing the box ID since again, the effect of changing OD influences the relative stiffness of the section and hence the rate of load transfer from pin to box. This is shown in Figure 4.51 and it is again possible to replot this data in terms of relative pin and box areas and the ratio of the tooth load at the first loaded tooth of pin and box, Figure 4.52. As would be expected from the pin results, this confirms that symmetry of loading is reached as the ratio of areas of the two components reach unity.

4.7.1.3 Case 3 - Tooth Height - Unpreloaded Section

The effect of tooth height is in fact difficult to isolate from other parameters. In this study, the pin ID and box OD were held constant. In order to model a fully meshing tooth of different height it is necessary to also change the root diameter of pin and box. Thus there is an influence of both the tooth height itself and the change in relative stiffness of the pin and box sections. However, a 1mm change in box and pin ID would result in only a small effect on the tooth load and hence the results from such a study will be secondary effect. The results are shown in Figure 4.53 where it is seen that a change in tooth height of 1mm affected the peak tooth load by between 10% and 15%. Figs.4.49 and 4.51 indicate the effect of change on the diameter would affect the tooth load by between 2% and 5% over the same range, for the tooth height chosen.

Figure 4.53 shows the effect of tooth height to be similar on the peak tooth loads for both pin and box, leading to a symmetric effect. It is seen that increasing the tooth height results in a more even distribution of tooth load. The reason for this is that the more flexible tooth will deflect more easily, thus leading to a take up of load in the central teeth and hence a slower transfer of load from pin to box, thus reducing the peak loading on the first loaded teeth.

4.7.1.4 Case 4 - Effect of Pitch - Unpreloaded Joint

Changing the tooth pitch has a similar influence to changing the tooth height, Figure 4.54. Changing the pitch for a given tooth height influences the tooth stiffness (in a similar way

to changing the height for a given pitch). The results are therefore as expected with increasing pitch leading to higher peak loads at the critical section due to the stiffer tooth section transmitting higher loads. Note that the effect of increasing pitch is to increase the connection length and this in turn has an influence of the relative stiffness of the tooth to the elastic stiffness of the pin and box components.

4.7.1.5 Case 5 - Effect of Taper - Unpreloaded Joint

The effect of taper was studied by reducing the pin diameter toward the free end. The taper angle (Defined as taper angle on diameter rather than radius) was varied between 0 and 18.4 degrees. It should be noted that a typical taper on a drillpipe threads is 9.5^0. It is seen, Figure 4.55, that the taper angle has a very strong influence on the peak load at the box, the reason being that the taper not only reduces the pin stiffness but increases the box stiffness at the same pint. This twofold effect on the relative stiffness means that for high taper angles the pin is much less stiff than the box and hence there is only a small load takeup in that region. The net effect is that this change in load takeup leads to higher loads on teeth away from the box critical section. Due to the load sharing with the central teeth, the increase in peak tooth load at the pin is lower than the reduction in peak load at the box.

4.7.1.6 Case 6 - Effect of Number of Teeth - Unpreloaded Joint

Figure 4.56 shows the effect of number of teeth in the connection. These results are interesting since the influence of number of teeth is seen to be very non-linear. For the connection considered, changing the number of teeth from 12 to 18 had very little effect on the peak tooth loads but that as the tooth number was reduced below 12 so the value of peak load for pin and box increased. It is noted that irrespective of number of teeth, the difference between the peak tooth load at pin and box was extremely small and varied by less than 0.25% of the applied load, Figure 4.57.

Figure 4.56 also shows how the rate of change of tooth load at the ends of the connector is similar irrespective of the number of tooth. This is due to the fact that the rate of load takeup at any section is influenced primarily by the relative stiffness at that section between pin, box and tooth. However, there is a limit to this since as the number of teeth reduces so the influence of the central teeth has relatively more importance to the overall connection geometry.

The increase in peak loading from a lower number of teeth is expected since the same load is transmitted through the connection. As the number of teeth reduces the mean tooth load increases with a resultant increase in peak loading. The most significant effect seen is that as the number of teeth is increased above approximately 12 there is little benefit to the peak loads.

It is seen that the rate of load transfer for the first and last three teeth is almost identical for the joints with 12 or more teeth with the central teeth taking proportionally less load as these numbers increase. This indicates clearly that a connection will have an optimum number of teeth for a given geometry and loading condition and that increasing the tooth numbers beyond that optimum derives no benefit.

4.7.2 Preloaded Connections

Section 4.7.1 has shown the effect of various geometric parameters on the tooth load distribution of unpreloaded connections. In the unpreloaded case the total applied load is transferred through the teeth, i.e. the sum of the tooth load for each case is equal to the applied load.

For a preloaded connection this is not the case and this has been discussed previously. The results presented here show the tooth load distribution for a number of cases and in all situations the value of load on any individual tooth is referred to as a percentage of the externally applied load. It should be noted however that due to the effect of preload, the sum of the "dynamic" tooth loads is less than the applied load and will not be equal in all cases. The last column in Table 4.3 gives details of the sum of the tooth loads for each test case for comparison.

4.7.2.1 Effect of ID - Preloaded

The effect of Pin Box on the tooth load distribution for a preloaded connection is shown in Figure 4.58. All cases show the typical behaviour of a preloaded pin indicating how the pin critical region is protected from the dynamic loadings. It is interesting to note also that the magnitude of the loading at the critical region of the box (Tooth 1) is very similar to that in the unpreloaded case. As an example, the results for Case 1a are plotted in Figure 4.59. This figure shows the effect of an identical applied load on a preloaded and unpreloaded joint. The distribution of static preload is also added, this has been calculated for an arbitrary

preload value. As would be expected, the effect of varying the bore diameter on a preloaded connection is seen to influence only the critical region of the box due to the same mechanism described for the unpreloaded connection above.

4.7.2.2 Case 2 - Outside Diameter - Preloaded Joint

Results for the influence of box OD are given in Figure 4.60. The effect of Box OD on a preloaded connection is similar to that for the unpreloaded joint except that, as for all preloaded connections, the influence is restricted to the critical region of the box, the pin being protected by the preload. As was the case for the effect of bore size, the tooth loads at the critical region of the box are very similar with or without preload.

4.7.2.3 Case 3 - Effect of Tooth Height - Preloaded Joint

The previous 2 cases showed very little effect on the absolute value of tooth load at the box with or without preload. The results for the effect of tooth height, Figure 4.61, whilst showing similar trends, do show an influence on the absolute value of tooth load as the teeth become more flexible. The explanation for this lies in the fact that as the teeth become more flexible, the load distribution was seen in the unpreloaded coupling to become more uniform. This trend is repeated for the preloaded coupling to the extent that there is an influence of applied load at the pin critical section (Tooth 15). The fact that the load distribution is more uniform, with all teeth taking the load leads to a slight reduction of tooth load at the critical box tooth.

It is also noted that there is a point in the connection where the tooth height has no effect on the tooth loading. For the unpreloaded joint, this occurs near to teeth 3 and 13. For the preloaded connection, the region is less well defined but appears to be closer to tooth No.4.

4.7.2.4 Case 4 - Effect of Pitch - Preloaded Joint

The effect of pitch has already been described as similar to that for tooth height since the pitch and tooth height combine to give a relative tooth stiffness. This effect of pitch is seen in Figure 4.62 and is seen to be similar to that for tooth height shown in Figure 4.61. It is also seen that for larger pitches (i.e. stiffer teeth for any given tooth height) there is no significant difference in tooth load at the critical box tooth (Tooth 1) between a preloaded or unpreloaded connection. However, as the tooth stiffness reduces (i.e. pitch decreases) the tooth load distribution improves and there is approximately 10% reduction in tooth load for Tooth 1 compared to the unpreloaded case.

4.7.2.5 Case 5 - Effect of Taper - Preloaded Joint

Case 5 for the unpreloaded joint showed a significant benefit of taper for the box critical region for high taper angles. Preload is expected to provide protection to the pin whilst giving little benefit to the box region. Thus there exists two competing effects in a preloaded tapered connection with the possibility of a connector design with a near uniform tooth load distribution.

Figure 4.63 shows the effect of taper angle on a preloaded connection. Comparing these results with those in Figure 4.55 shows how there is little difference in the tooth load at the box critical section with or without preload but that the effect at the pin critical region is dramatic. It is seen that for a preloaded connection, increasing the taper angle reduces the peak load at the box whilst increasing the peak load at the pin. For an angle of 18.4^0 the tooth load distribution is seen to be nearly uniform leading along the connection thus reducing the significance at the critical regions of pin and box. Of all of the parameters studied, the taper is the only parameter variation found to lead to a near uniform tooth load distribution.

4.7.2.6 Case 6 - Number of Teeth - Preloaded Joint

Unlike all other cases, the effect of number of teeth on a preloaded connection is very different to that observed on the unpreloaded connection. Figure 4.64 shows the effect of tooth number on a preloaded connection and it is seen that there is very little effect in the critical region (Tooth 1) as the number of teeth is increased from 6 to 18. The difference in behaviour is due to the fact that for the unpreloaded connection the total applied load is carried by the teeth whereas for the preloaded connection only a proportion of the applied load is shared between the teeth. Figure 4.64 shows that as the tooth number decreases, so the effect of the preload increases, that is to say, the proportion of the applied load carried by the teeth decreases.

At the critical section (Tooth 1) the load carried by the first tooth is controlled primarily by the local ratio of tooth stiffness to section stiffness. This ratio remains constant irrespective of the tooth number and hence the peak load remains unchanged. The tooth load distributions from 12, 15 and 18 teeth are very similar confirming the effect seen for the unpreloaded case whereby there appears to be an optimum number of teeth and that once this number has been reached there are no benefits from increasing the number further.

4.7.3 Summary

The results from studies conducted using the analog model show how various geometric parameters influence the tooth load distribution in threaded connections. The ease by which these results are obtained show the benefit of the mathematical models in rapid analysis of threaded connections to establish the important parameters for any particular design.

The study has shown how the model can be used to identify which parameters provide similar effects and which provide opposing effects.

Taper with a preloaded connection is identified as being of significant benefit in reducing the peak loads at both ends of the connection and can result in a near uniform tooth load distribution.

The results presented here are for an arbitrary connection and have been presented for each parameter in isolation. If one was commencing on a connection design, the model could be used to "tune" the connection geometry to give the required tooth load distribution. It could be possible to represent the connection behaviour in terms of a parametric equation, the parameters being those discussed here. If this is required it would still be necessary to study the effect of all parameters in isolation before the equations could be formulated. In view of the ease by which the model produces the results there would appear little benefit in deriving such equations, especially since each tooth profile would require a new data set.

The tooth load distribution identifies the most highly loaded section as well as allowing the load at any section be calculated. The model therefore provides the basic data from which further stress analysis studies can be conducted.

4.8 MODELLING OF OTHER MODES OF LOADING

The model and techniques described above have been developed for the case of threaded tether connections which are subject principally to cyclic axial loads. However, the model has proved sufficiently encouraging that its use for other situations should be considered. The other modes of loading likely are bending and torsion. For the drilling industry in particular, these three principle loading modes are all present and should be considered for further investigation. The principles are discussed here.

4.8.1 Bending

The application of a bending moment to a cylindrical section leads to axial stresses which are a maximum on the surfaces perpendicular to the loading axis and which reduce to zero at the neutral axis, the stress distribution being linear through the thickness, Figure 4.65.

It follows that if a thread is present within the section, the axial stiffness, and hence the axial strains will be different for the two members. From the earlier discussion on modelling tooth load, it is known that the tooth load distribution is dependent on the relative strains between box and pin and hence it is apparent that the application of a bending load will influence the tooth load distribution by much the same mechanism as axial loading. The problem is that there is no load axisymmetry and hence the 2D modelling is not directly applicable.

When considering bending, there are similarities with the model used for axial loading. Consider the pin and box in Figure 4.66.

At section AA, the box has the full moment acting; at BB the pin has the full moment acting. For an unpreloaded joint (with gaps across the preload force) the transfer mechanism must be via axial (shear) forces across the teeth. Note however that for this mode of transfer, compressive load transfer would be required on the teeth on the compression side of the neutral axis. For some thread geometries this is possible but on others the back faces are machined with clearance and in these geometries the axial loading to create the couple representing the moment, must be generated by a combination of compression and frictional loads. However, the example above is not very realistic since in most cases, the joint would at least be sufficiently tight that the mating (preload) faces BB in Figure 4.66 are touching. In this case, if no compression across the back of the teeth is generated, the load path is as shown schematically in Figure 4.67.

Now the compressive load P_B will be a distributed load across the section. Referring to Figure 4.67, the effective load acting on the face is P_B^1 at a radius of r_B. Now this must be balanced by a load distribution in the pin where P_P^1 is the equivalent load acting at a radius r_P. Now for the loads to balance,

$$P_P^1 = P_B^1$$

For balanced moments, the following equation holds

$$P_P^1 r_P = P_B^1 r_B$$

By inspection it is clear that this can only be satisfied if the neutral axis moves toward the compression part of the section.

Clearly this is a complex situation and one which merits further work.

Consider now the situation where a connection is fully preloaded as shown in Figure 4.68.

It has already been stated that the joint under axial load behaves as if it were welded. For bending loads the joint would be expected to behave in much the same way for the moment transfer. The moment transfer will be according to the section modulus,

$$\text{Total Section Modulus} = \frac{\pi(OD^4 - ID^4)}{64}$$

$$\text{Section Modulus of Pin at critical section} = \frac{\pi(dc^4 - ID^4)}{64}$$

Therefore

$$\text{Ratio of Moment carried by pin at critical section} = \frac{M \times (dc^4 - ID^4)}{(OD^4 - ID^4)}$$

Using typical dimensions of:-

$$dc = 1.5\ ID$$

$$OD = 2.5\ ID$$

$$M_{pin} = \frac{4.06}{38.06} = 0.1\ M$$

This compares to an axial load of P_i in the Pin due to an applied load of P

Where $\frac{P_i}{P} = \frac{\pi(dc^2 - ID^2)}{\pi(OD^2 - ID^2)} = 0.24$

Thus it is seen that the benefit for preload is extremely high under bending loads since it provides for this example a path for 90% of the applied moment.

When considering the tooth load in the pin due to the applied load, one needs to consider the transfer mechanism. Assuming the moment transfer into the pin is via a couple and considering the axisymmetric analogy, the total tooth load to transfer a moment of Mp into a parallel pin would be $\Sigma P_i = \frac{Mp}{dc}$. Where P_i is the total tooth load around the circumference and d_c is the effective diameter.

Using the example above, the axial load to produce the same tooth load is estimated as follows:

Tooth load due to moment of $M = \frac{0.1M}{dc}$

$$\Sigma P_i = \frac{0.1M}{dc} = 0.24P$$

$$P \approx \frac{0.42M}{dc}$$

Whilst this gives a first guide to the equivalence of the 2 loading modes in terms of severity, it is necessary to investigate the distribution of the equivalent axial forces before taking these comparisons further.

It is recommended that the model be reconsidered to investigate the relative strains at a thread due to an applied bending moment and that the same principle is then used to predict tooth loads due applied bending. Note that the analysis should only be conducted for a fully preloaded joint since the above discussion suggests a shift in the neutral axis for unpreloaded connection which could not be easily accommodated in the simple model.

4.8.2 Torsion

When considering torsion loading, one must first appreciate that preload is developed by torquing and that in the special case where relative movement of the pin and box are possible, applied torque manifests itself as axial loading as previously discussed. Note however that the preload situation is the result of an applied torque that has been removed. Consider now an unpreloaded joint where the torque is applied and then remains acting (i.e. this assumes a torque controlled situation where the applied torque level is maintained irrespective of displacement). Firstly it is noted that the joint is then in a preloaded situation (this means that torsion need only be considered for joints in the preloaded condition) and therefore can be analysed as detailed above. The fact that the torque is still applied has no direct effect on the axial loads generated in the connection since these only occur when there is relative movement between pin and box. The torsion load is therefore transferred via a mechanism other than shear forces across the teeth. This mechanism is friction. It is well known that one of the major problems associated with the torquing of threaded connections is the torque

used to overcome friction. For a joint under applied torsion loading 'T_o' as shown in Figure 4.69 the torsion transfers across the pin and box components via friction at the preloaded face and circumferential friction at the teeth.

It is therefore most unlikely that torsional effects, other than those which cause radial motion and hence affect preload, have any other effect at the thread root other than to affect that section as if it were part of a solid section. Referring again to Figure 4.69 one could consider two extremes.

Condition 1 is where the torsion is taken over the preload shoulder only, i.e. there is no elastic torsion in the pin.

For case 1,

$$\tau max = \frac{16T_o(OD)}{\pi(OD^4 - dc^4)}$$

$$\tau crit = \frac{16T_o(dc)}{\pi(OD^4 - dc^4)}$$

Using the sample sizes above

$$\tau crit = \frac{0.23T_o}{ID^3} \quad \text{at box root}$$

The second case is where the pin takes torsion load according to its torsional stiffness. Since the ratio of torsional stiffness of two hollow sections is identical to the ratio of section moduli, it follows from above that an applied torque of T_o' will result, using the above assumption, in a Torsion load of 0.1T in the pin.

For case 2,

$$\tau max = \frac{16T^1(dc)}{\pi(dc^4 - ID^4)}$$

$$= \frac{1.8T_o^1}{ID^3}$$

$$= \frac{0.18T_o}{ID^3} \quad \text{at pin root}$$

Thus it is seen that there is little difference in the result for the two conditions and that pin and box are similarly stressed. Note this has no effect whatsoever on the applied tooth loading and therefore no further modelling is required to predict tooth loads under torsion loading. It is recommended however that the effect on crack growth be investigated, particularly for a crack in the box.

This does raise an important point whereby it is seen that under torsion or bending loads, cracks in the box are growing into an area of increasing nominal stress whereas for the pin, the effect of torsion on bending leads to a reducing driving stress as the crack approaches the neutral axis.

	F.E.	Photo E.	Math Modelling	Proposed Model
2D Axisymmetric Analysis	✔	x	x	✔
3D Analysis	x	✔	✔ ?	x
Tooth Load Dist.	✔	x	✔	✔
Stress Analysis	✔	✔	x	✔
Tapered Geometry	✔	x	x	✔
Preload Considered	Difficult	✔	x	✔
Elastic/Plastic Analysis	✔	x	x	x
Easy to Use	x	x	x	✔
Flexible	x	x	✔	✔
No Special Equipment Required	✔	x	✔	✔
Quick to Use	x	x	✔	✔

Table 4.1 Capability of Thread Analysis Techniques

Model No.	Thread Form	Dimensions			Preloaded	Max Thread Root Stress	
		ID(mm)	OD(mm)	Length(mm)		FE	Hybrid
1	41/2" NC50	95.2	161.9	219	No	138	156
	41/2" NC50	95.2	161.9	219	Yes	69.6	68.8
2	65/8" REG	71.4	190.2	259	No	122	133
	65/8" REG	71.4	190.2	259	Yes	155	163
3	65/8" REG	71.4	210	259	No	648	700
	65/8" REG	71.4	210	259	Yes	369	393
4	65/8" REG	71.4	210	385	No	676	700
	65/8" REG	71.4	210	385	Yes	332	392

Table 4.2 Comparison of max thread root stresses derived using FE and Hybrid model [Ref.40]

Test Case	PIN ID(mm)	PIN OD(mm)	BOX ID(mm)	BOX OD(mm)	Tooth Height(mm)	Pitch(mm)	No.of Teeth	Taper Degs.	Preload Details for model Pin Area	Box Area	Stub (mm)	% of load transferred by teeth Preloaded Joint
1a	50	100	108	140	4	8	15	0	5890	6232	15	48.1
1b	40	100	108	140	4	8	15	0	6597	6232	15	49.2
1c	60	100	108	140	4	8	15	0	5027	6232	15	44.3
1d	70	100	108	140	4	8	15	0	4005	6232	15	38.9
2a	50	100	108	120	4	8	15	0	5890	2149	15	73.2
2b	50	100	108	130	4	8	15	0	5890	4112	15	58.6
2c	50	100	108	150	4	8	15	0	5890	8510	15	40.3
3a	50	101	107	140	3	8	15	0	5890	6232	15	48.4
3b	50	99	109	140	5	8	15	0	5890	6232	15	47.5
3c	50	98	110	140	6	8	15	0	5890	6232	15	46.4
3d	50	97	111	140	7	8	15	0	5890	6232	15	44.9
4a	50	100	108	140	4	6	15	0	5890	6232	15	46.3
4b	50	100	108	140	4	7	15	0	5890	6232	15	47.5
4c	50	100	108	140	4	9	15	0	5890	6232	15	48.4
4d	50	100	108	140	4	10	15	0	5890	6232	15	48.5
5a	50	60/100	68/108	140	4	8	15	18.4	5890	6232	15	41.0
5b	50	70/100	78/108	140	4	8	15	14	5890	6232	15	42.7
5c	50	80/100	88/108	140	4	8	15	9.5	5890	6232	15	44.4
5d	50	90/100	98/108	140	4	8	15	4.8	5890	6232	15	46.2
6a	50	100	108	140	4	8	6	0	5890	6232	15	39.3
6b	50	100	108	140	4	8	9	0	5890	6232	15	45.0
6c	50	100	108	140	4	8	12	0	5890	6232	15	47.3
6d	50	100	108	140	4	8	18	0	5890	6232	15	48.4
6e	50	100	108	140	4	8	7	0	5890	6232	15	
6f	50	100	108	140	4	8	8	0	5890	6232	15	

Table 4.3 Details of Test Cases

Case	**Parameter Studied**
1	Pin Bore (ID)
2	Box OD
3	Tooth Height
4	Tooth Pitch
5	Taper
6	Number of Teeth

Table 4.4 Parameters Investigated in the various test cases

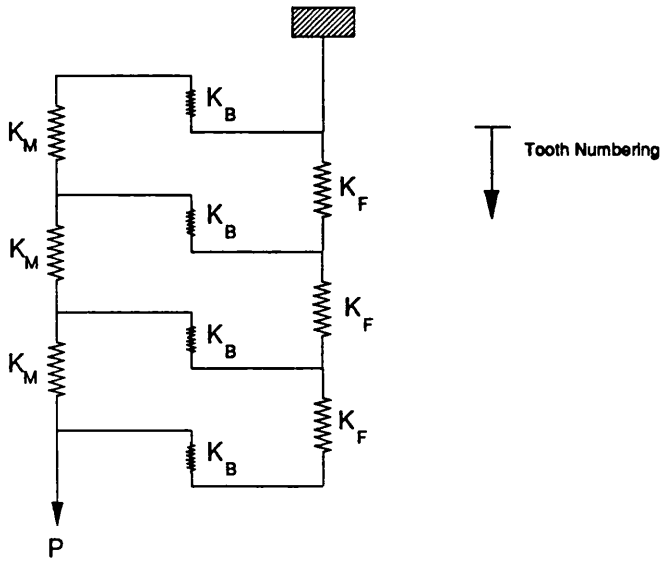

Fig. 4.1 Representation of a threaded connection by a series of springs

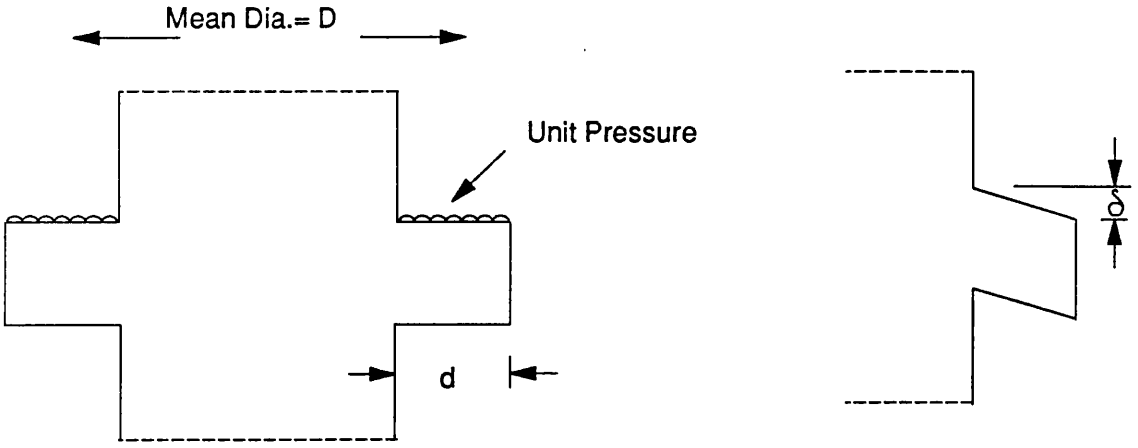

Fig. 4.2 Representation of tooth as an annular cantilever

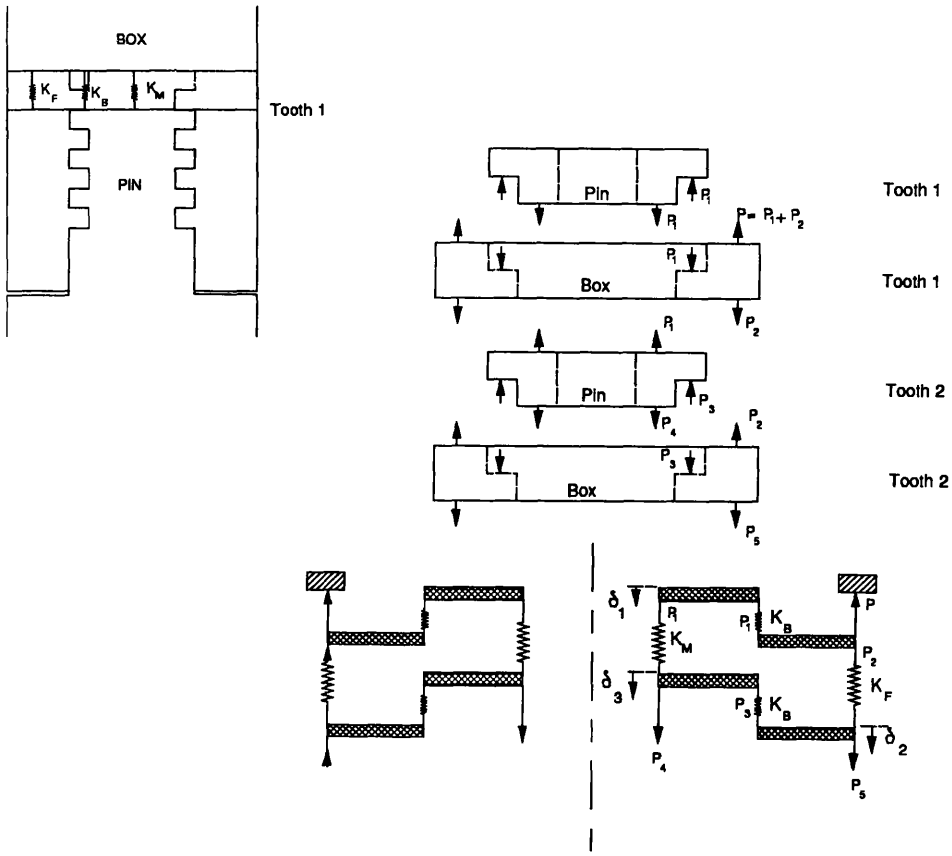

Fig. 4.3 Simple model of 2 teeth nearest free end of pin.

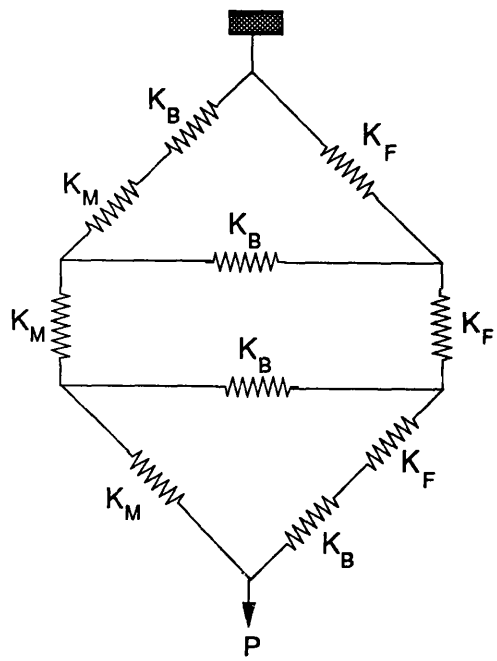

Fig. 4.4 Network representation of the mechanical model shown in Fig.4.1

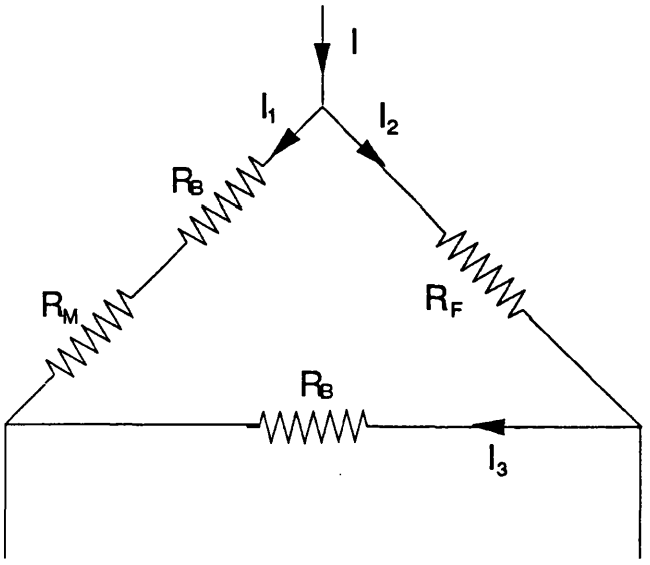

Fig. 4.5 Electrical representation of mechanical model shown in Figure 4.3

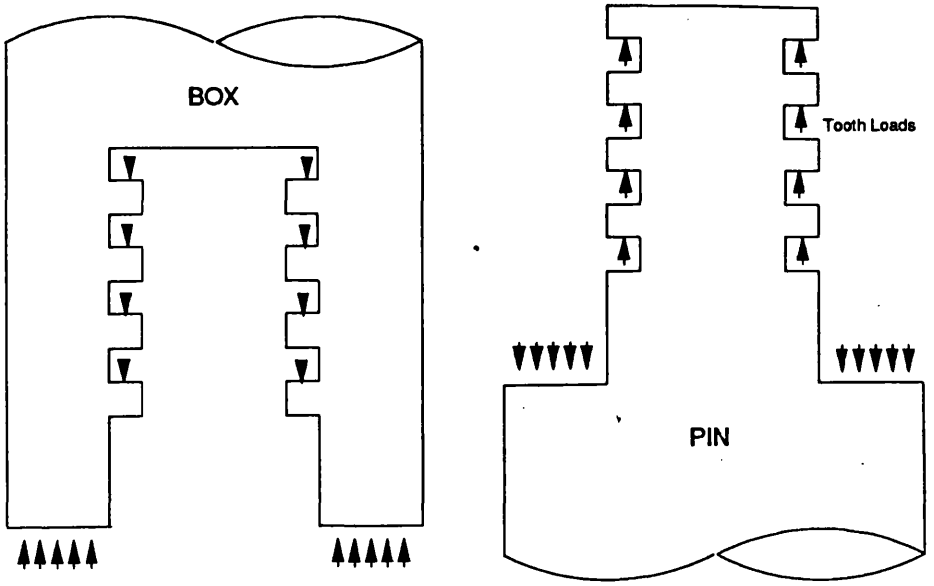

Fig. 4.6 Threaded Connection Under Preload

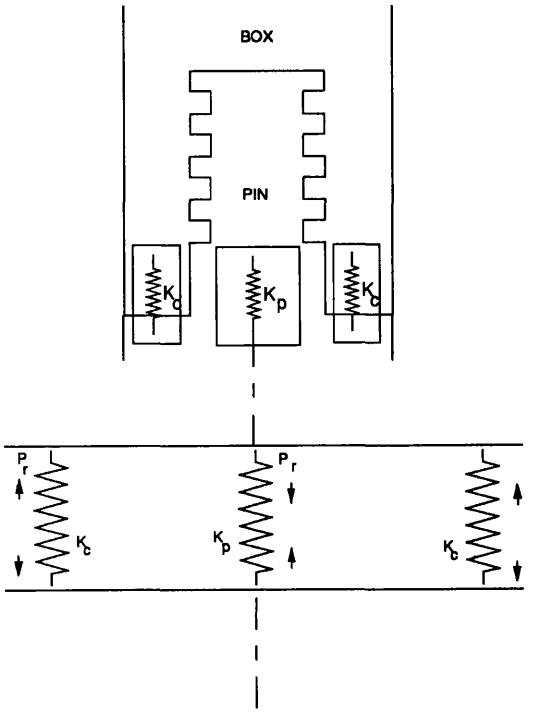

Fig. 4.7 Simplified model of preload condition

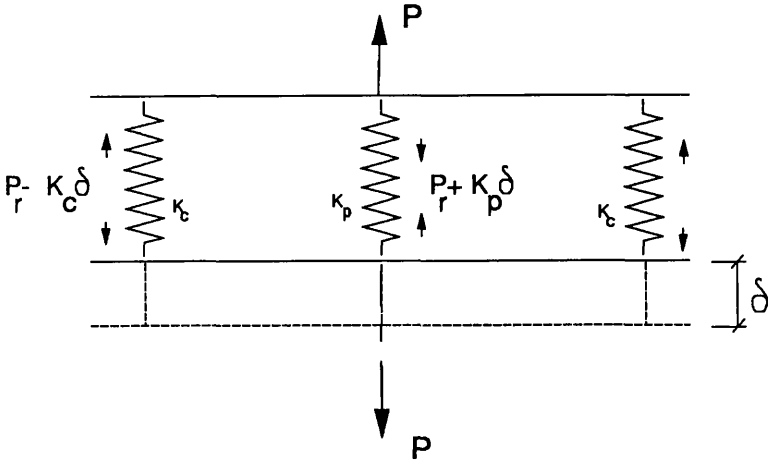

Fig. 4.8 Effect of externally applied load on a preloaded connection

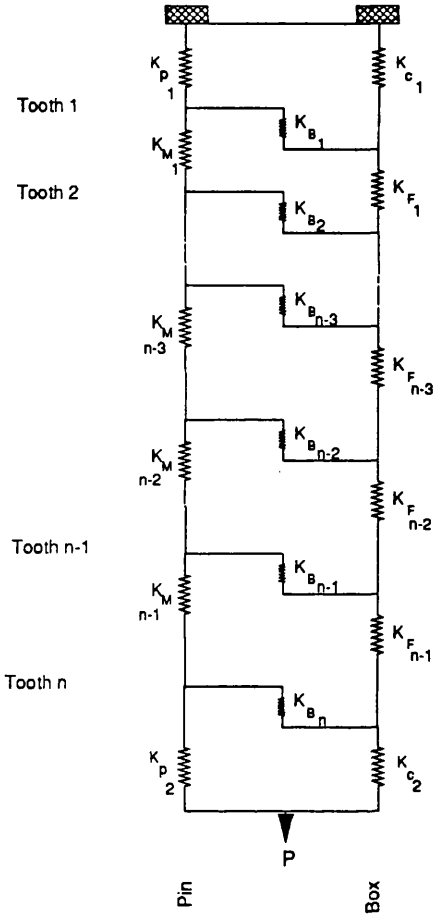

Fig. 4.9a Mechanical Model

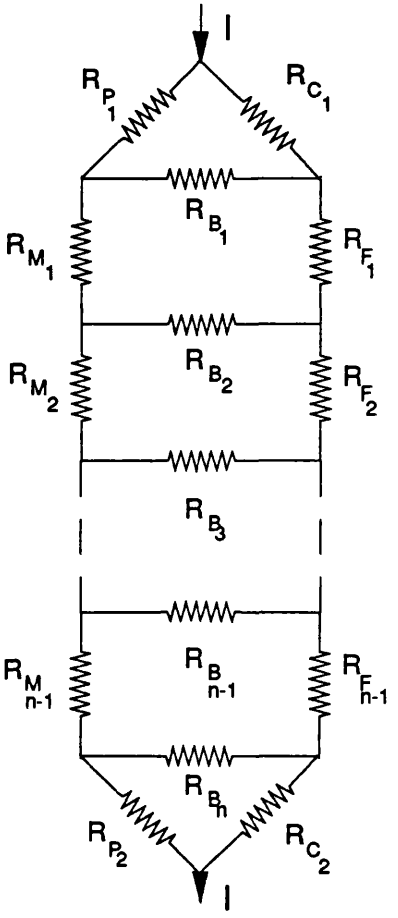

Fig. 4.9b Electrical Model

Fig.4.9 Representation of complete model with facility for preloading both ends

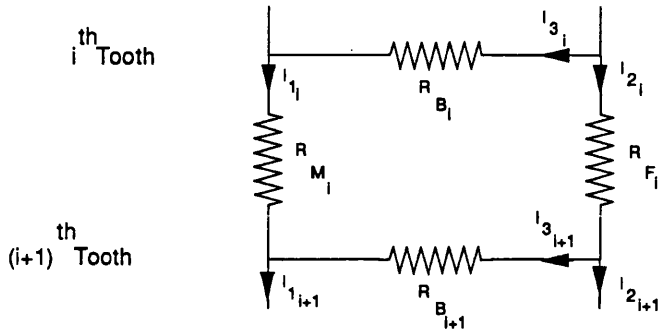

Fig.4.10 Model of General Tooth Load Case

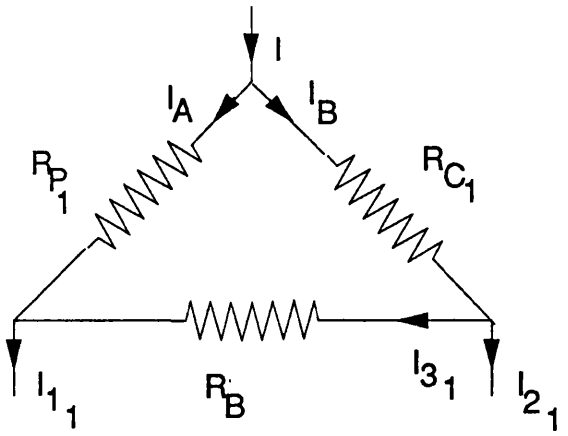

Fig. 4.11 Model of Tooth Number 1 (free end of pin)

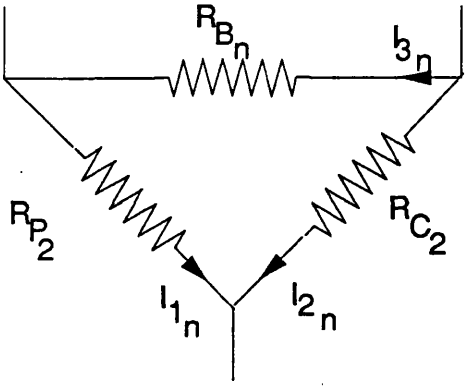

Fig.4.12 Model of Last Tooth

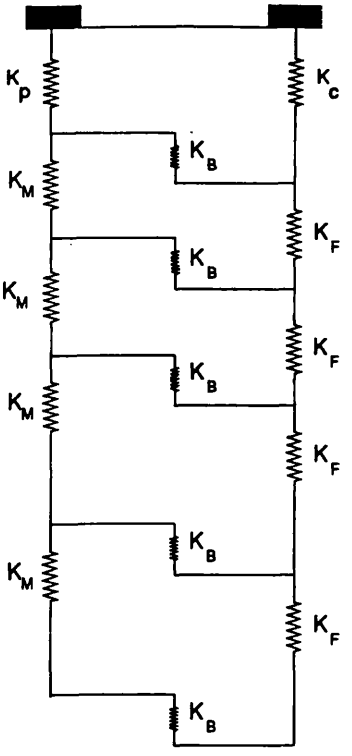

Fig 4.13 Mechanical Model of Preloaded Joint (Preloaded at free end of pin)

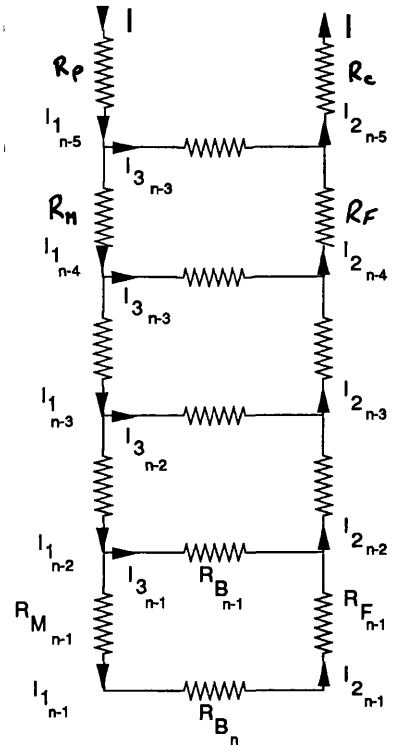

Fig 4.14 Electrical Model of the Preloaded Joint shown in Fig.4.13

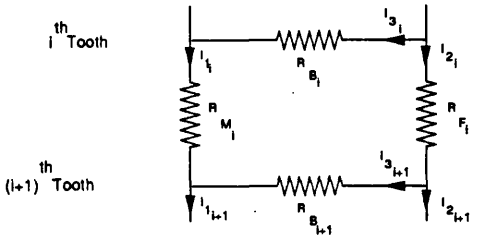

Fig 4.15 Model of General Tooth

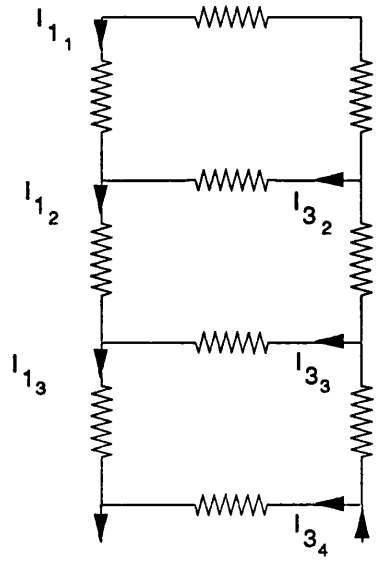

Fig. 4.16 Model of Preload at Free End of Box

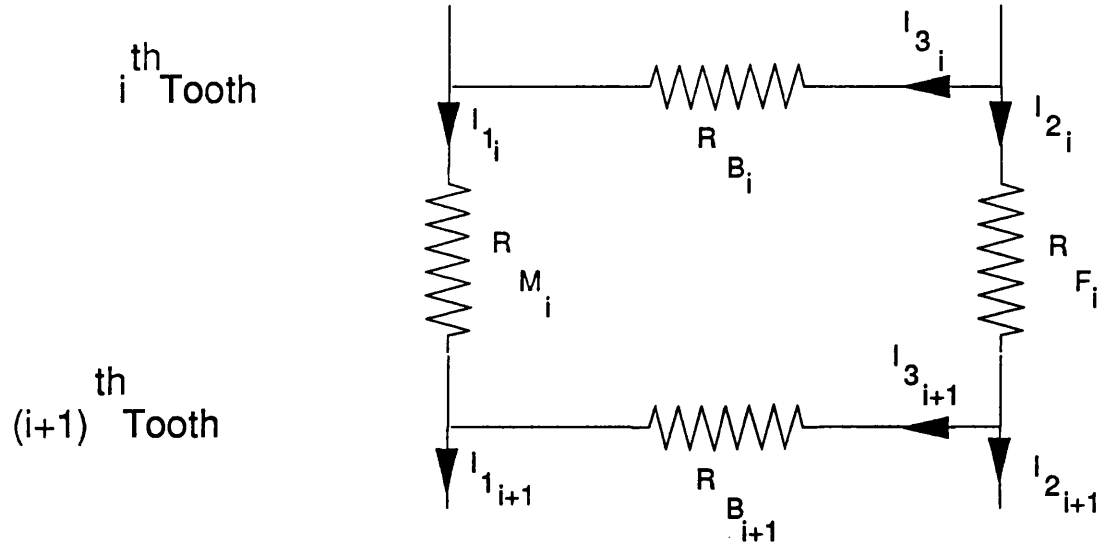

Fig. 4.17 General Case For Tooth

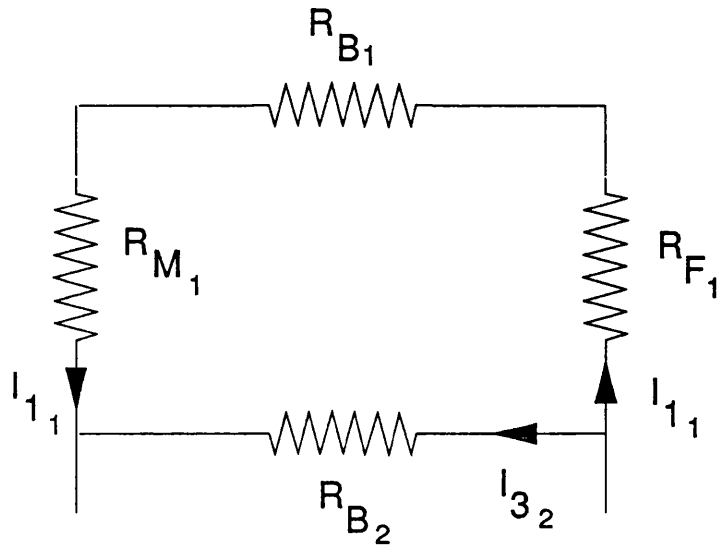

Fig. 4.18 Model of First Tooth

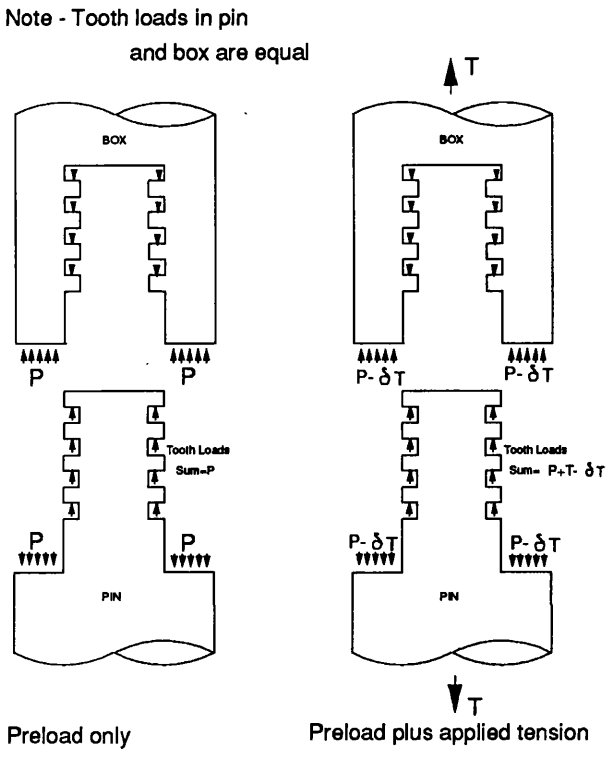

Fig. 4.19 Loads acting on a preloaded connection

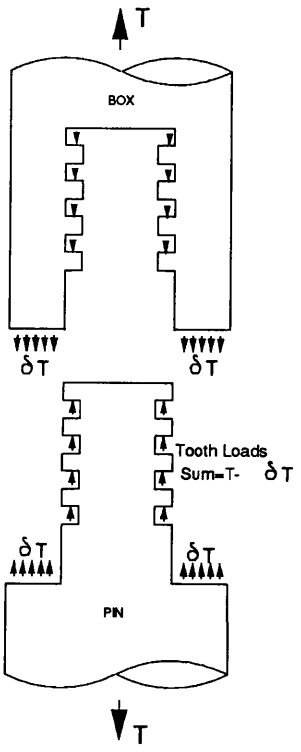

Fig. 4.20 Loads From General Model

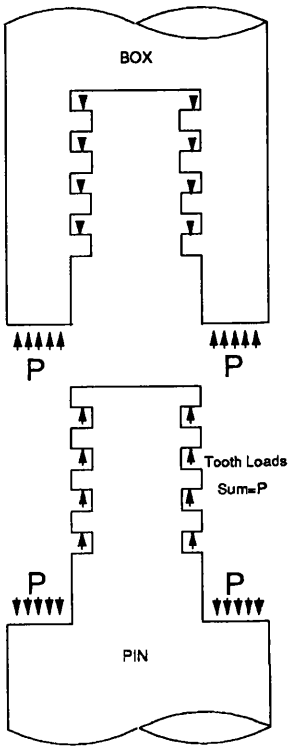

Fig. 4.21 Loads From Preload Model

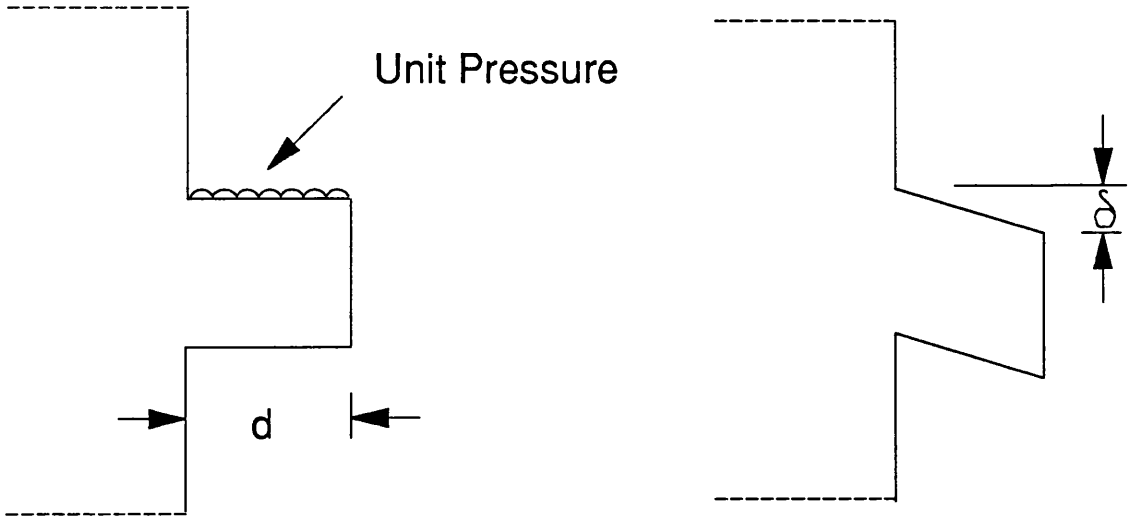

Fig.4.22 Model used for Tooth Stiffness Derivation

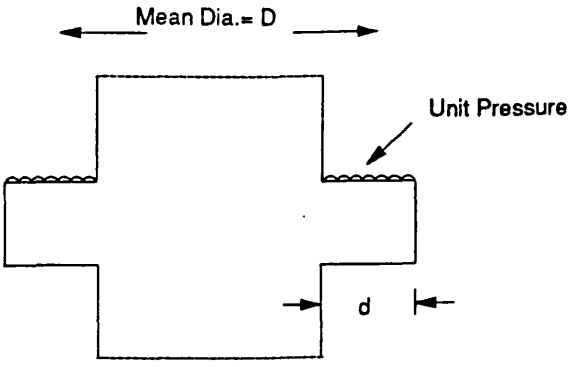

Fig.4.23 2D Representation of Thread Loading

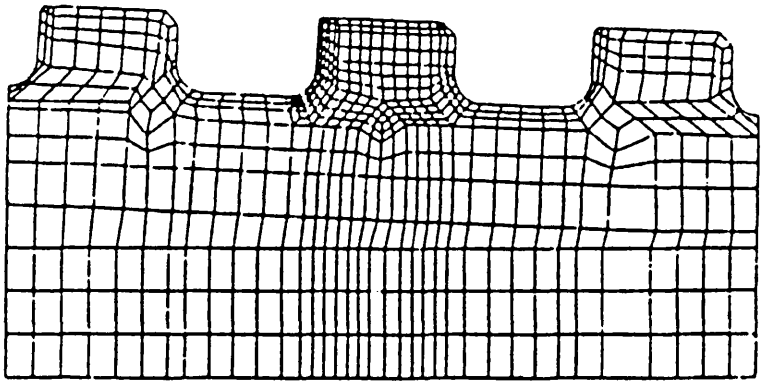

Fig. 4.24 Example of axisymmetric Finite Element sub model mesh (Thin Wall)

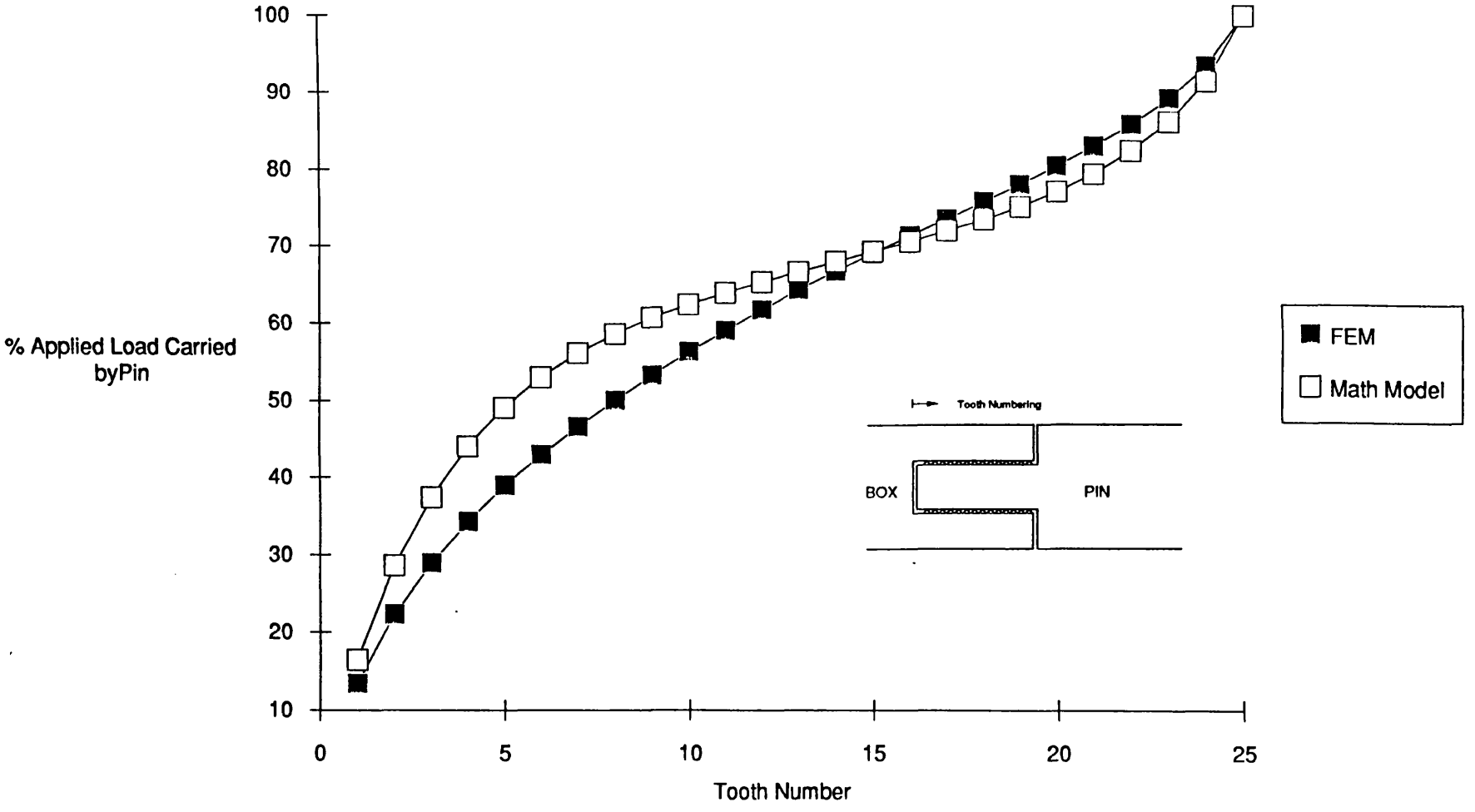

Fig.4.25 Comparison of pin load predictions between FE And Analogue Model - 120mm OD

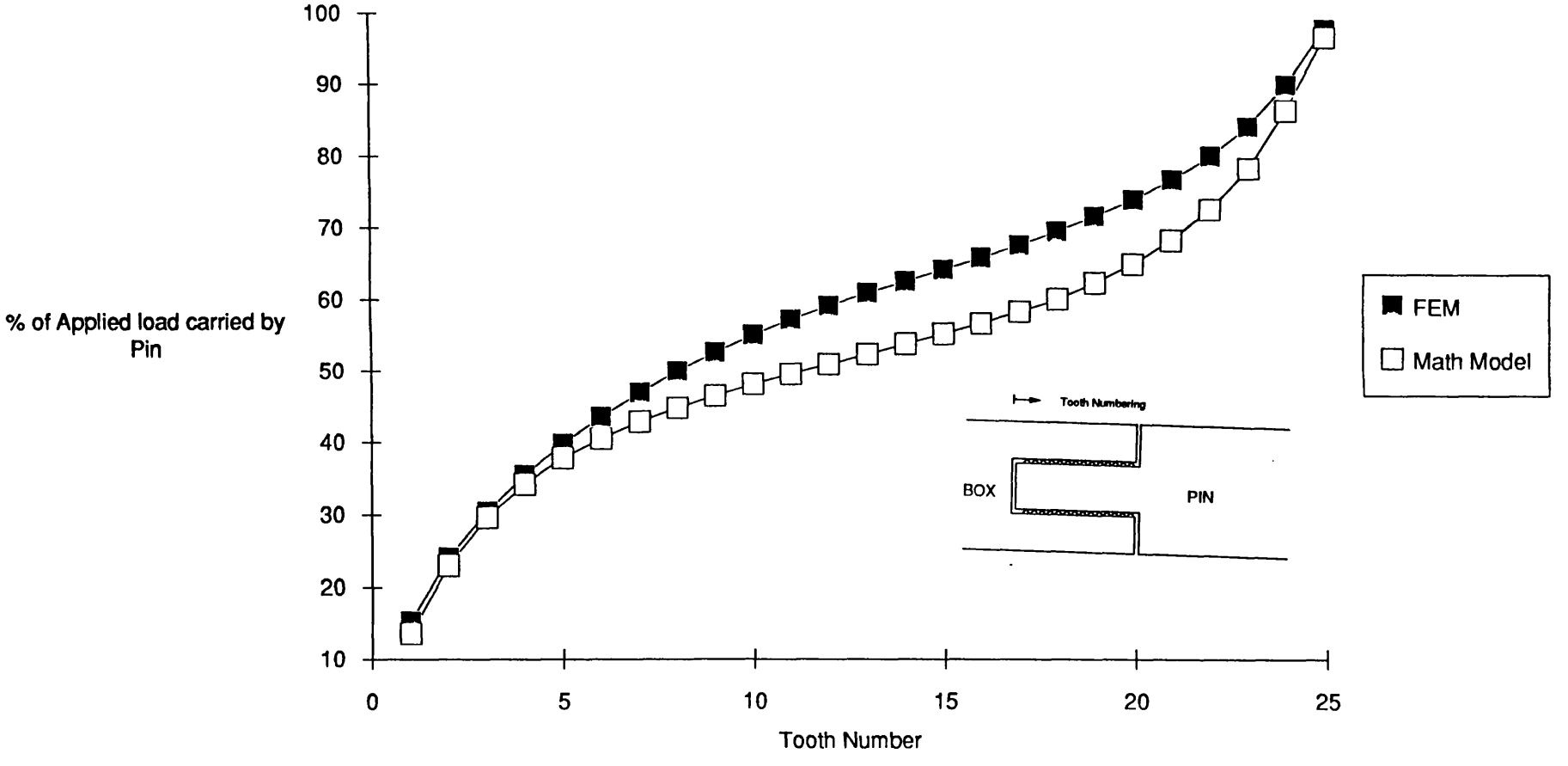

Fig. 4-26 Comparison of Tooth Load distribution between FEM and Analogue Model 140mm OD

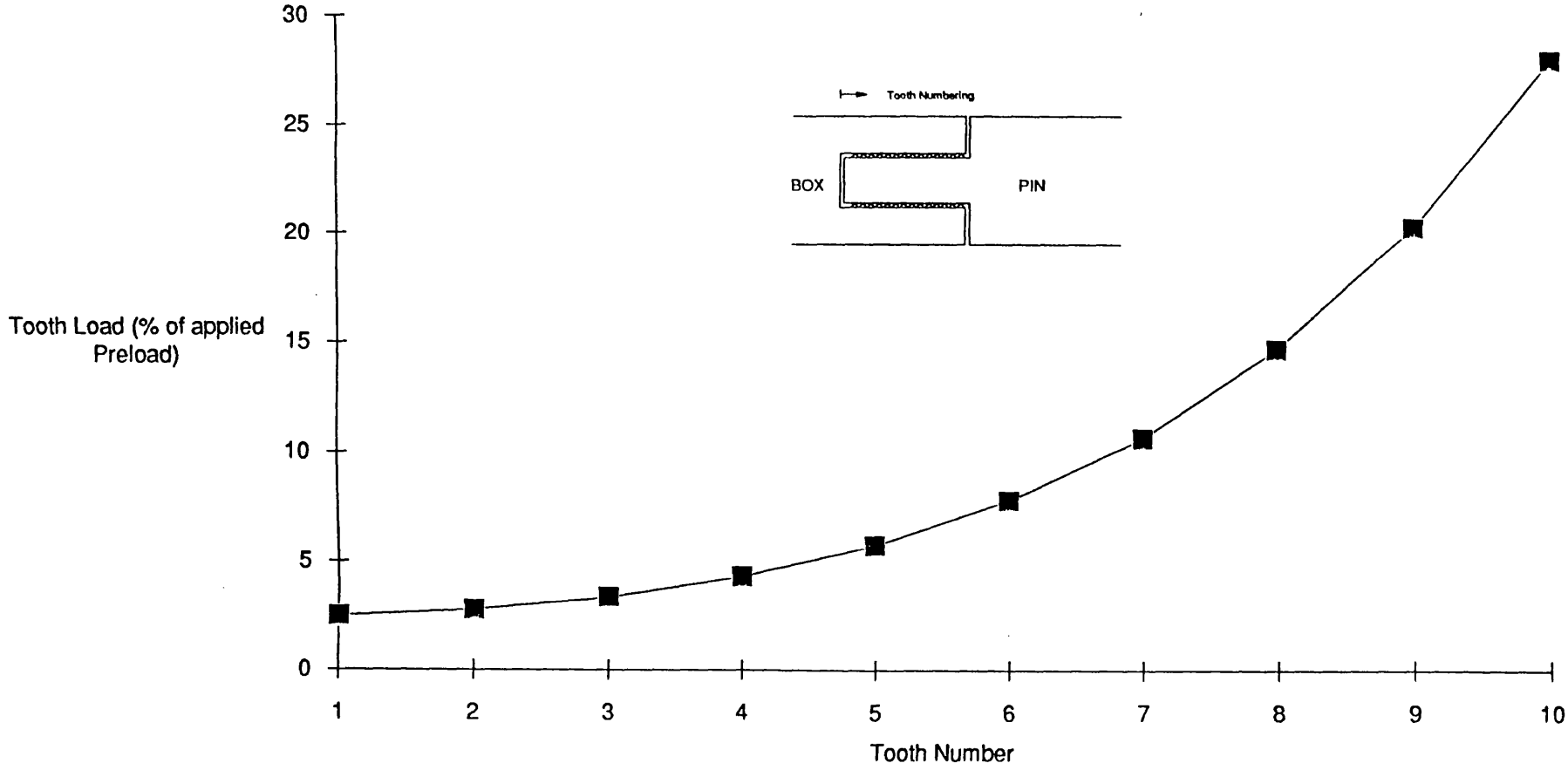

Fig 4.27 Tooth Loading due to Preload only

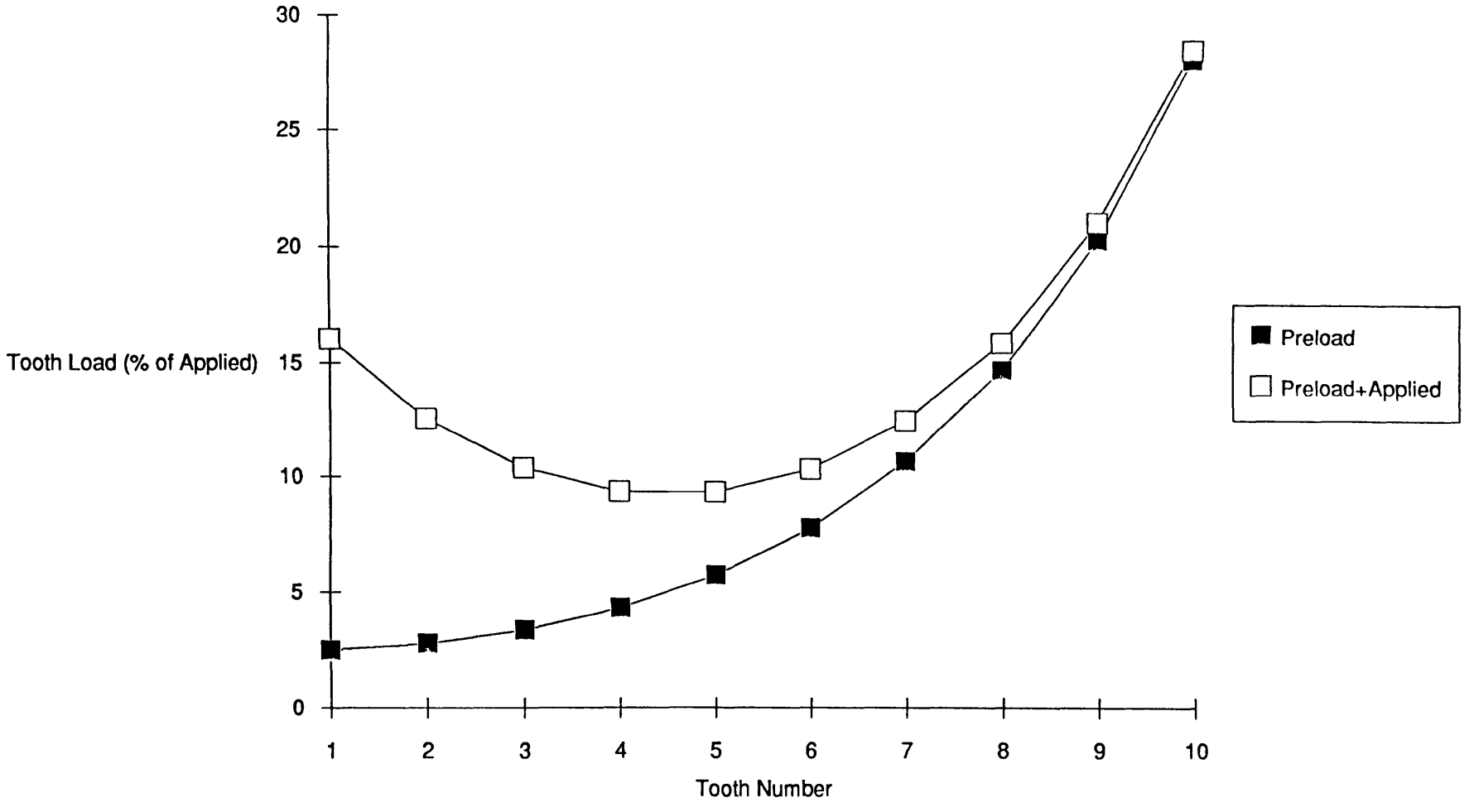

Fig 4.28 Effect of Axial load on a preloaded connection

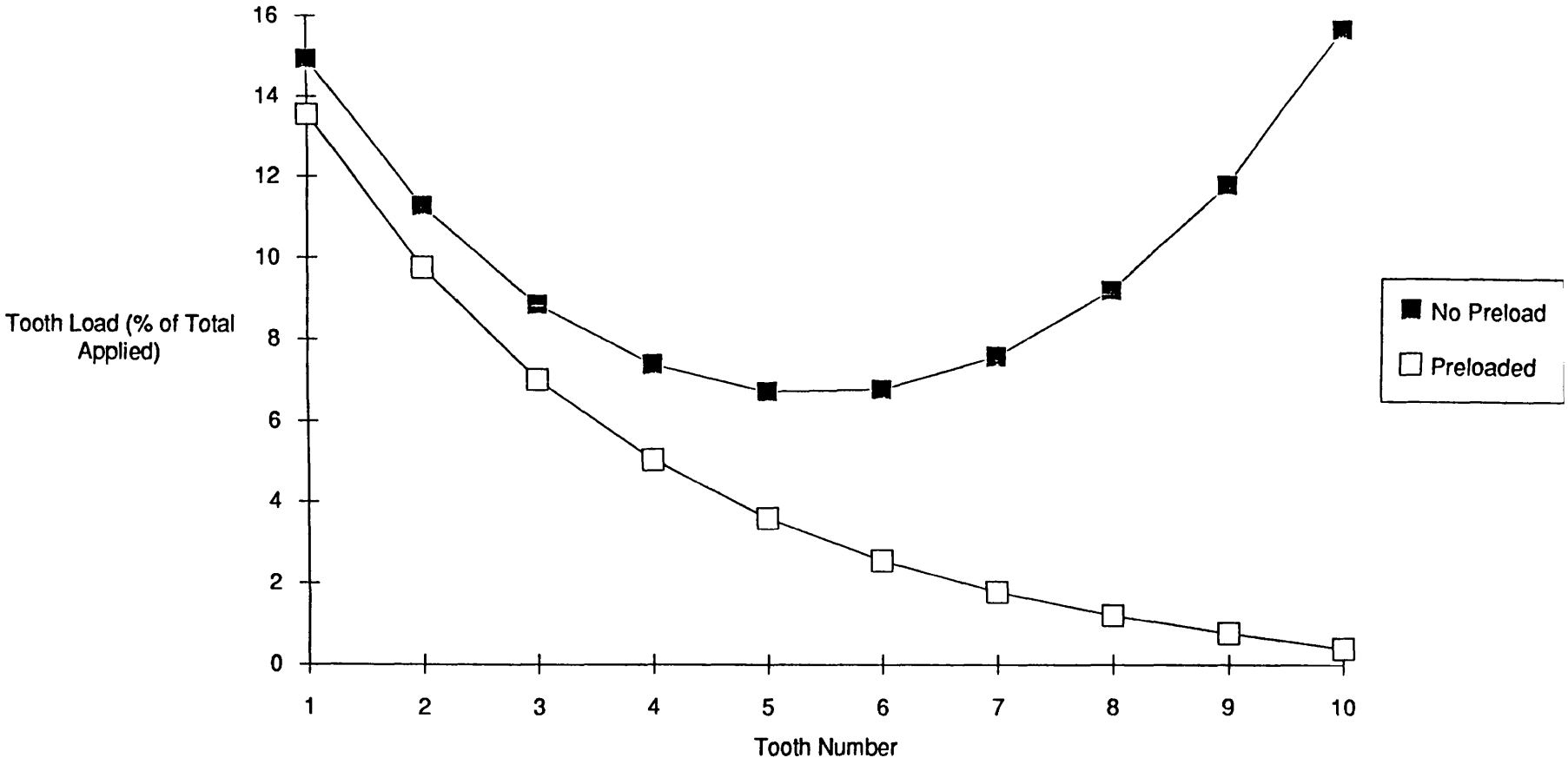

Fig. 4.29 Effect of an applied load on a preloaded and unpreloaded connection.

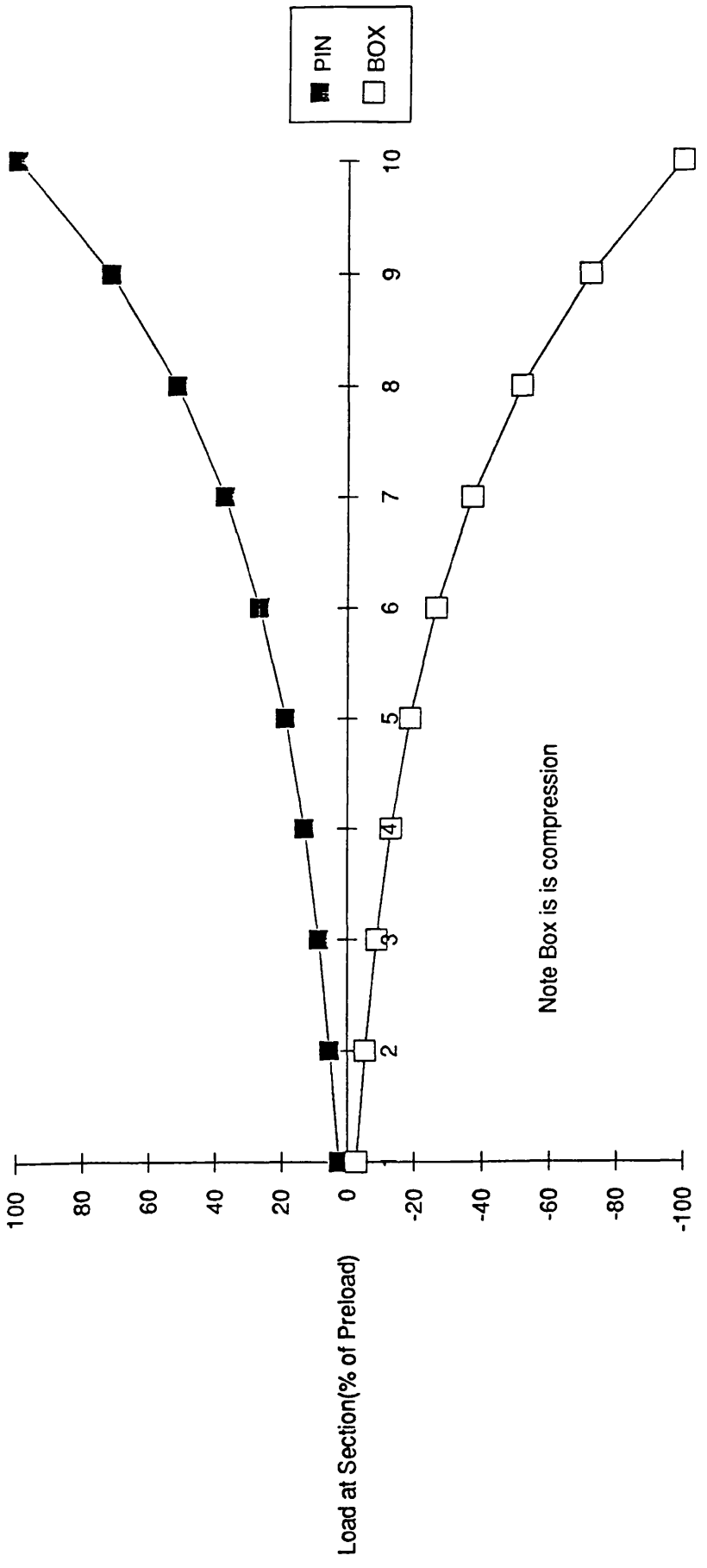

Fig 4.30 Load in Pin and Box due to preload only

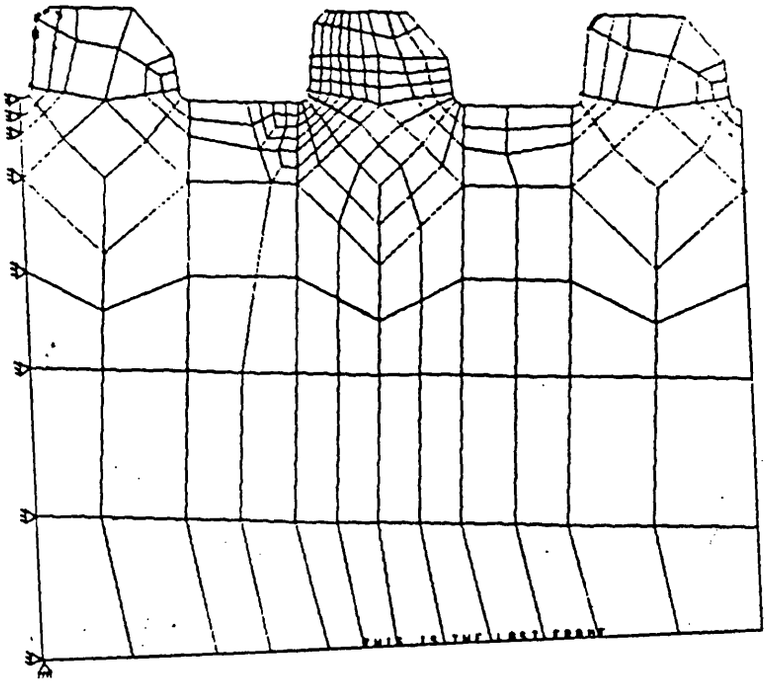

Fig. 4.31 Simple model of 3 axisymmetric teeth

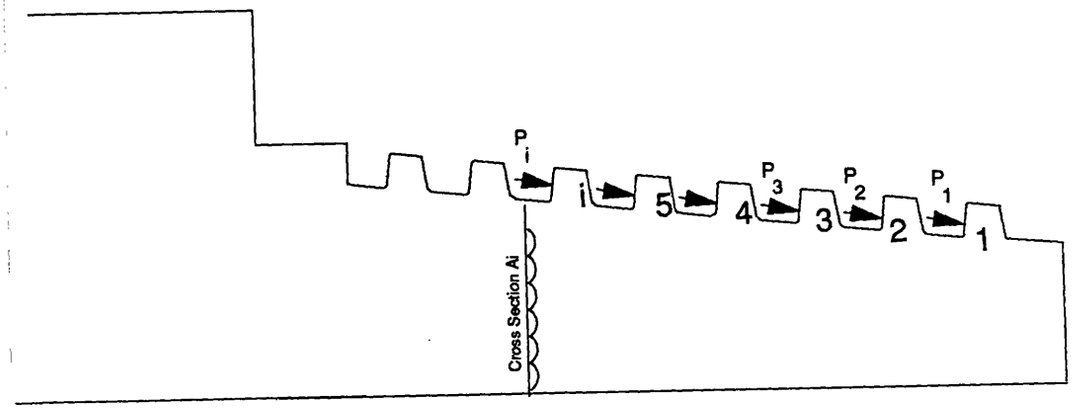

Fig 4.32 Notation for Local SCF Calculation

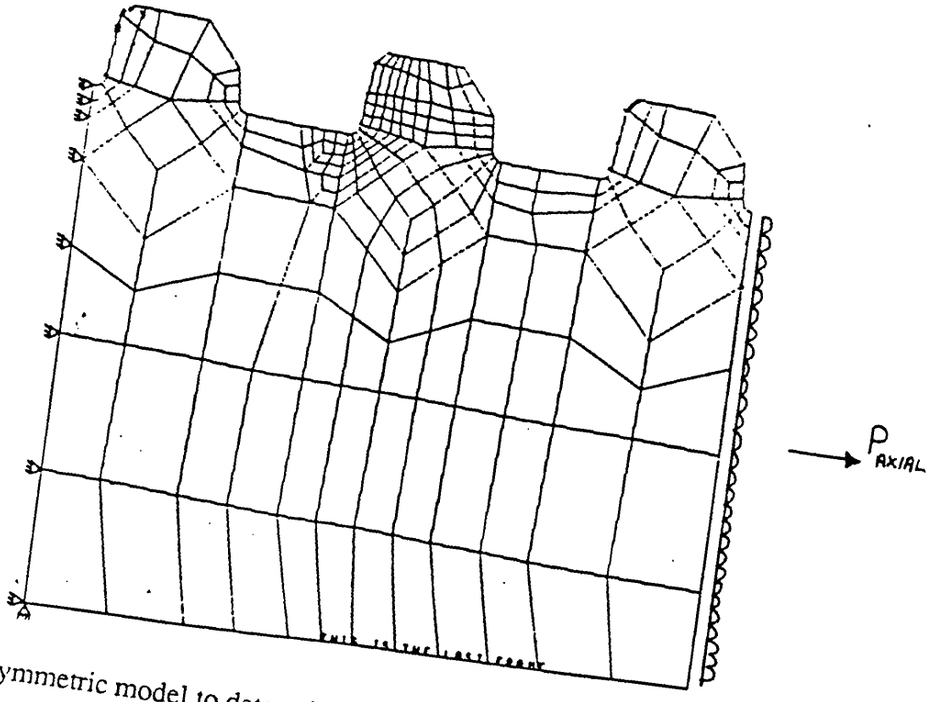

Fig. 4.33 Axisymmetric model to determine stress at thread root due to axial load only.

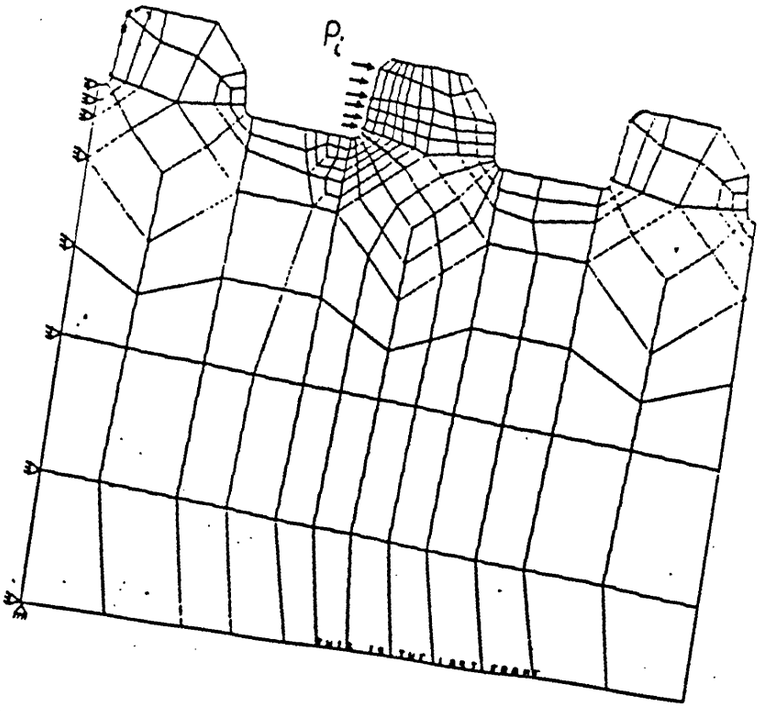

Fig. 4.34 Axisymmetric model to determine stress at thread root due to tooth load only.

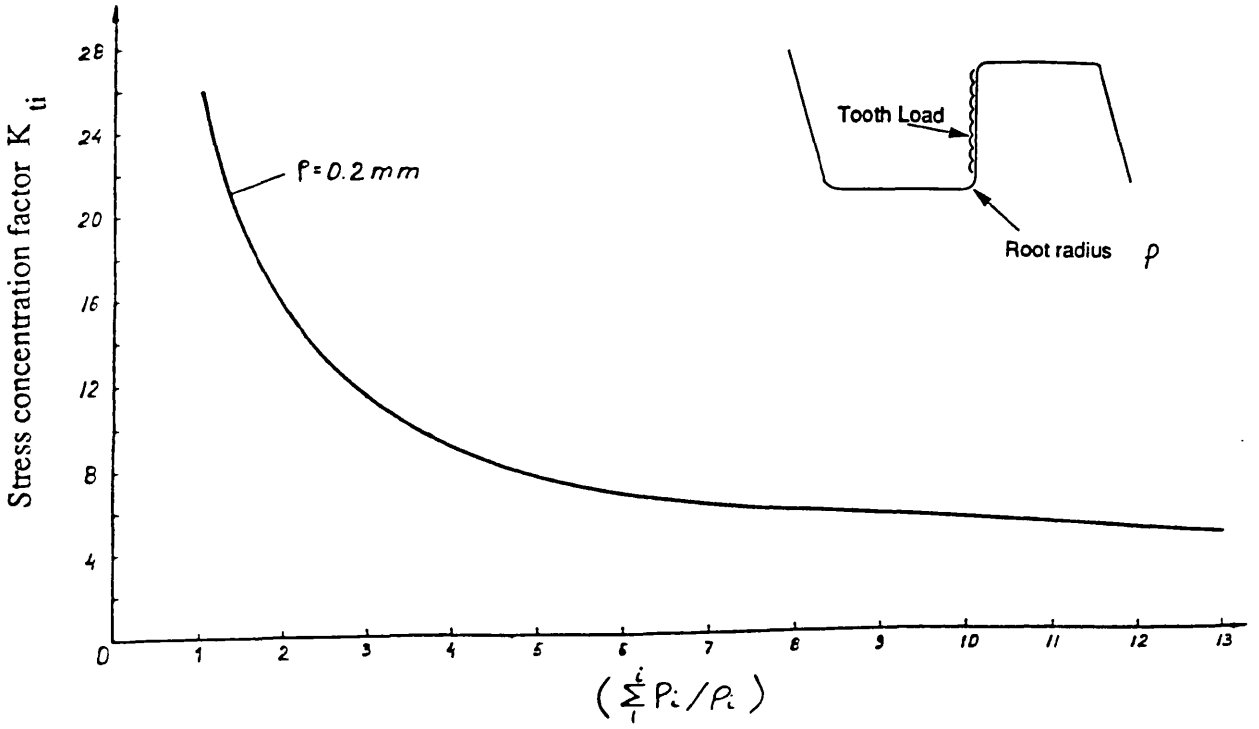

Fig. 4.35 Stress concentration factor as a function of tooth load ratio.

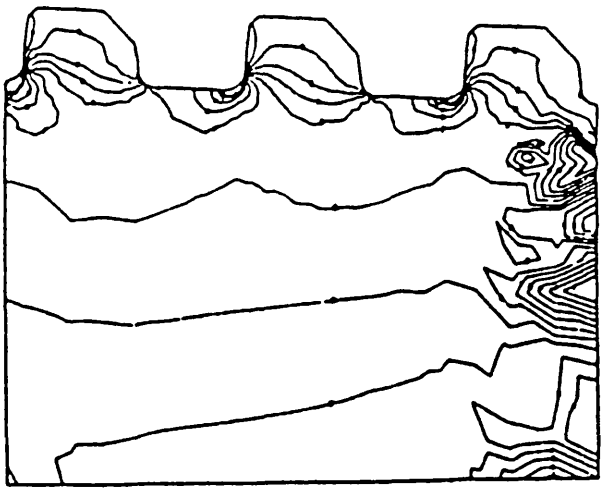

Fig. 4.36 Example of stress contours produced by FE sub model.(Axial Load)

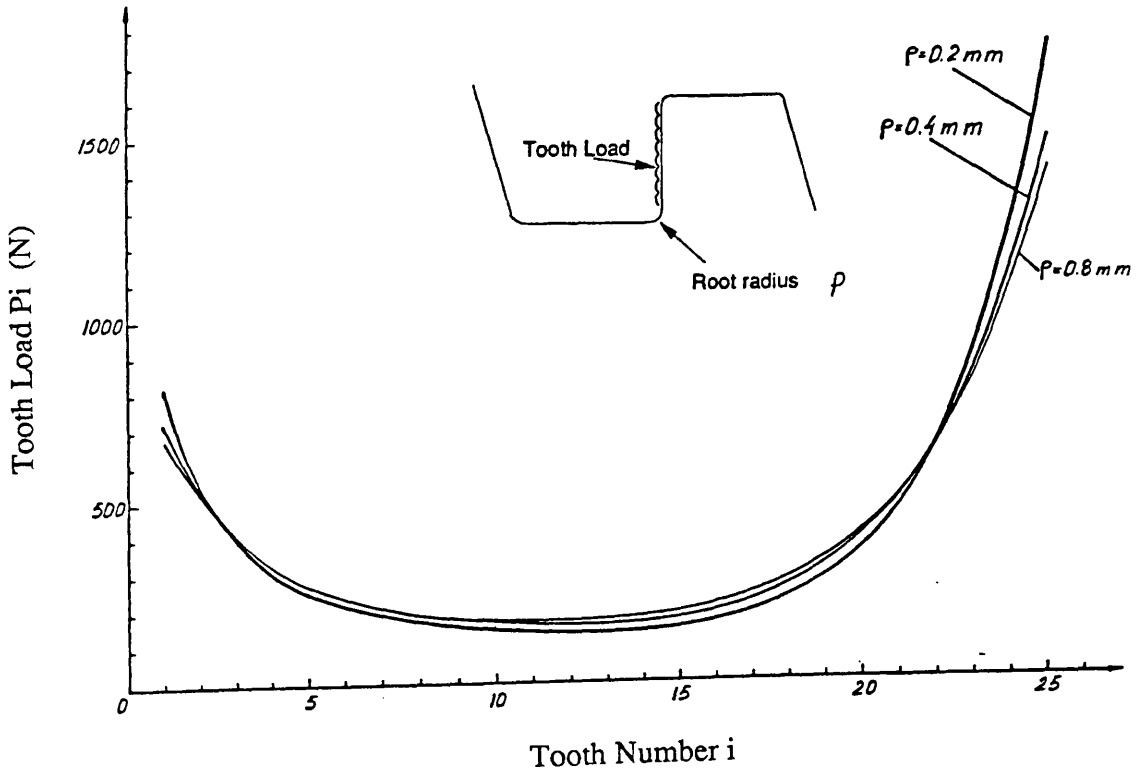

Fig. 4.37 Effect of root radius on tooth load distribution.

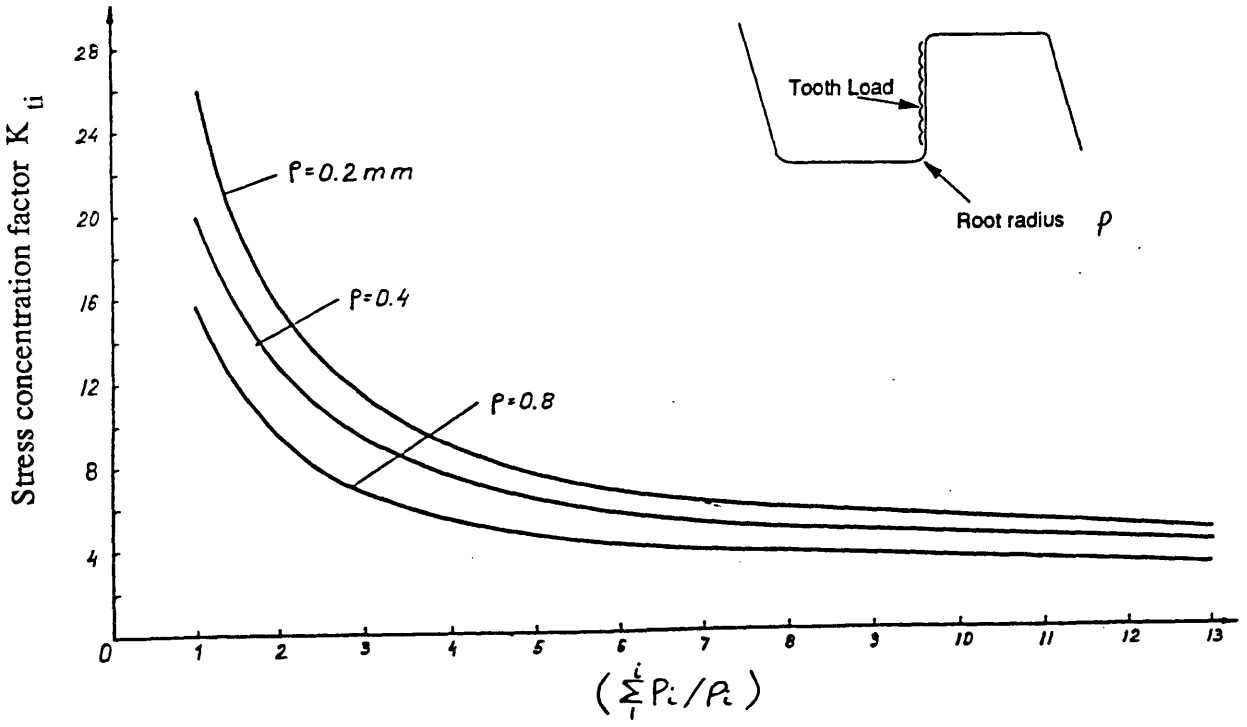

Fig. 4.38 Effect of root radius on stress concentration factor

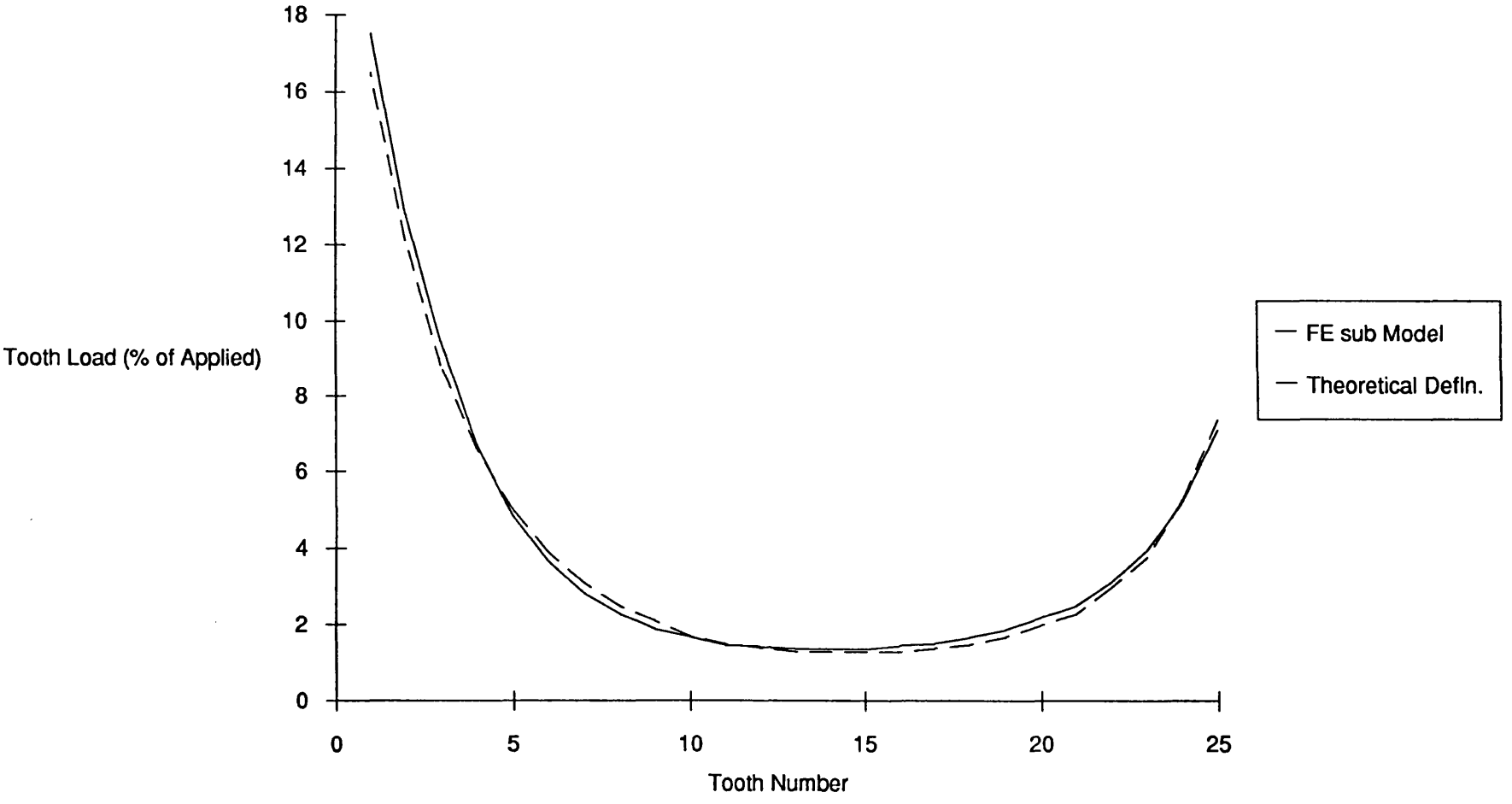

Fig. 4.39 Comparison of tooth load distributions calculated using tooth stiffnesses derived from theory and from FE Sub modelling.

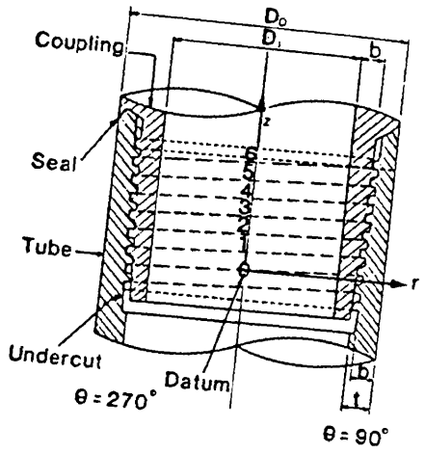

Fig 4.40a General Arrangement.

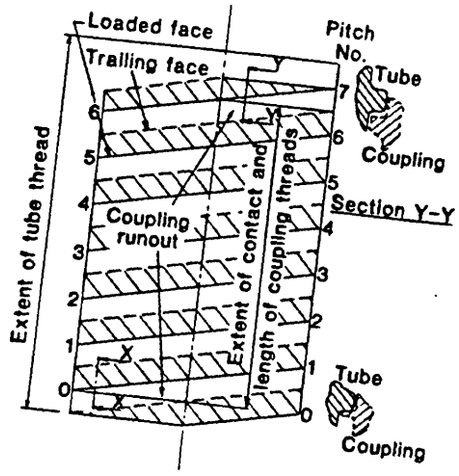

Fig 4.40b Details of thread runout.

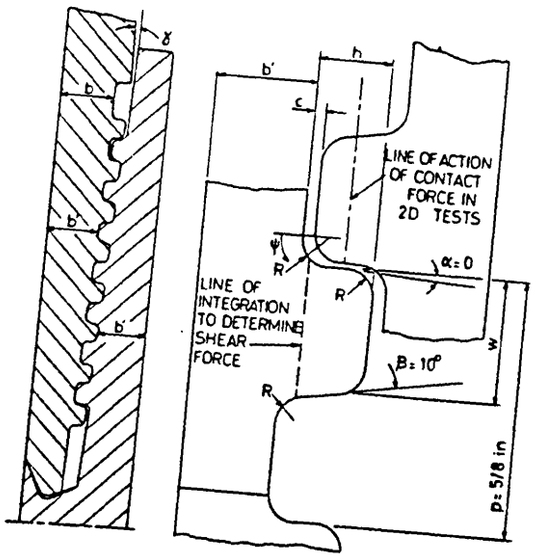

Fig 4.40c Tooth interface.

Fig. 4.40 Geometry of Photoelastic Models used by Broadbent. (Reproduced from ref.15)

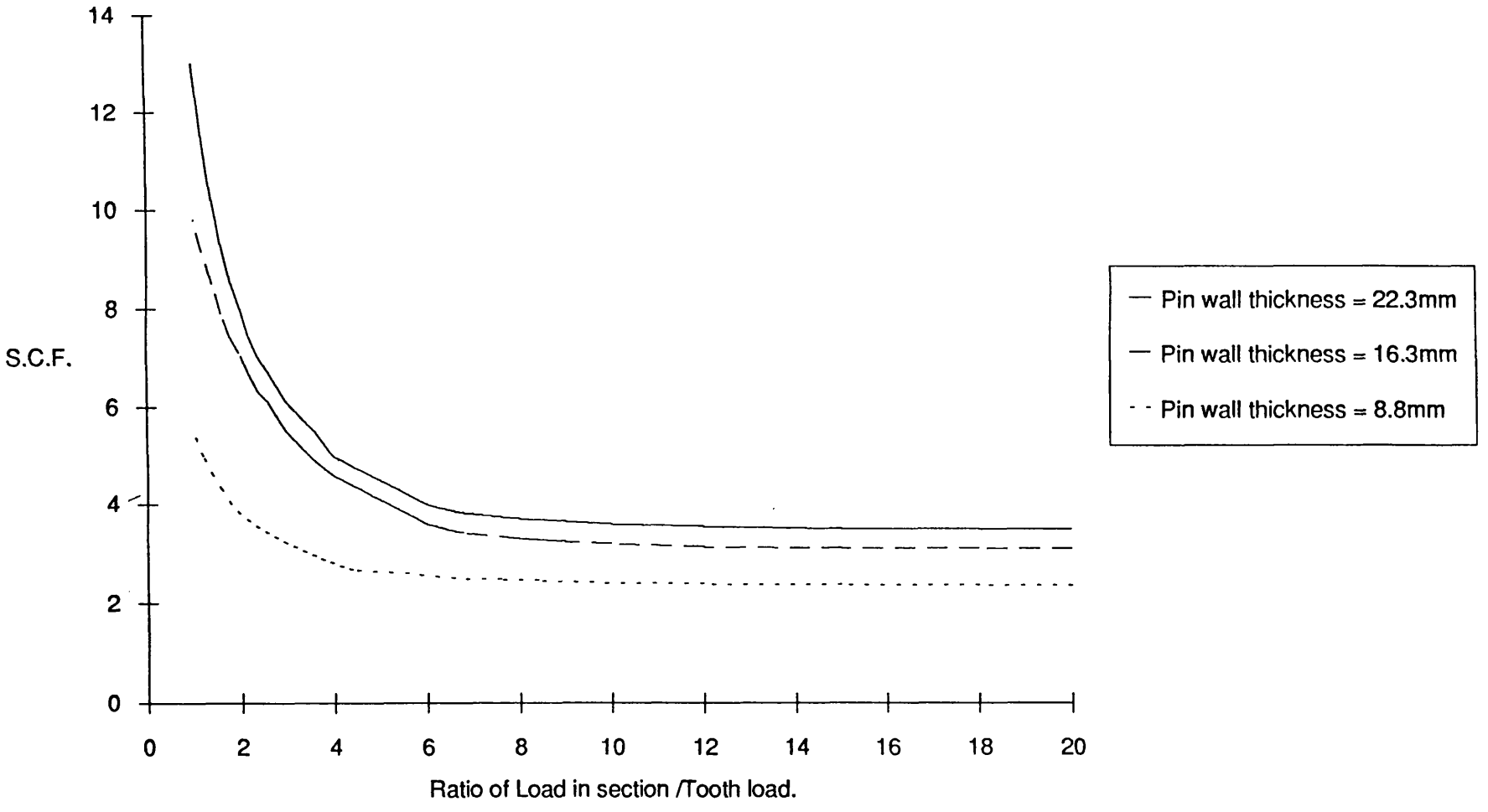

Fig 4.41 Stress concentration factors for different wall thicknesses.

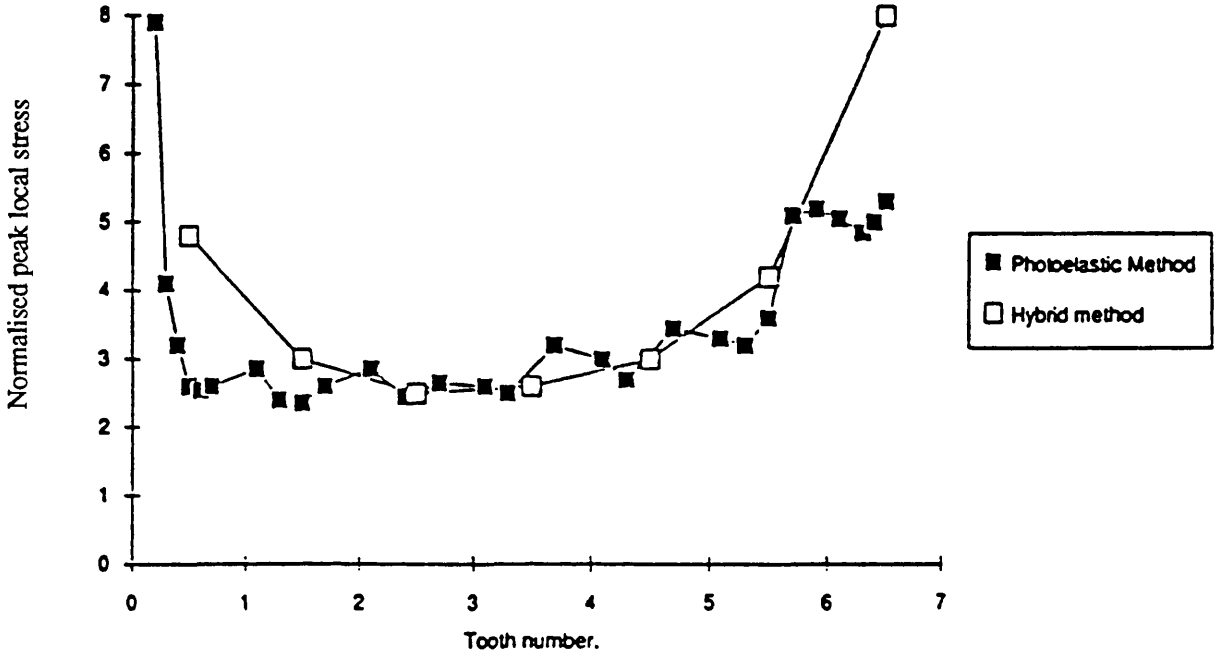

Fig. 4.42 Comparison of normalised peak local stresses obtained by the Hybrid model and by photoelasticity.

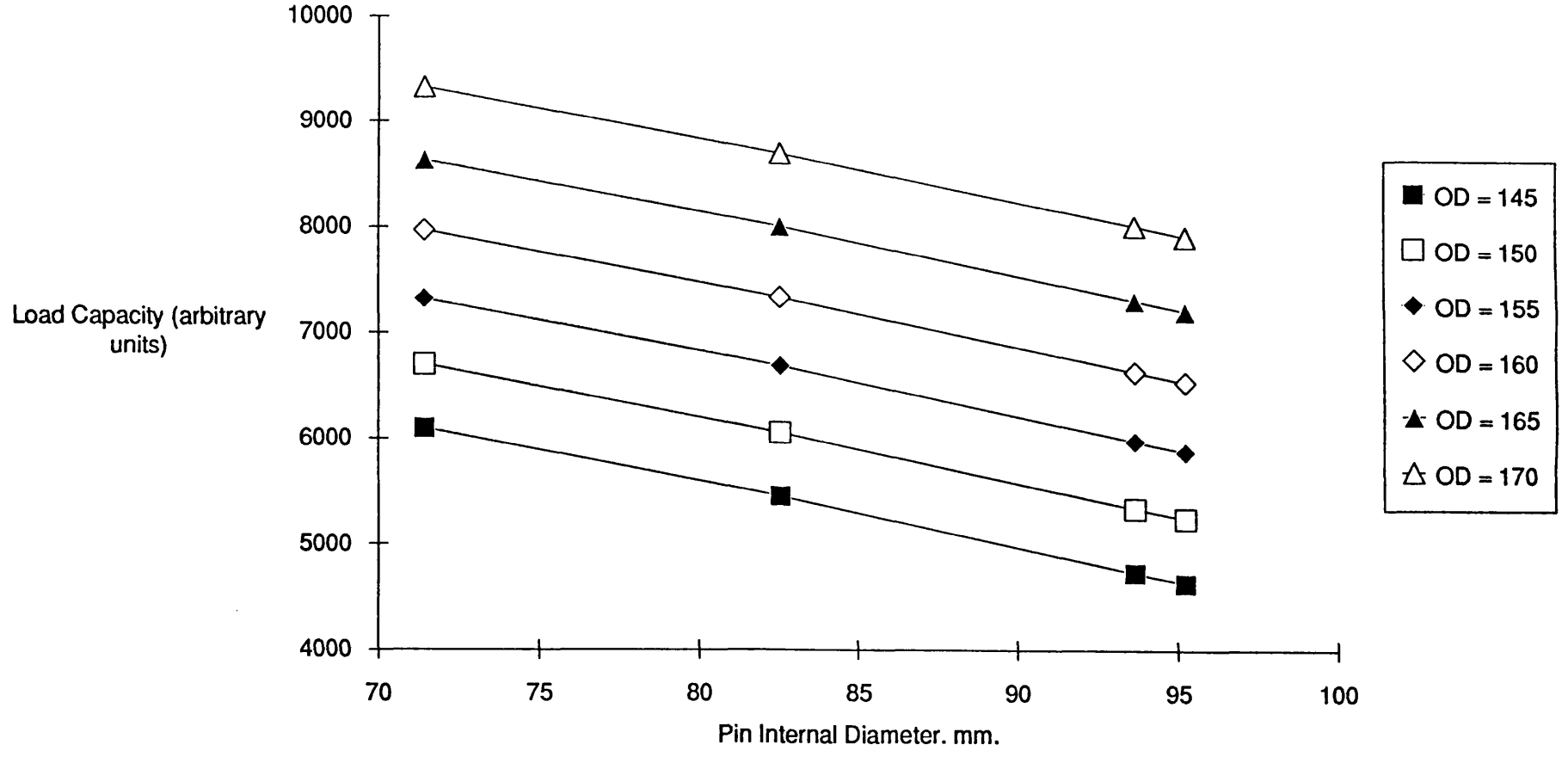

Fig 4.43. Variation in Load Capacity for 4.5 inch Drillpipe Pin with Preload.(ref.40)

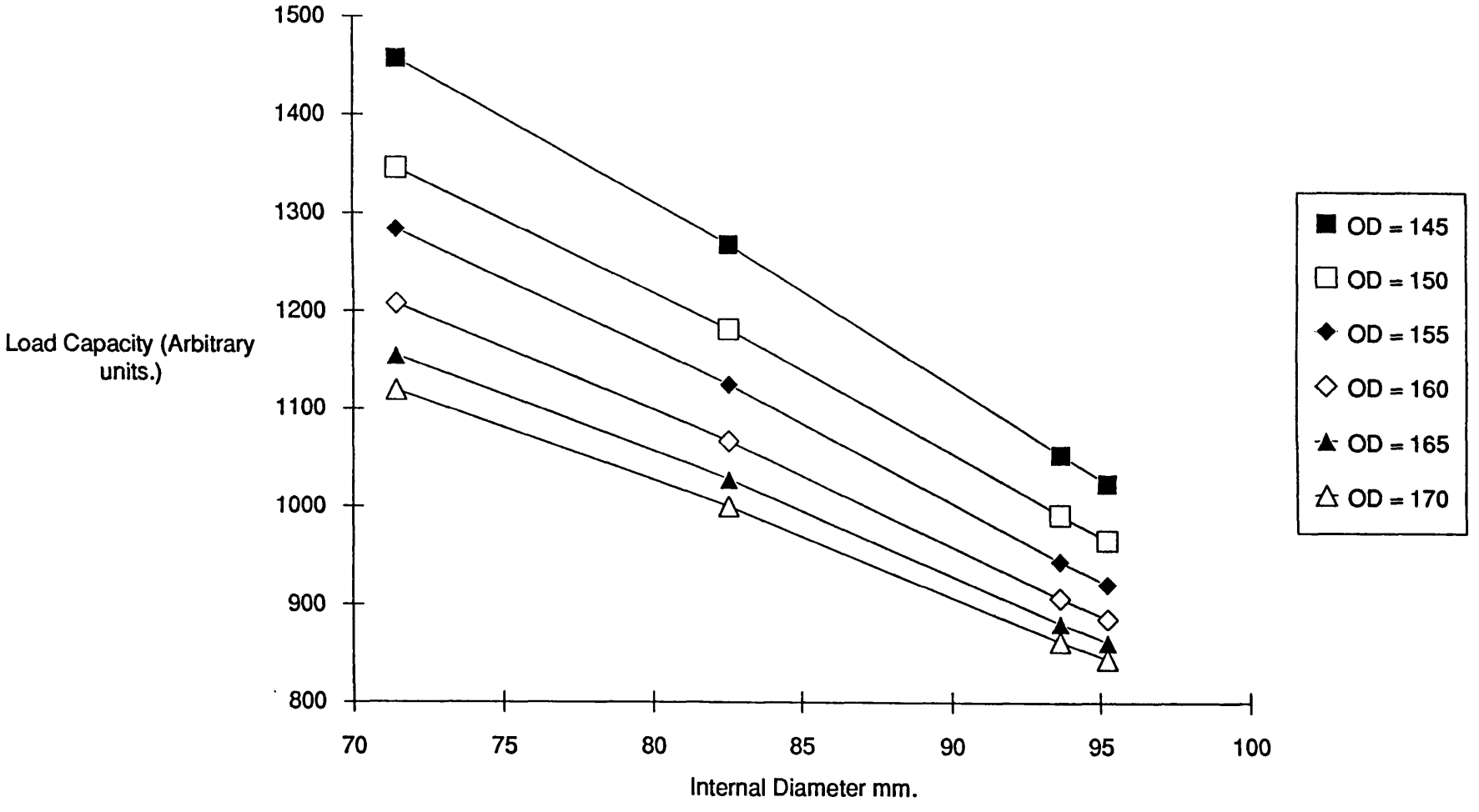

Fig 4.44. Variation in Load Capacity for a 4.5 inch Drillpipe Pin without Preload. (Ref 40)

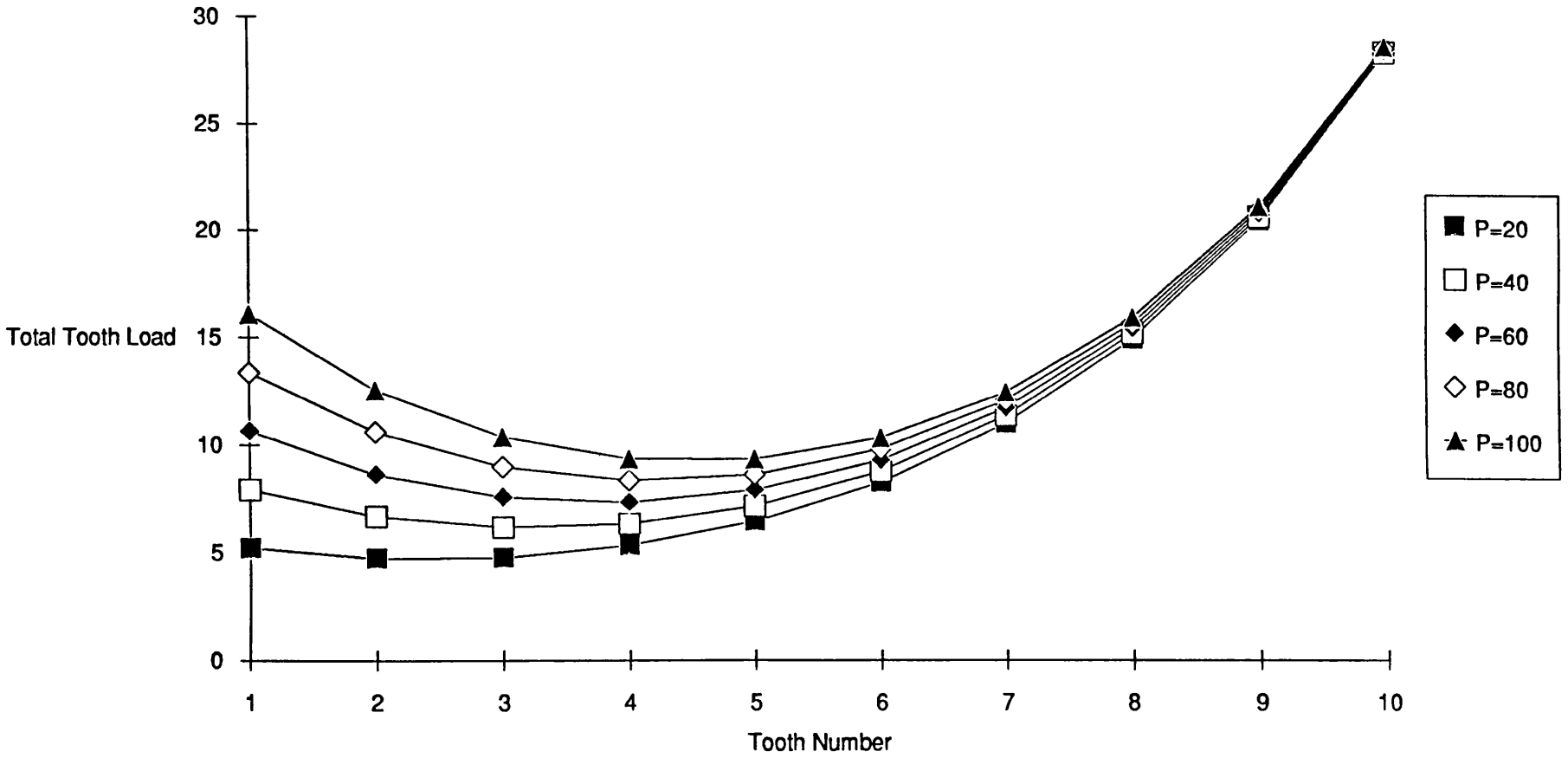

Fig4.45 Effect of Applied Load Level (P) on total tooth load in a preloaded connection

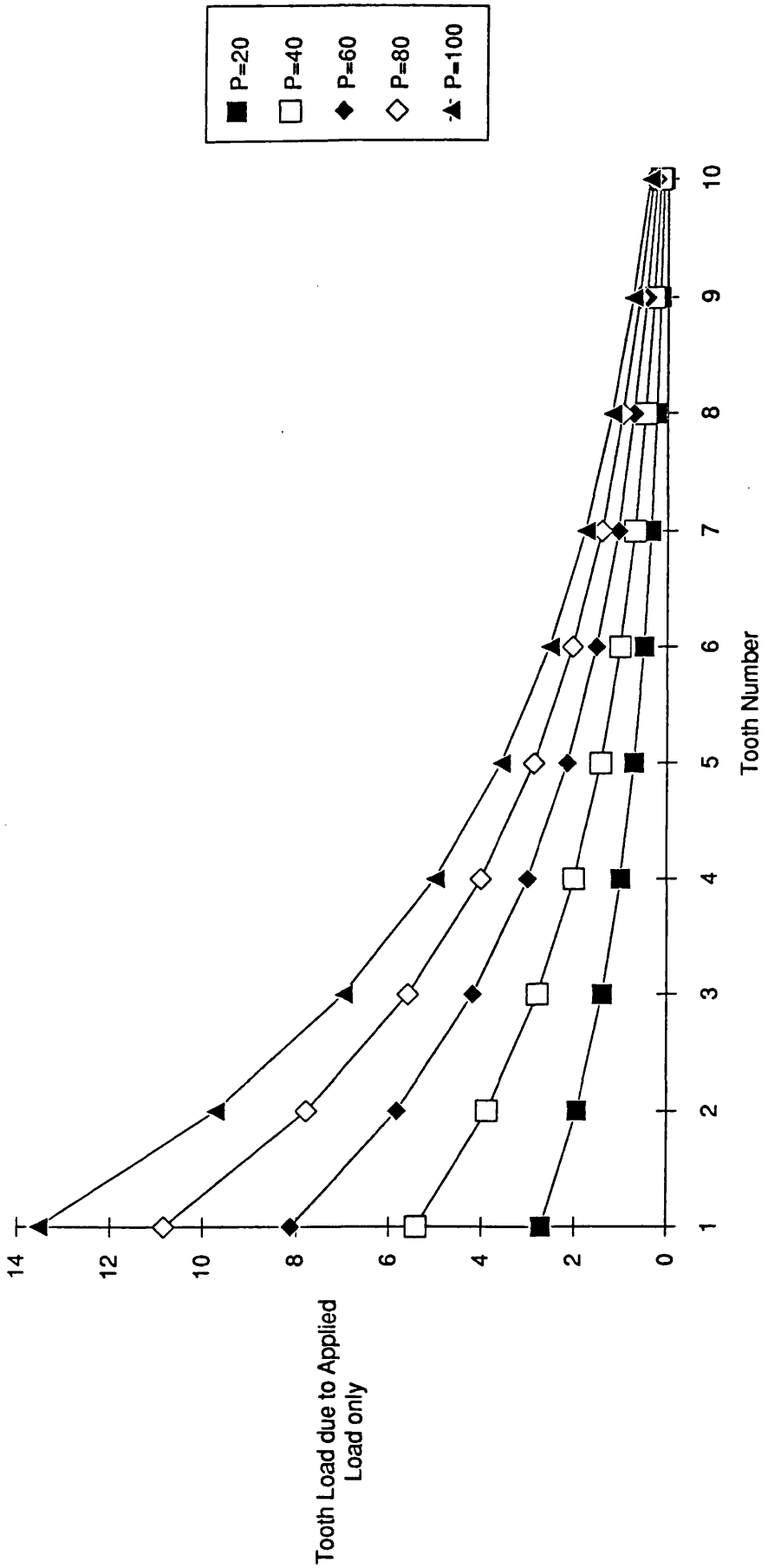

Fig 4.46 Effect of Applied Load level on the dynamic tooth load for a preloaded connection

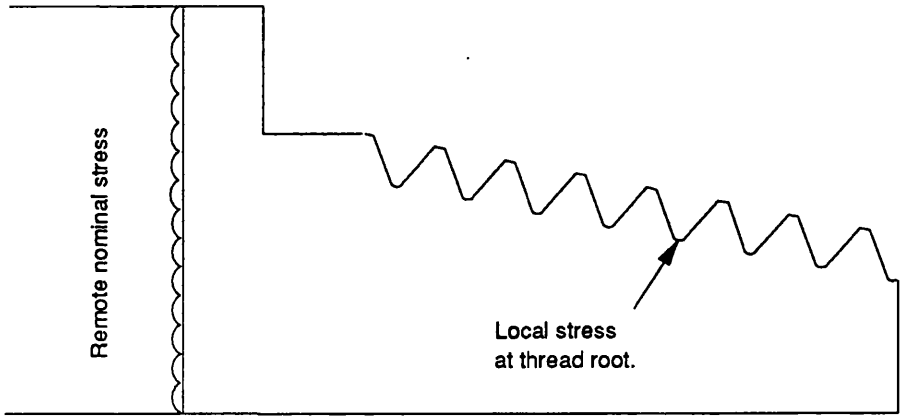

Fig 4.47 Notation for SCF Calculation

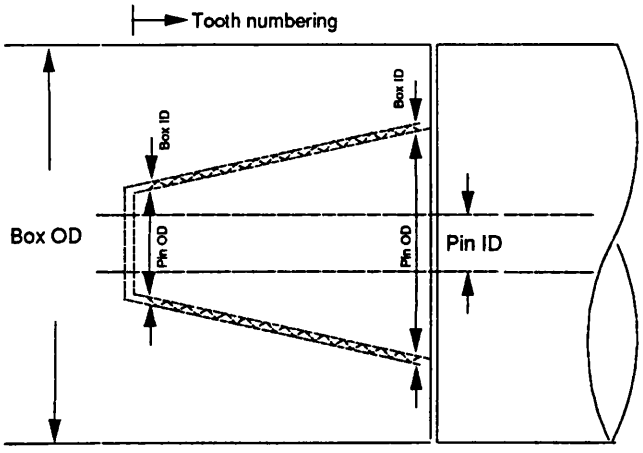

Fig 4.48 Notation used in Table 4.3

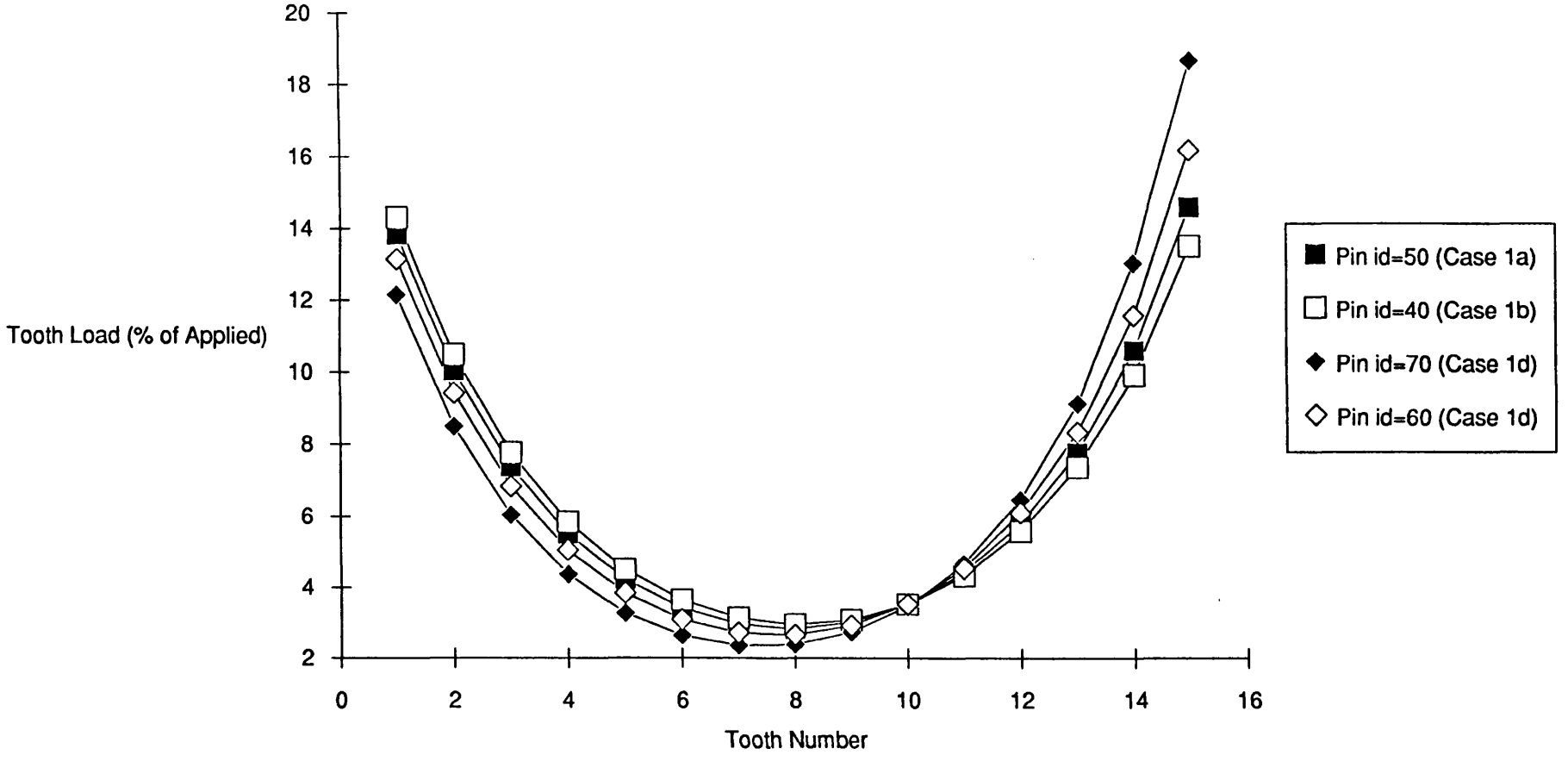

Fig 4.49 Effect of Pin inside diameter - No Preload

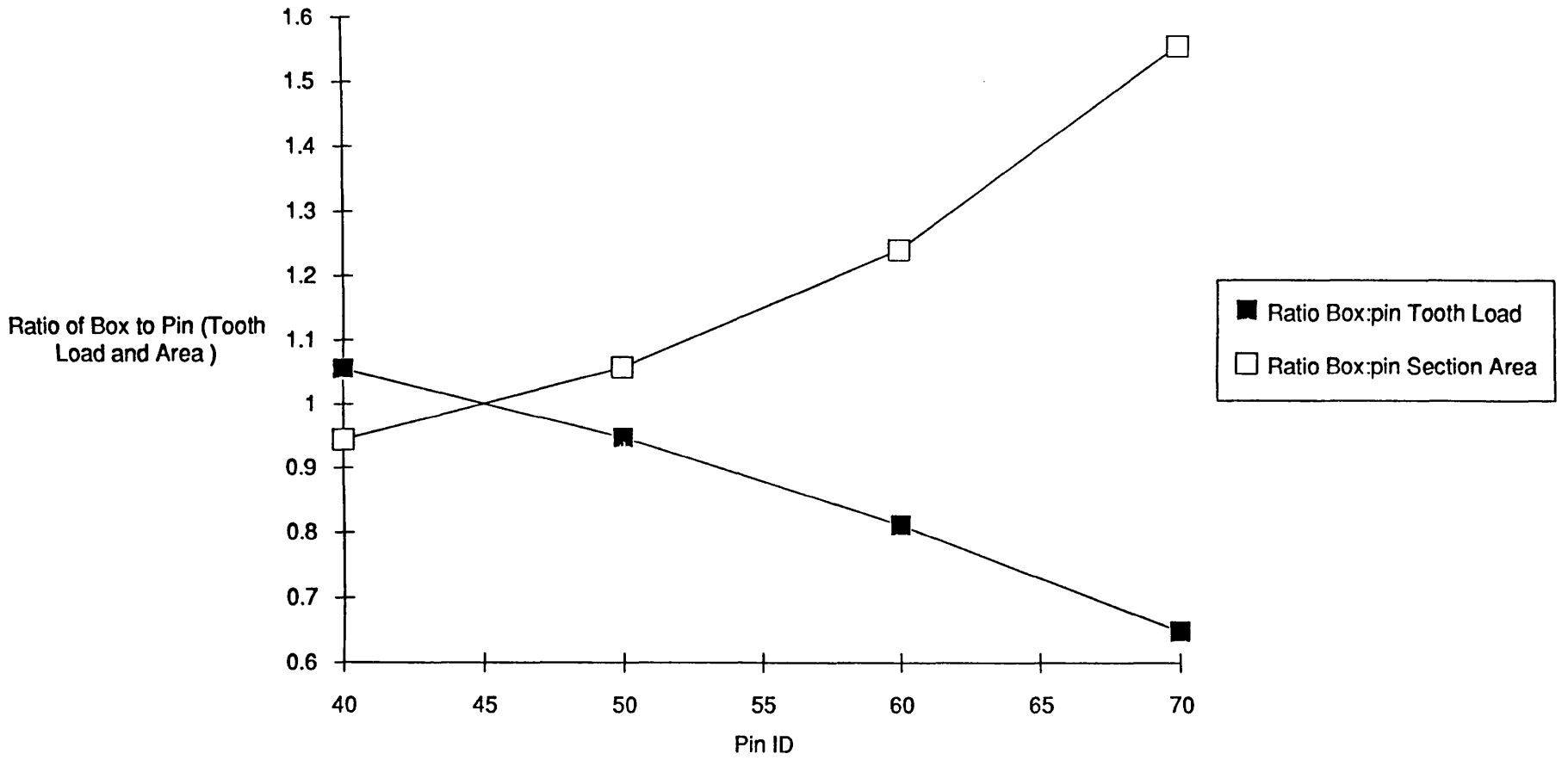

Fig 4.50 Effect of pin area on Load sharing between pin and box

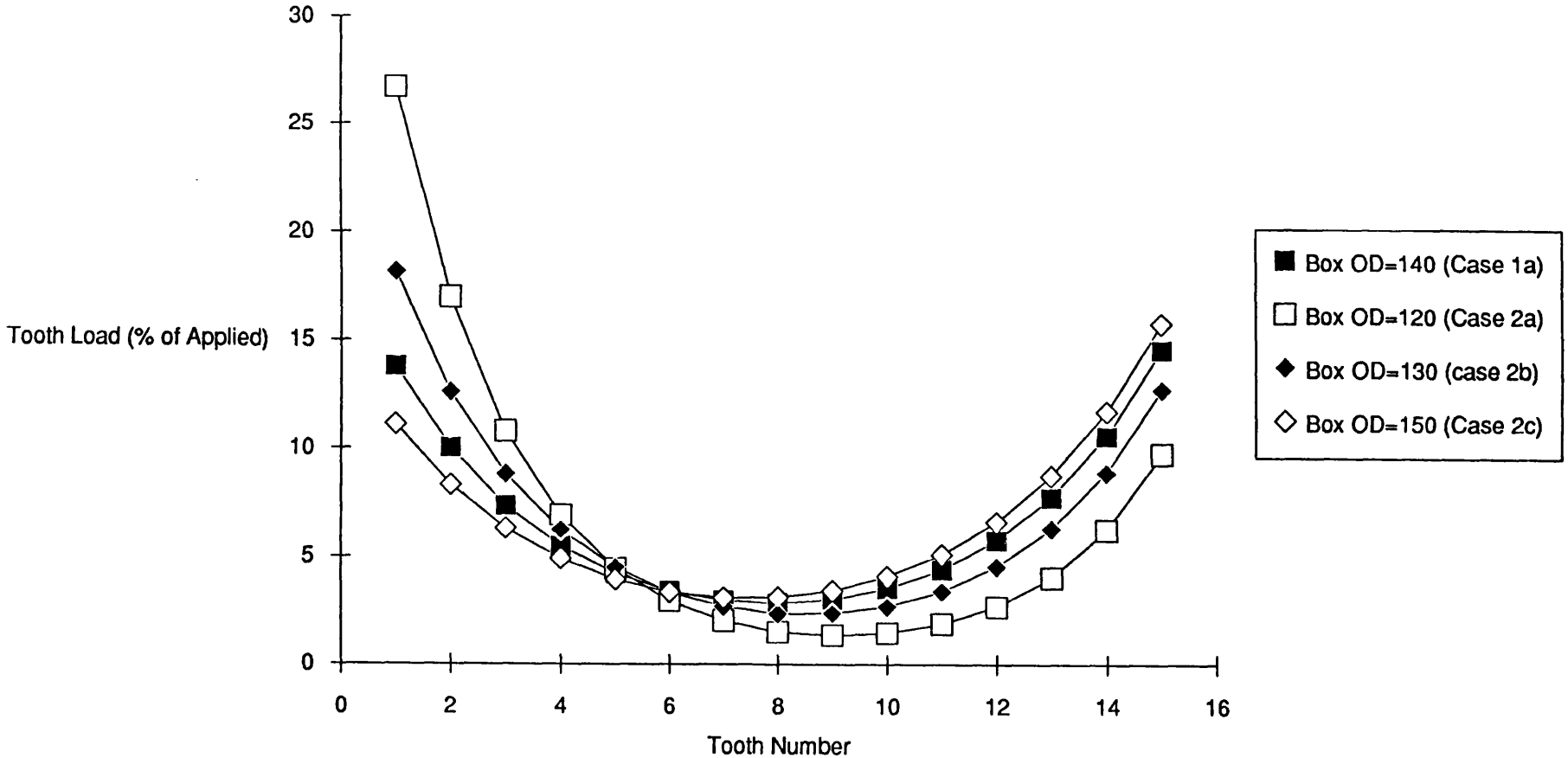

Fig 4.51 Effect of Box Outside Diameter - No Preload

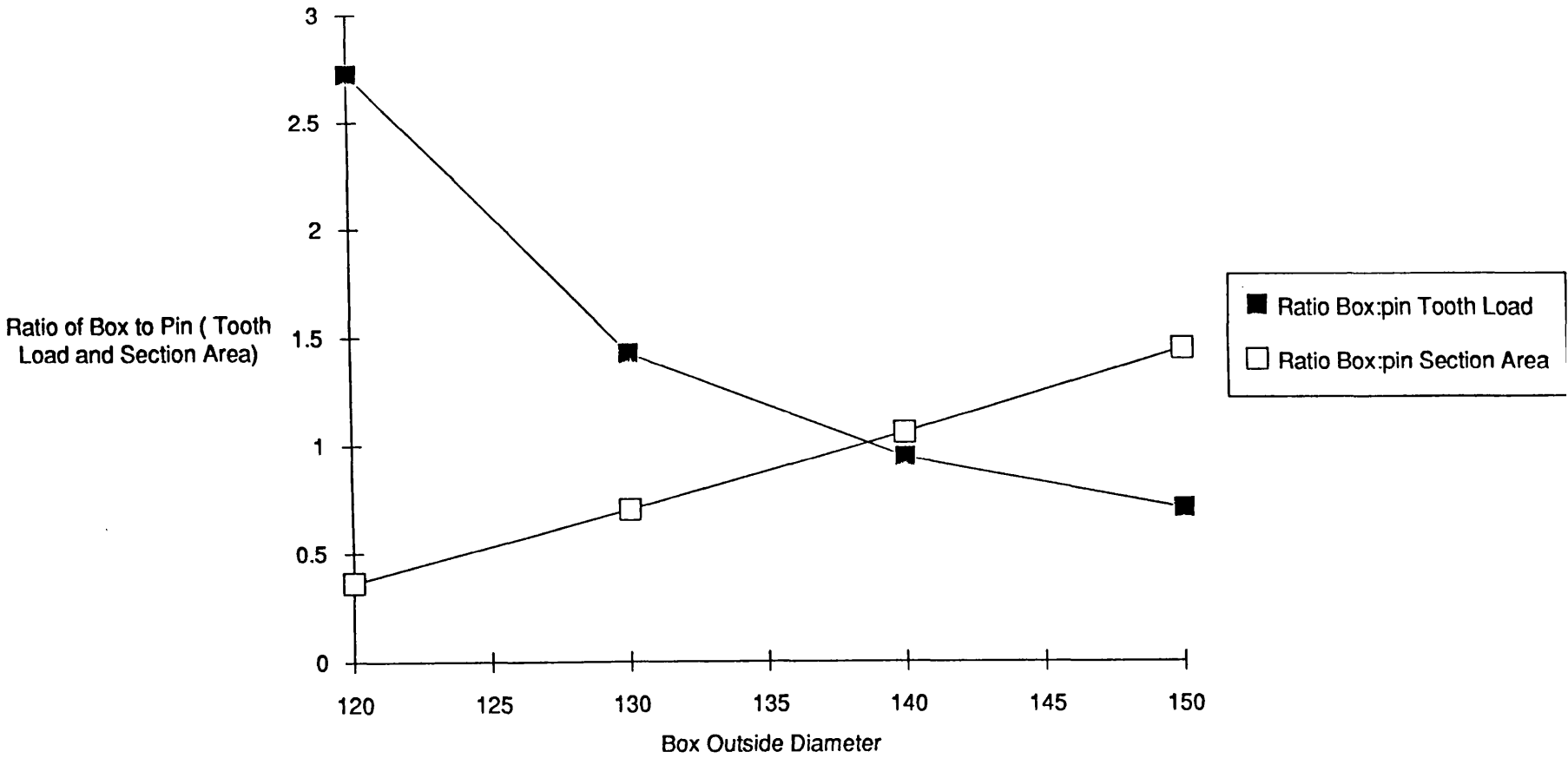

Fig 4.52 Effect of Box area on Load sharing between pin and box.

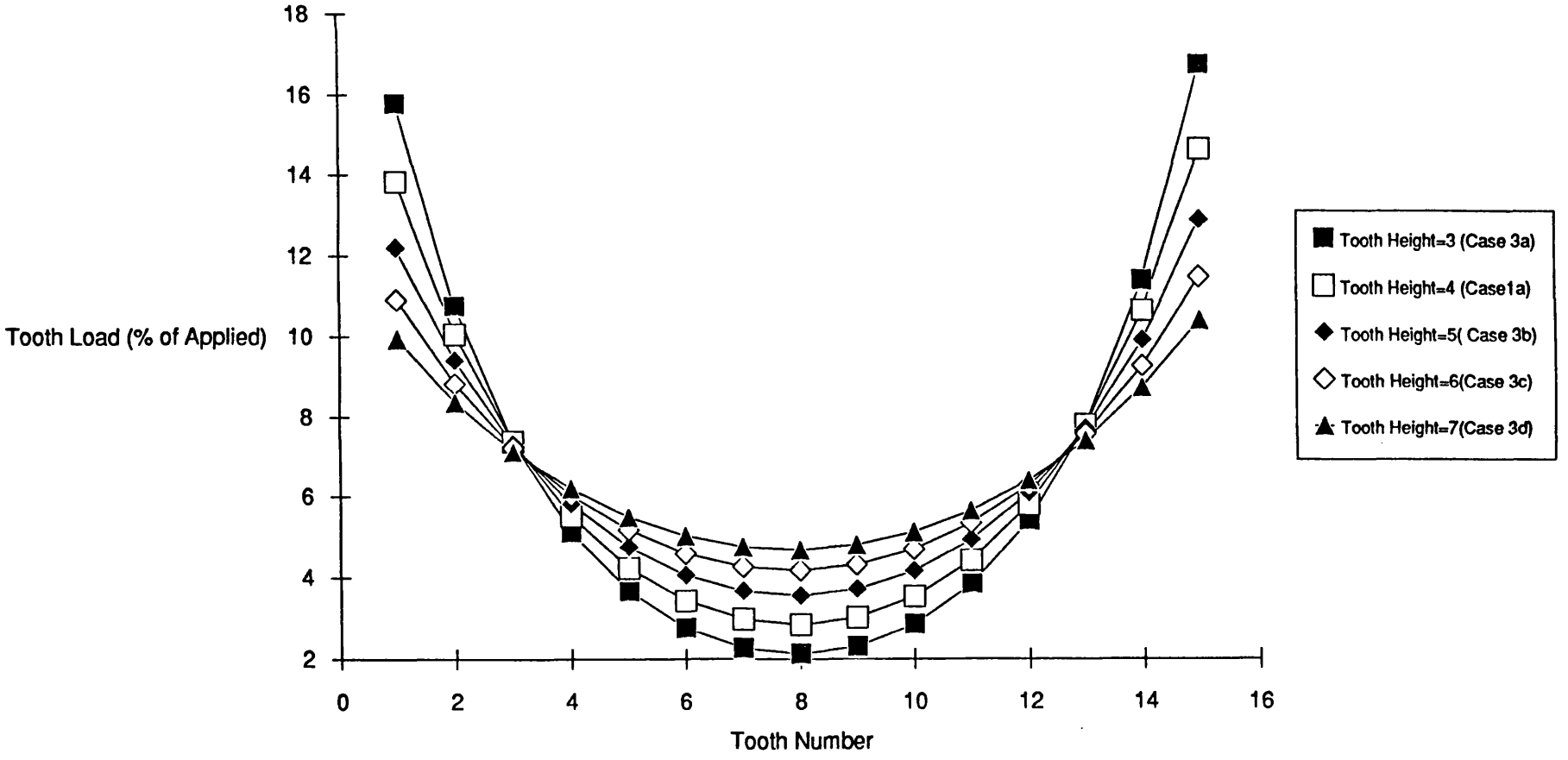

Fig 4.53 Effect of Tooth Height - No Preload

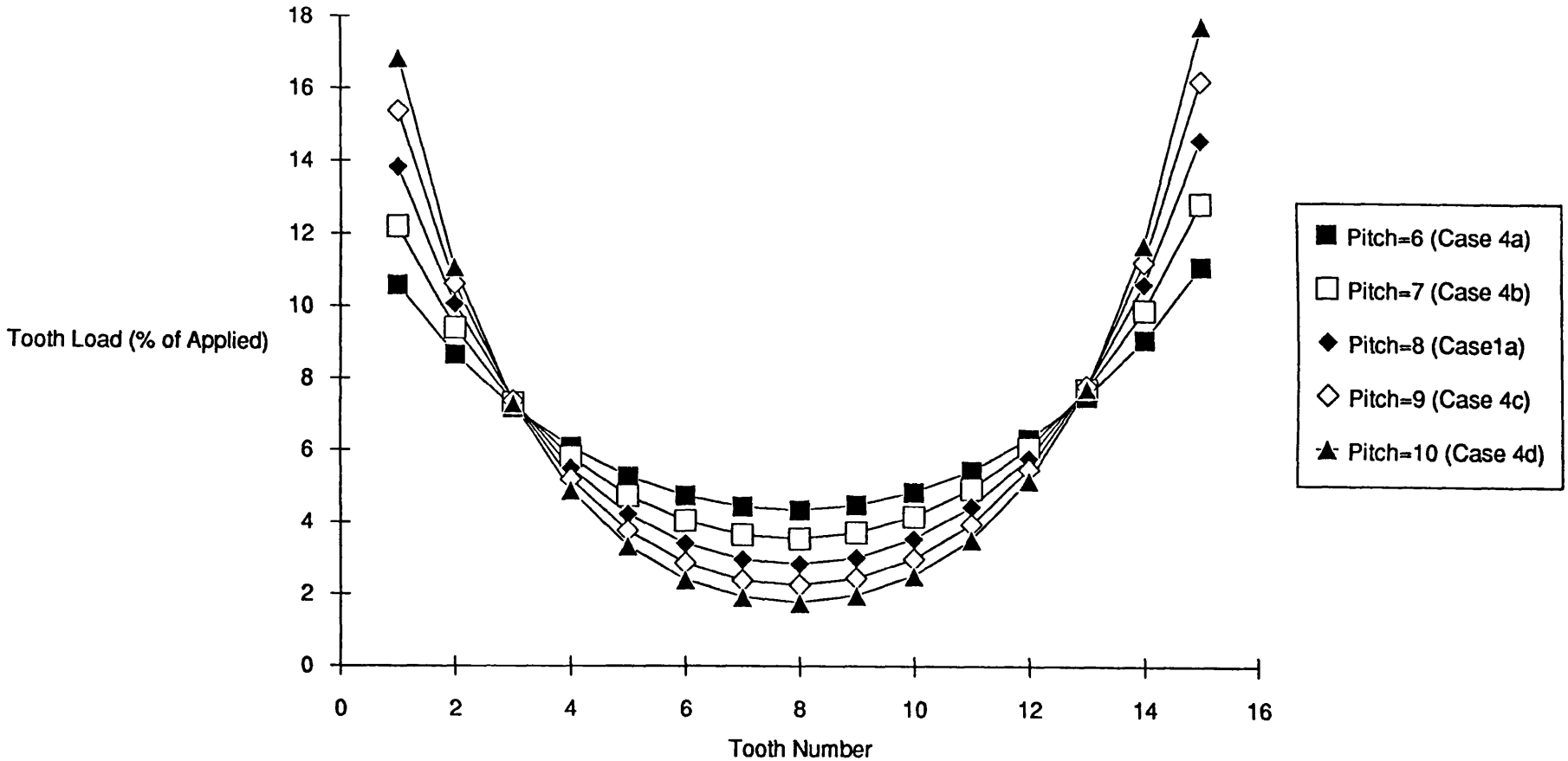

Fig 4.54 Effect of Thread Pitch - No Preload

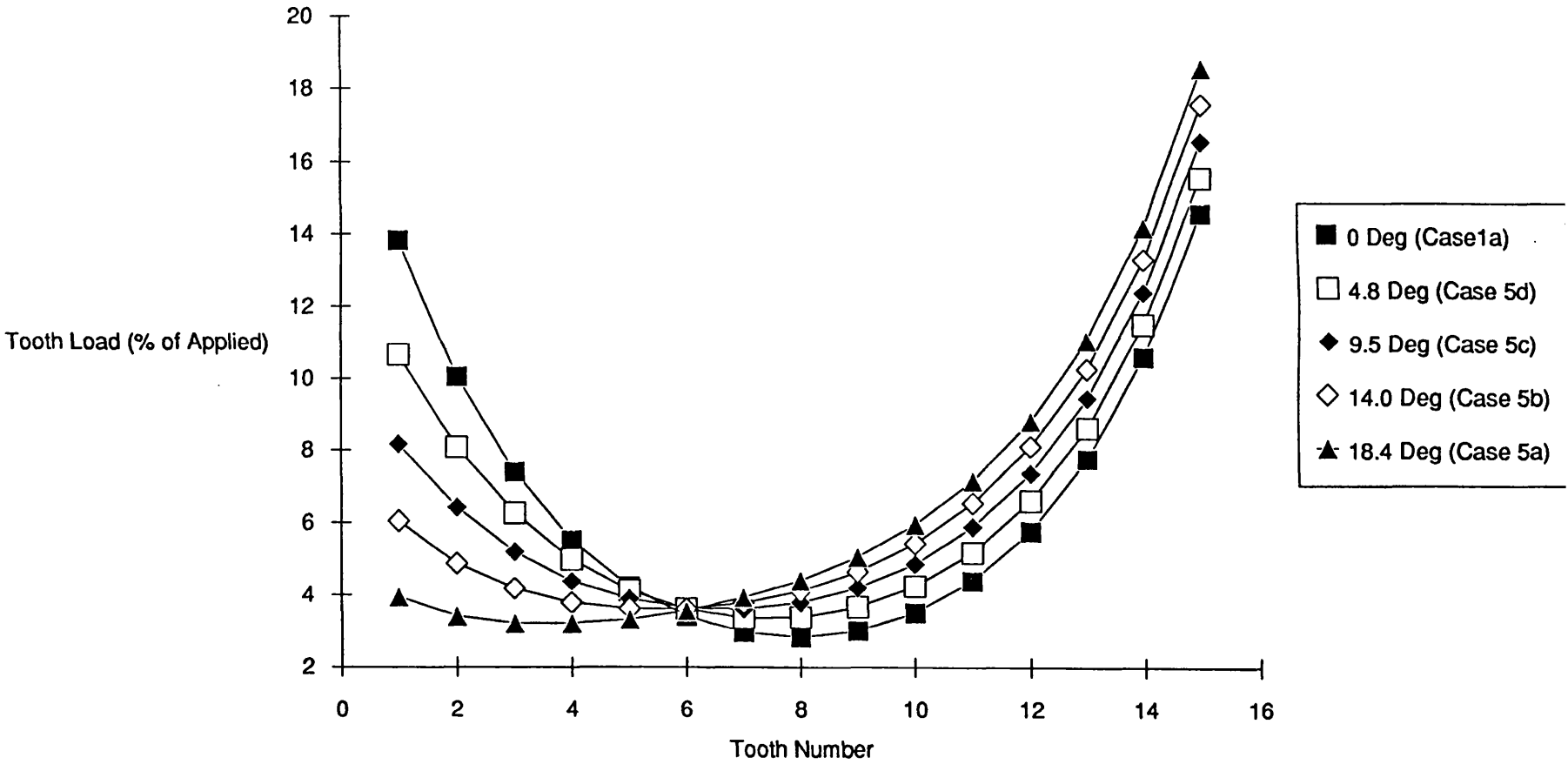

Fig 4.55 Effect of Taper Angle - No Preload

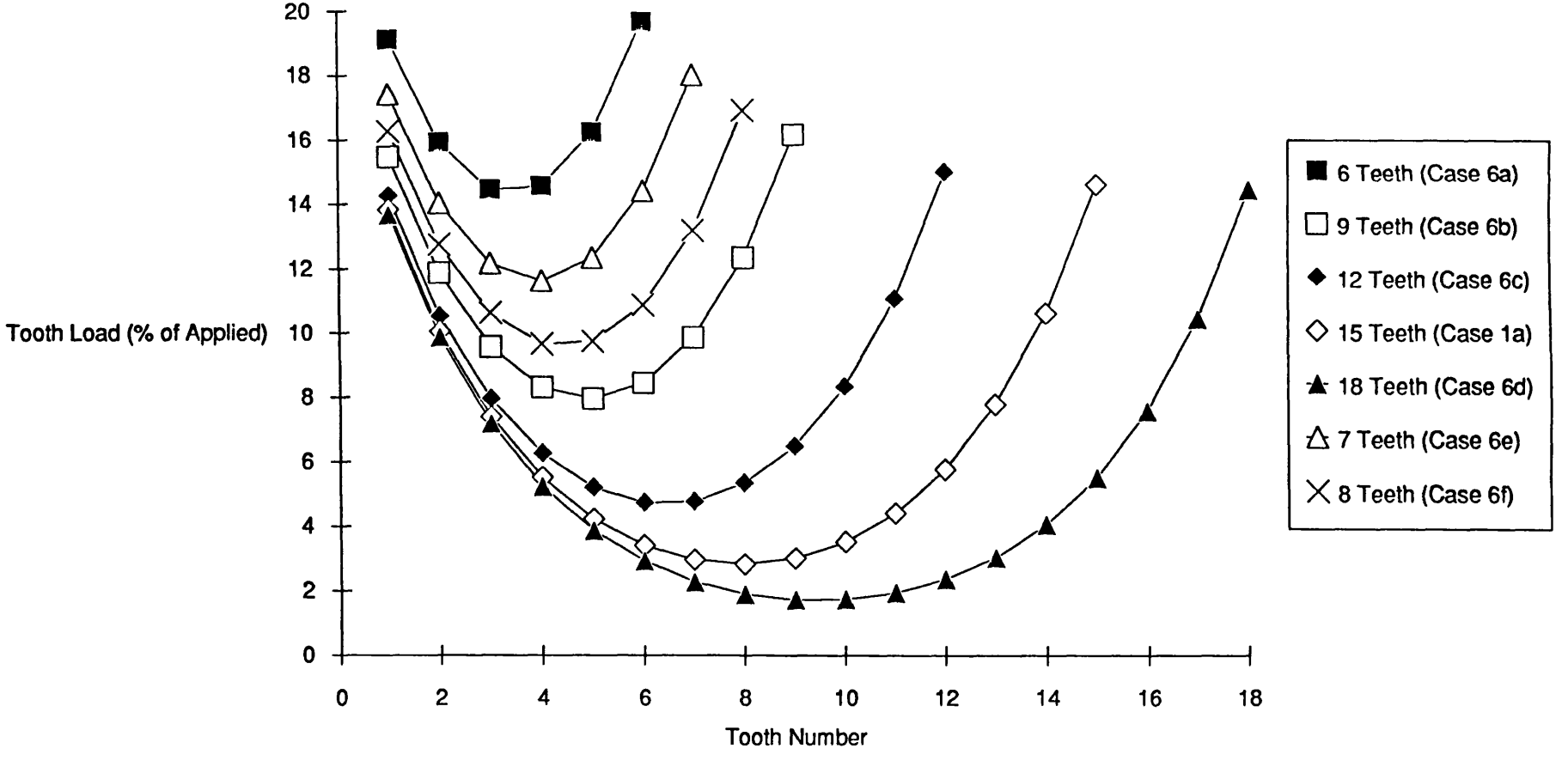

Fig 4.56 Effect of Number of Teeth - No Preload

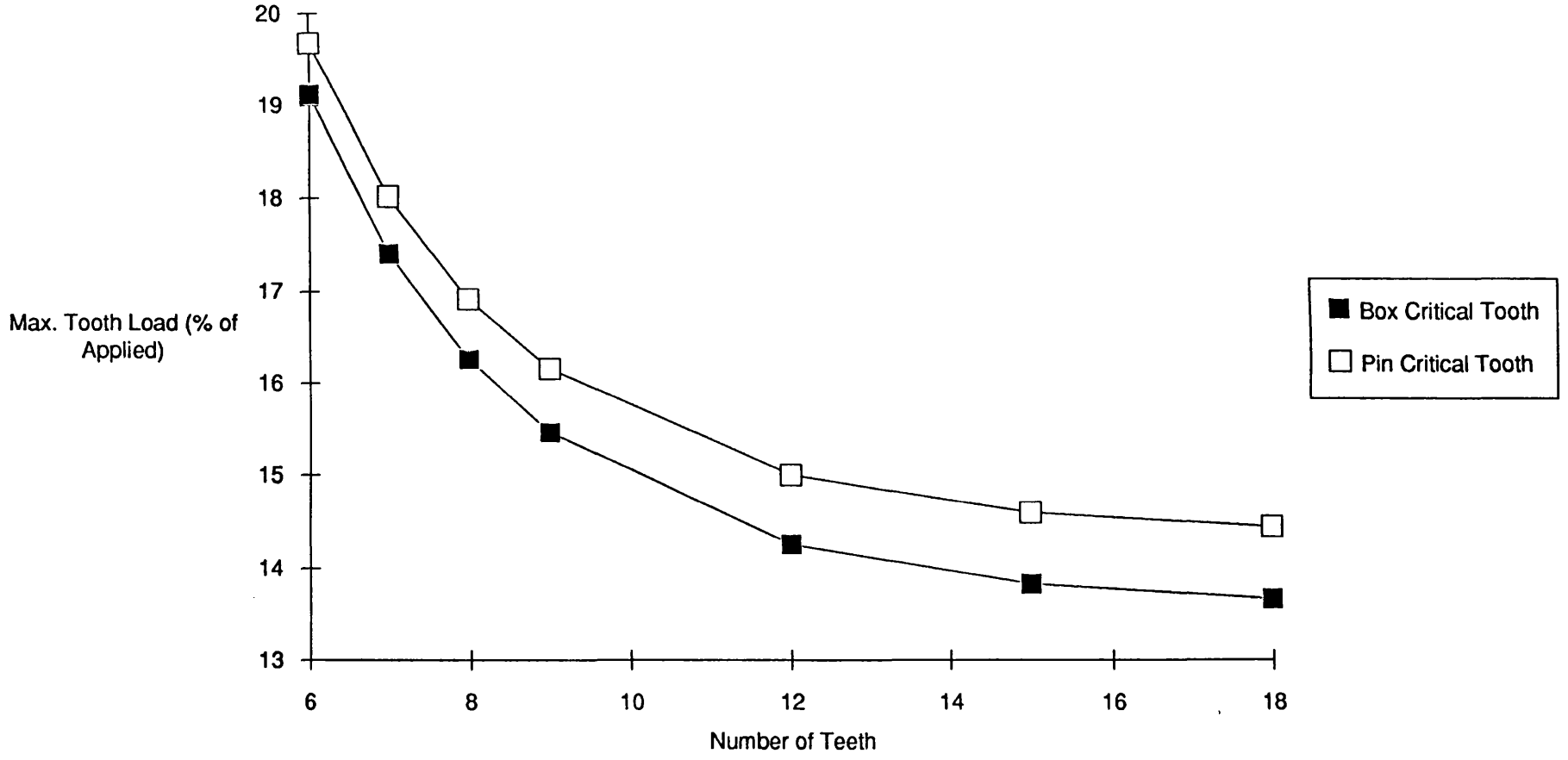

Fig 4.57 Effect of Number of teeth on load at critical tooth.

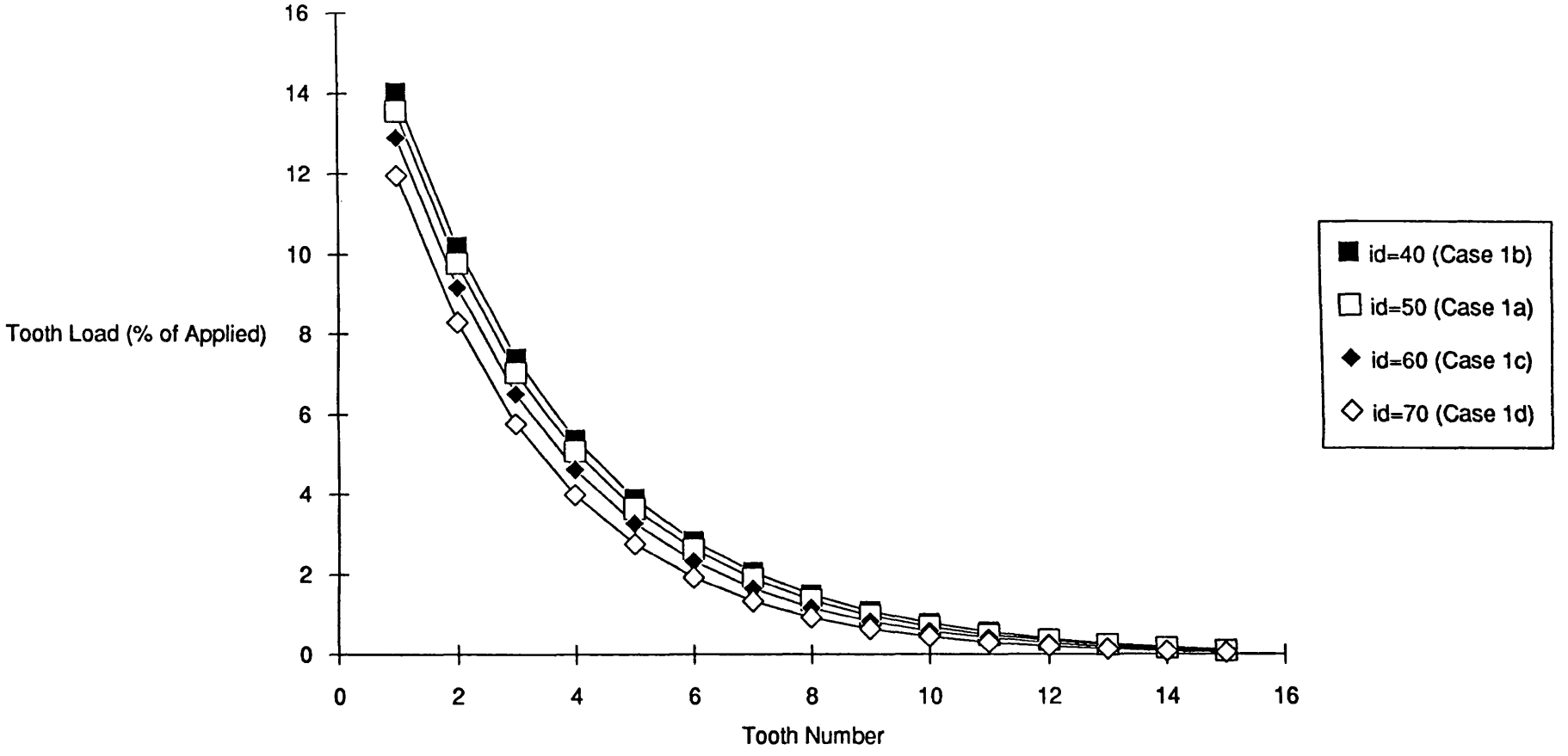

Fig 4.58 Effect of Pin Internal Diameter - Preloaded Joint

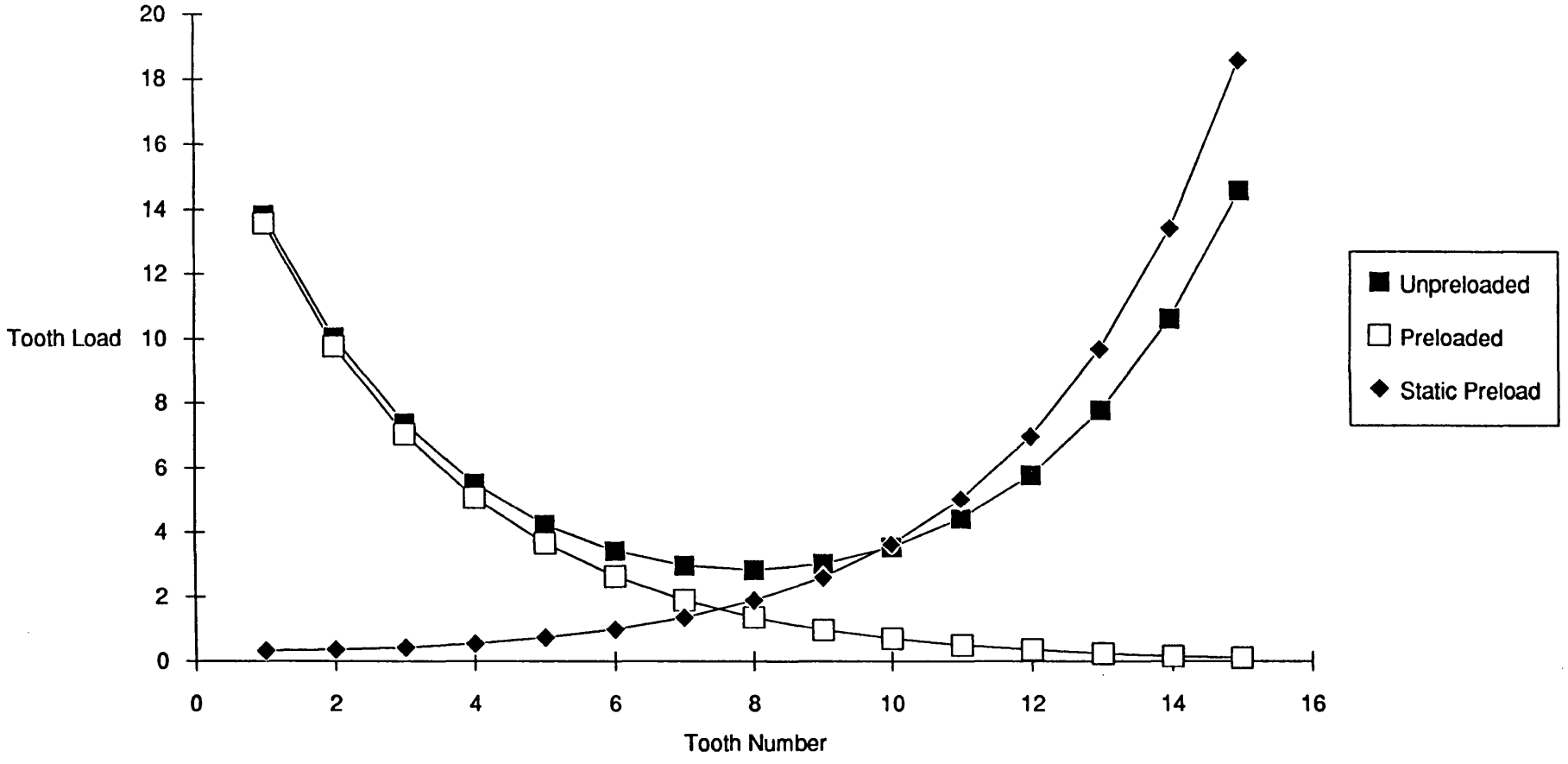

Fig 4.59 Complete results from Case 1a for a preloaded Connection

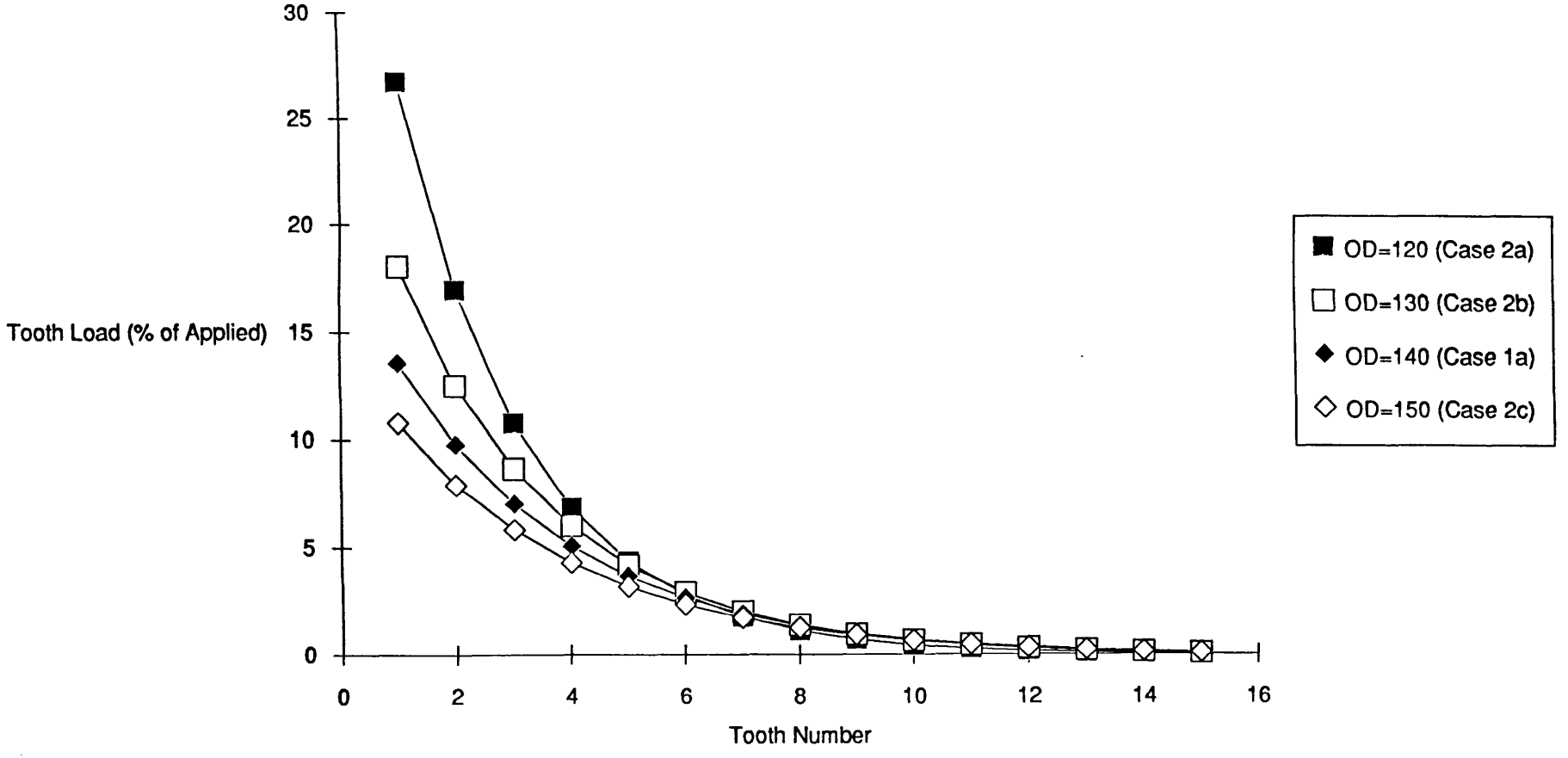

Fig4.60 Effect of Box Outside Diameter - Preloaded Joint

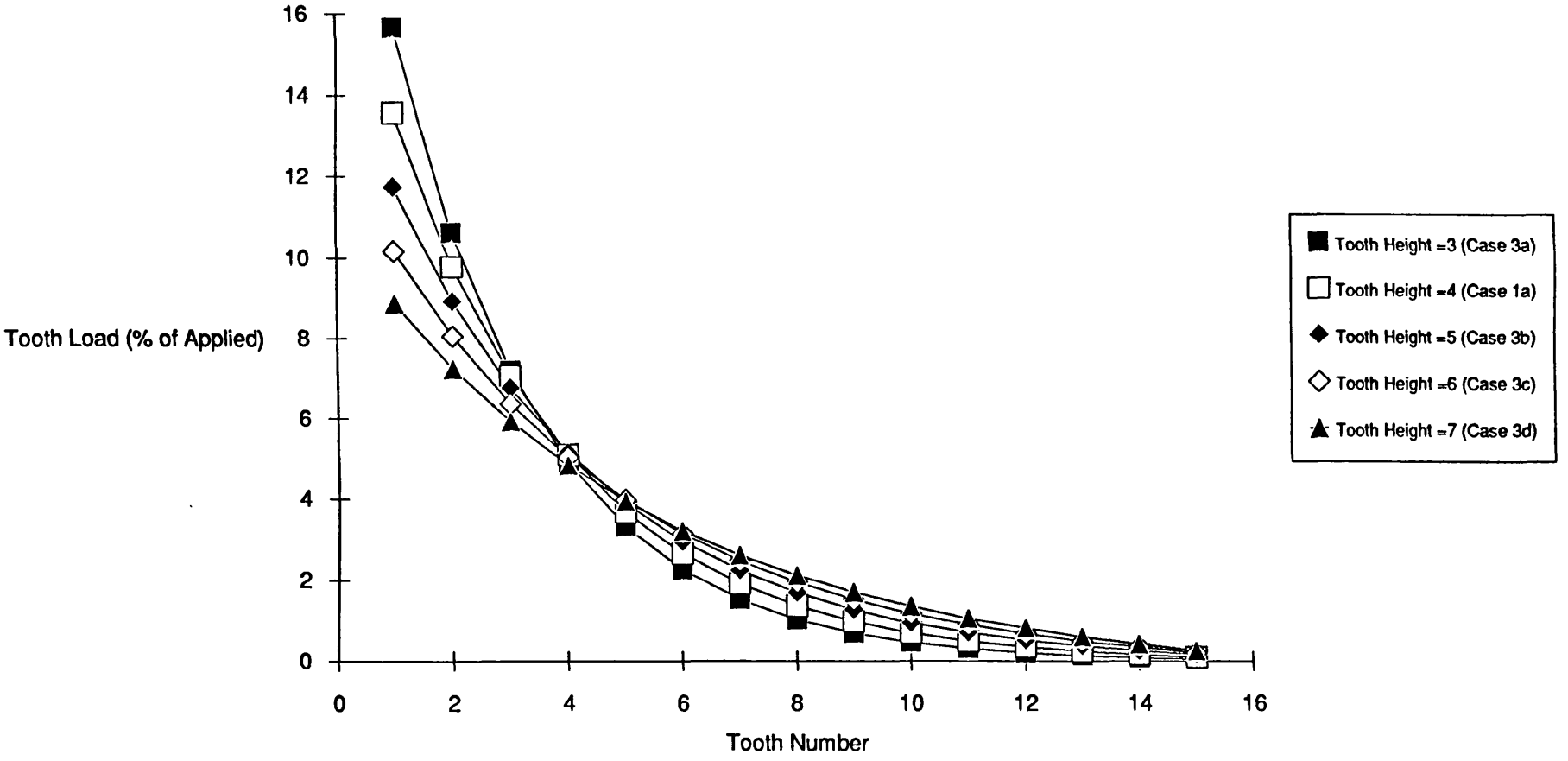

Fig 4.61 Effect of Tooth Height - Preloaded Joint

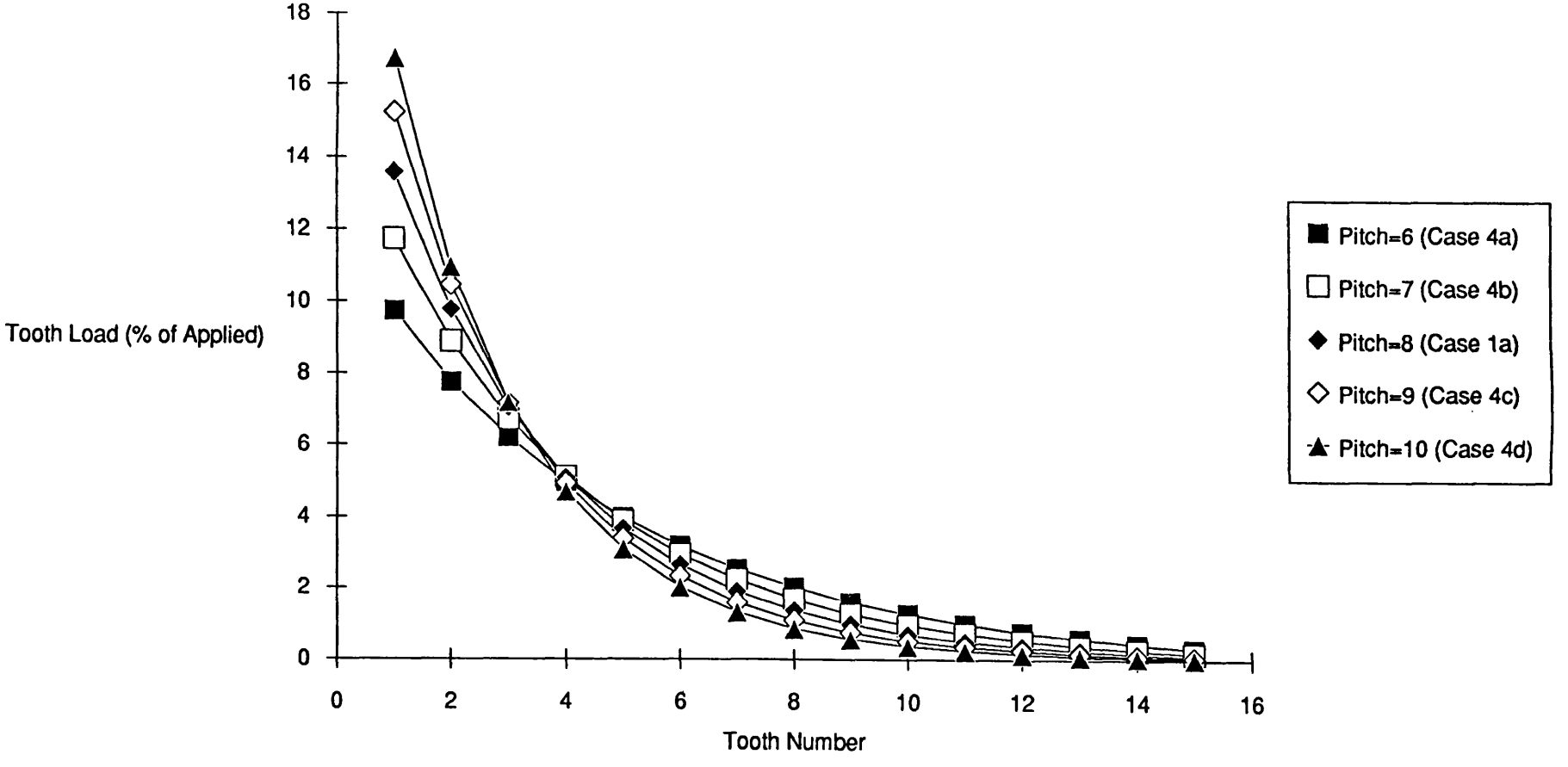

Fig 4.62 Effect of Pitch - Preloaded Joint

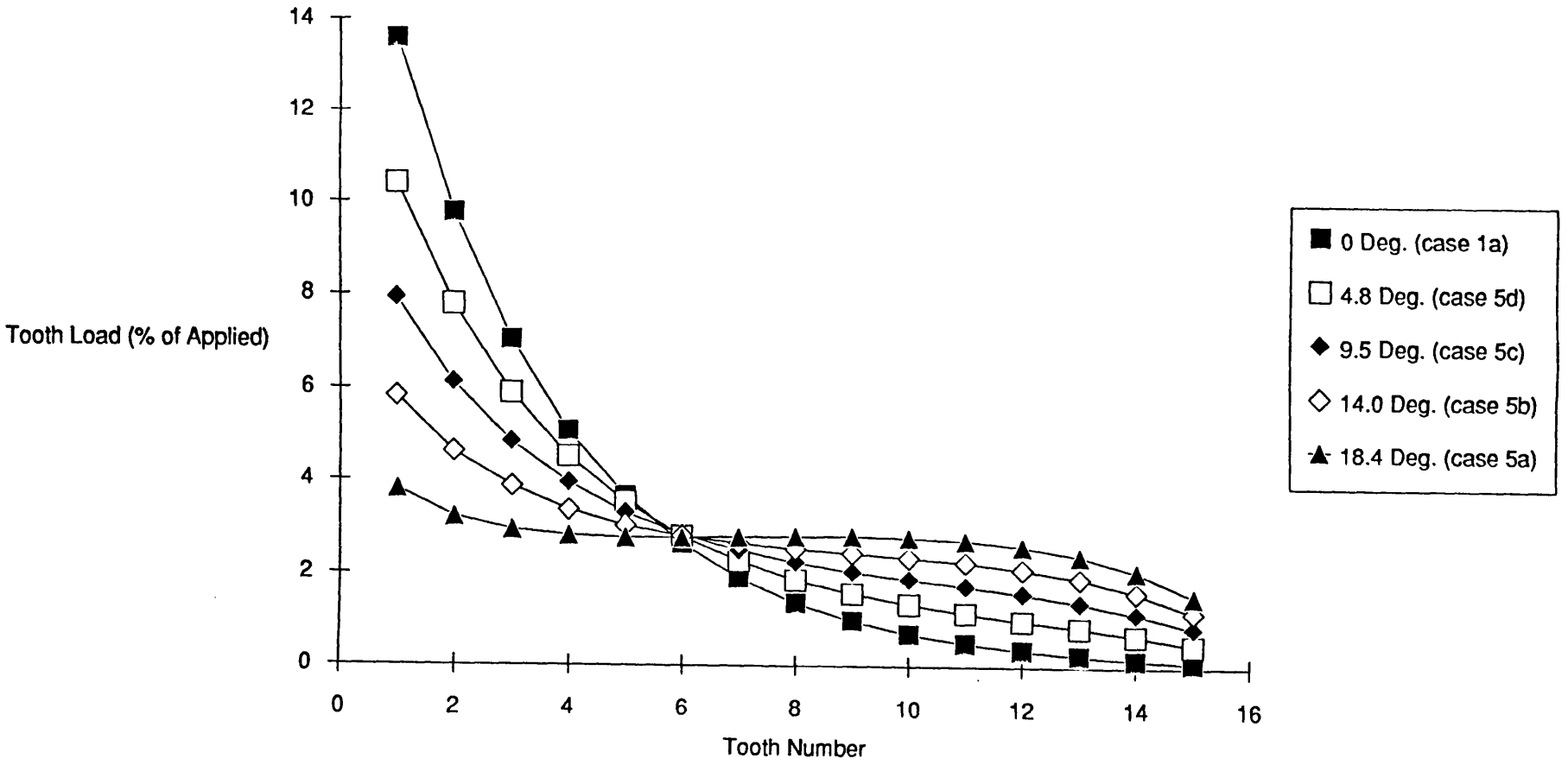

Fig 4.63 Effect of Taper Angle - Preloaded Joint

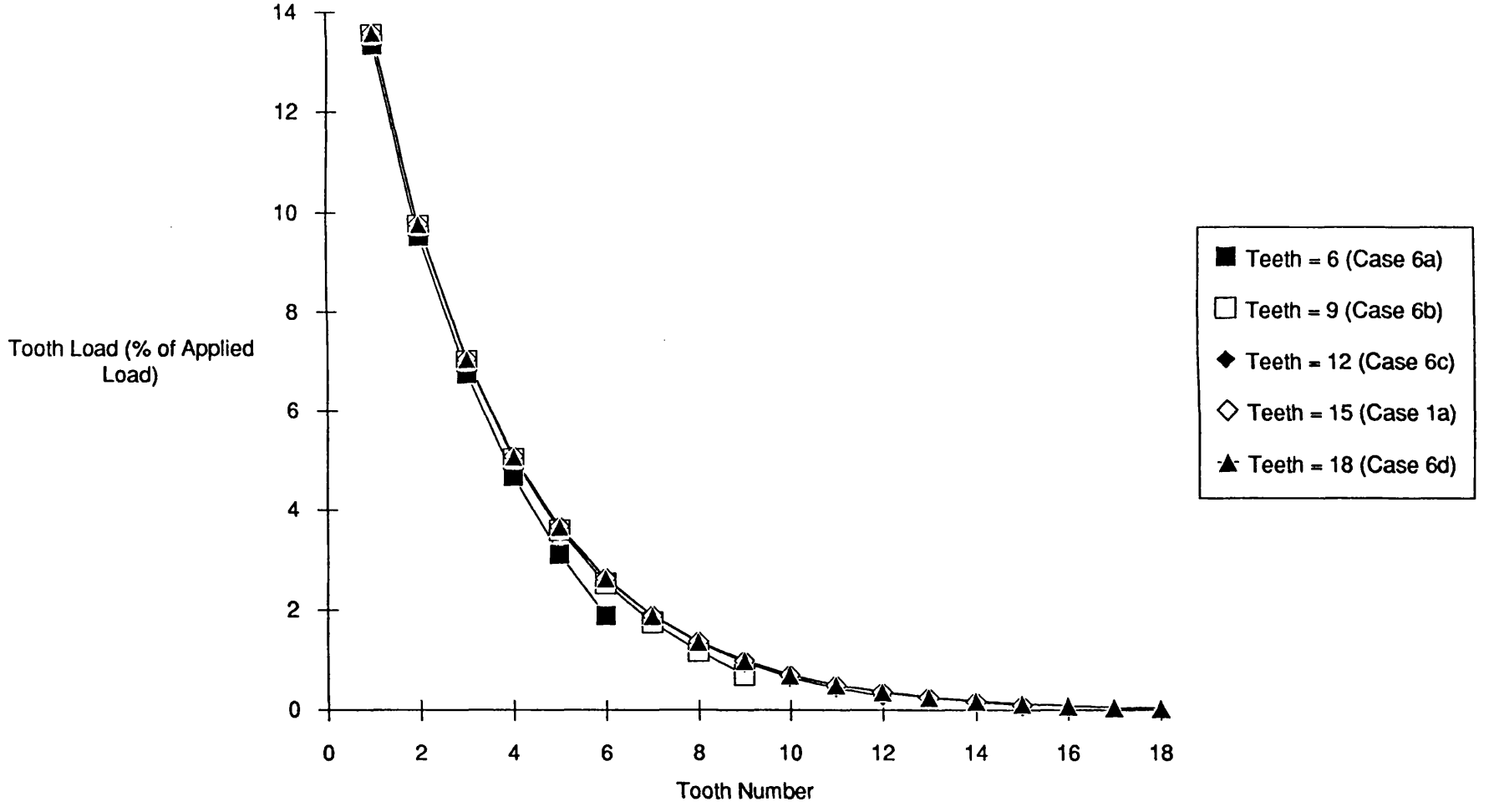

Fig4-64 Effect of Number of Teeth - Preloaded Joint

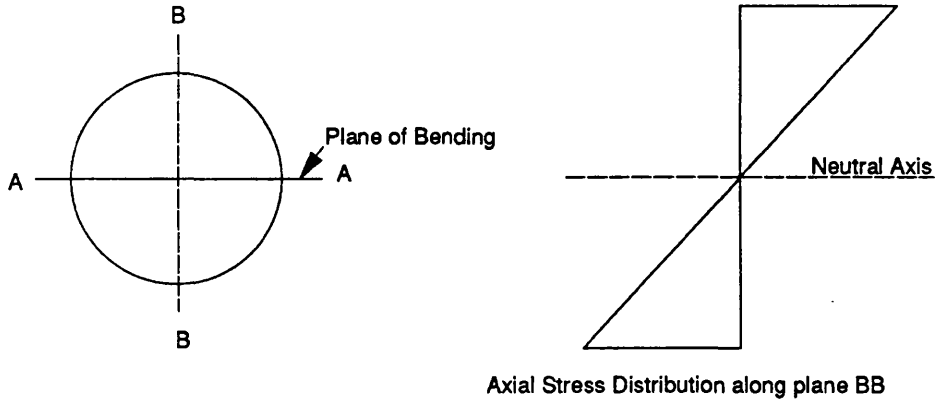

Fig. 4.65 Planes of Bending

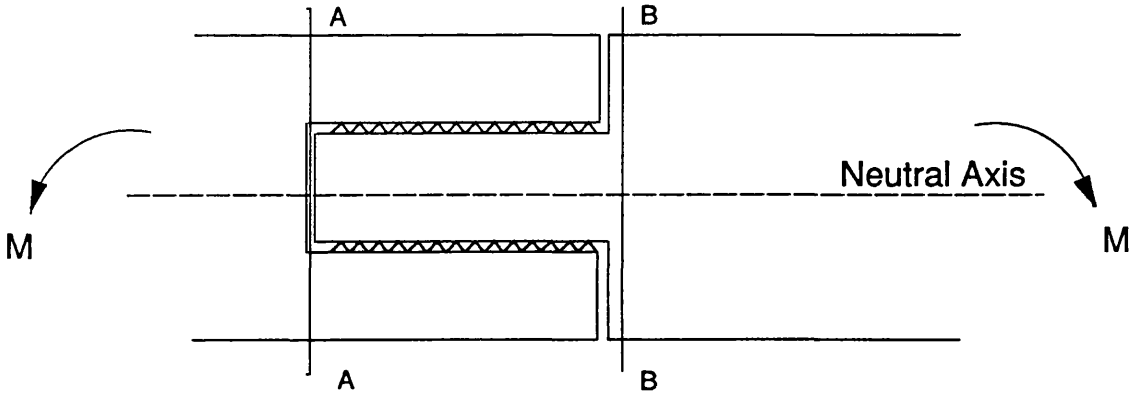

Fig. 4.66 Threaded connection under pure bending.

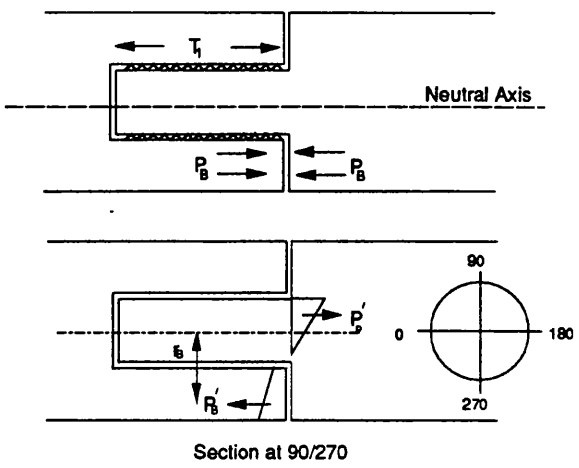

Fig 4.67 Effect of applied bending on location of neutral axis.

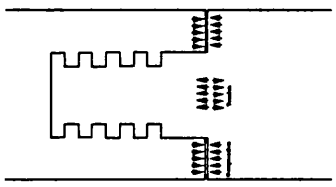

Fig 4.68 Preloaded Section.

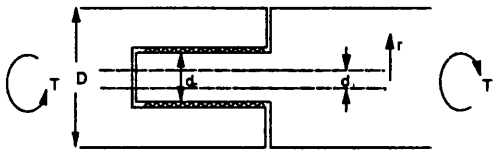

Fig 4.69 Torsion applied to a threaded connection.

CHAPTER 5

EXPERIMENTAL WORK

5.1 INTRODUCTION

Fatigue tests were conducted to investigate the behaviour of threaded connections under cyclic loading. The purpose of this exercise was to produce fatigue crack growth data that could then be used to verify fracture mechanics models of crack growth in threads.

This dictated a special requirement to be able to measure fatigue crack growth development in threaded members.

5.2 MODELS USED

Two types of threaded connector were used in the experimental studies.

I) **Thick Walled Specimen - Specimen No 1**
This model is shown in Figure 5.1 and was approximately 1/4 full size of the Conoco Hutton TLP connector although the thread form was different, in this case being a standard full size API buttress thread as shown in Figure 5.2. The geometry of the connection is the same as Model 1 studied in the FE modelling described in Chapter 3. The model was machined from ASI 4145 steel (Yield strength 870 MPa)

II) **Thin Walled Specimen - Specimen No's 2 and 3**
This model type was a standard VAM connector commercially available and licensed by Valourec. The configuration adopted is shown in Figure 5.3 and employs two pin connectors joined by a female coupling. The pins tested were 51/2" OD (20lb/ft) grade C75-2. The coupling was grade N80. Details of the geometry are given in Fig. 5.3.

5.3 TEST ARRANGEMENT

Both models were fatigue loaded in a standard Instron servo hydraulic fatigue machine of capacity ± 1000 kN. The models were loaded under cyclic axial loading at ambient pressure and temperature. The loading details are given in Tables 5.2 and 5.5. Special loading platens were produced to fix the models into the rig. The ends of the models were accurately machined to locate into the platens. No self aligning bearings were available and reliance on machine and fitting alignment was made. The models were strain gauged on the plain sections remote from the threaded connections to confirm correct alignment. Two sets of four gauges were mounted at 90° intervals, one set on the pin shaft, the other on the box. The alignment was found to be satisfactory.

The threaded connections were assembled out of the machine and the complete assembly then installed in the test rig. A special purpose lifting frame was built for this purpose. Plate 5.1 shows the test rig with a VAM joint under test.

There is no commercial technique available for the monitoring of crack growth in threads. For this reason, it was necessary to develop a system for crack detection and sizing. This is described in detail in Section 5.5.1 but did necessitate the threaded connection being disassembled for inspection. The models were inspected at regular intervals to determine crack development.

5.4 MODEL ASSEMBLY

The practice of torquing threads has been discussed earlier in Chapter 2. The requirement for high make-up torques led to particular difficulties in the Laboratory. The uncertainties associated with torquing were also a problem.. This was approached in different ways for the thick walled and thin walled models.

i) **Thick Walled Model**

The application of high torques could have been achieved in two ways. The first would be to apply the torque via the loading flange, remote from the coupling. This was considered inappropriate due to the possible damage of the plain tether section by the transfer of the torque.

A second option was to produce torquing splines on the coupling, as indeed Conoco did on the Hutton TLP. This would have been expensive to achieve and one was still left with the fundamental question of how do you monitor the torque and how much *preload* was being applied. It was the uncertainty on preload that led to an alternative approach being considered. It was considered the preload requirement was particularly important on this type of tether connection since the preload affords considerable benefit to the most highly loaded tooth, the first tooth on the pin. The solution adopted was similar to that used in Finite Element modelling, namely a "lack of fit" approach.

Figure 5.4 shows how a cam was inserted into the coupling. The coupling was then axially loaded in the test machine to just above the maximum test load. The cam was then tightened and the load released. This had the effect of compressing the cam when the specimen was in the unloaded state, hence preloading the collar of the coupling. This benefited from being totally controllable and repeatable and of course the opening load of the system was known. The disadvantage however was that the preloading sequence necessitated the loading of the model above the load at which the crack was growing. This overload type of situation can lead to blunting of the crack tip and deceleration or arrest of crack growth rate, however,

the magnitude of overload in this case was small, less than 5% of maximum dynamic load. A second effect was observed during the inspection phase and will be discussed in Section 5.5.

When considering the use of a cam lock arrangement, a number of factors needed to be considered. Firstly it was important to establish that the chosen method of preload application was realistic. In this case, the application of an applied tensile force was considered representative of the tensile force applied in the pin component during normal tightening against the preload face. Once the applied load was relaxed there was a residual load state representative of the load state applied during conventional preloading by torquing. However, the system did not have the complication of unknowns due to frictional forces in the thread and hence was considerably more repeatable with the opening load known absolutely.

However, load was not the only consideration since it is not only the load case that dictates the final stress in the component. If we consider the tapered thread, it is noted that the application of torque actually drives the joint along the taper thus reducing the radial clearance between pin and box. This has the effect of moving the contact area of the teeth toward the root and for a given load reducing the bending stresses at the thread root. Typical torque rotation are 7-10% of diameter for large steel threads used in the Offshore Industry and on this basis it was calculated this would result in a radial displacement of 0.05 mm, which was not introduced using the cam. Based on the unknown in preload due to friction on conventional torque methods, which can result in variation in a factor of 2 on applied load, this testing approach was considered an acceptable situation bearing in mind the advantages.

ii) **Thin Walled Model**

The wall thickness was too small to allow cam loading for the preload and the design, with sealing at the end of the pin precluded a similar arrangement being considered. In-service, VAM connectors are assembled using chain grips or tongs and a pre-determined rotation applied after assembly to "hand tight". It was feared that such a gripping method would damage the connector on repeated assembly/disassembly and therefore it was not adopted for these tests. Instead castellations were machined onto the end of the female coupling and a flange welded onto the end of the male component. A special purpose jig was designed to allow the coupling to be held firm whilst the pin was rotated. The applied torque was measured using a load cell developed especially for the task. The

torque used was 6500 lb.ft as recommended by the manufacturer. Both pins and coupling were then marked and subsequent assembly was achieved by applying sufficient loads to ensure exact alignment of the marks. In this way, it is guaranteed that the male and female threads mated in exactly the same place each time.

5.5 CRACK GROWTH MONITORING

The effect of a crack on the stiffness of the two types of joint were different. For the thick walled model, specimen 1, a shallow surface crack would be expected to have no measurable effect on the axial stiffness. However, it was envisaged that it may be possible to detect surface cracking on the VAM joint by monitoring the stiffness using strain gauges. In addition, the alternating current potential drop (acpd) technique was developed to allow inspection for cracking to be conducted on the unmade joints.

5.5.1 Crack Inspection Using Acpd

The ac potential drop technique has been successfully used for the sizing of fatigue cracks in many types of components [47]. Work at University College London as part of the space shuttle programme developed the technique for the manual inspection of high strength titanium and inconel bolts [48]. The technique was further developed during this study to allow the inspection of the steel tether models used here and an automated inspection system was produced.

The acpd technique makes use of the fact that an alternating electric current passes through a conductor in a thin "skin". The depth of the skin depends on the conductivity and magnetic permeability of the material and the frequency of the alternating current. The instrument used in this project was developed by staff at University College London and is now commercially available as the Crack Microgauge [49]. The model U7 used in this work operates at a frequency of 6KHz which, when used with carbon steels results in a skin depth of about 0.1mm. A probe was developed that allows the surface potential to be measured across adjacent thread crowns as shown in Figure 5.5. If a crack is present anywhere between the thread crowns, the measured surface potential increases as the probe spans the crack.

The acpd technique requires a uniform ac field to be applied to the area of interest. In the case of a bolt, this can be achieved by injecting the field on the axes of the bolt as shown in Figure 5.6.

In the case of hollow threaded component, the field cannot be applied at the axis and this introduces a major problem in that a uniform field is difficult achieve.

An alternative solution was developed in the form of an inducing probe. Figure 5.7 shows how an inducing coil was introduced into the measuring probe. By passing an ac current through the coil, a similar current was introduced locally into the material surface at the location where the field was to be measured. In this way, a uniform field could be imposed locally at the point of interest. This was a major improvement in the use of the technique, especially for difficult geometries and gave easily repeatable readings to within 0.25mm.

The probe was further developed into a part nut which meshed with the thread of the component being inspected (Fig 5.5). By constraining the probe in the radial direction, rotation of the component forced the probe to track along the thread, thus enabling the complete thread to be inspected. The rotation of the specimen was put under computer control and all acpd data captured by a DEC PDP 11 computer. The development of such an inspection system enabled crack detection as well as crack sizing (depth measurement). This system has recently been adopted by industry in the inspection of threaded drillpipe which has been removed from service [50].

By regular inspection during the fatigue tests, information was provided on three aspects.

i) Crack initiation
ii) Crack depth growth rates
iii) Crack shape evolution

This information was then used to study the crack growth characteristics and to validate the proposed fracture mechanics models.

The inspection capabilities of the acpd system as developed were limited to the inspection of the cracked face. This meant that the joint needed to be broken down each time to inspect for damage. It was not considered that there was a suitable alternative inspection system available. Conoco are reported to have spent in excess of $1m US to develop an ultrasonic tool for the inspection of threads in the made up condition and even then this was not completely successful. Bearing in mind the complex reflections from the thread roots, this is not surprising. The penetration depth of the 6kHz ac field was approximately 0.1mm and thus inspection with such high frequency would not be suitable for inspection from the remote face.

Two alternative inspection methods were employed on the thin walled model (Model 2). The first was another electric current flow method, DC potential drop (DCpd) and the second was conventional stress monitoring. Both are discussed below. The reason that these were both employed only on the thin wall tether is that as a crack develops, the crack would soon become significant in depth with respect to the wall thickness, a feature required from both these alternative methods as described below:-

5.5.2 DC Monitoring

One method used on small specimens is DC potential drop monitoring. A DC current flows through the whole section of the body and thus has the "potential" for interrogating the whole section. The principle is similar to that for acpd whereby the presence of a defect in the flow of current in the section results in disturbances in the surface voltage field. However, there are a number of drawbacks when applying the technique to large threaded connections.

1) Since the current flows through the whole section, the surface potential is rather insensitive to defects growing from the remote face since the net effect is small if the defect size in respect of both length and depth (particularly depth) is small compared to the wall thickness.

2) Since the current flows through the whole section, the surface potential is very much smaller than for an ac field where the current is concentrated near to the surface. As a result, currents of hundreds of amperes are necessary to produce measurable surface voltages. In the case of the tether, a current of 500A was used.

3) Since the whole section is inspected, the presence of a defect anywhere in the section can create surface voltage perturbations. There is therefore no general theoretical solution available for the prediction of crack size. In specimen testing where the crack location is predetermined, calibration procedures are produced by experimentation to correlate potential drop with crack depth. Such an approach was not considered possible for the threaded connections due to the size of the sample and the fact that the exact site of a defect was not known in advance.

4) In order to monitor a complete connection, it was necessary to pass the current from pin to coupling. Thus the current flow, and hence potential, depended totally on the electrical contact between the meshing teeth which would have been variable and uncontrolled.

Accepting these problems, a DC monitoring system was developed during the project. Surprisingly the system seemed to give repeatable readings despite the uncertainties regarding the current flow across the threads. Since moveable probes would be difficult to employ due to contact resistance variations, fixed probes were spot welded at a spacing of 10mm on the inside of the pins at 8 locations equally spaced around the circumference directly opposite the first loaded thread. Due to safety implications arising from the fact that the DC inputs were connected electrically (via the specimen) to the 100 tonne capacity test machine and controller, DC inspections were only conducted with the test machine off and the specimen unloaded. Typical measured voltages were of the order of 50-60 μV. Each probe site was multiplexed to a voltage measuring device using a proprietary manual strain gauge multiplexer. In the sample monitored, a defect of approximately 1mm depth was found using acpd which was not detected using the DC system probably due to the fact that the crack actually occurred mid way between two of the fixed probes, hence the surface voltage disturbance would have been too small to distinguish from the general variation in reading due to overall system performance, typically 2-4% of the mean value.

5.5.3 Strain Gauge Monitoring

There are similarities between the principle of strain gauge monitoring and DC monitoring. For strain monitoring, one is looking for variation in the surface strain field due to the disturbance of the internal stress field due to a defect. Like DC monitoring, it is necessary to monitor at fixed locations and it is therefore necessary to predict likely locations for fatigue cracking prior to the test. For the VAM joint under test, previous tests [42] suggested failure was likely at the first loaded thread of the pin, an observation borne out by the theoretical prediction and therefore strain gauges were sited on the outside surface of the coupling corresponding to the first loaded tooth position. The choice of site was dictated by two considerations.

1) It was not possible to accurately locate and reliably fix strain gauges on the inner face of the pin due to limited access. This was however the preferred site.

2) It was considered that the presence of a crack at the thread root of the pin would change the tooth stiffness of that tooth and thus modify the load transfer into the coupling. This was expected to result in a change in the strain distribution near the defect.

A total of 43 strain gauges were applied to the coupling as shown in Figure 5.9. Gauges 1-10 were linear gauges on the axis of the connection to investigate the overall coupling behaviour Gauges 11-15, 25-29 and 16-20 were in the form of 3 x 5 element linear strain concentration gauges, the remainder being linear gauges situated around the circumference close to the site of the first loaded thread. The gauges were located around a circumference rather than following the thread helix.

The gauges were connected to a Solatron data logger under computer control by a DEC PDP11 mini computer. All gauges were connected independently in the quarter bridge configuration.

It was not feasible to monitor the strain gauges during fatigue cycling since requirement for a strain measurement at the peak of the cycle could not be guaranteed with the hardware available. However this was not considered too serious since data could be collected by periodically stopping the test and measuring under static loads. At each monitoring interval, strain measurements were taken by monitoring the strain gauges as the load was increased and then decreased in fixed load increments.

However, this resulted in fixed interval monitoring rather than continuous monitoring which would obviously have been the ideal. Obviously with more sophisticated hardware it would be possible to co-ordinate the strain measurement at the cyclic peaks and thereby monitor long term trends. However, this type of monitoring does have a number of disadvantages in terms of the quality of data collected. It is normal to take a number of readings for each gauge and then average to give a single data point and for dynamic monitoring this would necessitate averaging over a number of peaks and hence introducing additional errors. A further disadvantage is that it is not possible to collect all channels of data simultaneously and hence any fluctuations in absolute value of load over a number of cycles will influence the results, the premise being that the static load stability would be better than the dynamic stability peak to peak. Finally there are additional problems of equipment stability when attempting to monitor over long periods (weeks or months). The quarter bridge gauge configuration does not incorporate

temperature compensation (although these gauges are specified as temperature compensated for steel) and therefore additional wiring and gauges would be required to minimise variations due to temperature.

5.6 LARGE SCALE TEST RESULTS

This section gives the large scale test results for the 2 models including the data obtained from the defect monitoring systems.

5.6.1 Model 1 - Thick Walled Tether

5.6.1.1 Static Preload

Preliminary studies were conducted to confirm the preloading mechanism using the cam rings. The cam rings were set by applying an axial testing load of 850kN and then locking the rings into place. The spacer ring was instrumented using 4 strain gauges spaced at 90°intervals around the outer surface. These were monitored during the initial set up phase to ensure that compressive loads were being induced into the joint. The procedure was as follows:

1. Load model to 850 kN
2. Tighten cam rings
3. Monitor strains on ring as load was decreased in increments to zero and then increased

Results are given in Table 5.1.

Whilst these results show very little change for loads in the range 400 kN to 850 kN, which implies that the compressive loading due to preload is not linear with applied load, it was observed that the cam rings and spacer were in fact under significant compressive loads even at an applied load of 800kN as evidenced by the fact that the cam rings could not be moved at that applied load.

These measurements were repeated several times and no-errors could be found. This apparent non-linearity could not be readily explained although it was thought possible that perhaps the preload which was clearly there since the cams were unmovable, was concentrated toward the inner face of the spacer nearest to the pin. However, even if this was the case, a linear effect would still have been expected providing that contact/compressive forces were maintained across the whole preload face ie the load path did not vary with load.

5.6.1.2 Dynamic Loading

The Instron test machine controller was set up for the particular experimental configuration by optimising the PID control loops under a square wave input. If this is not carried out, the dynamics of the control system can be influenced by the inertial effects of the specimen and fittings. The procedure was to use a square wave input of amplitude 100kN at a frequency of 1Hz and to "tune" the system for optimum load output response. The optimum setting were found to be:

Time Constant	=	3
Loan Gain	=	99.4%
Mass Compensation Setting	=	1

The loadings used for the test were then applied to the specimen and the input and output traces compared. These were found to be with 0.5% of the range of the load cell. All cyclic loads were measured as the load output.

The results for the subsequent fatigue tests are given in Table 5.2.

5.6.1.3 Crack Monitoring

As described earlier, the ac inspection system was used to inspect the pin periodically during the test. Both induced and injected field inputs were compared and since the induced field input gave similar results to the injected field system, and was much easier to deploy, the induced field system was used for all automated inspection.

Referring to Figure 5.8, the overall path length around the crowns was calculated to be 8.3mm. Denoting the potential reading across the crowns of an un-cracked thread as V_1 and the corresponding measurement across a cracked thread as V_2, the crack depth is calculated [47] as

$$a = \left(\frac{V_2}{V_1} - 1\right)\frac{8.3}{2}$$

Since the system relies on voltage ratios, there is no need for calibration.

After 59,700 cycles, the inspection using acpd revealed 2 cracks. The calculated depths are:

Induced Field	Crack 1	0.64mm
	Crack 2	0.46mm
Injected Field	Crack 1	0.68mm
	Crack 2	0.47mm

This gave confidence in the new induced field probe development which was then used for all subsequent inspections.

Figures 5.10 and 5.11 show the raw output from some typical acpd inspections conducted during the test with the crack fronts clearly shown.

The crack depth was also measured using a probe with a shorter leg length which actually reduced the path length between probe tips to 3.6mm. This is shown schematically in Figure 5.12. Table 5.3 summarises the calculated crack depths from the acpd inspection for the first 3 inspections.

These are plotted in Figure 5.14 and it is seen that whilst Cracks 1 and 3 appeared to be growing as expected. Crack 2 had not developed. This is unlikely to be the case and therefore it was suspected that the acpd monitoring was being affected in some way. It was thought most likely that the process of making and breaking the model with the associated overload to tighten the cam rings could have created markings on the fracture crack surface due to excess plasticity on the crack tip and that these were creating electrical short circuits across the crack face loading to an underestimate of crack depth. This is shown schematically in Figure 5.13. The overload could also lead to crack closure stresses which could again increase the possibility of shorting across the crack face.

In an attempt to investigate this, it was decided to apply a low amplitude R = -1 loading sequence to the specimen to "shake down" the closure stress. A load range of ± 70kN (ie ±10% of the original stress range) was applied with the cam rings undone (ie no preload) 126,000 cycles were applied and the specimen removed. The result of this exercise is given in Table 5.4.

These results show that the crack readings that were suspected (Cracks 2 and 3) had indeed increased by a small amount and that the greatest increase was on that crack (crack 3) that showed the most significant growth rate reduction. Additional cycles were applied on the normal test load ($\delta P = 750kN$) and the specimen then inspected after a total of 207,000 and 284,400 cycles. Again the results indicated that there were problems with the acpd inspection as the cracks appeared not to be growing at anything like the required rate (a constant or accelerating crack growth behaviour would be expected rather than decelerating).

Since it was not possible to apply a tensile load whilst monitoring the crack with acpd, a bending jig was produced (Fig 5.21) which, although of limited load capacity, allowed the pin threads to have a moment applied. It was only possible to apply a surface bending stress of between 10-15 N/mm^2 at the crack location but monitoring with acpd during the applications of load indicated no effect whatsoever.

The testing then continued until 374,700 cycles had been applied when a fracture occurred.

5.6.1.4 Examination of Crack Surface

The final fracture surface indicated that cracking had occurred over a surface length greater than 1 circumference, this was predicted from the acpd monitoring.

The fracture occurred such that Crack 1 and 2 were completely visible with only part of crack No 3 exposed. Figure 5.15 shows the exposed crack profiles measured from the fracture surface. It is evident from the fracture surface that the overloads did result in crack markings on the fracture surface with three clearly defined features on cracks 1 and 2 and two clearly visible markings on crack 3. These appeared as "beach marks" which are characteristic of fracture surfaces where crack markings by overloading has been attempted. These marks on the surface were therefore considered to be attributed to the overloads applied during the make and break operation for the specimen removal and therefore were considered to represent the crack shape at the time of specimen inspection.

The best acpd results were obtained from cracks 1 and 3. The acpd inspection results from the first 3 inspections of all 3 cracks are compared with the crack shape measurements on the fracture surface in Figure 5.17. It is seen that there is excellent agreement in the crack shape development between acpd and optical readings which appears to confirm that in the early stages of crack growth, the acpd crack

measurements were reliable but that as the crack grew, and hence the SIF at the crack tip due to the applied overload necessary to undo the cam rings increased, so the effect on the electrical contact increased resulting in significant underestimates of crack depth as the test progressed.

Using a combination of acpd and optical measurements (Fig. 5.17) crack growth curves for cracks 1, 2 and 3 were produced and are presented in Figure 5.16. Here it is seen that the crack growth is seen to accelerate toward the end of the test as the nominal stresses due to the reducing net section combined with the increasing crack tip severity.

5.6.2 Thin Walled Tether, Model 2

A series of VAM joint tests had previously been conducted by British Steel Corporation on 5" diameter J55 VAM joints [42]. The results which are confidential were released to enable the test proposed here on 5.5 " OD joint to be designed. Based on the BSC results, it was predicted that a load range of 534 kN would produce a failure after 300,000 cycles, based on the same nominal stresses for the two different joint sizes. Table 5.5 summarises the test data for the VAM Joint test (Model 2).

5.6.2.1 Acpd Inspection

A similar inspection arrangement to that used on Model 1 was used for the VAM joint except that it was necessary to redesign the automated rig to accommodate the different joint geometry. An induced field probe was used for all acpd inspections and it was necessary to develop a special probe to allow for the inspection of the thread run out on the pin. The pin design is such that the taper thread is cut into the outside of the plain tube and hence runs out at the end furthest from the free end, as the outside diameter becomes too small to accomodate the thread taper (Fig.5.3). ACPD inspections of both pins showed no cracking after 32,400 cycles. The specimen was then removed again from the test rig for inspection after 65,400 cycles. Unfortunately the bottom pin was damaged as it was unscrewed resulting in considerable damage to the thread crowns which made any acpd inspection impossible. It was therefore decided to continue the test with the strain gauge monitoring only, which avoided the necessity to remove the specimen. The specimen was therefore re-assembled and the test continued to failure.

5.6.2.2 Strain Gauge Monitoring

The readings for gauges placed around the circumferences at 15,000 cycle increments are given in Figure 5.18. Whilst the absolute strain values were not uniform around the circumference, the distribution remained similar throughout the test.

The plots of strain axially along the length of the coupling are given in Figure 5.19. From Figure 5.19 it is seen that overall, the strain distribution is similar for both connections within the coupling. However, local monitoring of strains using strain concentration gauges gave unexpected results. Figures 5.20a and 5.20b show the detailed strain distributions for different loads, at each end of the coupling and it is seen that there is a change from tension to compression near the free end of the coupling. This is due to the belling effect described below and suggests the surface of the coupling is assuming a concave shape in the axial direction.

It is also observed that the changeover point remains constant at any load. Thus there is apparently a point of zero strain on the coupling surface irrespective of applied load. This is seen to occur at both free ends of the coupling. As for the circumferential gauges, the strain distribution did not alter significantly throughout the test.

No significant changes in strain distribution were observed, even close to the end of the test so as a monitoring technique, the success of strain gauging was not fully established in these tests. The fact that no information on crack growth was collected means that the sensitivity of the system could not be defined. However such a strain survey did highlight an interesting feature of this type of commercial connector.

Close examination revealed that the connector has an interference radial fit between pin and couplings. As the connection is torqued, the taper of the pin leads to a "belling" of the coupling near the free end, where the wall thickness is a minimum. During applied axial loading, this effect is maintained with axial loading from the pin resulting in radial expansion of the coupling in proportion to the load. Hence, what is observed in the strain monitoring is an elastic belling of the coupling superimposed on the applied axial strain resulting in the phenomenon of a zero strain location around the joint. A basic analysis of the axial loading suggested that the pin was the most highly stressed component. However, the belling phenomenon just described does have the effect of inducing tensile stresses at the root of the threads at the free ends of the coupling. This could explain the failure of coupling components in some instances in service.

5.6.2.3 Failure

The VAM model failed after 373,000 cycles by through wall cracking of the top pin. The crack had developed in the first loaded thread of the pin (which is a partial depth thread) and had grown from the thread root around 50% of the circumference. The fact that the strain gauges indicated no changes after 360,000 cycles, and the compliance had been checked at that time, suggests the through thickness crack had not developed at that stage.

This suggests that very rapid through thickness crack growth had occurred with the last 12,000 cycles. The specimen did not fail by brittle fracture as had occurred with the thick walled model. The through thickness cracking had in fact resulted in extreme lateral displacement as the cracking led to an eccentric load path as the net section reduced. When an axial load was applied, the cracked section was displaced approximately 6mm horizontally as the remaining load carrying section tried to align itself along the specimen axis.

Subsequent acpd inspection of the other pin connection indicated a small surface crack in the first loaded tooth. This crack extended for a length of 20 mm around the thread root and had a measured depth of 1.5mm. No cracking was found on the coupling component although inspection of this was restricted to manual acpd inspection since the coupling was too small to fit into the automated inspection rig.

5.7 DISCUSSION OF RESULTS OF LARGE SCALE TESTING

The large scale tests conducted have given a valuable insight into the behaviour of threaded connections under cyclic fatigue loading and, where acpd monitoring was conducted provided information on the crack growth behaviour. It was unfortunate that mechanical damage prevented the VAM joint from being periodically inspected during the test using acpd.

The acpd system for semi automated inspection developed here provided vital information on the development of the shape of the defect. By using this data it is possible to compare actual crack behaviour to that predicted for Fracture Mechanics analysis (See Chapter 6). The problems with the VAM joint test clearly showed that without the use of acpd, the fatigue test was only able to provide one data point in terms of crack growth which was through wall penetration. In contrast, the acpd system gave a number of data points for the thick walled joint which allowed an estimate of initiation life and crack growth rates to be made.

However, it is clear that the acpd system was affected by the experimental technique used to apply to preload. That technique, involving small overloads damaged the crack surface sufficiently to lead to electrical short circuits and underestimate of depth. The data clearly showed that the results for crack length prediction were not affected. This would be expected since the short circuits would occur on the crack front and not significantly affect the electric flow near the end of the crack where it breaks the surface.

The implications for this is that the acpd system could be used on full scale threads to detect cracking at the thread roots, that is to say, to establish the presence of a crack.

The possible problems in depth predictions due to overloads damaging the crack surface could lead to underestimates of crack depth. These effects may be reduced in service where the presence of corrosive fluids could quickly eliminate the possibility of electrical short circuits across the crack face. In practical situations however, it is unlikely that any cracked component would be used, irrespective of the measured (predicted) crack depth, and this suggests that the inspection system developed here for laboratory use could be developed for commercial applications for the verification of components prior to use. This is particularly true for situations where the defect reporting is based on crack depth and for which the depth at which defects are reported would be small. The experiments here showed the underestimates of crack depth would only occur at large crack sizes well above the rejection threshold.

The DC inspection system did not prove very successful and was very difficult to use. For large scale applications the DC system is impractical due to the requirement for large DC currents and the ensuing safety implications. This, together with the complexity of interpretation, makes the DC potential drop system unsuitable for any in service inspection or industrial thread inspection systems. The stability of readings was however, surprisingly good considering the possibility for variable contact resistance across the thread faces and it is considered that further refinement could make the system suitable for the detection of the occurrence of gross damage in the laboratory.

The strain monitoring on the VAM connection provided a valuable insight into the belling effects which are characteristic of this type of interference fit tapered connection. There were however, no significant effects seen during the VAM tests but, due to the experimental difficulties discussed earlier, it was not possible to know whether this was indicative of the fact that no cracking was occurring or whether indeed cracking was taking place and the monitoring system was insensitive to it. For larger scale tests, it is considered that the use of strain monitoring on the inside of the pin would be significantly more sensitive to cracks in the pin and that circumferentially applied gauges at the first loaded tooth may be able to monitor a change in stress distribution due to crack development.

The results from the thick walled model clearly shows the design to be "defect tolerant". That is to say, the defects were first detected after approximately 60,000 cycles and yet failure occurred after a total of 373,00 cycles. The fact that 85% of the fatigue life was taken in crack growth indicates clearly that the design is capable of operating whilst cracked which allows an in-service inspection procedure based on regular routine inspections for the presence of a crack greater than a certain size to be adopted.

For the thin walled tube, there is insufficient information to be able to judge whether the design is defect tolerant to the same extent. It is considered likely that the percentage of the total fatigue life occupied by crack growth will be significantly less for this design since the thin wall would lead to the earlier wall penetration and the more rapid growth characteristics of a through crack.

The most significant comparison however, is in the nature of the failure. The thick walled modelled failed by brittle fracture before through wall penetration whereas the thin walled member failed by through wall penetration and subsequent ductile crack growth around the circumference. This is a particularly important observation when considering typical service conditions for such connections. It has already been discussed that to date there are no adequate in-service inspection systems for threaded connections. This is due to the geometric complexity of an assembled connection which makes inspection from a remote face extremely difficult. The crack tolerance of the thick walled connections means that externally these would be an indication of impending problems, the first indication being a brittle failure. However, for the thin walled connection, the wall penetration prior to failure will lead to a "leak before break" situation which can be extremely beneficial as an indication of a problem. For example, should the tubing be filled with a fluid at a higher pressure than surrounding medium, the through crack will lead to fluid leakage which can be detected by a loss of internal pressure.

It must be noted that these discussions refer to the results as observed here and are not necessarily general to thin or thick wall designed connectors. Clearly the fracture toughness of the material plays an important role in dictating exactly how a connection fails. However, in general, the thicker the material, the greater the opportunity for high stress intensity factors to develop at the tip of the surface breaking crack and hence the likelihood of a fracture condition being reached. Whilst discusing leak before break systems it is important to consider the consequences in the short term following a leak, for example, drilling pipe which normally contains erosive drilling muds have been shown [51] to suffer from very severe (and probably rapid) erosion as the mud leaks from the inside to the outside. This effect, known generally as washout, results in a very significant enlarging of the original crack which can rapidly increase the defect severity.

Axial Applied Load (kN)	Gauge No. 1	2	3	4
850	0	0	0	0
600	0	0	0	0
400	-1	-1	-3	0
200	-9	-8	-12	-8
0	-20	-17	-19	-20
200	-9	-9	-11	-8
400	-1	-1	-3	0
600	0	0	0	0

Table 5.1 Strain gauge readings on spacer ring (microstrain)

Preload Opening Load	850kN
Max Load	+ 800kN
Min Load	+ 50kN
Load Range	750kN
Nominal Pin Area (Gross) See Fig. 3.6	5890mm^2
Nominal Pin area at preloaded section	7540mm^2
Cyclic Frequency	1 Hz
Environment	air
Temperature	ambient
Cycles to Fracture	374,700

Table 5.2 Summary of Test Data - Specimen No.1

	Crack Depth (mm)		
Cycles	**Crack 1**	**Crack 2**	**Crack 3**
58,700	0.65	0.25	0.45
107,100	1.35	1.1	1.45
157,800	1.5	1.2	2.2

Table 5.3 ACPD Inspection Results for early part of test

Crack	Crack Depth (mm)	
	Before	After
1	(2.49) 2.50	(2.46) 2.47
2	(1.40) 1.20	(1.65) 1.52
3	(2.2) 2.2	(2.68) 2.89

( ) Denotes measurements taken using short probe

Table 5.4 Effect of R = -1 Loading on measured crack depth

Maximum Load	695 kN
Minimum Load	161 kN
Load Range	534 kN
Nominal Pin Area (Gross)	3760 mm^2
Cyclic Frequency	2 Hz
Environment	Air
Temperature	Ambient
Cycles to Failure	362,600

Table 5.5 Test Data for VAM test (Model 2)

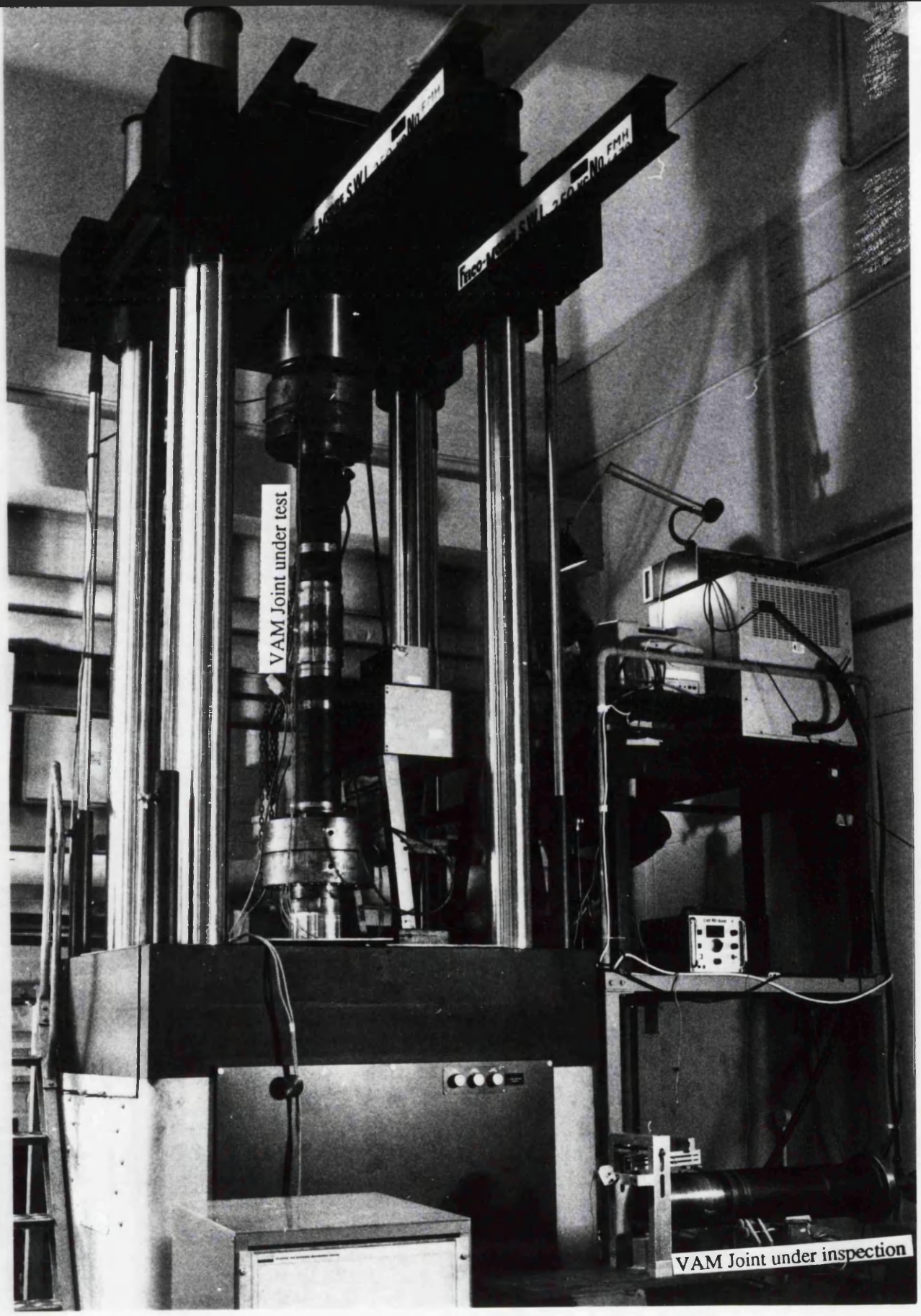

Plate 1 - Test Rig and Inspection Rig used for Large Scale Tests

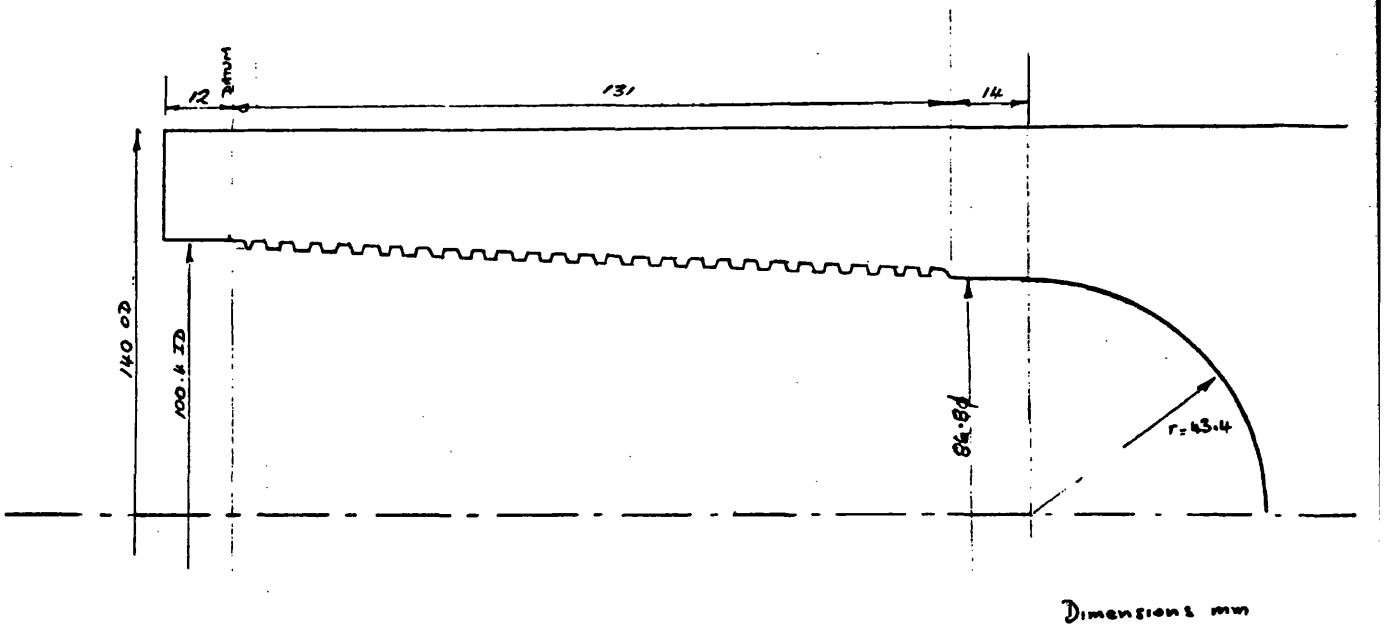

FIG. 5.1b Box Geometry - Model 1

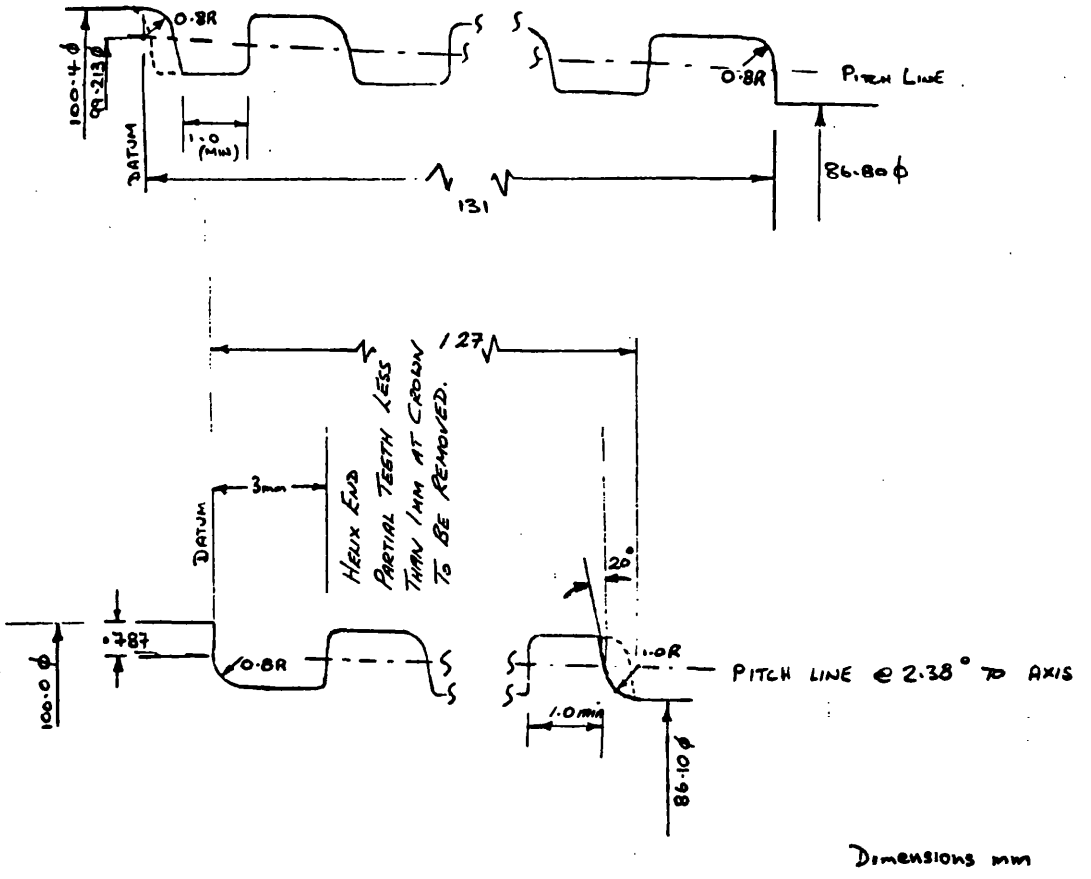

FIG. 5.1c Tooth Detail at Ends of Pin and Box

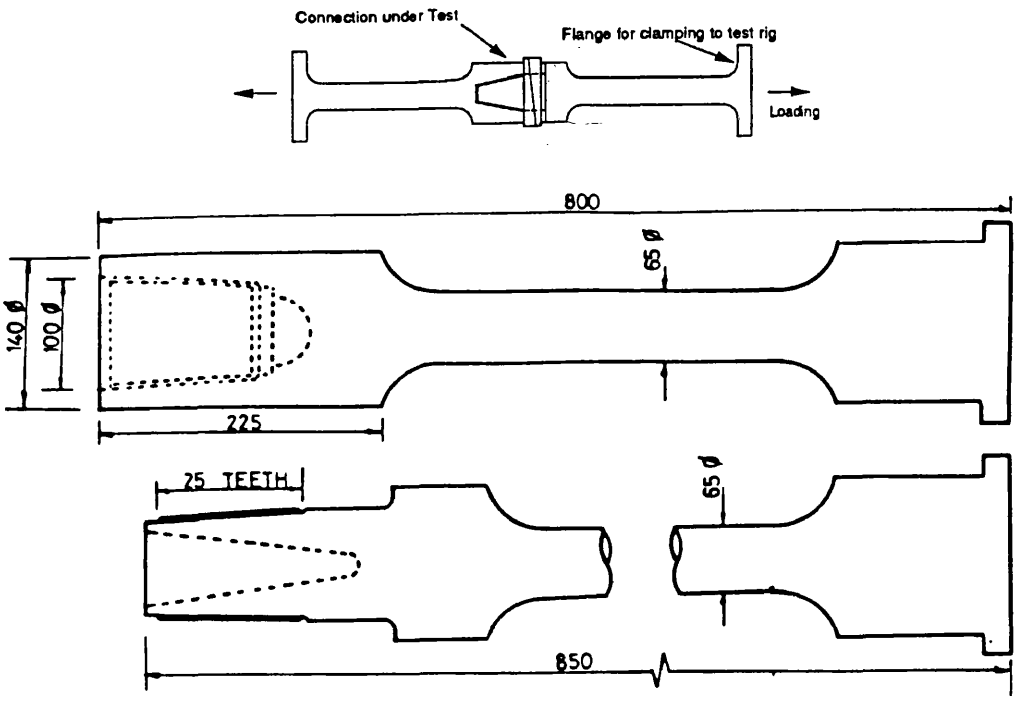

Fig. 5.1a Thick walled specimen and general test arrangement Dimensions in mm.
For Details see Figs 5.1b & 5.1c Opposite & Fig. 5.1d over

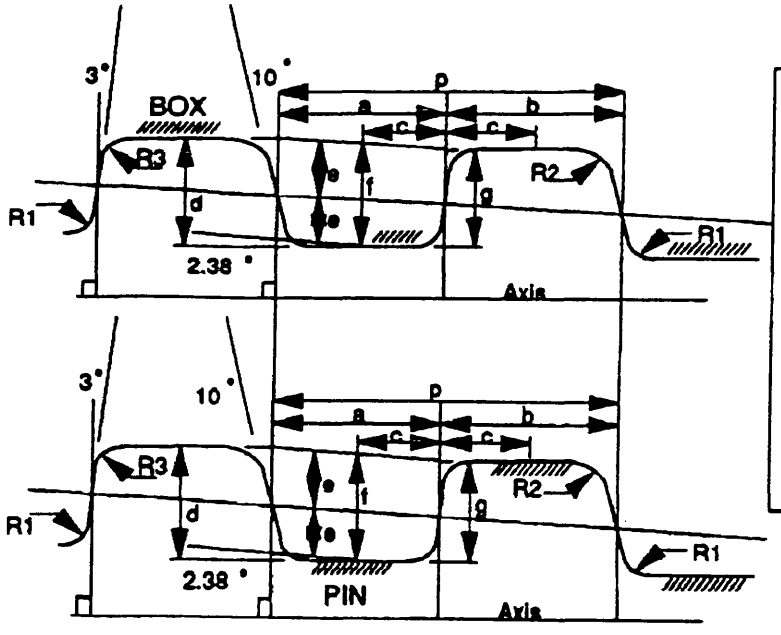

	PIN			BOX	
a	0.100	+0.005 -0.000	a	0.099	+0.000 -0.003
b	0.100	+0.000 -0.005	b	0.101	+0.003 -0.000
c	0.050		c	0.050	
d	0.662		d	0.662	
e	0.031		e	0.031	
f	0.062	±0.001	f	0.062	±0.001
g	0.0578		g	0.0578	
R1	0.008	+0.000 -0.002	R1	0.008	+0.002 -0.000
R2	0.03	+0.002 -0.000	R2	0.03	+0.000 -0.002
R3	0.008	+0.002 -0.000	R3	0.008	+0.000 -0.002
p	0.200		p	0.200	

Dimensions in inches

Fig 5.2 Geometry of API buttress thread [Ref.7]

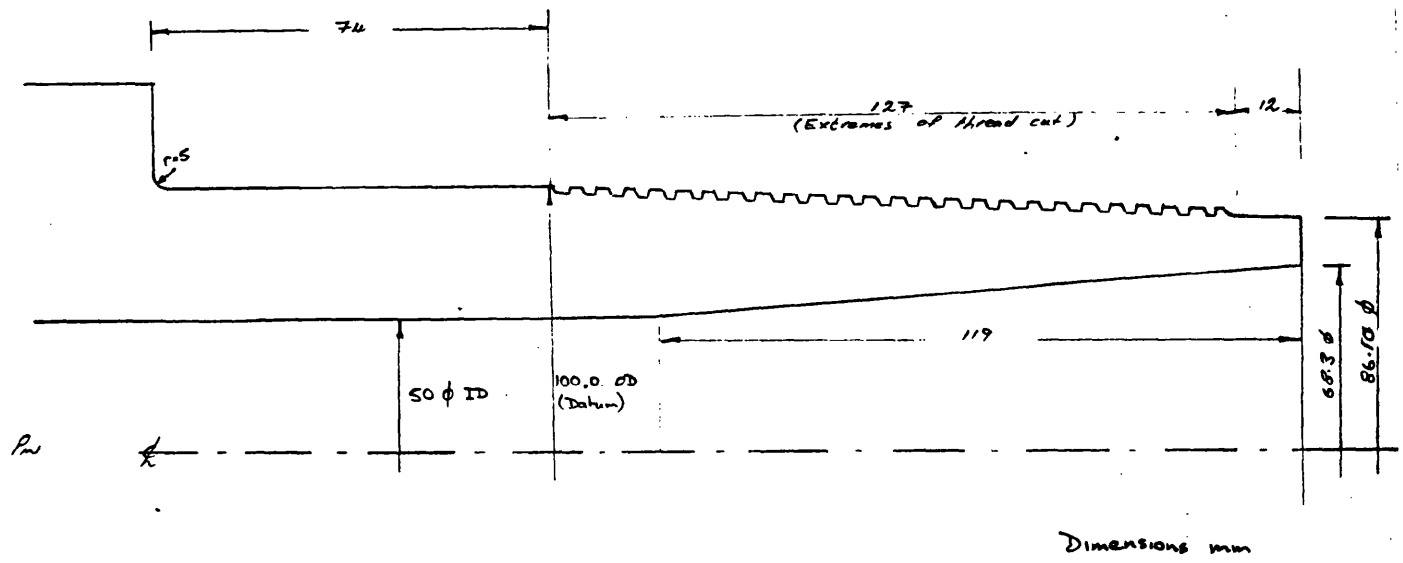

FIG. 5.1d PIN GEOMETRY - MODEL 1

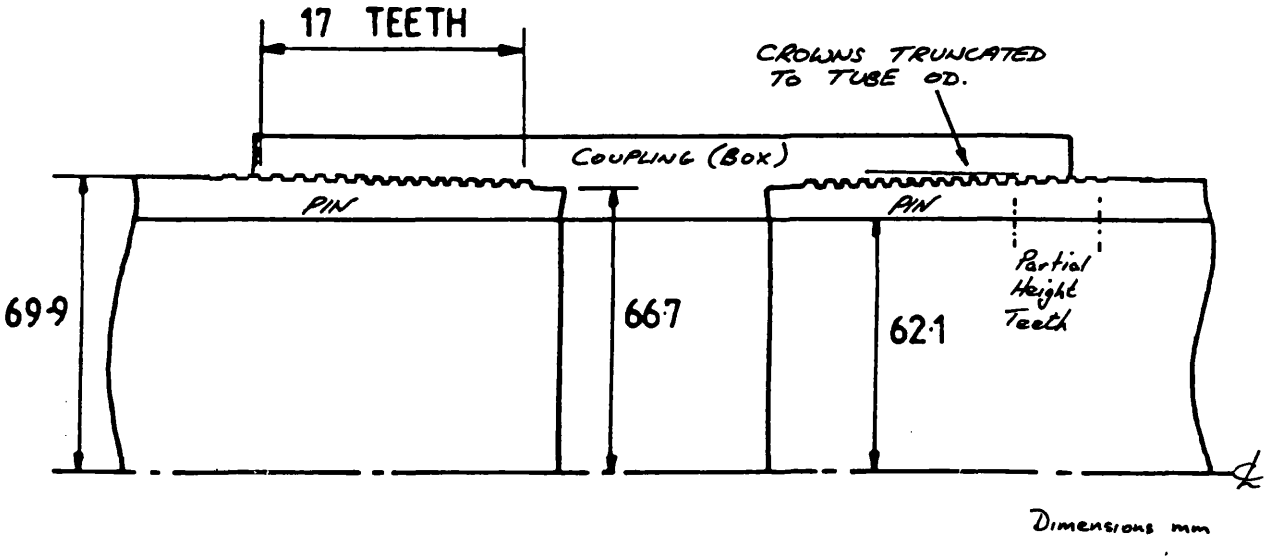

Fig 5.3 Schematic section through VAM Connector

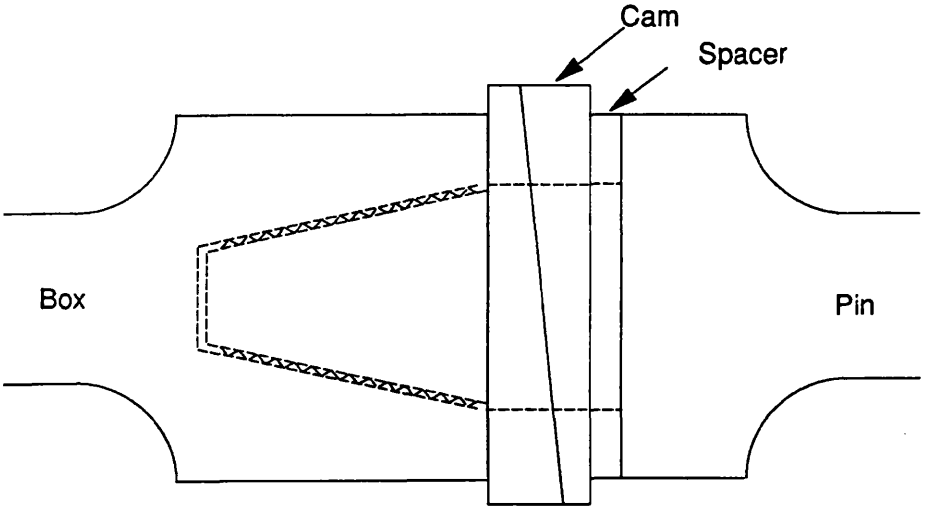

Fig. 5.4 General Arrangement Showing Preload Cam TO CONTROL OPENING LOAD

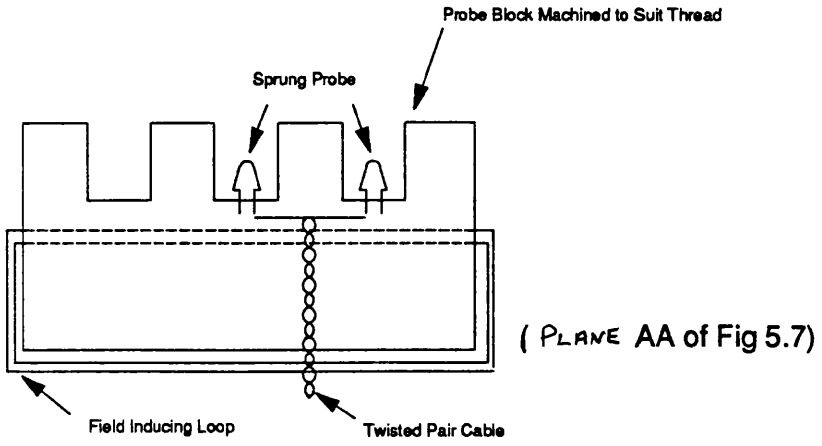

Fig 5.5 Schematic View of ac Measurement Probe

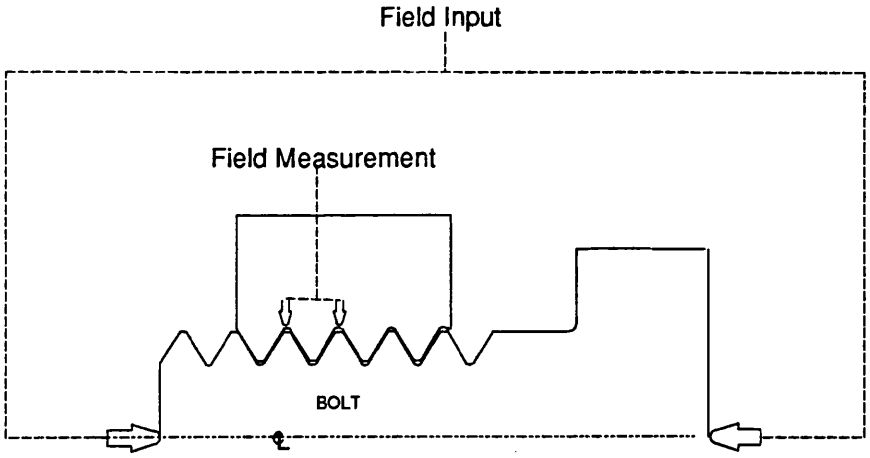

Fig 5.6 ACPD Bolt inspection using injected field.

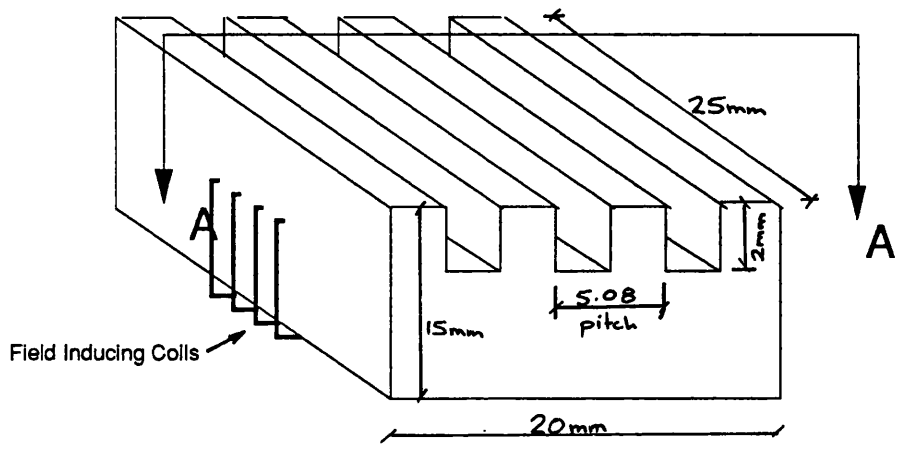

Fig 5.7 General arrangement of induced field probe

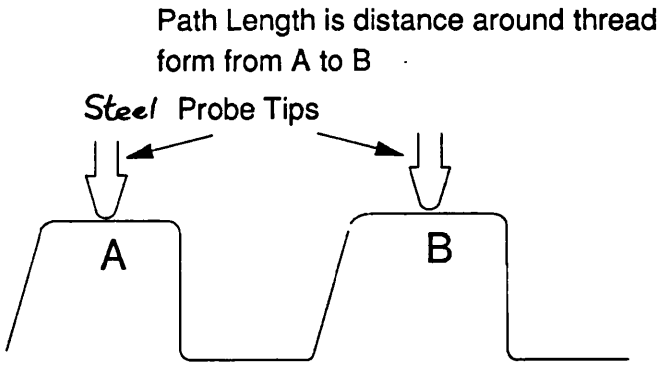

Fig 5.8 Definition of probe spacing for ACPD

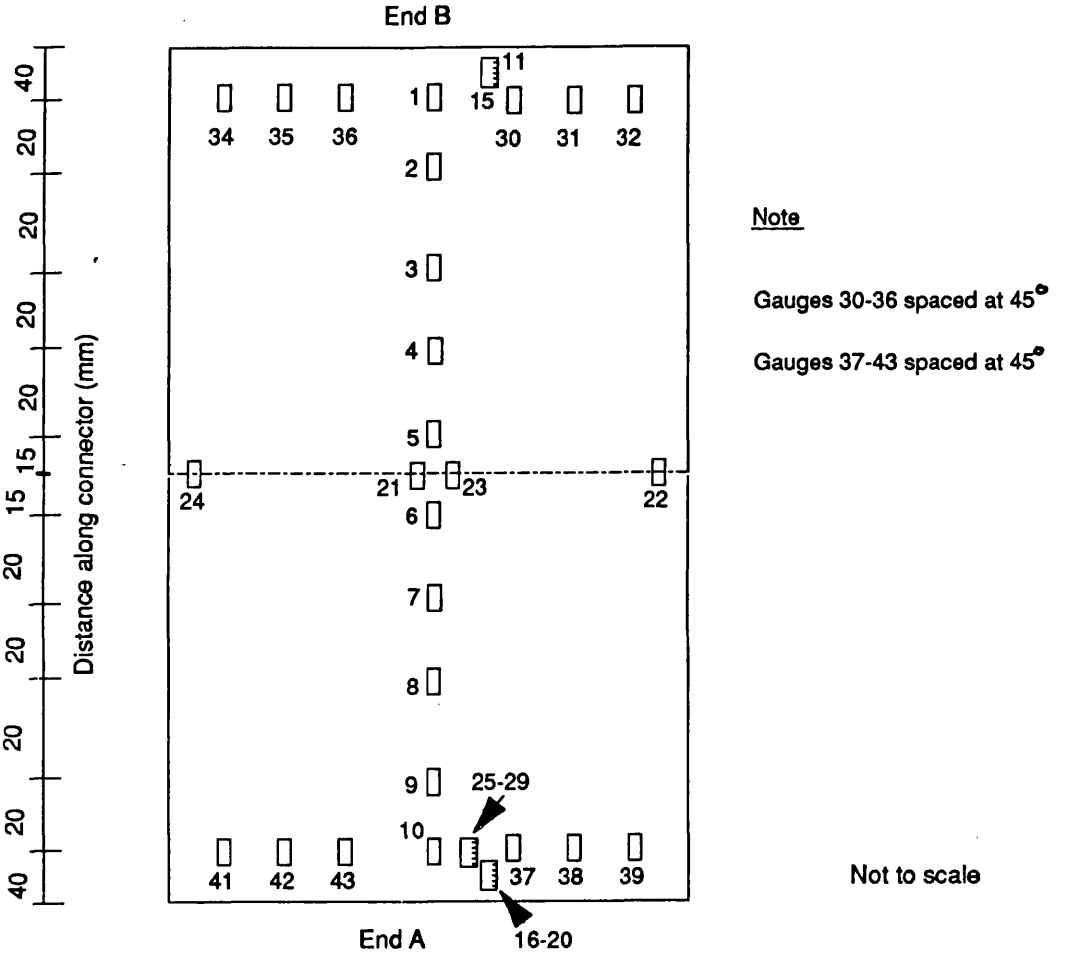

Fig. 5.9 Strain Gauge Layout on VAM Coupling

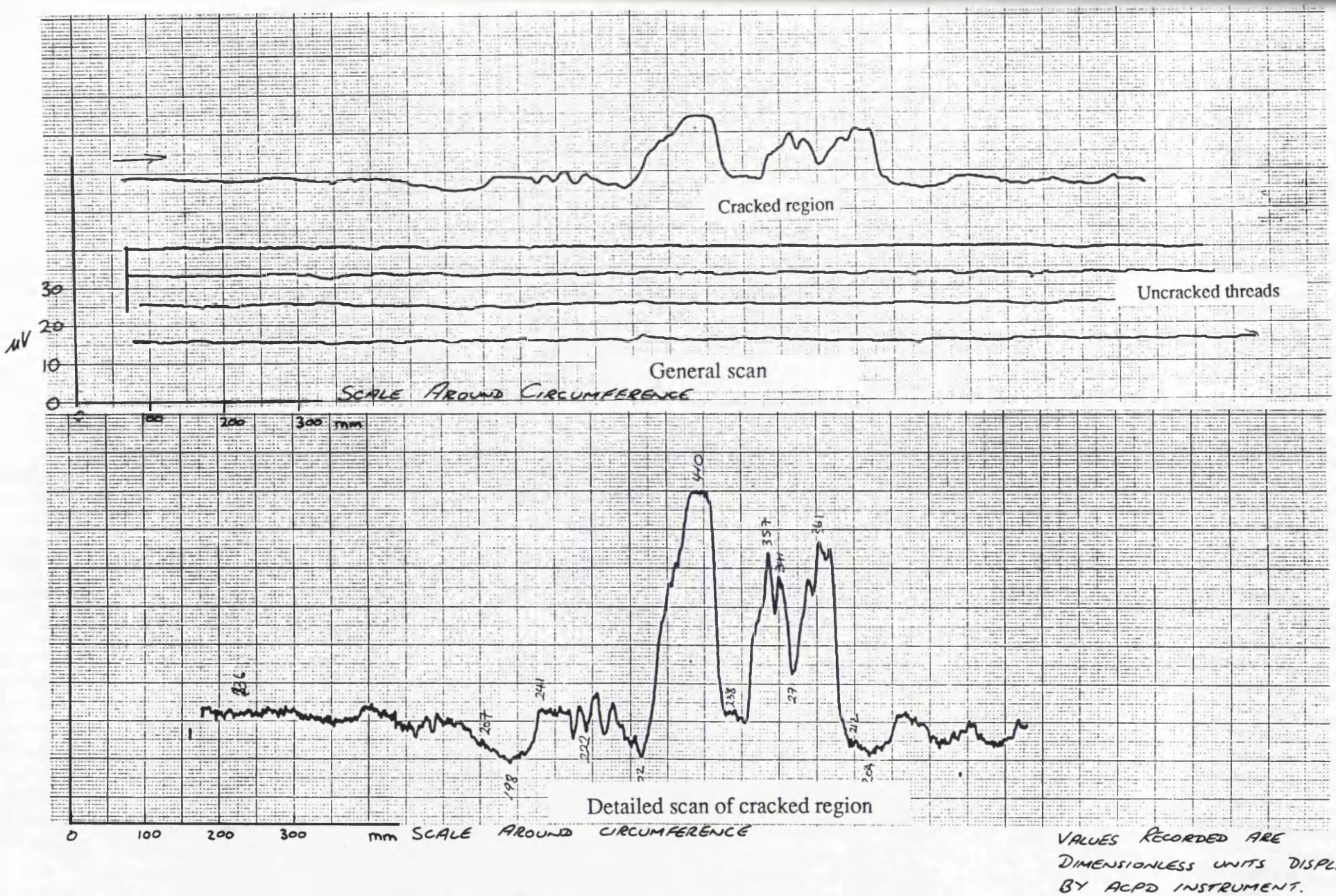

Fig. 5.10 ACPD Inspection data taken after 207,000 Cycles

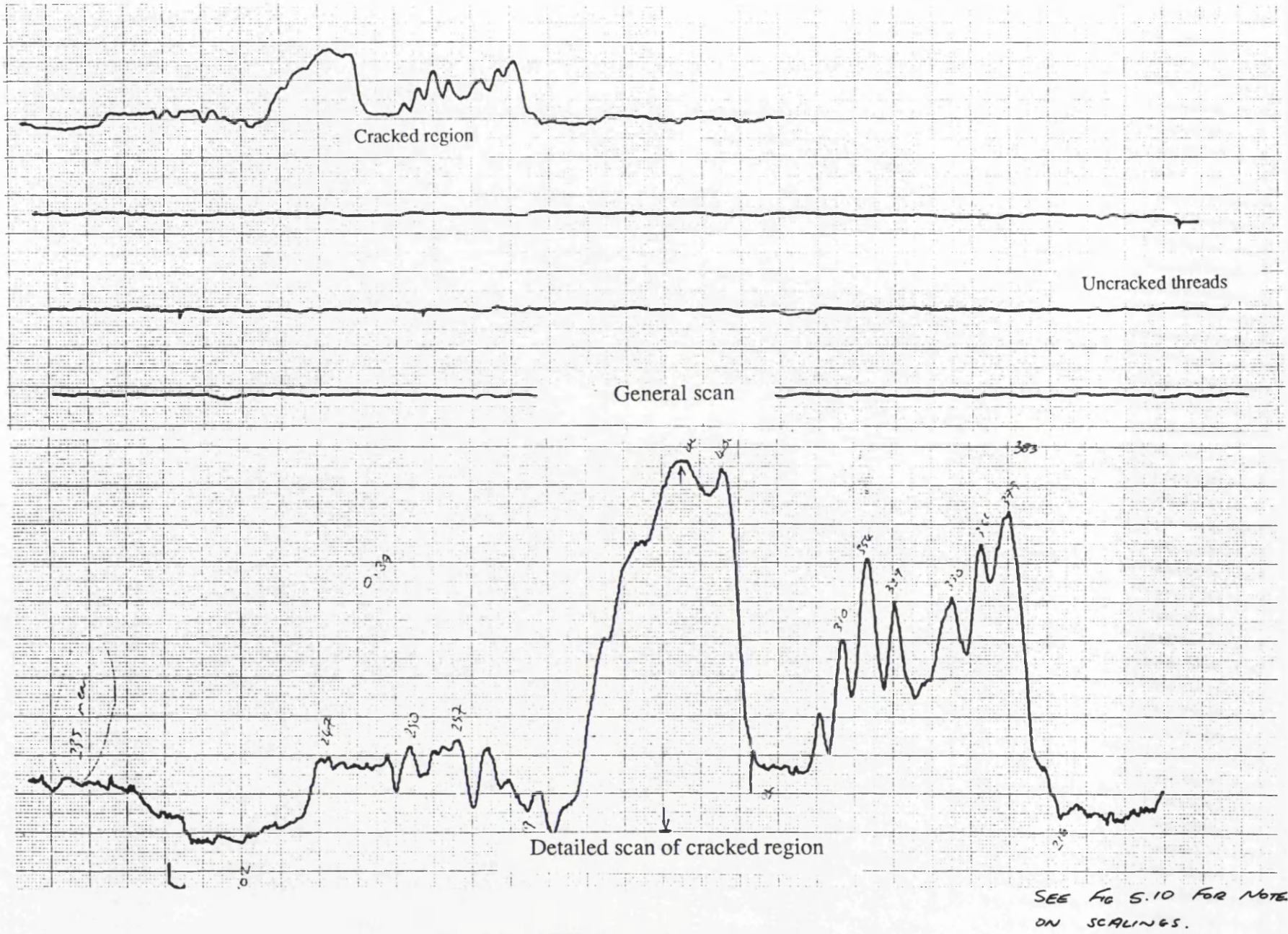

Fig. 5.11 ACPD inspection data taken after 285,000 Cycles

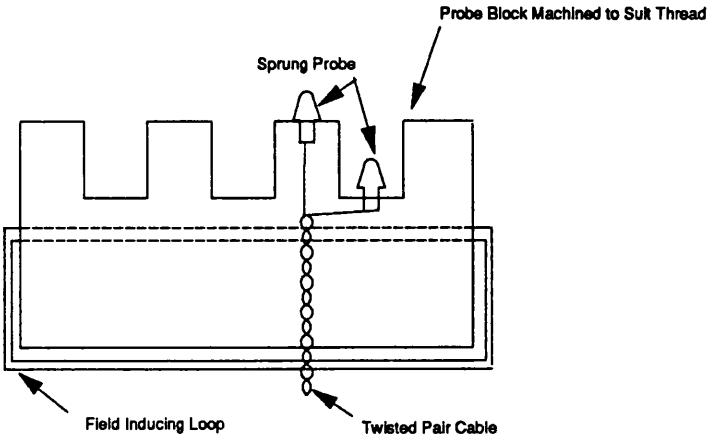

Fig 5.12 Modified Probe with reduced probe spacing

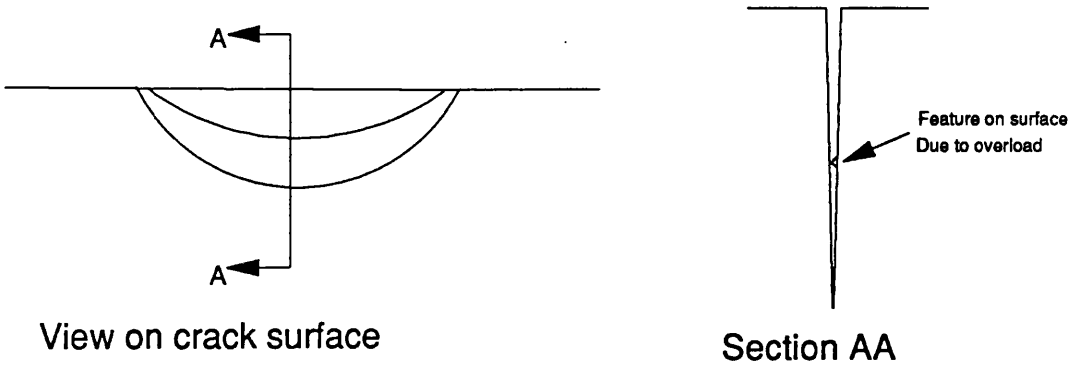

Fig. 5.13 Effect of overload on crack surface

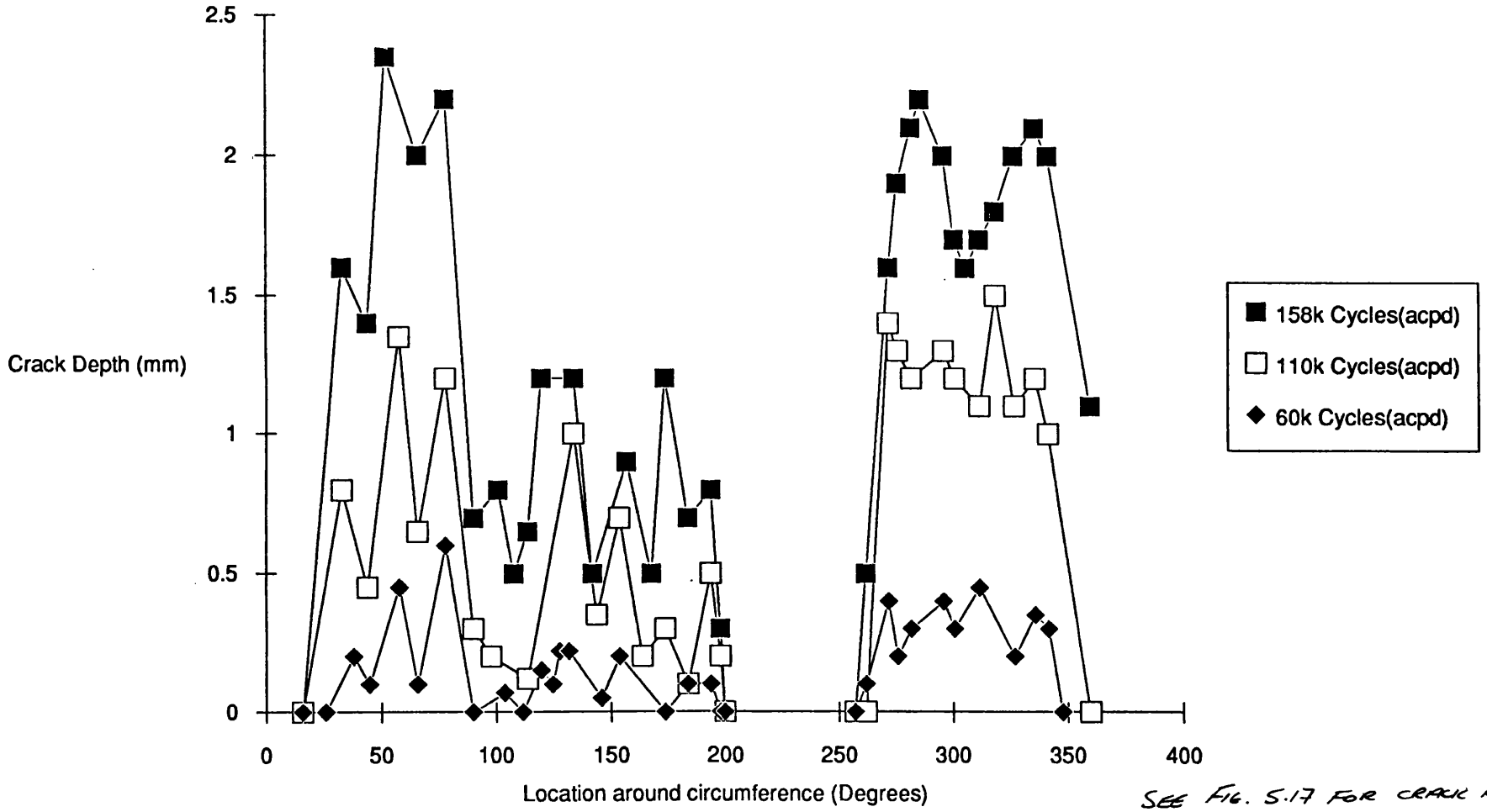

Fig. 5.14 Crack Depths measured by acpd.

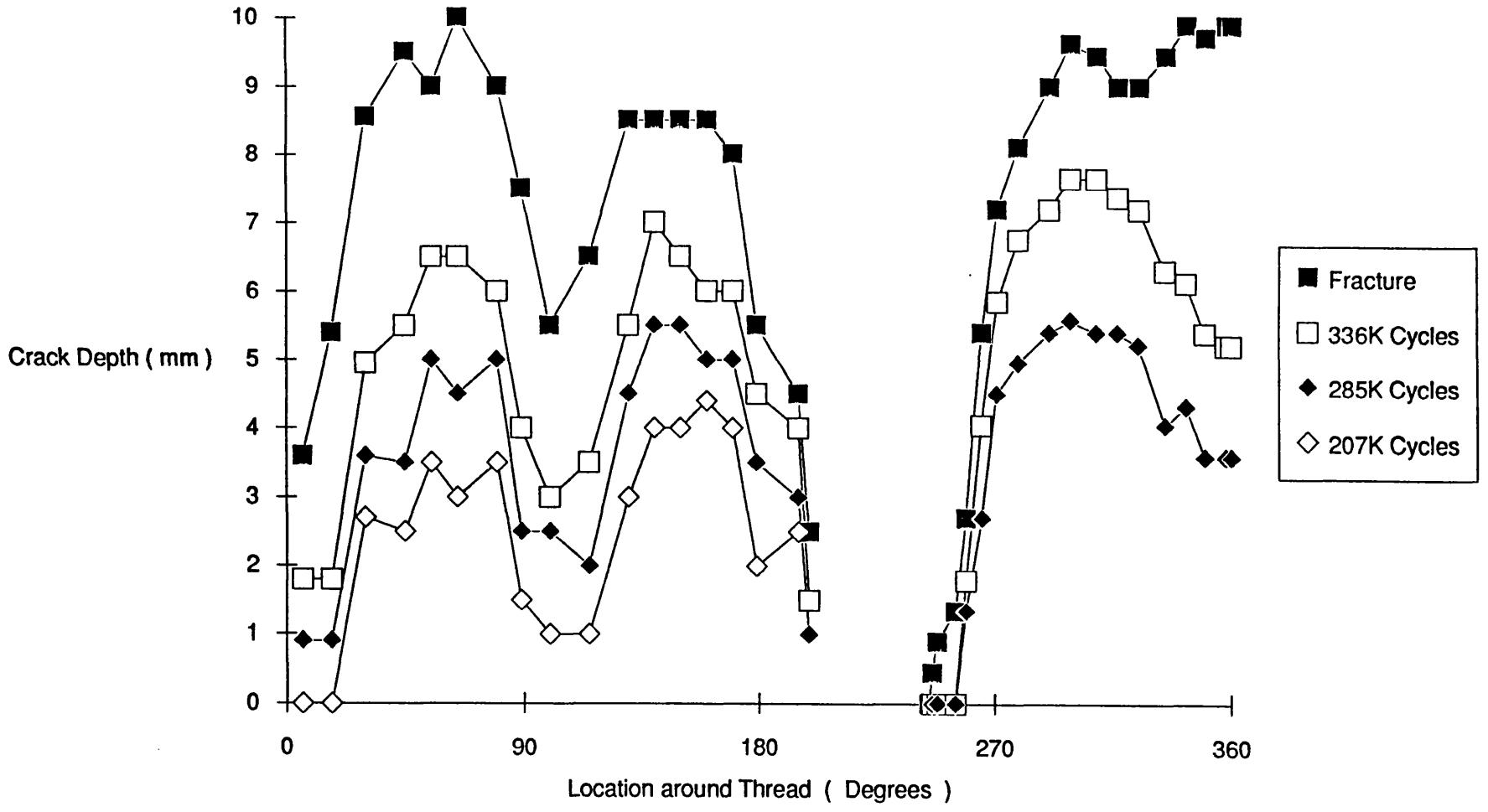

Fig. 5.15 Crack shape measurements made on fracture surface.

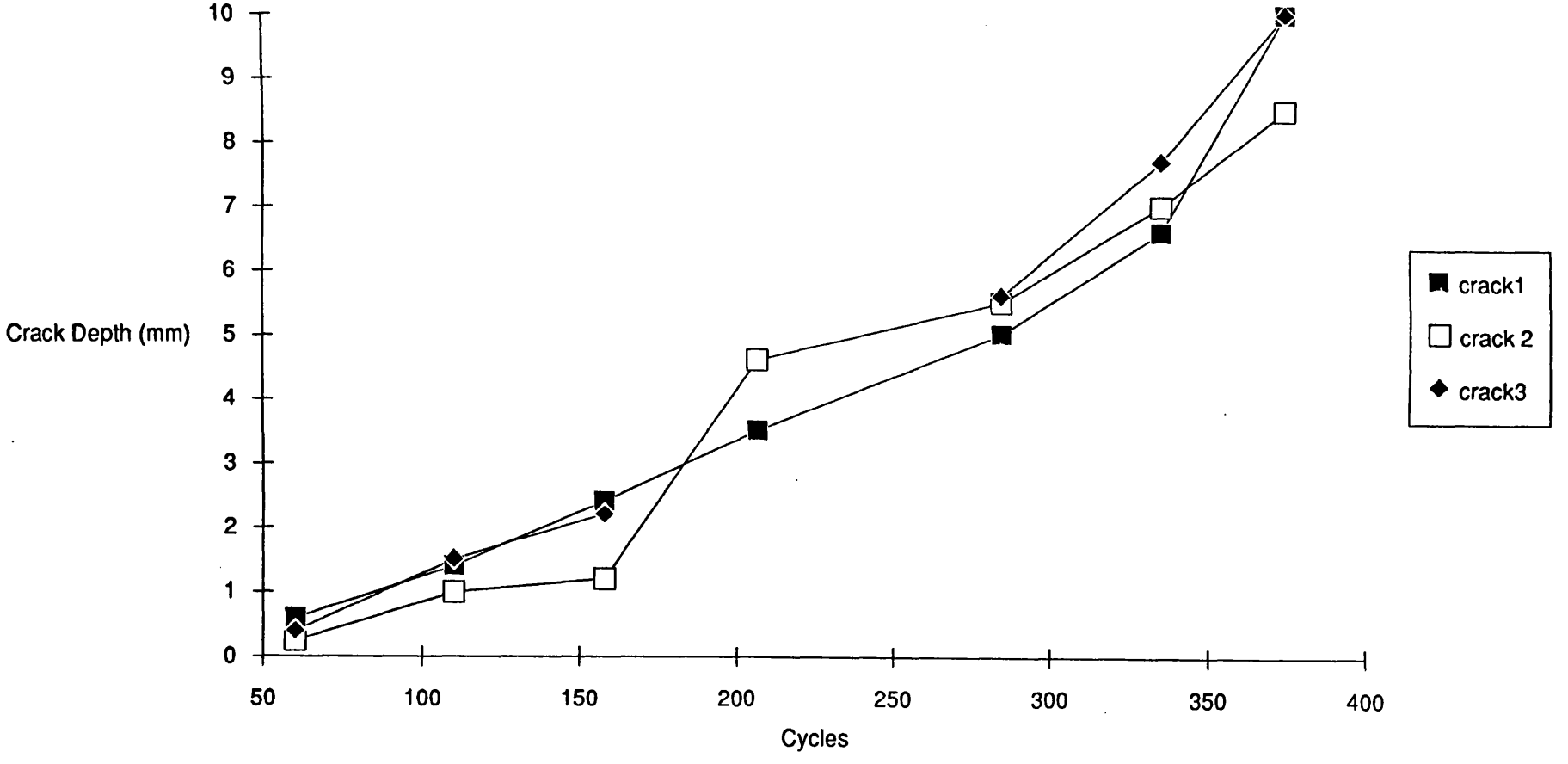

Fig. 5.16 Experimental crack growth curves

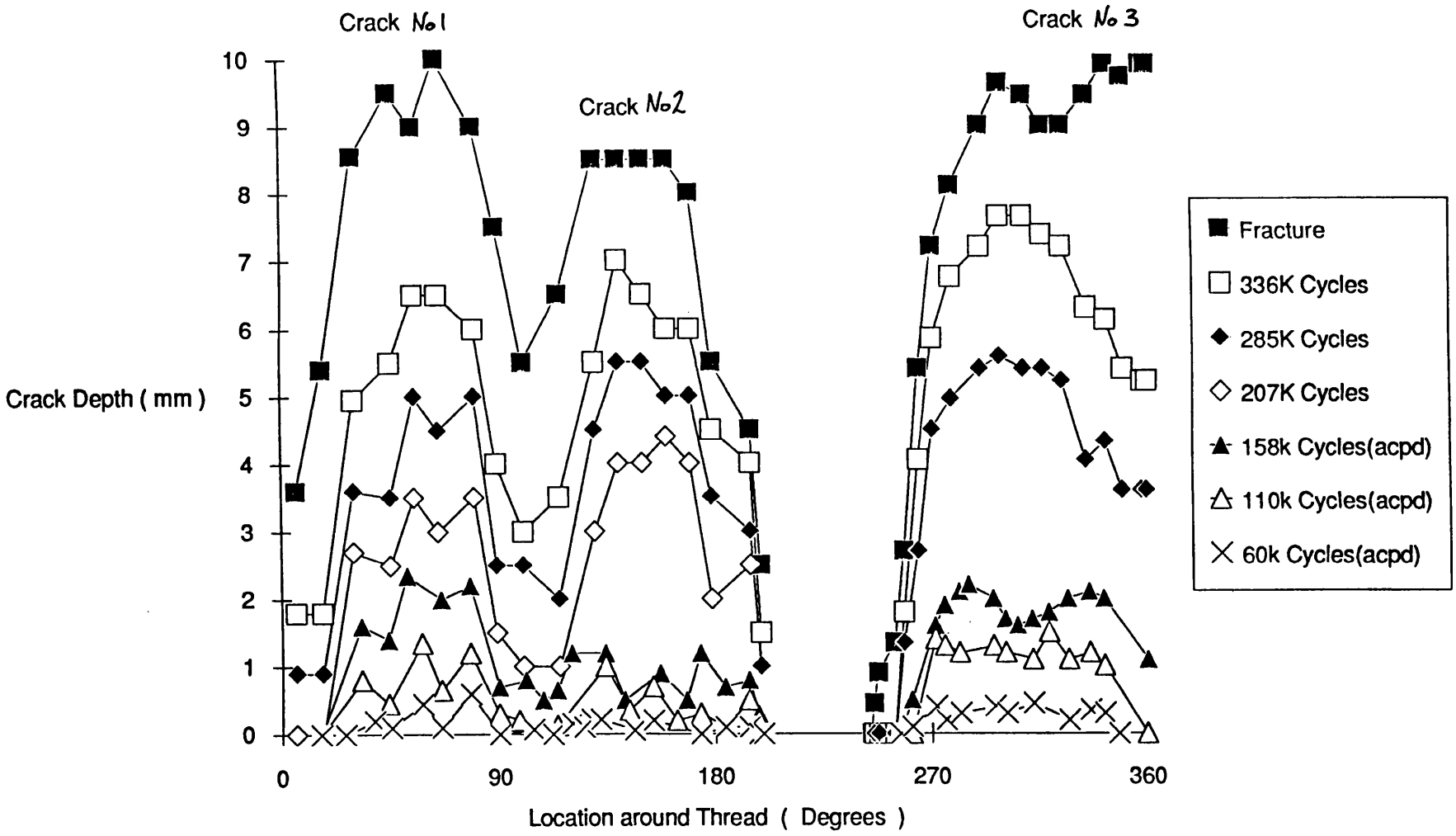

Fig. 5.17 Crack shape measurements from fracture surface and acpd.

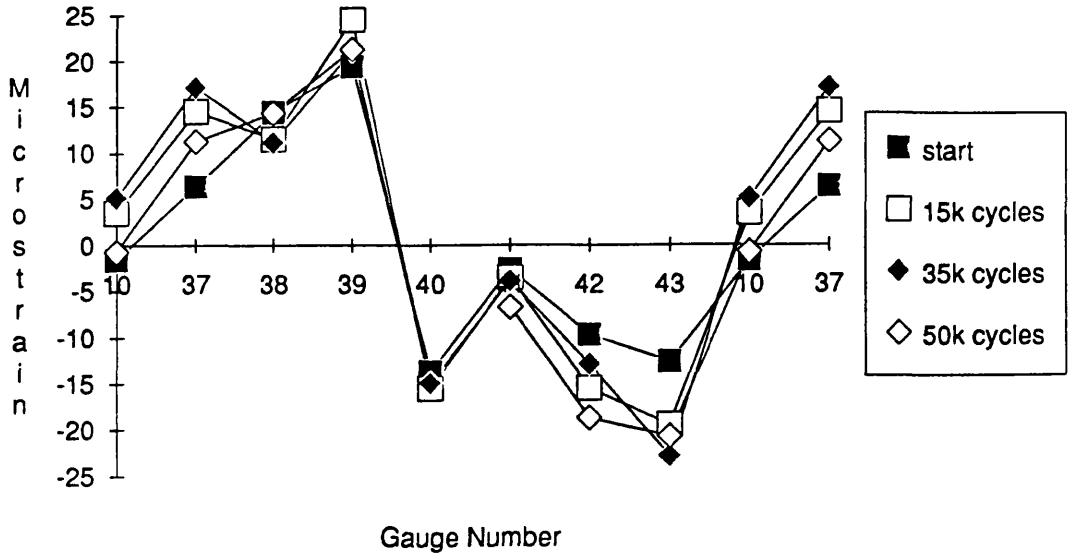

Fig . 5.18a Circumferential strain distributions around end "a".

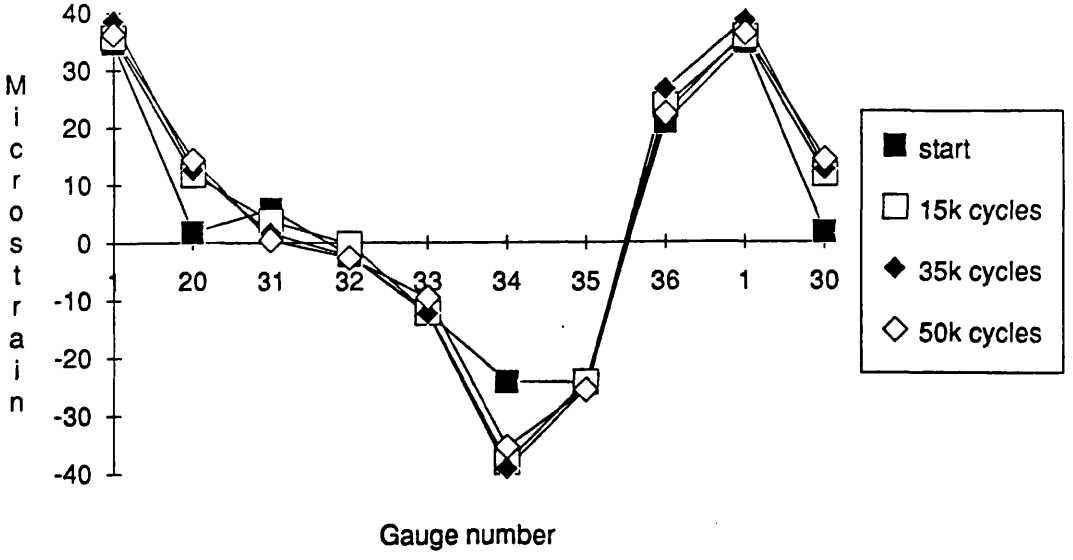

Fig 5.18b Circumferential strain distribution around end "b"

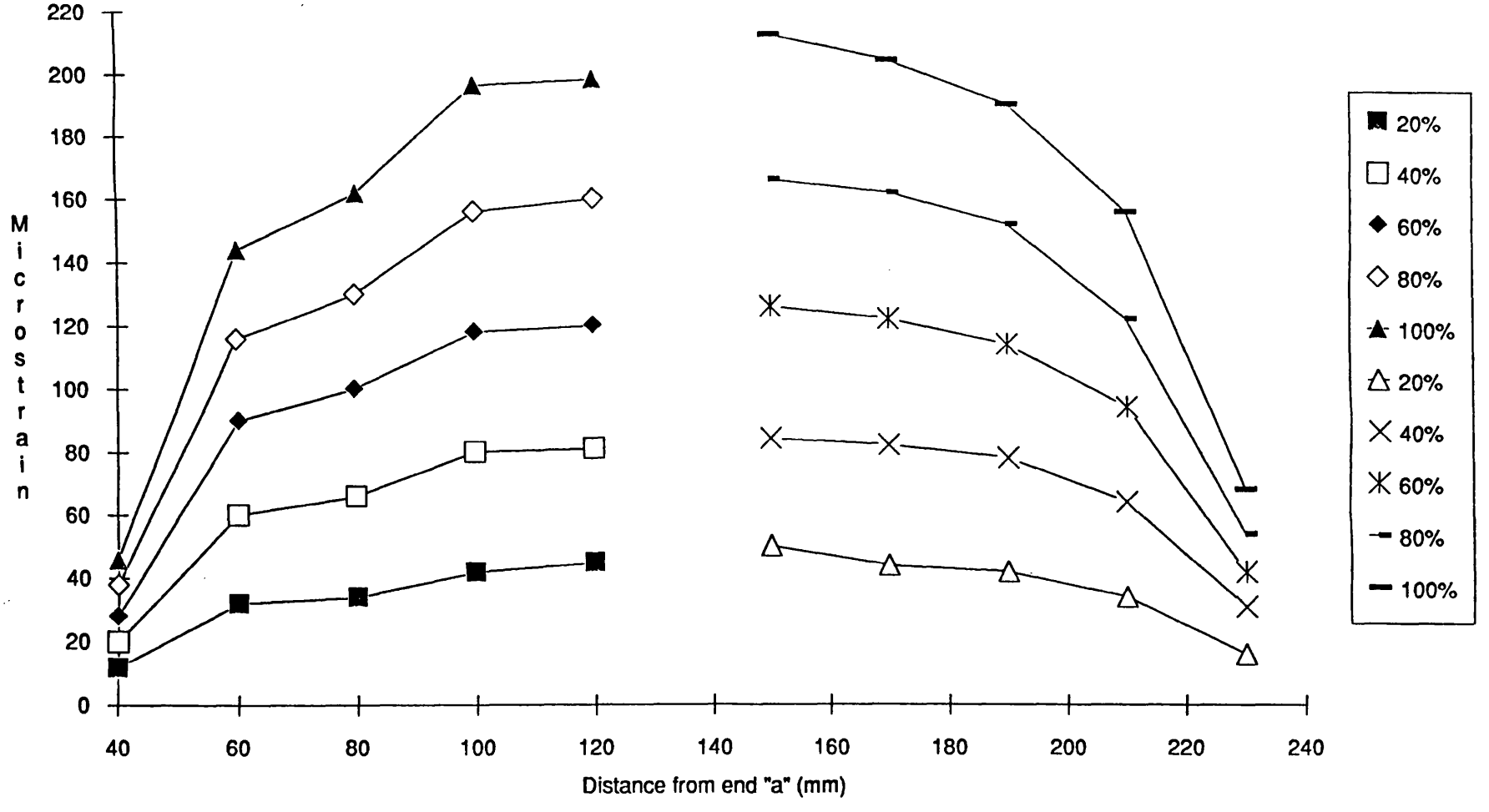

Fig 5.19 Distribution of longitudinal strains under increasing loads

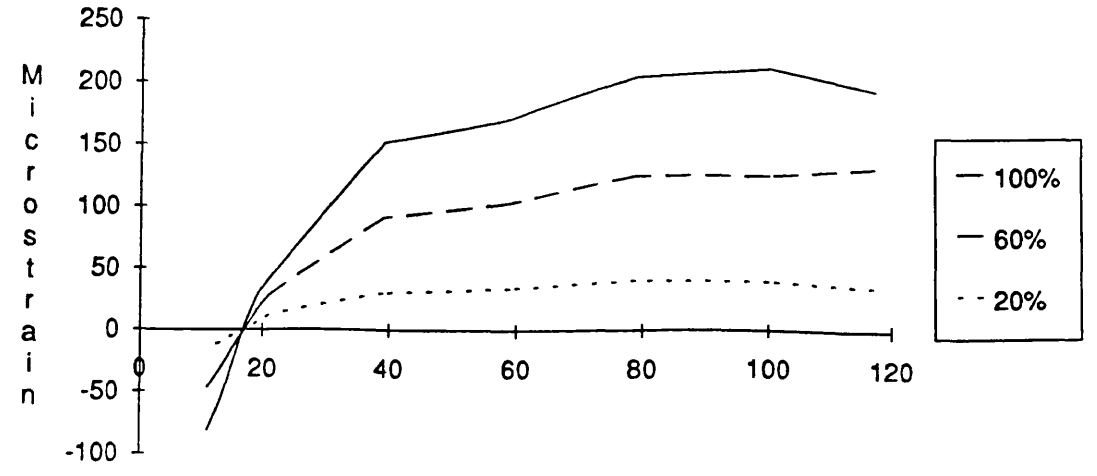

Fig. 5.20a Strain distribution at end "b" under different loads (After 15k cycles)

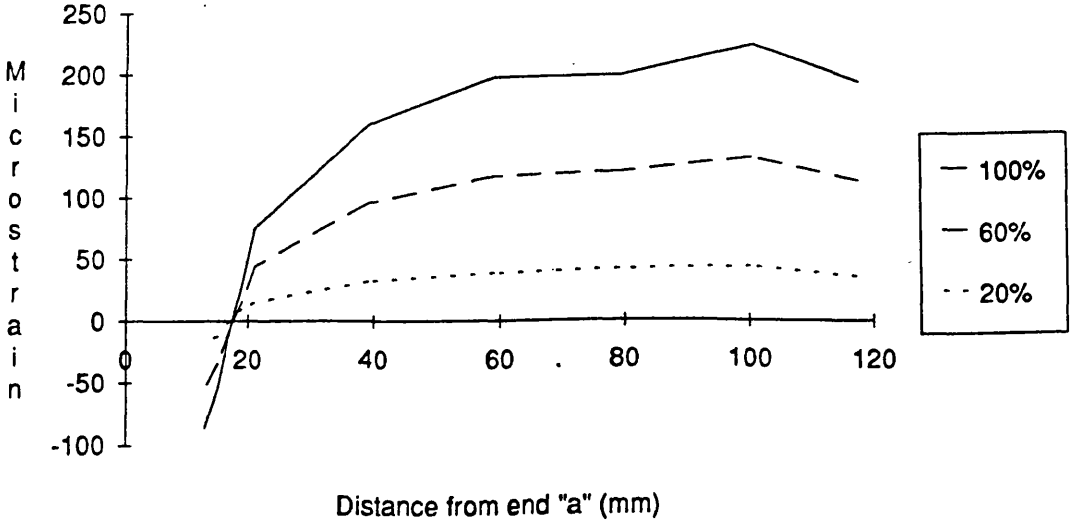

Fig 5.20b Strain distribution at end "a" under different loads (After 15k cycles)

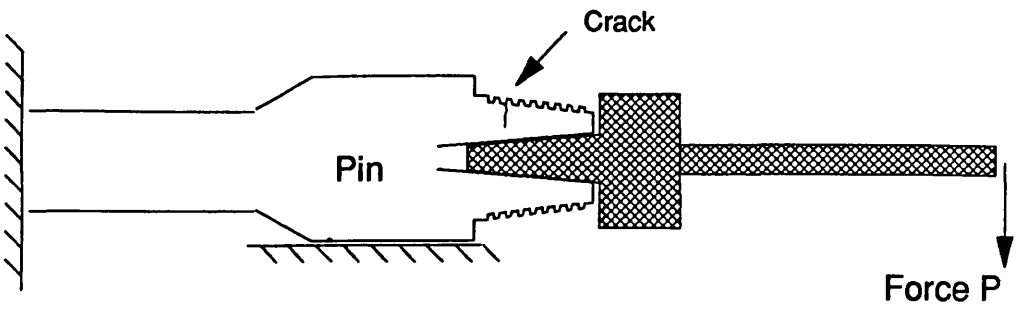

Fig 5.21 System used to apply a bending load to the pin to open the crack.

CHAPTER 6

FATIGUE AND FRACTURE MECHANICS MODELLING

of

CRACK GROWTH IN THREADED COMPONENTS

6.1 INTRODUCTION - The Fatigue Process

All components operating under cyclic stress may be susceptible to damage by fatigue. In order for fatigue damage to occur, cyclic stresses are necessary, these could be in the form of a low number of very high stresses or a large number of low stress cycles where these must be of a magnitude above the fatigue limit for the material. The fatigue process can be considered in two phases, initiation and propagation. The initiation phase is that portion of the fatigue life where the damage is occurring on a microscopic scale, prior to the first appearance of a crack. The period of growth of the initial crack to a size at which the component fails is known as the propagation or crack growth phase. Material behaviour under crack growth conditions can be described by the Paris [52] Law which is stated in Equation 6.1. Paris Law of crack growth states that

$$\frac{da}{dn} = C(\Delta K)^m \qquad 6.1$$

where C and m are material constants, ΔK is the stress intensity factor range and *da/dn* is the rate of crack growth through the thickness of the material and refers to the crack depth. For common engineering steels, the value of m is in the region of 3 to 5 and the above relationship shows that the power relationship with respect to ΔK (which is proportional to $\Delta\sigma$ the cyclic stress range) means that crack growth rates are strongly influenced by the levels of cyclic stress.

Almost every engineering component exhibits geometric stress concentration factors resulting in "local" regions of high stress. The overall fatigue behaviour will be dictated by the size of the stress field created by the geometric SCF.

i) ***Low SCF with large applied stress***

If a low SCF exists, the applied cyclic stress must be high to satisfy the demand for high fluctuating stress range.

This situation results in a large high stress field and any crack initiating will be driven by such a stress state which will result in a rapidly growing crack, almost certainly accelerating.

ii) ***High SCF with small applied stress***

In contrast, this situation results in a small highly stressed region as was described for the buttress thread in Chapter 3. A crack initiating in this region will grow rapidly in the high stress field but is seen to be growing into a region of low stress (Figure 3.7). This situation tends to lead to a lower more uniform crack growth rate or even a decelerating rate of crack growth.

6.1.1 Application to threaded connections

Consider now the two geometries of tether being investigated.

The thin walled tether represents the situation where a large stress field is created by the relatively close proximity of the thread to the opposite surface of the member. The smaller section area leads to higher mean stresses. This would therefore be expected to result in an accelerating crack growth rate.

The thick walled tether however results in local high stress region close to the thread root but this rapidly decreases to a uniform stress state (as shown in Figure 3.7). This would therefore be expected to exhibit slower crack growth characteristics.

6.1.2 Crack initiation and propagation

Consider now the generalised case of fatigue behaviour.

i) ***Crack Initiation***

Cracks do not occur instantaneously once a component is subjected to fatigue loading, instead there is an "initiation" period during which time it is considered that microstructural damage occurs which finally develops into a "crack". Quite when a crack is deemed to exist, i.e. has initiated, depends very much on who is asked! Many workers [e.g. 53, 54] are conducting studies on "short cracks" which, to metallurgists could be on the same scale as the atomic grains. On the other hand, inspection engineers perhaps in the aircraft industry for example consider small cracks to be one or two millimetres long. If you ask an inspection diver working in the North Sea to define a short crack he would say a few centimetres in length.

There is clearly some scope for defining crack initiation.

The D.En. [55], when referring to cracking in welded offshore structures refer to the stage when a crack is first observed. Again this is unsatisfactory because it depends on who is observing and using what technique. In this study, reference will be made to the point at which cracking was first observed using the Inspection techniques described in Chapter 5. This may or may not be acceptable as an initiation point.

ii) Crack Propagation

Once beyond the problems of initiation, description of the remaining fatigue life is relatively straight forward. A crack under sufficient cyclic loading will extend and under these conditions, the component is said to be undergoing crack propagation. The rate of crack propagation depends on the material properties and the stress fields acting at any particular time. It is generally accepted that the crack propagation phase occupies the time between initiation and failure of the component.

6.2 THE S-N APPROACH

Many Engineering components are intolerant to cracks and, once a crack occurs, the propagation rates are such that failure rapidly ensues. For such components, a stress-life approach can be used to describe the fatigue behaviour. This is known as the S-N approach whereby the information is presented in terms of the number of cycles (N) at a given stress level (S) required to cause failure of the component. It is noted that N refers to the total number of cycles for initiation and propagation.

Indeed this approach can be adopted for any type of component irrespective of the ratio of initiation to propagation. However, the S/N approach simply describes the overall life of the component. For many applications, where full scale component testing is feasible to determine experimentally the life, this approach is adequate for design purposes where a specific design life is defined.

The weakness of the S/N approach is that it does not consider the crack growth behaviour specifically. For high integrity components, subjected to regular in-service inspections fatigue information in the form of S-N data will provide no information for decision making if a defect is found in-service.

The S-N approach has developed as a design tool but is not adequate as an analytical tool. For this reason, improved methods of fatigue analysis have developed and in particular the Fracture Mechanics (FM) Approach.

6.3 THE FRACTURE MECHANICS APPROACH

Fracture Mechanics involves the analysis of crack propagation behaviour. The benefits of such an approach are significant in that subsequent behaviour can be predicted at any point during the propagation life, enabling predictions of remaining life to be made. This makes the fracture mechanics approach particularly useful in situations where the component is tolerant to cracking resulting in a significant proportion of the fatigue life being fatigue crack propagation.

An example is a welded steel offshore structure where cracking is likely at an early stage due to the manufacturing process and inherent high local stresses but where crack propagation through the thickness can occupy around 80% of the total fatigue life [56]. For such structure, the fracture mechanics approach has been used to predict fatigue behaviour [57] and to enable remaining life calculations to be made.

The study of such behaviour experimentally has been significantly advanced by the acpd technique [47] which enables crack growth and crack development to be measured during fatigue tests.

Stress Intensity Factor

Studies on the fatigue behaviour of common Engineering materials have shown that the crack growth rate can be described by the Paris Law, Equation 6.1.

The stress intensity factor is a function of the stress field acting and the crack shape and is defined in general terms as

$$K = (Y_\sigma)\sigma\sqrt{\pi a} \qquad 6.2$$

Where σ is nominal stress acting, a is the depth of the crack and Y_σ is a function that takes into account the stress distribution (stress field) on the plane of interest due to the nominal applied stress σ. The stress intensity range ΔK is calculated from equation 6.2 by substituting the stress range $\Delta\sigma$ for σ, the other parameters remaining the same.

It is observed from equation 6.1 and 6.2 that the crack growth rate can be calculated knowing the material properties and the stress intensity factor. Material properties are obtained from standard tests on small specimens [58] for which the stress intensity solution is known. The problem then reduces to the derivation of the K factor for the particular geometry under investigation.

6.3.1 Theoretical Solutions

The application of fracture mechanics techniques was pioneered by Griffith [37] and has been subsequently developed by workers such as Irwin [36]. The stress intensity factor (SIF) can be determined theoretically using the localised stress concentration factor as described by Griffith [37]. Whilst theoretical models for SIF do not generally appear in the literature for threaded connections, Harris [23] presented SIF's for hollow circumferentially notched round bars, which clearly bear close similarity to threads. Harris presents SIF's for tensile, bending and Torsion loads calculated from stress concentration factors after Neuber [35].

In the case of a tether, axial loading is predominate and it is possible, using the results for SCF from Neuber, to verify the results of Harris as follows.

6.3.1.1 Calculation of SIF from SCF

Consider a hollow cylinder containing a deep notch with a large diameter hole as shown in Figure 6.1.

$$\sigma_{nom} = \frac{T}{\pi\{(r+c)^2 - c^2\}} \qquad 6.3$$

Neuber [35] has analysed a cylinder with deep circumferential notch, as shown in Figure 6.1, under axial load and derives the SCF at the root of a notch of radius ρ as

$$SCF = \alpha_1 + C_t\alpha_3 \qquad 6.4$$

Noting that σ_{nom} is defined as the nominal stress in the reduced section,
Where

$$\alpha_1 = \frac{2(r/\rho+1)\sqrt{r/\rho}}{[(r/\rho+1)\,arctan\,\sqrt{r/\rho}+\sqrt{r/\rho}]} \qquad 6.5$$

For a crack, ρ is small and, neglecting small terms, equation 6.5 reduces to

$$\alpha_{1_0} = \frac{2(r/\rho)\sqrt{r/\rho}}{(r/\rho)\pi/2+\sqrt{r/\rho}} = \frac{4r^{1/2}\rho^{-1/2}}{\pi} \qquad 6.6$$

(Note that the sub-script 0 refers to the case for small notch tip radius)

From Ref.[35]:-

$$\alpha_3 = \frac{2(r/\rho+1)-\alpha_1\sqrt{r/\rho+1}}{\frac{4}{\alpha_2}(r/\rho+1)-3\alpha_1} \qquad 6.7$$

Where

$$\alpha_2 = \frac{4r/\rho\sqrt{r/\rho}}{3[\sqrt{r/\rho}+(r/\rho-1)\ \ arctan\ \ \sqrt{r/\rho}]} \qquad 6.8$$

By inspection with equation 6.5

$$\alpha_2 = 2/3\ \ \alpha_1$$

Similarly, for small ρ and neglecting small terms,

$$\alpha_{2_0} = \frac{8r^{1/2}\rho^{-1/2}}{3\pi}$$

Substituting for α_1 and α_2 into equation 6.7 and for small ρ gives:-

$$\alpha_{3_0} = \frac{2(r/\rho)-\frac{4}{\pi}(r/\rho)}{\frac{3\pi}{2}(r/\rho)^{1/2}-\frac{12}{\pi}(r/\rho)^{1/2}}$$

$$\alpha_{3_0} = 0.814(r/\rho)^{1/2} \qquad 6.9$$

Ref[35]

Putting $C_t = 0.8$ and substituting into equation 6.4 gives

$$SCF = (r/\rho)^{1/2}\left[\frac{4}{\pi}+0.8(0.817)\right]$$

$$SCF = 1.93(r/\rho)^{1/2} \qquad 6.10$$

For Fracture Mechanics Analysis, the SIF is the controlling parameter and by definition [37]

$$K_I = \sqrt{\pi/2}\,\lim_{\rho \to 0} \rho^{1/2}\,\sigma_{max} \qquad 6.11$$

where $\sigma_{max} = SCF \times \sigma_{nom}$

and $$\sigma_{nom} = \frac{T}{\pi[(c+r)^2 - c^2]}$$

The stress intensity factor is found as

$$K_I = \sqrt{\pi/2}\frac{T}{\pi(r^2+2cr)}\rho^{1/2}[1.93(r/\rho)^{1/2}]$$

$$= \frac{0.965T}{\sqrt{\pi r}(r+2c)} \qquad 6.12$$

This solution assumes a deep notch where a' » r and c » r.

Neuber [35] has studied the more complex case of a shallow notch and this will be used to provide a general solution.

Neuber states the general case as:-

$$\alpha_{tk_o} = (r/\rho)^{1/2} \qquad 6.13$$

$$\alpha_{fk} = 2(r/\rho)^{1/2} \qquad 6.14$$

$$\alpha_{tb} = 1.92(r/\rho)^{1/2} \qquad 6.15$$

Note that Neuber's value of α_{tb} corresponds to the total SCF calculated from Equation 6.10. Writing α_k as the unknown general SCF, Neuber gives the general case as

$$\frac{1}{(\alpha_k - 1)^2} = \frac{1}{(\alpha_{fk} - 1)^2} + \frac{1}{(\alpha_{tb} - 1)^2} - \frac{1}{(\alpha_{tb} - 1)^2} + \frac{1}{(\alpha_{tk} - 1)^2} \qquad 6.16$$

with r + c instead of r

Writing $$\frac{1}{(\alpha_n-1)^2} = \frac{1}{(\alpha_{tk}-1)^2} - \frac{1}{(\alpha_{tb}-1)^2}$$

gives $$\frac{1}{(\alpha_n-1)^2} = \frac{1}{\frac{r+c}{\rho}} - \frac{1}{\left[1.92\left(\frac{r+c}{\rho}\right)^{1/2}\right]^2}$$

$$= \frac{2.69}{3.69\left(\frac{r+c}{\rho}\right)}$$

$$= \frac{1}{1.37\left(\frac{r+c}{\rho}\right)}$$

Note from Equation 6.14 that according to Neuber,

$$\alpha_{fk} = 2(a'/\rho)^{1/2}$$

Using Equation 6.11

$$K_{I(fk)} = \sigma_{max}\sqrt{\pi a}$$

But previous work [38] on the stress intensity factors for an edge notch in a plate shows that $K_I = 1.12\sigma\sqrt{\pi a}$. Harris [23] recommends therefore that the value of the constant in α_{fk} be increased from 2 to 2.24 to comply. Putting this revised value into Equation 6.16 and neglecting small terms as $\rho \rightarrow 0$ gives:-

$$\frac{1}{(\alpha_k-1)^2} = \frac{1}{2.24^2(a'/\rho)} + \frac{1}{1.92^2(r/\rho)} + \frac{1}{1.37\left(\frac{r+c}{\rho}\right)}$$

$$= \rho\frac{(5.05r(r+c)+6.87a'(r+c)+18.51a'r)}{25.36a'r(r+c)}$$

$$(\alpha_k-1) = \rho^{-1/2}\frac{(5.05+6.87a'/r+18.51(a'/r+c))^{-1/2}}{25.36a'}$$

$$\alpha_k = \rho^{-1/2}a'^{1/2}\left[\frac{5.05+\frac{6.87a'(r+c)+18.51a'r}{r(r+c)}}{25.36}\right]^{-1/2}$$

$$= \rho^{-1/2}a'^{1/2}\left[\frac{5.05+\frac{a'}{r+c}(25.38+6.87c/r)}{25.36}\right]^{-1/2}$$

Again,

$$K_I = \frac{\sqrt{\pi}}{2} \lim \rho \to o \rho^{1/2} \sigma_{max}$$

$$K_I = \sigma_{nom} \sqrt{\pi a'} \left[0.80 + \frac{a'}{r+c} (4 + 1.08\, c/r) \right]^{-1/2}$$

For this general case, the nominal stress is the net section stress at the crack plane, hence:-

$$K_I = \frac{T}{\pi[(c+r)^2 - c^2]} \sqrt{\pi a'} \left[0.80 + \frac{a'}{r+c} (4 + 1.08 c/r) \right]^{-1/2} \qquad 6.17$$

Note that if $a' \gg r$, a deep notch situation exists.

Rewriting 6.17 whilst ignoring negligible terms gives:-

$$K_I = \frac{T}{\pi r(r+2c)} \sqrt{\pi a'} \, [0.80 + a'/c(4 + 1.08 c/r)]^{-1/2}$$

$$= \frac{T}{\pi r(2c+r)} \sqrt{\pi} \left[\frac{0.80}{a'} + 4/c + 1.08/r \right]^{-1/2}$$

$$= \frac{T}{\sqrt{\pi}(2c+r)r} \left[\frac{1.08}{r} \right]^{-1/2}$$

$$= \frac{T}{\sqrt{\pi}(r+2c)r} \left(\frac{r}{1.08} \right)^{1/2}$$

$$K_I = \frac{0.962T}{\sqrt{\pi r}(r+2c)}$$

which compares well with Equation 6.12.

6.3.1.2 Application of theoretical SIF to threaded connections

The foregoing section describes an SIF solution for a circumferentially notched (cracked) hollow cylinder. If one looks at the result from the large scale fatigue test reported in Chapter 5, it is seen that the crack did grow around at least one circumference of the thread although the crack depth was not uniform around the thread. If however one considers the nominal stress acting over the cracked section, an estimate of the SIF can be obtained using Equation 6.17.

Note that the ***local nominal*** stress acting is used in this calculation. The FE analysis reported in Chapter 3 indicated that the stress gradient on the uncracked joint, through the section, was slight away from the thread root (Figure 3.7). This suggests that any cracking from the thread would soon be in a region of nominal stress and thus it is apparent that the analysis here is representative of the true situation once the crack has grown away from the thread root. At the thread root, there is a very high stress gradient as indicated from the FE results in Figure 3.7. This region requires a different analysis technique since the stress driving the crack is significantly higher than the nominal stress in the section and is heavily influenced by tooth loading and the local root radius.

In this region, a different theoretical approach is required. The experimental results from Chapt. 5 show how the crack initiated as a short sharp defect at the thread root. In this situation, it is unlikely that there are any other influences on the crack other than the local thread root stress. The crack can therefore be interpreted, on the local scale, as being a surface crack in a wide plate, for which the SIF is well documented [38] as

$$K = 1.1\sigma\sqrt{\pi a}$$

In this way, the two regions of crack growth can be modelled and an "envelope" of crack growth behaviour constructed as described in Section 6.5.

6.4 EXPERIMENTALLY DERIVED STRESS INTENSITY FACTORS

The advancement of crack measurement techniques, and in particular the acpd technique described in Chapter 5, have led to the ability to determine crack growth behaviour experimentally. Using such techniques, the crack growth can be monitored during the test and consequently experimental growth rates can be derived as shown in Figure 5.16.

Such information can then be used to determine experimental values for SIF.

Equation 6.1 gave the relationship between crack growth rate and SIF as

$$\frac{da}{dn} = C(\Delta K)^m$$

which can be written as

$$\log\left(\frac{da}{dn}\right) = \log C + m \log \Delta K \qquad 6.18$$

$$\log \Delta K = \frac{1}{m}\log\left[\frac{\left(\frac{da}{dn}\right)}{C}\right]$$

Noting from equation 6.2 that

$$\Delta K = (Y_\sigma)\Delta\sigma\sqrt{\pi a} \qquad 6.18a$$

Y_σ can be calculated from experimental data and is expressed as a Stress Intensity Calibration Function.

6.4.1 Results for Thick Walled Tether

Theoretical Analysis

i) Rigorous Analysis

The analysis described in Section 6.3.1.1. describes a stress intensity factor for a crack in a notch in a hollow round bar as:-

$$K_I = \frac{T}{Net \quad Area}\sqrt{\pi a}(0.8 + \frac{a'}{r+c}(4 + 1.08c/r))^{-1/2} \qquad 6.19$$

or in general terms,

$K_I = (Y_\sigma)\sigma\sqrt{\pi a}$ | (a = crack depth)

Table 6.1 gives values of Y_σ calculated from the forged tether model. The values given in Table 1 have been calculated on the basis of a nominal stress applied on the section. Thus the values from equation 6.19 can be presented in terms of nominal stress as shown in the example below.

Sample Calculation

Equation 6.17 gives

$$K_I = \frac{T}{\pi[(c+r)^2 - c^2]}\sqrt{\pi a}\left\{0.8 + \frac{a'}{c+r}(4 + 1.08c/r)\right\}^{-1/2}$$

Putting a'= crack + notch = 14mm with c = 25 and r = (25 - a) gives

$$K_I = \frac{T}{\pi[(c+r)^2 - c^2]}\sqrt{\pi a}[0.55]$$

Defining σ_{nom}=stress in unnotched section and noting nominal section area for the pin = 5890mm, gives

$T = \sigma_{nom} x\ 5890$ and

$$K_I = \sigma_{nom}\sqrt{\pi a}\left[0.55 \times \frac{5890}{\pi[(r+c)^2 - c^2]}\right]$$

$$K_1 = 1.54\sigma_{nom}\sqrt{\pi a'}$$

Note however that a' = crack depth (a) + notch depth.
Considering the tooth height (=1.575mm) as the notch, the above expression can be re written as

$$K_1 = 1.54\sqrt{\frac{a'}{a}}\sigma_{nom}\sqrt{\pi a}$$

$$K_1 = 1.34\sigma_{nom}\sqrt{\pi a}$$

ii) Simplified Analysis

The simplest model that could be used to described the behaviour of the crack in a thread is that which is used to describe the behaviour of a crack in a plate. As discussed earlier, this type of analysis would be expected to be appropriate for early crack growth.

Taking the simple solution for a crack in a plate gives

$$K = 1.1\sigma_{nom}\sqrt{\pi a} \qquad 6.20$$

Noting that the stress analysis described in Chapter 3 indicated high stress at the thread root as shown in Figure 3.7, these must be accounted for in equation 6.20 as follows

$$K_{Thread} = K_{plate} \times SCF \text{ due to thread}$$

i.e. $K_I = (1.1 \times SCF)\sigma_{nom_{thread}}\sqrt{\pi a}$

Hence $(Y\sigma) = 1.1 \times SCF$

Table 6.2 gives values for Yσ based on this simplified model

6.4.1.1 Experimental Study of Crack Growth Behaviour

Figure 5.16 shows the experimental crack growth curves. It is observed that all three crack fronts exhibited roughly the same growth characteristics. In order to described this behaviour using the FM approach, it is necessary to express the growth curves in terms of crack growth rates. This has been done for the experimental crack growth

behaviour and is presented in Table 6.4 in terms of *da/dN* i.e. crack growth rate per cycle. The experimental crack growth rates have been used to calculate an experimental value of ΔK, using equation 6.18. Equation 6.18a is then used to calculate experimental values of Y_σ. The cyclic stress range was calculated as 52.7 MPa at the nominal section. This accounts for the reduction in cyclic stress due to preload and was calculated on basis of the ratio of the areas of pin and box, as discussed in section 4.2.4. In this analysis, the following Paris materials data, derived from a similar steel [59] was used.

$$C = 1.8 \times 10^{-11}$$

$$m = 3.2$$

The results of Cracks 1 and 3 are presented in Tables 6.5 and 6.6. These represent the fastest and slowest growing cracks.

6.5 DISCUSSION OF CRACK GROWTH RESULTS

Figure 6.2 summarises the results from the experimental measurement and theoretical calculations. It is seen that the Y Factor calculated assuming an infinitely long edge notch is initially high and decreases rapidly as the influence of SCF due to the notch decreases as the crack tip grows away from it. In contrast, the solution for the circumferentially notched bar, which ignores the effect of SCF due to the notch itself, steadily increases from a value of 1.1. The two solutions converge, in this case at a value of a = 5mm approximately. Thus it is possible to consider an envelope of applicability created by the 2 solutions whereby for values of crack depth greater than 5mm equation 6.17 is used and for values less than 5mm the edge notch solution is used. The experimental results for cracks 1 and 3 clearly demonstrate the expected trend and lie close to the proposed combined solution as seen in Figure 6.2.

Whilst the amount of experimental data is limited, this approach shows considerable promise and it is recommended that further studies be conducted to confirm these results. It should be noted that the solutions proposed here are both based upon the assumption of a circumferential notch (considered as analogous to an infinitely long edge notch if the flat plate solution is adopted). This is reasonable since the very sharp radius at the thread root would be expected to lead to rapid initiation circumferentially, as was indeed observed from the fracture surface. This arises from the very high local SCF which rapidly decays into the section as the crack grows into the section.

Another reason for the long crack behaviour could be the relatively high stress conditions under which the thread was tested. In general, high stress/short life tests tend to lead to long crack behaviour. In contrast, a low stress long life test can lead to shorter deeper cracks.

The reason being that in the early stages, the general peak SIF at the root would be lower and crack growth would be concentrated on local stress concentrations such as mechanical damage on local material imperfections leading to concentrated rather than general crack growth, particularly during the early stages of the fatigue life.

For thread forms with larger root radii, the crack growth behaviour could lead to part circumferential cracks where it would be necessary to consider the crack aspect ratio in the solutions. Whilst rigourous approaches have recently been developed based on Weight Function Solutions [41] a simplified approach would be to consider the effect of aspect ratio on an edge notch [38] and apply this factor to both solutions proposed here.

Further studies would need to be conducted to determine the nature of the aspect ratio development of other thread geometries before developing the methodology for their assessment.

The studies here considered only axial loading. For TLP tethers this is the predominant load with bending moments being relatively small due to the taut configuration. For other applications using threaded connections, bending and torsional loads could be present as well as axial tension and under these conditions careful consideration of the effect of combined loading would be required.

6.6 STRESS STRAIN BEHAVIOUR OF MATERIAL UNDER CYCLIC LOADING

The stress strain characteristics of a material can be described using the Ramberg-Osgood relationship given in equation 6.21

$$\varepsilon = \frac{\sigma}{E} + \left(\frac{\sigma}{K'}\right)^{1/n'} \qquad 6.21$$

A typical stress strain curve is shown in Figure 6.3. It is generally assumed that all stable hysteresis behaviour can be described by expanding this basic cyclic stress strain curve by a factor of 2 and shifting its origin - Figure 6.4. Thus the dynamic behaviour of the material under cyclic loading can be described by equation 6.22

$$\frac{\Delta\varepsilon}{2} = \frac{\Delta\sigma}{2E} + \left(\frac{\Delta\sigma}{2K'}\right)^{1/n'} \qquad 6.22$$

Where $\Delta\sigma$ is the stress range.

When a notch is present in the material, as in the case for a thread, an elastic cyclic nominal stress leads to elastic plastic behaviour at the notch tip. Neuber [4.5] has investigated this behaviour and describes the material behaviour in terms of two geometric concentration factors, one being a stress concentration factor K_σ and the second a strain concentration factor K_ε where:-

$$K_\sigma = \frac{\text{Max Notch Stress}}{\text{Nominal notch Stress}} = \frac{\sigma}{S_t}$$

and

$$K_\varepsilon = \frac{\text{Max Notch Strain}}{\text{Nominal notch Strain}} = \frac{\varepsilon}{e}$$

Defining nominal strain = $\dfrac{\text{Elastic nominal stress}}{\text{Youngs Modulus of Elasticity}} = \dfrac{S_t}{E} = e$

and the elastic SCF as $K_t = (\sqrt{K_\sigma K_\varepsilon})$

Gives $K_t^2 = \dfrac{\sigma\varepsilon E}{S_t^2}$

or $\sigma\varepsilon = \dfrac{(K_t S_t)^2}{E}$

This can be written in terms of stress ranges as:-

$$\Delta\sigma\Delta\varepsilon = \frac{(K_t\Delta S)^2}{E} \qquad 6.23$$

From 6.22 and 6.23, the complete stress strain history can be predicted for any value of applied load range and elastic SCF.

Now, knowing the cyclic stress strain condition, the material behaviour can then be investigated.

6.7 FATIGUE CRACK INITIATION

Section 6.1 discussed the definition of crack initiation and described the way in which repeated stress cycles produce microscopic damage which accumulates to form a microscopic defect, the crack. This effect can be investigated in the laboratory using smooth tensile specimens whereby the applied stress is calculated simply by considering the specimen geometry and the number of cycles to failure is counted. For situations where a notch exists, the uniform stress fields found in the simple specimen do not exist. However, by considering the local stress strain behaviour of the notch tip, as described in the previous section, it is possible to infer the behaviour of the notch from that of smooth specimens by considering the notch tip as being a part of the small tensile specimen. This model is shown in Figure 6.5.

From Figure 6.5 it is seen that the cyclic stress/strain behaviour at the notch could be applied to a smooth specimen and that, since the crack growth rate on a smooth specimen would be extremely rapid, due to the rapidly increasing stress intensity, the cycles to cause failure of the smooth specimen is a closer approximation to the cycles to defect initiation.

Such a model has been investigated by a number of workers [61,45] and it is found that crack initiation predictions were good when compared to experimental data on notched specimens. Glinka [62] has found that the Neuber [45] theory for predicting elastic/plastic strains at the notch tip tends to overestimate the local strains in situations where the elastic SCF is high and suggests a better approximation to be predicted using the Equivalent Energy Density Method [62].

As a comparison, Neuber gives from equation 6.23

$$\frac{(K_t S_t)^2}{E} = \sigma\varepsilon$$

Whereas the energy density concept would predict

$$\frac{(K_t S_t)^2}{2E} = \frac{\sigma^2}{2E} + \frac{\sigma}{(n'+1)}\left(\frac{\sigma}{K'}\right)^{1/n'} \qquad 6.24$$

It is seen that the additional term is material dependent and is derived from the material stress strain curve (Equation 6.21).

A graphical interpretation of this is shown in Figure 6.6

The Equivalent Strain Energy Density Concept is based on the assumption that the total strain energy density in the plastic zone ahead of a notch tip is equal to the strain energy density calculated on the basis of the hypothetical elastic stress field which would be present in the absence of plastic yielding.

In the absence of plastic yielding the area under the stress strain curve represents the strain energy and is seen to be equal to

$$W_s = \int_0^e S(e)de = \frac{S_t^2}{2E} \qquad 6.25$$

When the notch yields, the equivalent elastic energy W_e is given by

$$W_e = K_t^2 W_s \qquad 6.26$$

However, for local plastic yielding at the notch tip, the strain energy W_p is given by

$$W_p = \frac{\sigma^2}{2E} + \frac{\sigma}{n^1+1}\left(\frac{\sigma}{K^1}\right)^{1/n^1} \qquad 6.27$$

Equations 6.26 and 6.27 give

$$\frac{(K_t S_t)^2}{2E} = \frac{\sigma^2}{2E} + \frac{\sigma}{n^1+1}\left(\frac{\sigma}{K^1}\right)^{1/n^1} \qquad 6.28$$

Where

$$\varepsilon = \frac{\sigma}{E} + \left(\frac{\sigma}{K^1}\right)^{1/n^1} \qquad (\text{Equ}^{\text{n}}\ 6.21)$$

Note that Neuber gives

$$\frac{(K_t S_t)^2}{2E} = \frac{\sigma\varepsilon}{2}$$

Referring to Figure 6.6. The area of triangle ODE represents the equivalent elastic energy and it is seen that

$$W_e = \frac{K_t^2 S_t e_t}{2}$$

The solution using the Neuber solution would be represented by the transfer OA^1B^1 which has an identical area of ODE and results in the solution of σ_n and ε_n. For the equivalent energy density method, the solution is σ, ε where area OCAB is equal to ODE.

6.7.1 Calculation Of Fatigue Initiation Life

Once the local notch tip stress strain response has been calculated, the fatigue initiation life prediction can be conducted using a modified version of the Manson-Coffin strain life relationship given in Equation 6.29.

$$\frac{\Delta\varepsilon}{2} = \frac{\sigma_f - \sigma_m}{E} (2N_f)^b + \varepsilon_f (2N_f)^j \qquad 6.29$$

Thus it is seen that the solution for N_f, the number of cycles to failure can be found as follows:-

1. Use the notch/equivalent energy density concept with Ramberg-Osgood material behaviour to calculate cyclic strain behaviour.

2. Use equation 6.29 to calculate N_f.

Note that the above solution route is for constant amplitude loading. If variable amplitude loading is used, the material memory effect must be considered in counting strain ranges together with a damage accumulation procedure such as the Miner approach [63].

6.7.2 Calculation Of Crack Initiation For The Large Scale Model

The above approach was used to predict a fatigue initiation life for the large scale model tested (Model 1) but without preload. The lack of information about the absolute value of preload used in the experiments precluded the calcultaion of mean load for a preloaded connection.

Cyclic strain data from a similar material was published by Chen and Lawrence [59] and used in this calculation. The properties of the HY 130 steel are given in Table 6.7

This allows the material stress strain curve to be produced using equation 6.1. This is shown in Figure 6.7.

The materials curve was then used to predict the cyclic stress strain relationship using equation 6.22. As explained earlier, this in effect means expanding the scale by a factor of 2 and moving the origin. The cyclic materials curve was then broken down into 7 segments. This piecemeal presentation of the curve was used to allow a numerical technique to be employed for the solution of the cyclic stress and strain ranges due to the applied nominal stress range.

The above analysis was run with both the Neuber and Equivalent Energy Models which yielded the following results:-

Input Data

Nominal Stress Range ΔS_t = 136 MPA (From FE analysis)

K_t= = 12.0 (From FE analysis)

Results

For Energy Model

σ_{max} = 895 MP_a σ_{mean} = 190 MPa

$\Delta\sigma$ = 1411.42 $\Delta\varepsilon$ = 0.00791

For Neuber Model

σ_{max} = 942 MP_a σ_{mean} = 212 MPa

$\Delta\sigma$ = 1460.03 $\Delta\varepsilon$ = 0.00873

Equation 6.27 was then used to calculate the value of N_f.

Equation 6.29 gave

$$\frac{\Delta\varepsilon}{2} = \frac{\sigma_f - \sigma_m}{E}(2N_f)^b + \varepsilon_f(2N_f)^j$$

The constants for this material are given in Table 6.7

Using the Energy Method, $N_f = 32{,}000$ Cycles
Using the Neuber Method, $N_f = 17{,}700$ Cycles

6.8 DISCUSSION OF INITIATION RESULTS

These results show clearly the sensitivity to the method of calculation of the notch tip stress-strain characteristics with almost of factor of 2 between the results from the different models with Neuber producing the lower (more conservative) prediction. The lives calculated here are for a connection with no preload and thus cannot be directly compared with the experimental results. It is however interesting to note that if the early crack growth curves for all three cracks (See figure 5.16) are extrapolated linearly to the zero axis, they cross at between 12,000 and 44,000 cycles.

6.8.1 Prediction of Crack Initiation in Threads

The theoretical models described here are applicable to plane stress situations but can readily be modified for plane strain situations. It must be noted however that the modelling is based on the assumption that the behaviour of the notch tip can be represented by a smooth specimen. This fundamental assumption is questionable for the case of a machined component on two counts.

1) The surface of a machined component such as a thread is unlikely to be smooth in metallurgical terms. Any machining marks on the surface of a cut thread tend to be perpendicular to the axis and therefore are in a critical orientation. Likewise thread damage occurring in service due to debris in the threads is unlikely to result in a "perfect" thread profile. Bearing in mind that the stress analysis and the initiation

analyses are based on perfect root radii and smooth specimen prediction, it is likely that the predictions for initiation are in fact based on a non-conservative situation in reality.

2) The very high stress gradients at the thread root surface, as predicted using FE modelling and shown in Figure 3.7 lead to the likelihood of very small regions of plasticity which may not be correctly represented by the assumption that the notch tip can locally be modelled as a tensile specimen under uniform stress.

The fatigue life predictions based on initiation are also extremely sensitive to mean stress effects. For preloaded threaded connections, where the preload is not known, the uncertainties in absolute value of the mean stress level can lead to wide variations in predicted initiation life.

The use of initiation predictions described above should therefore be treated with caution when applied to threaded connections. Whilst such calculations will allow comparison of alternative design feature, the absolute value of fatigue initiation life could be significantly in error due to the practicalities of thread production and uncertainties in torquing procedures. The initiation life will also be affected by production techniques such as thread root rolling. This process tends to increase initiation resistance and can be modelled using the same methodology but the same geometric influences apply.

In terms of remaining fatigue life prediction, it is recommended that initiation life for threads should be ignored and it should be assumed that any thread that has been used in service contains defects of a certain size unless sufficient inspection data is available to determine otherwise. This approach is conservative and is discussed in more detail in Chapter 7. It is recommended as a practical approach since fatigue initiation calculations tend to be non-conservative for the reasons discussed above.

Crack Depth a (mm)	Notch+Crack Depth a' (mm)	Normalised Crack Depth (a'/t)	Y_σ
0.23	1.8	.01	2.83
0.43	2	.09	2.40
2.43	4	.17	1.44
4.43	6	.26	1.34
6.45	8	.34	1.35
8.43	10	.43	1.40
10.43	12	.51	1.49
12.43	14	.60	1.63

Note: Calculations based on Gross Section (Nominal stress)

Table 6.1 Stress Intensity Factors Calculated using the Harris Solution (Section 6.3.1.1)

Crack Depth (a)mm	Normalised Crack Depth a/t	SCF (Ref. Fig.3.7)	Y_σ
0.2	.01	8.5	9.35
0.5	.02	2.9	3.19
1.0	.04	2.1	2.31
2.0	.09	1.4	1.54
4.0	.17	1.2	1.32
6.0	.26	1.0	1.10
8.0	.34	0.9	0.99
10.0	.43	0.9	0.99

Table 6.2 Results for $Y(\sigma)$ calculated using the Simplified FM model

	Crack Depth (mm)		
N (Cycles) x 1000	Crack 1	Crack 2	Crack 3
60	.65	.25	.45
110	1.35	1.12	1.45
158	2.5	1.20	2.20
207	3.5	4.5	-
285	5.0	5.5	5.6
336	6.5	7.0	7.7
375	10.0	8.5	10.0

Table 6.3 Experimental Crack Depths (Depth at Deepest Point)

	Crack Depth (mm)					
	.5	2	4	6	8	10
Crack 1	1.88×10^{-8}	2.0×10^{-8}	2.38×10^{-8}	4.75×10^{-8}	7.13×10^{-8}	14.7×10^{-8}
Crack 3	1.75×10^{-8}	2.1×10^{-8}	2.75×10^{-8}	3.9×10^{-8}	5.0×10^{-8}	7.0×10^{-8}

Table 6.4 Experimental Crack Growth Rates da/dn for Cracks 1 and 3 at various depths (m/cycle)

Depth (mm)	da/dn x 10^{-8} m/cycle	ΔK $MPa\sqrt{m}$	Y_σ
1	1.88	8.78	2.97
2	2.00	8.95	2.14
4	2.38	9.45	1.60
6	4.75	11.73	1.62
8	7.13	13.31	1.59
10	14.70	16.70	1.78

Table 6.5 Analysis of Crack 1

Depth (mm)	da/dn x 10^{-8} m/cycle	ΔK $MPa\sqrt{m}$	Y_σ
0.5	1.75	8.58	4.10
2	2.10	9.09	2.18
4	2.75	9.88	1.67
6	3.90	11.03	1.52
8	5.0	11.92	1.43
10	7.0	13.24	1.42

Table 6.6 Analysis of Crack 3

K^1	=	1517
n^1	=	0.1
E	=	209,000
b	=	-0.06
j	=	-0.64
ε_f	=	0.9
σ_f	=	1489

Table 6.7 Material Properties of HY 130

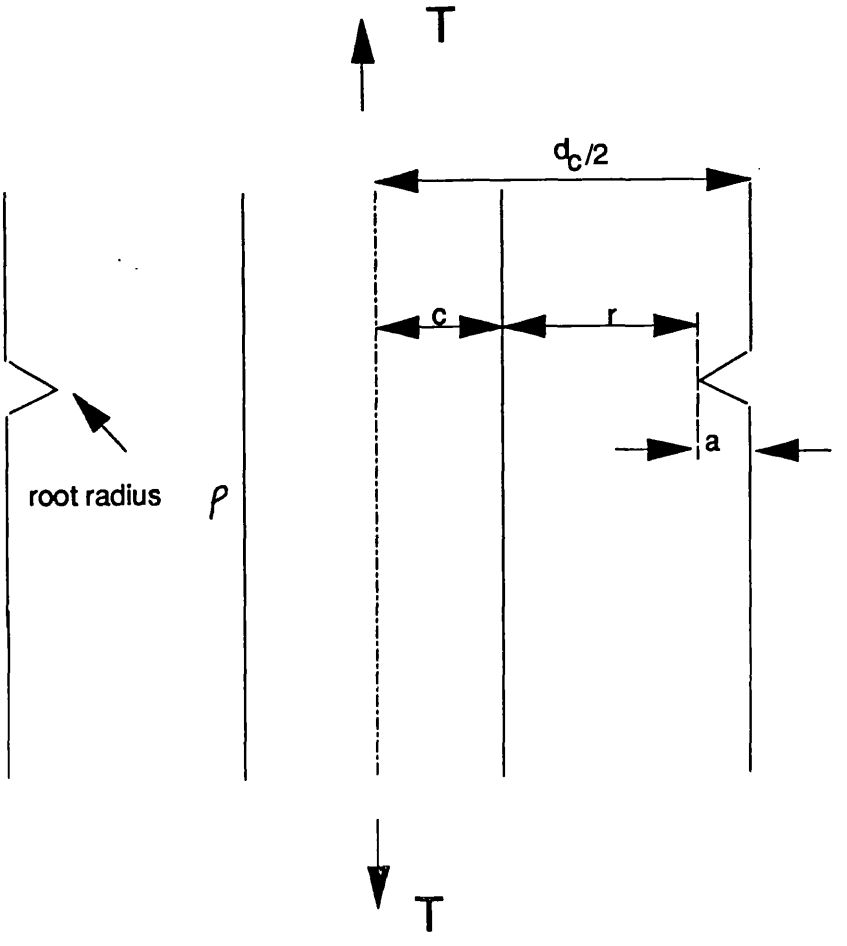

Fig 6.1 Hollow cylinder modelled by Harris.

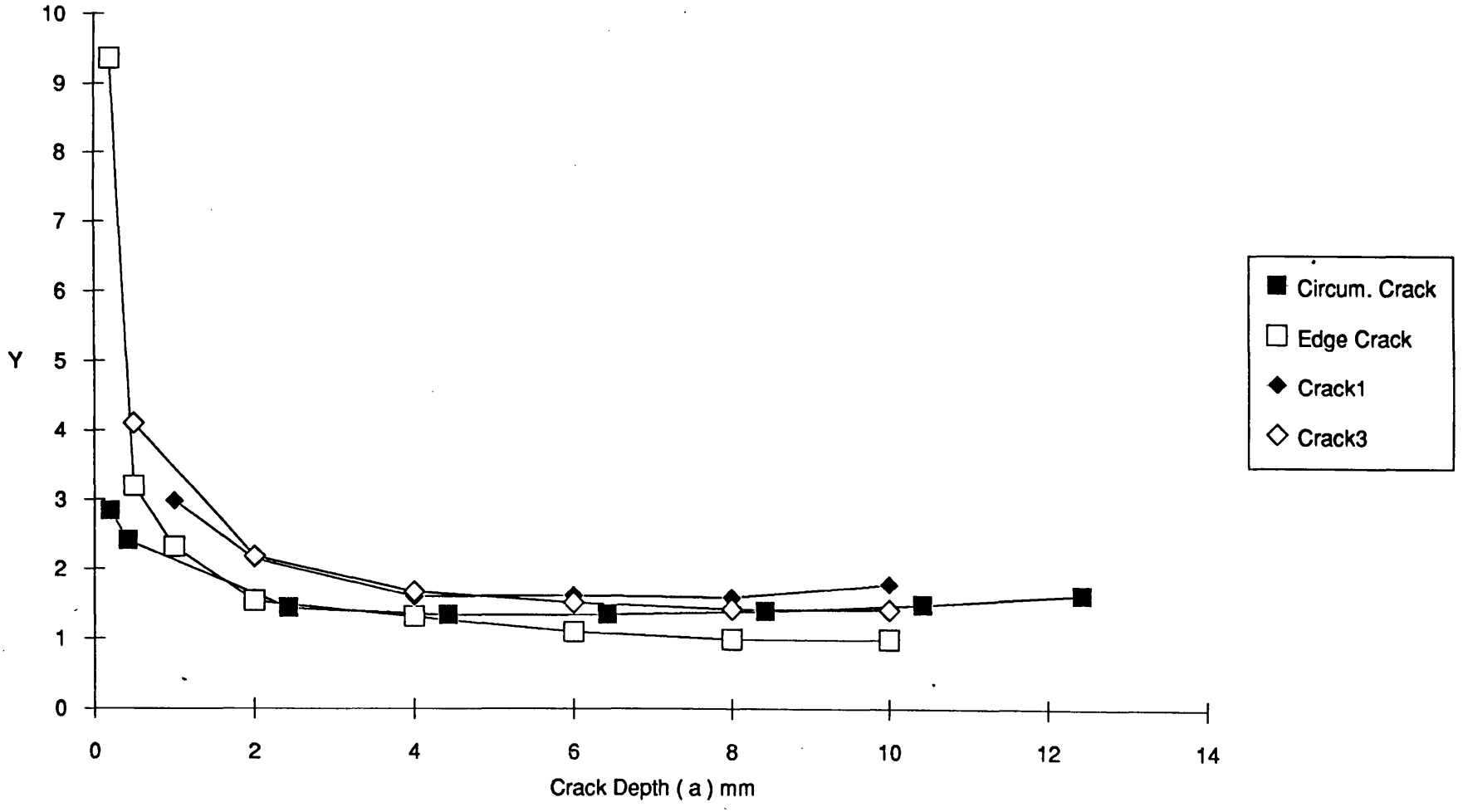

Fig. 6.2 Comparison of Experimental and Theoretical Y Factors

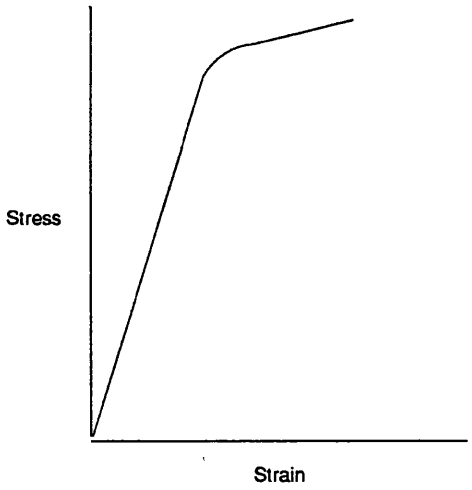

Fig. 6.3 Basic material stress-strain behaviour

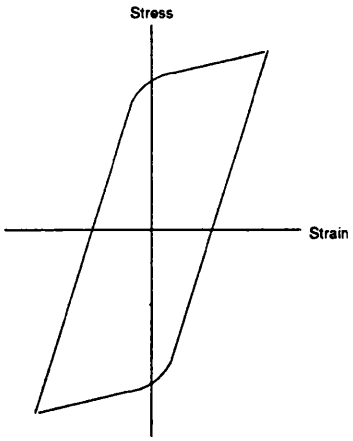

Fig 6.4 Stable Hysteresis Behaviour

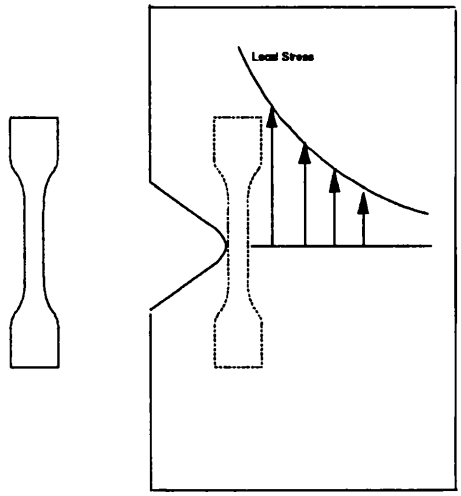

Fig. 6.5 Use of Small specimen data to predict notch effect

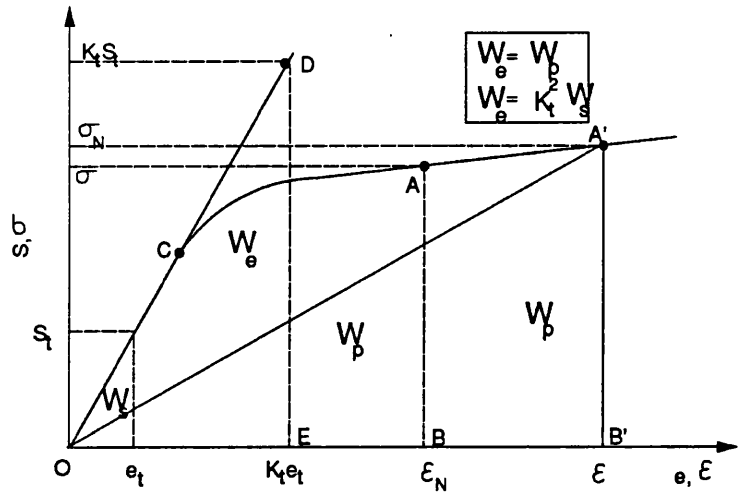

Fig. 6.6 Graphical Presentation of the strain energy density concept.

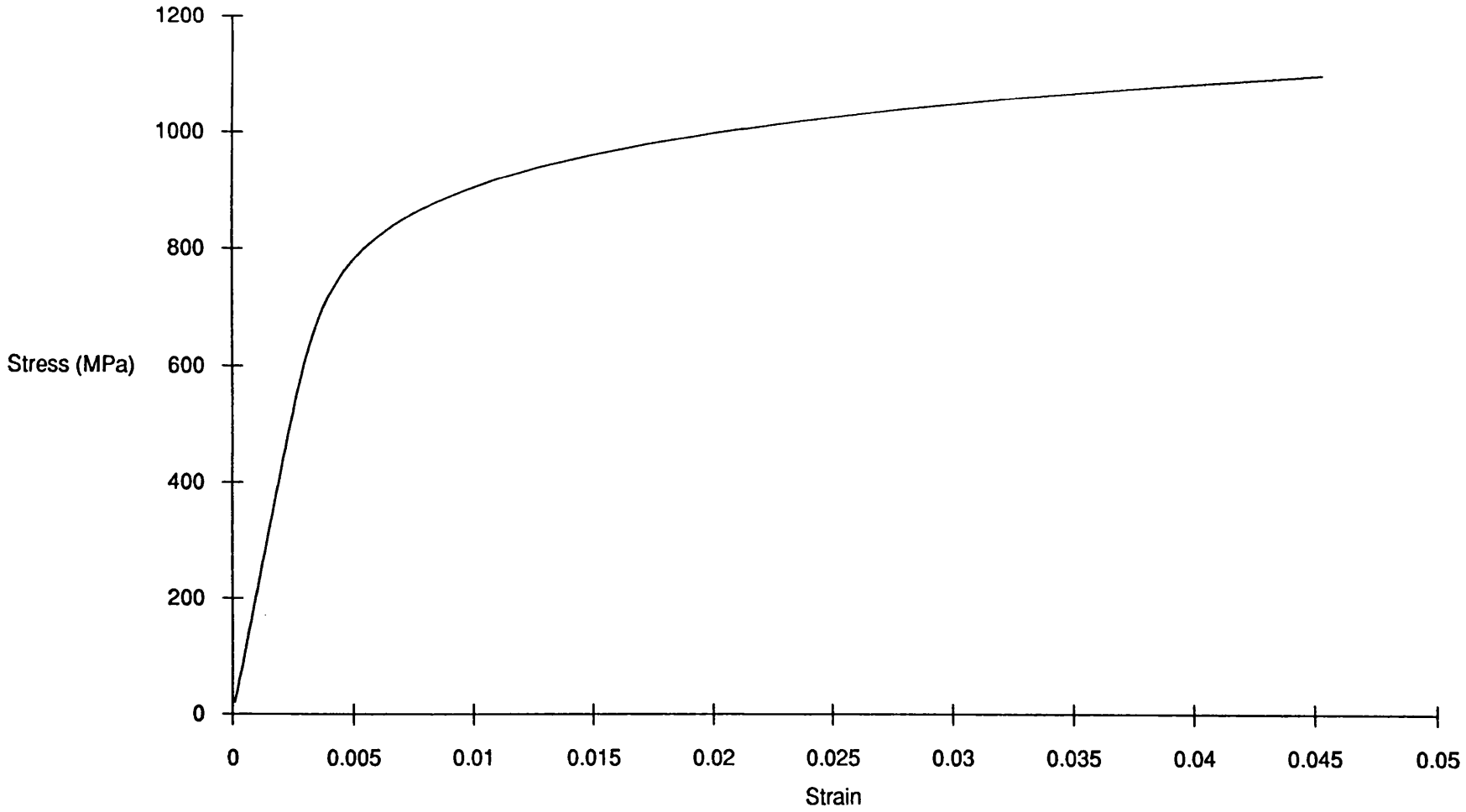

Fig 6.7 Stress Strain Curve for HY 130 Steel

CHAPTER 7

THE USE OF CONTROLLED INSPECTION

for

MAINTAINING COMPONENT INTEGRITY

7.1 INTRODUCTION

The foregoing sections have shown how mathematical models can be used to predict the stresses in threaded connections and how Fracture Mechanics methods can be used to predict fatigue behaviour. The work in Chapter 5 also showed how non-destructive testing or inspections can be carried out on threads to measure the amount of cracking that has occurred. This demonstrates the possibility of monitoring at regular intervals to determine whether fatigue damage is occurring in service and whether the component is performing as predicted.

The use of in-service inspection during the life of critical components obviously provides verification that no unforeseen problems are occurring whilst also providing valuable feedback to the designers. Another major benefit is that the life of a component could be extended if the design proves to have been excessively conservative. This is a particularly important benefit for offshore platform structural components which, whilst designed originally for a life of, say 25 years, may be required to be used for an extended period due to improvements in well recovery and economic situations which could make marginal recovery economic in the future. It should of course be noted that there is a statutory requirement to inspect key structural components of platforms at regular intervals and tethering systems would be included in this requirement.

Thus there is already a requirement for in-service inspection of threaded components and models for crack growth behaviour have been produced. It is therefore possible to consider how the two considerations can interact to provide safe and economic operations of tethering systems.

Before looking at the specific case of a TLP tether, the general philosophy of using fatigue predictions with regular inspections will be considered under the general banner of Retirement for Cause.

7.2 THE RETIREMENT FOR CAUSE APPROACH TO STRUCTURAL INTEGRITY

For many structural components, the combination of material properties, geometric factors and fabrication processes make the presence of cracks inevitable, even for components that have been used for a small percentage of their fatigue life. A typical example of this is the tubular welded joint used extensively for the construction of

offshore structures. Here the combination of very high local stresses with site fabricated multi-pass manual welding result in very short fatigue crack initiation lives with crack growth occupying perhaps 80 - 90% of the total fatigue life of the component.

In such situations, the presence of a crack, which is not dramatically accelerating due to load shedding mechanisms, provides ample opportunity for the detection of the defect prior to failure of the component. The same is true for the thick walled threaded connection, as investigated in this study. In Chapter 5, the crack growth curves clearly indicate a situation of fairly constant crack growth over approximately 80% of the total fatigue life of the component. This means that, given an ideal inspection system, if the components were inspected at any time during the life when a crack was present, the component could have been identified as flawed and removed from service prior to failure.

Such an approach is known as "retirement for cause" whereby components are removed from service on the basis of a known defect being present, rather than after a fixed period in service.

7.3 APPLICATION OF THE "RETIREMENT FOR CAUSE" TO THREADED COMPONENTS

Some threaded connections can be shown to be defect tolerant in that the presence of a defect is not necessarily catastrophic. The presence of high geometric stress concentration factors at the thread root, combined with load concentrations at the first loaded tooth, can lead to the initiation of defects at the first loaded thread, but since the stress concentrations are very localised, the crack is actually growing into a region of low stress and the results from the large scale tests clearly indicate (Fig: 5.16) that the crack growth rates which are controlled by the lower stress regions, can be fairly uniform over a large proportion of the fatigue crack growth phase. These features of crack growth behaviour mean that a Fracture Mechanics approach can be used to predict how rapidly a crack will grow from a known size and this information can be used to determine an inspection procedure aimed at ensuring that a crack is identified prior to it becoming critical. Thus, the component could be used under known conditions for which Fracture Mechanics could predict crack growth rates and then these could be used to define suitable inspection periods, with the results of the inspection being used to determine whether there is cause to retire the component from service, or whether it could be re-used.

As an example of the way in which the approach is used in practice, consider a simple fatigue life curve for a particular threaded component under service loading conditions as shown if Figure 7.1

Note that the crack size is referred to here as crack depth, since for a surface crack at the thread root, it is the depth rather than the length that controls crack growth. Let us assume that the inspection system is perfect and is guaranteed to find any defect greater than 10% of the critical depth, the "NDT Target", and does not pick up any defects less than 10% of the critical depth. From the idealised fatigue life curve, it is seen that, if the component were to be inspected at intervals representing 25% of the predicted life, the first inspection would not show any defect, since the crack depth is below the inspection threshold. The second inspection would show a defect present and the component would be removed from service. In this simple example, with idealised fatigue characteristics and inspection system, the principle of the "retirement from cause" approach is demonstrated. In practice, however, the situation is far less simple and whether such an approach could be used for a particular application depends on a number of factors which are:-

i) Crack growth characteristics for the connection
ii) Reliability of the Fracture Mechanics Modelling
iii) Reliability of the inspection system
iv) Significance of a failure.

7.3.1 Crack Growth Characteristics

The "retirement for cause" approach should only be adopted where it can be shown that, for the particular connection and service conditions, the crack growth phase occupies in excess of 50% of the fatigue life under service conditions, and that for a significant proportion of that crack growth phase, the crack is not accelerating.

7.3.2 Reliability of the F.M. Modelling

There is clearly a close interaction between the prediction of crack growth rate and inspection requirements. If the rate of crack growth is underestimated, the component could fail due to a critical crack depth being reached between inspection intervals which would be unacceptable. It is therefore important to make due allowance for any uncertainties in growth rate predictions when defining inspection intervals. It is likely that the most significant factor contributing to unreliable fracture mechanics modelling is the loading input to the models. For many offshore applications, threaded members

are used in applications where load prediction is extremely difficult. For example, the loading in a TLP tether are extremely complex and have contributions from deck/wave interaction, deck/current interaction, vortex induced vibrations and direct environmental loading on the tethers themselves. The same complexities apply to drillpipe which is subjected to axial loading, torsion, rotating bending loads as the pipe negotiates dog legs, axial and lateral vibrations and drill bit induced vibration. With such uncertainties in the fundamental loads on the component, any FM predictions need to be carefully considered.

The reliability of FM modelling to predict fatigue damage is also influenced by the material properties used in the calculations. Material property variations, particularly in the Paris constants C and m can have a strong influence on crack growth rate predictions. It should be noted that the so-called material properties are not strictly properties of the material itself but rather the combination of material and environment. The interaction of material with environment is extremely complex and has been the subject of a great deal of research. Unfortunately there are no general rules that can be applied to the effect of environment and the behaviour of the type of steels used for tether and drilling applications, the reason being the competing effects of corrosion, crack closure, hydrogen embrittlement and even stress corrosion cracking. The following parameters all influence the material behaviour and it is thought necessary to consider all of these prior to selecting material properties for use in the final analysis.

i) Material microstructure (composition, manufacturing process, heat treatment)

ii) Environment (acidity, temperature, viscosity of any fluids, pressure)

iii) Environmental protection (level of protection, nature of protection i.e. surface coating and electrical)

iv) Loading "R" ratio

v) Loading level (Near threshold or close to stress corrosion plateau).

7.3.3 Reliability of Inspection System

A "Retirement for Cause" approach relies heavily on the ability of the inspection system to be able to reliably detect the presence of a crack. The ability of any inspection system to detect defects relies on many factors. These can be categorised into two groups, the first relating to the inspection system and the way it is utilised and the second being dependent on the nature of defect itself.

7.3.3.1 Influence of Inspection System on Inspection Reliability

The Inspection System referred to here means the entire system including hardware and operator. Clearly the choice of physical principle on which the inspection system is based will influence its ability to reliably inspect threaded connections. In general it is fair to say that any system requiring interpretation by an operator is likely to be more variable in overall performance than a system that is automated and requires little operator interaction. That is not to imply that machines are better than people but rather that the human operator's interpretation of inspection data is influenced by many factors, not least the variability between human operators. For example, MPI inspection requires the recording of visual indications, this depends on the operator's eyesight. For inspection in difficult areas, it depends on the operator's ability to perform various contortions to get to an ideal location.

The physical principle on which an inspection system is based will also have a strong influence on the overall performance for a specific application. For example, the use of ultrasonics for detection of cracks in flat plates is well established. However, the same system does not perform well on threads because the principle on which it is based relies on reflections from features such as the crack tip. A threaded connection has many corners and geometric features which also create reflection and therefore can confuse or swamp the signal from a crack of the same order of size on the thread.

The other prime influence on the system reliability is the procedure to which the inspection is conducted. For repeatable inspection results, it is necessary to minimise as many variables as possible, which means carefully controlling the way in which the inspection is conducted and this will cover all aspects of the inspection including set up of equipment, conduct of the inspection and recording and reporting of results.

7.3.3.2 Influence of Defect Type on Inspection Reliability

Whilst the influence of defect type can be discussed for a variety of different defects, the discussion here relating to threaded connections will be limited to surface breaking defects since these are the primary defects likely to be developing whilst the component is in service. Some features of fatigue cracks in threaded connections that could have an important influence on how easy they are to detect and measure are:-

1) **Crack Location**

Cracks could be located in pin or box members and could be in a variety of locations within the thread itself. This must be considered when choosing an inspection system and procedure, since a system which is targeted at finding cracks specifically at the root of the thread could fail to detect significant defects growing on the flank.

2) **Crack Size**

In simple terms, big cracks are easier to find than small cracks. However, "big" and "small" need to be carefully considered. For example, a long, very shallow crack could be less significant than a short deep crack which may be difficult to detect. Whether the length or depth of the crack controls the detectability depends very much on the inspection system. For systems such as acpd, eddy currents, and ultrasonics, a deep defect generally gives a better signal to noise ratio.

3) **Crack Roughness**

The degree of crack roughness can influence some techniques which rely on reflections/absorbtion such as ultrasonics and radiography.

4) **Crack Opening**

The degree of crack opening, i.e. the width of the mouth of the crack, can be a significant factor in it's detectability. In general, the greater the crack opening, the greater the detectability.

5) **Deposits on crack surface.**

Cracks that grow in corrosive environments can develop corrosion products on the crack surface. If cathodic protection is present, calcarious deposits on the crack surface can result. Also the deposit can be due to the penetration into the crack of various fluids that can leave a deposit such as oil or mud on the crack surface. The wide variety of possible crack face deposits make full generalisation of the effects impossible, but it can be said that deposits that lead to electrical isolation between the surfaces can improve detectability to electromagnetic systems (e.g. acpd/acfm and eddy currents) and deposits that wedge open the defect mechanically and thus reduce the possibility of crack closure are likely to enhance detectability.

6) **Crack Branching**

Crack branching either through thickness or on the surface can lead to erroneous prediction of crack size. This can work both ways. For example, a series of multiple surface cracks which are all short in their own right, can be interpreted as a much larger defect, whereas an overlapping pair of cracks can lead to serious underprediction on crack depth when using electromagnetic techniques, unless the feature is identified and correction applied.

7.4 INSPECTION SYSTEMS FOR TETHERS

It is obvious that any inspection system being used for the assessment of structural integrity must be reliable both in operation and the results it gives. Inspection Reliability is addressed in the next Section but it is necessary to state at this point that the performance of any inspection system being used to monitor structural integrity must be readily quantifiable with a high confidence.

7.4.1 In Situ - Inspection Systems

In situ monitoring of tether connections is an extremely onerous requirement. The fact that the threads are made up means that any inspection system needs to inspect from an uncracked remote face. Such inspections are conventionally attempted using ultrasonic or radiographic techniques.

7.4.1.1 Ultrasonic Methods

The simplest mode of ultrasonic inspection involves a pulse echo technique as shown schematically in Figure 7.2. This works well for flat plates but is more difficult to use on a threaded component where the back face contains notches (thread roots) which create their own echoes. More sophisticated inspection techniques such as Time of Flight Diffraction [43] are available but require complex probe deployment and considerable interpretation. Bearing in mind that it would be desirable to inspect both pin and box from the same system, rather than the box inspection being done from the outside and the pin being inspected from the internal bore, the ultrasonic path becomes extremely complex. Added to this the fact that interpretation of ultrasonic signals relies heavily on a knowledge of the exact location of the probes, it is extremely unlikely that reliable inspection of a tethering system could be conducted from the internal bore with a high degree of confidence. The criteria being for indication of the presence of a defect and its size and location.

7.4.1.2 Radiographic Methods

In-service radiography would require access from both inside and outside to achieve single wall (pin plus box) penetration or the outside for double wall penetration (2 x pin plus 2 x box). The fact that the cracks would probably be circumferential makes the likelihood of radiography succeeding extremely small.

7.4.2 Inspection of Tethers Removed from Service

If the elements were removed from service and recovered, the inspection problem becomes much easier. Once access to the threaded section is available, techniques such as MPI, Eddy Currents and acpd can be deployed. The acpd system developed in Chapter 5 could be easily adapted for service use and it is obvious that this be considered as a major new advance for quantitative thread inspection since it is not only capable of detecting defects but measuring the size as well without prior calibration.

The key factor in selecting an inspection system is whether it is reliable and repeatable. Any systems that do not require operator interpretation will have major benefits over competitors. A brief summary of the state of the art for thread inspection is given below:-

7.4.2.1 Magnetic Particle Inspection (MPI)

Magnetic Particle Inspection is widely used in many areas of industry for component inspection. It is used for the inspection of threads for the drilling industry and for that application is deployed manually. The technique is extremely sensitive to operator interpretation and relies heavily on the operator's skills. It cannot easily be automated for thread inspection.

7.4.2.2 Eddy Current Systems

Eddy Current (EC) inspection is becoming more popular for general applications and is widely used in the aircraft industry. It has not been widely used for thread inspection. To be effective, the probe needs to deployed close to the root of the thread and on ferritic steels the thread flanks would cause interface with the measuring signals. EC systems can be automated but this has not been done for thread work.

EC is really a detection tool although claims for some depth predictions are made. The signal decays exponentially with depth and thus a detailed calibration procedure is required for any depth interpretation and any defects above about 5mm deep could be seriously underestimated.

7.4.2.3 ACPD Inspection

The acpd technique was described in Chapter 5 and used to monitor crack growth in the large scale tests. The same technique has been used successfully for inspection of tether connections which have been removed from service from the Hutton TLP. The acpd technique depends on electrical contact between the probe and the component and hence requires a high degree of surface cleaning. The technique has proved to be extremely sensitive and reliable and is capable of detection and sizing (depth measurement). The requirement for electrical contact can however lead to difficulties for detection where it is preferable to "sweep" the probes around the thread, the probe movement sometimes leading to momentary loss of contact between probe and component.

A development from the contacting acpd technique is the non-contacting ac field measurement (acfm) technique [64]. Like the acpd technique, this is a field perturbation technique but instead of measuring surface voltages measures the associated magnetic fields above the surface. Whilst the interpretation of the signals is more difficult than for acpd, mathematical modelling can be used to interpret the magnetic field perturbation in terms of crack length and depth [65]. The non contacting method requires no electrical contact between probe and component and is therefore much easier to deploy than conventional acpd.

An acfm system for drillstring inspection has been developed [50] and this takes advantage of the fact that the interpretation of acfm signals can be conducted by microprocessor, without any need for any form of calibration. This has resulted in a fully automated system for the inspection of drillpipe threads which requires no operator interpretation whatsoever. The result is a system that gives reliable and repeatable results from a single scan capable of detecting the presence of any defects and measuring their length and depth.

This technique is equally applicable to the inspection of tethering-components and is likely to make a significant contribution to quantitative thread inspection. The technique can be applied to magnetic and non-magnetic components.

7.4.2.4 Flux Leakage Inspection

Flux Leakage techniques rely on the measurement of magnetic flux disturbances in the presence of a defect. Unlike the acpd/acfm techniques where known, uniform fields are applied, leakage techniques can be applied in situations where the nature of input flux (magnetic field) is unknown, indeed they can be used in residual fields.

Hall effect sensors are often used to measure the leakage flux. The technique is not generally supported by any form of modelling and hence requires prior calibration on known defects. This is often carried out on notches and represents a major disadvantage for quantitative inspection. The response from the calibration sample relies on the magnetic properties of the test piece and the geometry of the defect. If either are not exactly the same as in the component the interpretation will be in error. Since calibrations are rarely carried out on a range of defect geometries and materials, this is generally a source of concern if any interpretation of defect severity is to be made. Detection would be less of a problem but the setting of detection thresholds, based on calibration would of course introduce errors.

A semi-automated system, based on flux leakage has been developed for drillstring inspection [66] and this could be applicable to tethered connections.

7.5 INSPECTION RELIABILITY

The foregoing discussion has identified reliable inspection as a principle requirement for the "retirement for cause" approach to be adopted. This leads to a requirement for a quantification of the inspection performance of a particular system, the emphasis being on the reliability of the system, rather than the equipment alone. This section describes how inspection performance can be quantified in terms of the "Probability of Detection" for a crack of a certain size and how this statistical parameter can be used to define inspection intervals for components in service.

The performance of inspection can be expressed in terms of 'Probability of Detection' (POD) curves. These curves show how the inspection success varies with parameters such as defect size. POD curves are determined by inspecting only a sample of the total possible flawed components (the population) during trials and the predictions from the sample to population behaviour depend critically on the sample being truly representative of the nature of the population. Here the population represents any defect occurring in a component during service. The nature of the sample is therefore extremely important and is a critical factor in setting up trials. The size of the sample is also important

however, as a trial will only produce a few estimates (P) of the population POD (p). These individual values of POD (P) are based on the sample at each flaw size and are unbiased estimates of p but cannot be assumed to be equal to p. Instead it is necessary to assume that P is only one value of a range that could be measured and that all the possible values of P are spread around a mean value of p. The scatter in values of P is dependent on the sample size. Hence the prediction of p from the single estimate of P depends on the sample size. These two concepts are illustrated in Figure 7.3.

It can be seen from Figure 7.3 that the choice of a sample which is not representative of the population gives a useless answer and the trial would be valueless. Choice of sample size is simpler, as statistical analysis can be used to guide the decision but small sample sizes lead to wide confidence limits and again unusable results. Inspecting several components containing the same size defect can give additional confidence in predicted behaviour if general trend lines emerge. The nature of the sample and the choice of sample size are addressed in the following sections.

For many components subject to fatigue the basis of design is a pre-defined design life which is based on assumed service loading. For threaded components such as tethers, the service loading can to some extent be monitored and compared with prediction. In this application, in-service inspection would be used to primarily ensure either that the component was performing as designed or, that the component was not suffering damage due to parameters not considered during the design process (i.e. manufacturers defects or increased loadings).

For components such as drillpipe, the service loading is never known, and neither is the previous service history for the vast majority of components. In this case, the role of inspection is very different in that the sole purpose is to confirm the condition of the component prior to further service. Whilst different in nature, continued use of either component will be based on the result of the inspection.

7.5.1 Inspection Reliability Trials

In order therefore to establish the performance of the inspection system, trials need to be conducted on real components containing fatigue damage of the type most likely to be found in service.

These trials are conducted on a finite number of flawed components usually chosen so that a required confidence level can be established. It is impractical to consider including all features that might influence inspection performance and, for this reason one must assess the importance of various features to crack 'visibility' so that the most important can be included in the sample. It is necessary to base the sample on fatigue cracks in appropriate materials and consider the features listed below as well as the geometry of the components to be included in the sample.

Some of the features of fatigue cracks that could have an important influence on how easy it is to detect and size are as follows:

1) Crack type - i.e. surface or corner
2) Crack size (area)
3) Crack roughness
4) Presence of deposits on crack surfaces
5) Crack opening
6) Single/multiple cracking

These features are related to the microstructure and the nature of the fatigue loading (high temperature, low cycle, variable amplitude) and also to the fact that inspection will take place with the component under zero stress.

Some of these features may significantly affect inspection performance and must be included in any trials. Among these are crack type (surface or corner), crack shape, crack face corrosion (deposits), crack size and crack opening. Of all these, only crack opening can be changed during trials and it is possible that a detailed study of this important factor should be incorporated in any trial.

Surface cracks (or corner cracks) of a given length can have a variety of crack mouth openings and depths depending on the aspect ratio. The aspect ratio in each case may well be a function of the initial flaw distribution, the applied cyclic stress level and the final crack size. An inspection reliability trial should be based on a sample containing a range of aspect ratios as this is an important factor that could influence successful detection. Surface fatigue cracks are the most likely service flaw and it is essential that Inspection Reliability trials are conducted on these cracks.

The samples required for trials, and the defects contained in them need to be carefully planned and in general need to be produced specifically for that purpose. It is possible that some tethers removed from service would posses surface flaws that could be used for trials. It is however unlikely that these will be sufficient in number or will contain the appropriate range of defect sizes. Tethers with flaws should be regarded as useful supplementary specimens to complement the main sample. The sample would consist mainly of specimens with fatigue cracks introduced under controlled conditions.

Crack face corrosion influences crack closure and hence crack visibility and should be included in the sample. It can be introduced by conducting some of the precracking in corrosive fluids (hydraulic fluids or sea-water). It should not be necessary to produce the complete sample with oxidised crack surfaces and indeed would be inadvisable, for some NDT techniques might find this an advantage whereas others would not.

For trials on a thread inspection system, the crack sizes to be included need to reflect desirable aims based on economic lifing strategies and likely inspection performance. In practice, these will coincide but for the purposes of the trials, the sizes will need to range from those necessary for acceptable reuse to those approaching failure critical size. Both are a matter of conjecture in that, as discussed above, inspection intervals, design stresses and choice of material are major factors. Final decisions would be made in conjunction with designers, users and other interested authorities.

The probability of Detection Approach is described in detail in Appendix C together with some statistical aspects of the way in which trials can be organised and the effect of sample size in the resulting Probability of Detection estimates.

7.6 CONCLUSIONS

The development of commercial thread inspection systems together will Fracture Mechanics modelling of fatigue behaviour means that the retirement for cause approach to structural integrity of tethers is an available option to the operator. The implementation of such an approach will require detailed studies of the inspection system performance and the fatigue prediction methods to determine the level of confidence that can be put on them.

The fact that the tethering system is one of the most important components of the TLP means that careful consideration of uncertainties need to be made before embarking on such an approach.

However, previous trends suggest that during the life of long service components, systems improve and analysis techniques advance to the stage where subsequent complete re-analysis of existing designs are often conducted. These can lead to revisions of design life predictions and there is then pressure to verify, by practical methods, that the structure is still safe. In these situations, knowledge of fatigue behaviour and inspection capability can enable inspection schedules to be assessed and revised according to likely fatigue damage in the intervening interval.

Inspection scheduling, based on quantitative assessments of the integrity at any time during the component life is an important outcome of such an approach. As an integrated part of the retirement for cause approach, revision of inspection schedule will depend on many factors. The rate of crack growth depends on the input parameters to the fracture mechanics model and the suitability of the model itself. Of course the capability of the inspection technique to achieve the NDT target has a strong influence on the reliability of the results. These aspects were shown schematically in Figure 7.4. The work presented in this study shows that the first steps toward fracture mechanics modelling and methodology for the determination of inspection reliability have been made and that the application of retirement for cause is possible for threaded connections. Considerable work now needs to be carried out to determine the reliability of the fracture mechanics models, given the scatter in input data, together with the reliability of thread inspection systems in order to assess the true potential of the approach.

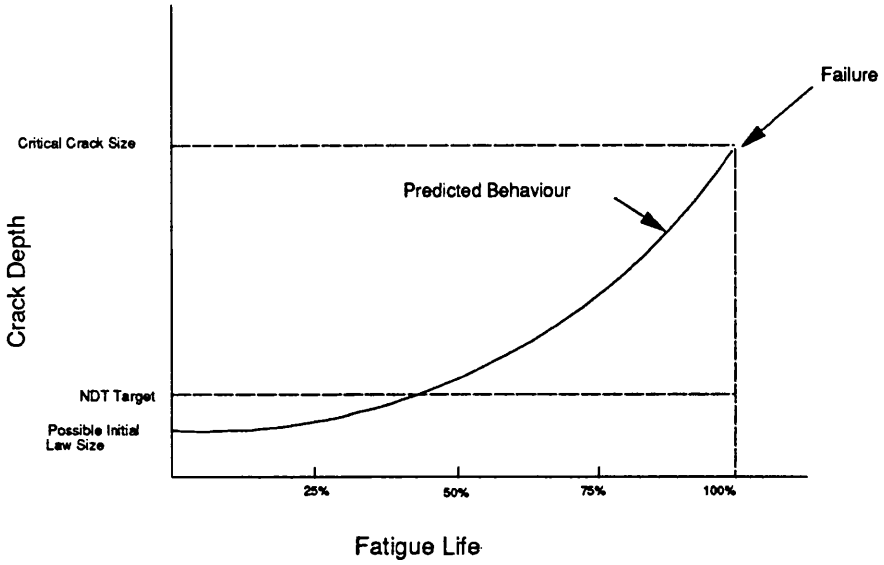

Fig 7.1 Idealised fatigue life curve for threaded connection under service loading

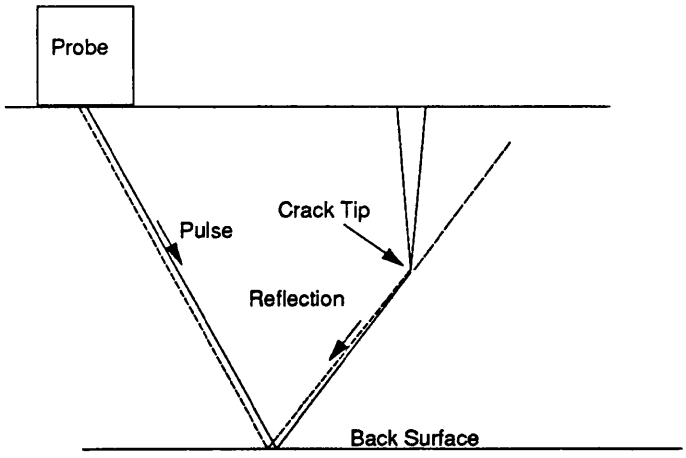

Fig7.2 Principle of pulse echo ultrasonics

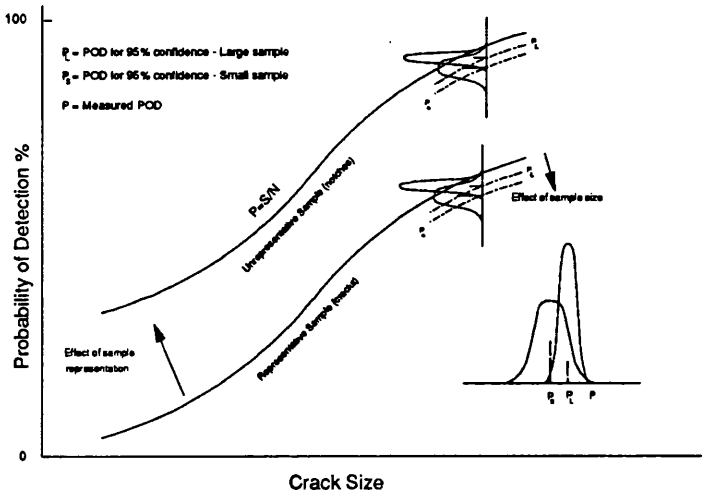

Fig 7.3 The relative effect of the nature of the sample and sample size on POD

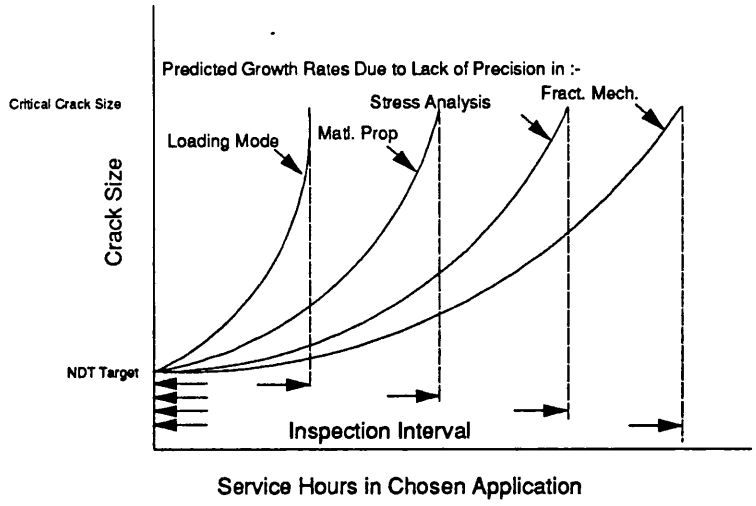

Fig.7.4 Influence of input parameters on inspection schedule

CHAPTER 8

CONCLUSIONS AND RECOMMENDATIONS

8.1 CONCLUSION

Large threaded connections are now being used to connect high integrity tethering components in Tension Leg Platforms. The safety of the platform relies totally on the integrity of the tethering system and analysis has shown that the threaded connection can be the most highly stressed section in the mooring system. For such critical structural components there is a requirement to assess, on a regular basis, the integrity of the component and this involves routine inspections. This leads to requirements for a knowledge of the type and nature of damage that may occur in such components and a subsequent confirmation that the inspection strategy is capable of detecting such damage before it becomes a risk to the platform integrity. It must be emphasised that the failure of a tether would be catastrophic since, as discussed in Chapter 2, a tethering system does not exhibit true structural redundancy, even when there are multiple tethering elements operating in parallel. For this reason, the performance of the tethering system throughout the service life of the platform is of the utmost importance.

Tethering systems are subjected to significant cyclic loading due to environmental loading both on the platform and the tether itself and as a result, fatigue is identified as a primary damage mechanism during the service life. This study considered the fatigue mechanism both in terms of crack initiation and fatigue crack propagation. Both aspects require knowledge of the cyclic and static stresses acting and material properties. Fatigue crack growth analysis involves the use of fracture mechanics which in addition requires a knowledge of the nature of the defect, its size, shape and location.

The first consideration of this study was the determination of the stresses acting in a threaded connection. Here it was evident that the analysis of stress distribution in threaded connections was extremely complex due to the highly non-linear load distribution which is a feature of all threaded connections. Chapter 2 discussed aspects of earlier work on the analysis of threads and considered methods for determining the stress distributions. These are broken down into experimental and theoretical/mathematical methods and it is concluded that all of the analysis techniques suffered drawbacks in terms of their ability to determine the dynamic stresses acting in preloaded connections. Of the methods discussed it was seen that the photo-elastic method (an experimental technique) required sophisticated modelling and specialist experimental equipment in order to predict stresses in threaded connections. Whilst being the only practical method of conducting a full 3 dimensional analysis, it was not

capable of predicting dynamic stresses for a preloaded joint from a single model and for this reason was unsuitable for use in parametric type studies where the effect of various geometric parameters required investigation.

Finite element techniques were considered in detail in Chapter 3 where it was shown that a 2D analysis could provide stress distribution in preloaded joints in a single run by using a special modelling technique developed to overcome the necessity to model preload in detail. The method adopted made modelling far simpler and avoided the need for multiple runs to determine dynamic stresses. The use of 2D analysis, effectively ignoring the helix angle was discussed in detail and considered to be acceptable bearing in mind the uncertainties inherent in a 3D photo-elastic analysis. The implications of ignoring the helix angle were considered in detail in Appendix A where it was shown that the peak stresses were likely to be underestimated by approximately 15% around the first tooth. The 2D FE modelling described in Chapter 3 was still considered prohibitive, in terms of its complexity, for general parametric purposes and for this reason our alternative analysis method was developed. This development formed a major part of the study and provided very significant advantages in terms of simplicity of use, over any other technique. The suitability of 2D linear elastic analysis was investigated and it was concluded that for the tethering situation using thick walled connectors, the assumptions are justified.

Chapter 4 described in detail the development of a simplified model to allow the prediction of load distribution in both preloaded and unpreloaded connections. The tooth loads were then used in conjunction with a simple FE model to determine thread root stresses. The model, the results from which compared well with FE, mathematical and photo-elastic results, allowed rapid analysis of a whole range of connection geometries and allowed the effect of geometric parameters to be studied. The work also clearly indicated the advantages of preloading threaded connections.

The effect of connector size, preload, thread form are all discussed in Chapter 4. The work concluded that for a preloaded connection, the section at the first loaded tooth of the box is critical in most situations from a fatigue stand point. It also shows however that if a preloaded connection is not properly preloaded, the first loaded tooth of the pin can become critical. Thus preload is seen to have a very significant effect on the behaviour of a threaded connection. It is concluded that whilst the effect of preload is so important,

it is not possible to determine, with any degree of confidence, the amount of preload introduced into a connection. This must be a point of major concern for the designer and users of threaded connections for TLP applications.

The stress analysis conducted in Chapters 3 and 4 was used as input into fatigue models described in Chapter 6. Chapter 6 considers the use of fatigue initiation analysis, based on the results of tests on small samples of material, and concludes that the results require treating with caution due principally to two effects. The first is the effect of mean stress which has a strong influence on the fatigue initiation life and which, due to the uncertainties in preload level can vary considerably in practice. The second effect is that of surface finish at the thread root. Fatigue initiation data is generally gathered from smooth specimens tested under cyclic loading and it is assumed that, for a notched component, the root of the notch is smooth like the test specimen. In practice, many types of large thread are produced by cutting processes which lead to machining marks (circumferential defects). These lead to local stress raisers and a consequent reduction in fatigue initiation life compared to that predicted.

The fatigue and growth analysis investigates the use of Fracture Mechanics modelling to predict the fatigue crack growth behaviour. The modelling was based on a simplified analysis using flat plate solution and a solution for crack growth in a circumferentially notched bar. The flat plate analysis was considered appropriate for early crack growth whilst the circumferentially notched bar solution was appropriate for cracks away from the highly stressed thread root. Experimental crack growth data obtained from the results of monitoring crack growth in large scale laboratory fatigue tests provided information for the prediction of experimental values of Stress Intensity Factors. These were compared with those predicted from theory and there was seen to be reasonable agreement. It was considered however that the simple theoretical modelling could perhaps be refined. A larger database of experimental data would be required for a more complete validation. However, the results do highlight the benefit of experimental data for fatigue crack growth.

The large scale tests, described in Chapter 5, were unique in that they provided data on crack development using non-destructive testing methods, rather than simply providing fatigue life. This was made possible by the development of a thread inspection system based on the alternating current potential drop (acpd) technique. Despite the fact that the test was complicated by the need to regularly inspect the threads, the benefits were significant in that the tests provided information on the crack development behaviour in

threaded connections subjected to fatigue loading. The experimental data also revealed the way in which failure mechanisms vary between different designs of connection. The thick walled connection failed by final fracture from a surface crack and gave no prior indication of impending failure whereas a thin walled connection failed by through wall penetration which resulted in significant deflection, early visible, and of course a "leak before break" situation. These points are discussed in detail in Chapter 5 and are important considerations when considering the suitability of different connection types for tethering applications.

The fatigue studies, both experimental and theoretical, indicated that the fatigue crack growth characteristics of thick walled tethers shows a large proportion of the total fatigue life is occupied by fatigue crack growth. This means that such a system is crack tolerant and indicates that the presence of a defect would not necessarily mean the component is in danger of failing. The requirements for routine inspection to confirm the integrity of the component should therefore take this into account. For any component, susceptible to fatigue damage, the inspection requirement in terms of frequency of inspection and sensitivity of the equipment should be related to the fatigue behaviour of the component under service loading.

In its simplest form this means that if the time interval between a crack initiating and final failure is short then the inspection interval must be considerably shorter and the inspection system must be extremely sensitive to ensure that any defects are found. It is therefore seen that for most critical structural components a knowledge of fatigue behaviour must be complemented by an understanding of the inspection process. Chapter 7 describes such a methodology and Appendix C describes how an inspection system can be evaluated to determine its true capabilities.

This study has therefore investigated the concepts of structural integrity for a critical structural component, the threaded tether connection. The study highlighted several areas that necessitated the development of new techniques including a solution to the difficulties of predicting cyclic stresses in threaded connections and the development of large scale testing techniques to enable fatigue crack growth data to be collected. The development of a simplified model for the prediction of dynamic stress in threads enables very rapid modelling of different geometric parameters and in particular enabled an extensive study to be carried out into the effect of preload and the preload mechanism.

These developments have recently been applied to industrial situations where fatigue studies [40] are being complemented by inspection system development [50] in an effort to reduce the incidence of failure in the threaded connections of drillstrings.

The next Section discusses recommendation for extending this work to allow the same approach to be extended to a broader range of applications.

8.2 RECOMMENDATIONS FOR FURTHER WORK

The analysis techniques developed here have addressed the elastic analysis of threaded connections under axial loading. In order that the methodologies can be extended to other applications, where the loadings could include bending and torsional loading, it is recommended that the simplified model for load analysis be extended to accommodate these additional modes of loading. Some ideas on how this could be achieved are included in Chapter 4.

The fracture mechanics modelling described in Chapter 6 would benefit from experimental data in order to assess its suitability over a range of geometries. The fracture mechanics models used here have been derived from simplified solutions and it is recommended that some of the more advanced methods for determining stress intensity factor, such as the weight function approach [67] be considered for use with threaded connections. There is also a need for models to be considered for the box member.

Threaded connections generally rely on the use of preload and it is a major weakness that preload levels cannot be verified in a torqued connection. It is recommended that this problem be considered since it would have not only a significant effect on the reliability of threaded connections but could have very significant commercial potential as an in-service monitoring technique.

Finally advances in the hardware available for FE analysis have been significant in recent years. This means that the FE technique would be able to be used for more complex analyses without the time/computing constraints experienced in this study. These advances could make possible the use of FE techniques for elastic/plastic analysis and FM analysis by the use of crack tip elements. These would likely still be constrained to 2D analysis for most situations but would have significant benefits if the design of threaded connections lead to either large displacements or the development of plastic deformation.

APPENDIX A

SOPWITH'S ANALYSIS

of

LOAD DISTRIBUTION IN THREADS

1 INTRODUCTION

This Section shows how the work of Sopwith [2] can be used to determine the tooth load distribution in a threaded coupling (turnbuckle). Whilst the analysis was derived primarily for a nut and bolt connection, it can be applied to a tension - tension connector like a trunbuckle or indeed an offshore tether connection. It must be noted that the analysis as presented does not consider preload or tapering sections. This is a serious drawback since, as discussed in Chapter 4, many threaded connectors depend on the preload mechanism and body tapers for fatigue resistance.

2 ANALYSIS

The tooth load distribution is dependent on the relative displacements of the two components.

Using Sopwith's notation:

Pitch	=	a
Pin area	=	A_1
Box area	=	A_2
Mean thread diameter	=	D
w_m	=	Mean tooth load/unit length
w	=	Tooth load/unit length at any point
x	=	Proportion of length of thread from free end
L	=	Length of thread engagement
k	=	$\frac{A_1}{A_1+A_2}$

The distribution of load is given as

$$\frac{w}{w_m} = \frac{\theta_1}{\sinh\theta_1}[(1-k)\cosh x\theta_1 + k\cosh(1-x)\theta_1] \qquad \text{A1}$$

The function θ_1 is derived from:-

$$\theta_1^2 = \frac{\pi D L^2}{a(h_1+h_2+k_1+k_2)}\left(\frac{1}{A_1}+\frac{1}{A_2}\right) \qquad \text{A2}$$

Now h_1, h_2, k_1 k_2 are defined as deflection co-efficients and refer to the axial separation of the mating teeth of the pin and box.

Sopwith considered primarily 'V' threads which deflect and deform as shown in Figure A1. In the case of a buttress thread, radial separation is small and hence the only deflection is that due to tooth bending (and shear).

In equation A2, the function h_1 and h_2 refer to the bending deflection of the contact point of the two teeth and k_1, k_2 refer to the axial deflection (Referred to as recession factors). For a buttress thread one needs only to consider the tip deflection, Figure A2.

For a buttress thread, equation A2 reduces to

$$\theta_1 = L\sqrt{\frac{\pi D}{ah}\left(\frac{1}{A_1}+\frac{1}{A_2}\right)}$$

which can be written $\theta_1 = mL$

Expanding $\cosh(1-x)\theta_1 = \cosh\theta_1 \cosh x\theta_1 - \sinh\theta_1 \sinh x\theta_1$

and putting into equations A1 gives

$$\frac{w}{w_m} = \frac{\theta_1}{\sinh\theta_1}[(1-k)\cosh x\theta_1 + k(\cosh\theta_1 \cosh x\theta_1 - \sinh\theta_1 \sinh x\theta_1)]$$

$$= \frac{\theta_1}{\sinh\theta_1}[\cosh x\theta_1(1-k+k\cosh\theta_1) - k\sinh\theta_1 \sinh x\theta_2$$

$$= \theta_1 k\left[\left(\frac{\frac{1}{k}-1+\cosh\theta_1}{\sinh\theta_1}\right) - \sinh x\theta_1\right] \qquad \text{A3}$$

Now $$k = \frac{A_1}{A_1+A_2} \qquad \text{A4}$$

$$\frac{w}{w_m} = \frac{\theta_1 A_1}{A_1+A_2}\left[\left(\frac{A_1+A_2}{A_1} - 1 + \cosh\theta_1\right)\frac{\cosh x\theta_1}{\sinh\theta_1} - \sinh x\theta_1\right]$$

$$\frac{w}{w_m} = \frac{\theta_1 A_1}{A_1+A_2}\left[\frac{(A_2+A_1\cosh\theta_1)\cosh x\theta_1}{A_1\sinh\theta_1} - \sinh x\theta_1\right] \qquad \text{A5}$$

Now w_m is the mean load on the thread.
For an applied load P

$$w_m = \frac{P}{\left(\frac{\pi DL}{a}\right)}$$

and writing $\theta_1 = mL$ equation A5 yields

$$w = \frac{Pma}{\pi D}\frac{A_1}{A_1+A_2}\left[\frac{(A_2+A_1\cosh mL)}{A_1\sinh mL}\cosh mZ - \sinh mZ\right] \qquad \text{A6}$$

where Z is the distance measured along the thread axis to the point of interest and

$$m = \sqrt{\frac{\pi D}{ah}\left(\frac{1}{A_1}+\frac{1}{A_2}\right)} = \sqrt{\frac{\pi D}{ah}\left(\frac{A_1+A_2}{A_1A_2}\right)}$$

It is seen that the only unknown becomes the tip deflection factor h.

Tip deflection $\delta = \frac{hw}{E}$

Consider the tooth as a cantilever as shown in Figure A3.

Using beam theory and assuming a udl, tip deflection $\delta = \frac{Wl^3}{8EI}$

where W is the total applied load.

Considering unit width,

$$W = w \quad \text{(from equation A6)}$$

$$I = \frac{1(d)^3}{12}$$

$$\delta = \frac{3w}{2E}(l/d)^3 = \frac{hw}{E}$$

$$\text{hence } h = 1.5(l/d)^3 \qquad \text{A7}$$

Now this does assume elastic beam theory. In practice, as detailed in Appendix B, this does not apply and a factor must be used to modify this to allow for shear.

The analysis using Stress Functions as described in Appendix B allows the tip deflection of any shape beam to be determined.

3 CALCULATION OF LOAD AT ANY SECTION

Equation A6 allows the load per unit length at any point on the helix to be calculated. The total load transferred by any part of the thread can be obtained by integrating the load per unit length over that part, thus it can be seen that this analysis can be used to calculate the load at any section since, for conditions of no preload, the load transferred by the thread represents the total load in the section. Referring to Figure A4, the total load transferred by the thread between sections AA and BB represents the load in the ***pin*** at section AA.

Equation A6 gave, for a unit width,

$$W = \frac{ma}{\pi D}\frac{PA_1}{A_1+A_2}\left[\frac{(A_2+A_1\cosh mL)\cosh mZ}{A_1\sinh mL} - \sinh mZ\right] \qquad \text{A8}$$

Noting that Z can be expressed in terms of s since

$$s = \frac{\pi D Z}{a}$$

Thus $$\int \cosh mZ\, ds = \left(\frac{ma}{\pi D}\right)^{-1}\sinh mZ$$

$$\int w ds = \frac{PA_1}{A_1+A_2}\left[\frac{(A_2+A_1\cosh mL)}{A_1\sinh mL}\sinh mZ - \cosh mZ + K\right] \qquad \text{A9}$$

Use boundary conditions to determine K

Putting Z = L gives

$$\int w = \frac{PA_1}{A_1+A_2}\left[\frac{(A_2+A_1)}{A_1}\cosh mL - \cosh mL + K\right] \qquad \text{A10}$$

$$P = \frac{PA_1}{A_1+A_2}\left[\frac{A_2}{A_1}+K\right]$$

$$\frac{A_1+A_2}{A_1} = \frac{A_2}{A_1}+K$$

$$K = \frac{A_1+A_2}{A_1} - \frac{A_2}{A_1} = 1$$

When $Z=0, \int w = 0$ this is correct since this is the free end of the pin.

Now, from A9, between Z = 0 and Z = S

$$\Sigma w = \frac{PA_1}{A_1+A_2}\left[\frac{(A_2+A_1\cosh mL)}{A_1\sinh mL}\sinh mZ - \cosh mZ + 1\right] \qquad \text{A11}$$

Now Σw, as defined, would be the ***box*** load. The pin load is therefore given as:-

$$P_s = P - \frac{PA_1}{A_1+A_2}\left[\frac{(A_2+A_1\cosh mL)}{A_1\sinh mL}\sinh mZ - \cosh mZ + 1\right]$$

$$= P\left(1-\frac{A_1}{A_1+A_2}\right)+P\left(\frac{A_1}{A_1+A_2}\right)\left[-\frac{(A_2+A_1\cosh mL)}{A_1\sinh mL}\sinh mZ+\cosh mZ\right]$$

$$= P\left(\frac{A_2}{A_1+A_2}\right)+P\left(\frac{A_1}{A_1+A_2}\right)\left[-\frac{(A_2+A_1\cosh mL)}{A_1\sinh mL}\sinh mZ+\cosh mZ\right]$$

$$= P\left(\frac{A_1}{A_1+A_2}\right)\left[-\frac{(A_2+A_1\cosh mL)}{A_1\sinh mL}\sinh mZ+\cosh mZ+\frac{A_2}{A_1}\right] \qquad \text{A12}$$

Equation A12 therefore gives the distribution of Box load along the thread.

4 COMPARISON OF RESULTS WITH HYBRID MODEL DESCRIBED IN CHAPTER 4

This analysis was used to compare the results from the analysis by Sopwith as modified above to those from the model proposed in Chapter 4. Note that it is only possible to compare non-preloaded joints and for parallel threads.

The comparison was conducted for a simple threaded connection of the following dimensions

Pin ID	=	25mm
Pin OD	=	50mm
Box ID	=	54mm
Box OD	=	70mm
Tooth Depth	=	2.0mm
Pitch	=	4.0mm
Number of Teeth	=	10

The tooth is of rectangular cross section 2mm x 2mm. Equation A8 enables h to be calculated using beam theory. However, Appendix B shows that this is not appropriate for such a cross section. When calculated using the analysis in Appendix B, it is seen that the tip deflection due to shear plus bending is in fact a factor of 2.83 greater than if only bending is considered. It is therefore necessary to modify equation A8 to give, for this thread,

$$h = 2.83 \times 1.5\ (1)^3 = 4.25$$

This calculated value of h had been used in the analysis. The results are presented in Table A1. These are presented graphically in Figure A5.

It is also possible to investigate the distribution of load around the helix using this extension of Sopwith's analysis Figures A6 and A7 show the variation in tooth load per unit length around the first and last teeth in the coupling respectively.

5 DISCUSSION OF RESULTS

This comparison of the 2D and 3D analyses indicates the excellent agreement on averaged tooth loads, again indicating the merits of the 2D analysis together with a justification of the assumptions made. It must be noted that the extended Sopwith analysis discussed here is very limited in that it cannot accommodate tapering sections or preload. These are serious limitations which do not affect the Hybrid model.

The variation in tooth load around the circumference indicates the magnitude of the likely errors associated with the 2D analysis to be in the order of 15% if the load is averaged around each circumference. The error is not large considering the benfits in ease of use and flexibility allowed by choosing a 2D analysis but must of course be considered when reviewing 2D results.

	Percentage of Total Load	
Tooth No.	**Hybrid Model**	**Modified Sopwith**
1	14.92	15.13
2	11.27	11.31
3	8.84	8.80
4	7.38	7.27
5	6.71	6.59
6	6.76	6.64
7	7.55	7.45
8	9.16	9.12
9	11.76	11.82
10	15.64	15.87

Table A1 Comparison of average tooth loads from the 2 Models

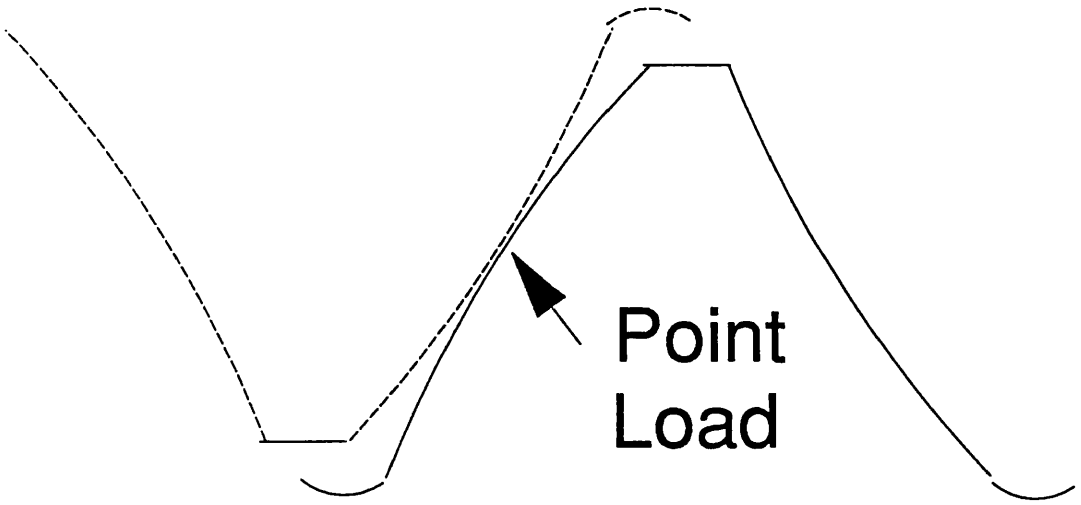

Fig.A1 Deformation of nut and bolt under load (After Sopwith)

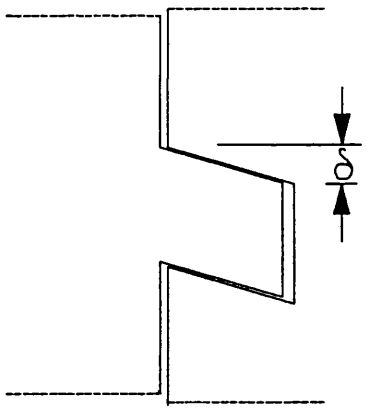

Fig. A2 Tip deflection of buttress thread

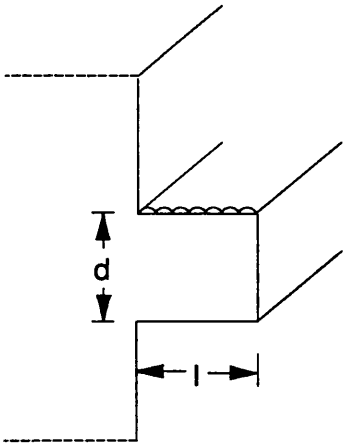

Fig. A3 Representation of buttress thread as a cantilever.

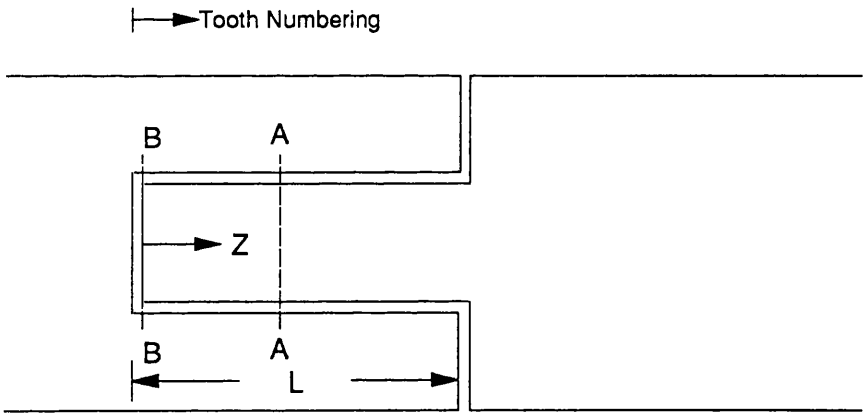

Fig. A4 Notation used in analysis

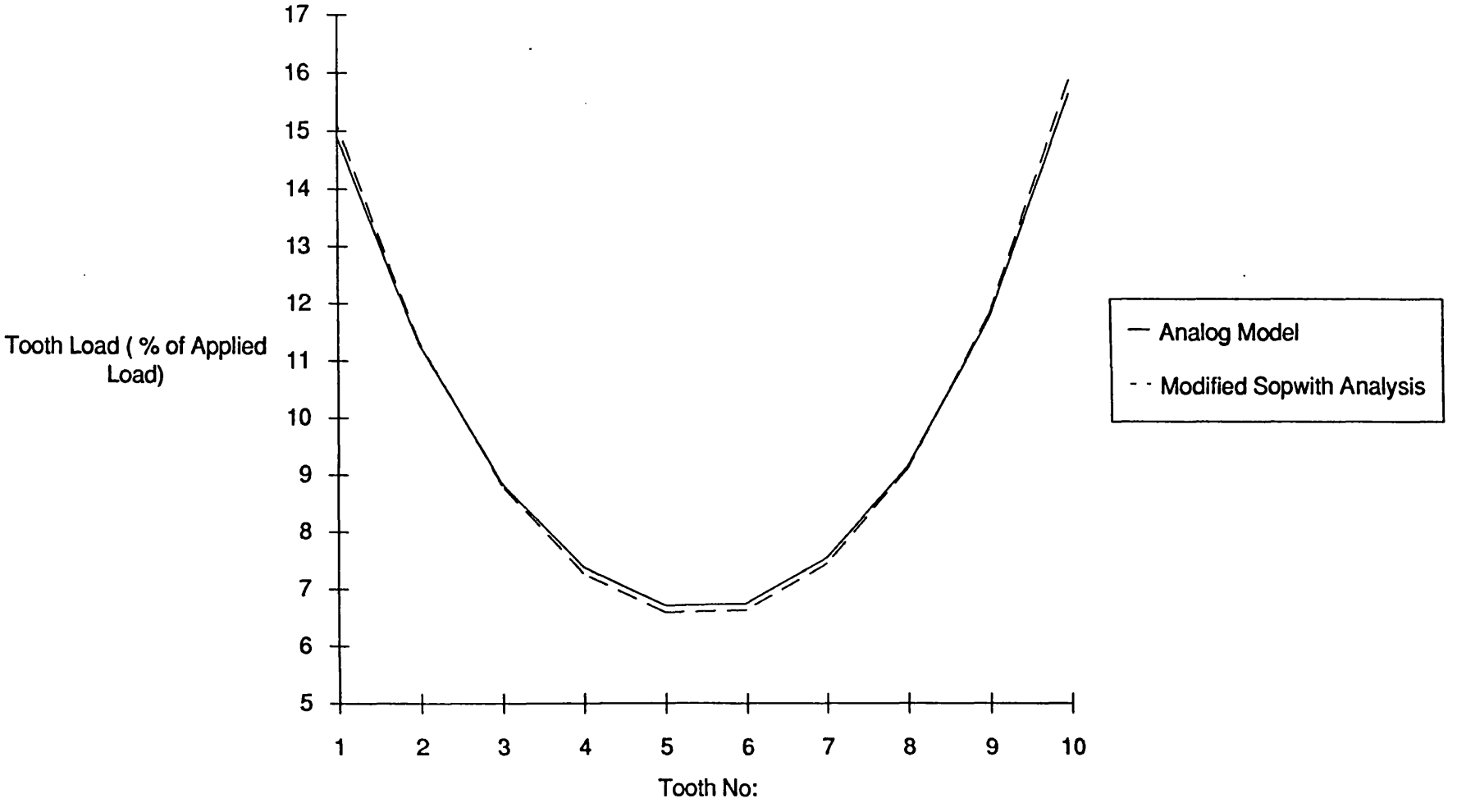

Figure A5. Comparison of Averaged tooth load from different models.

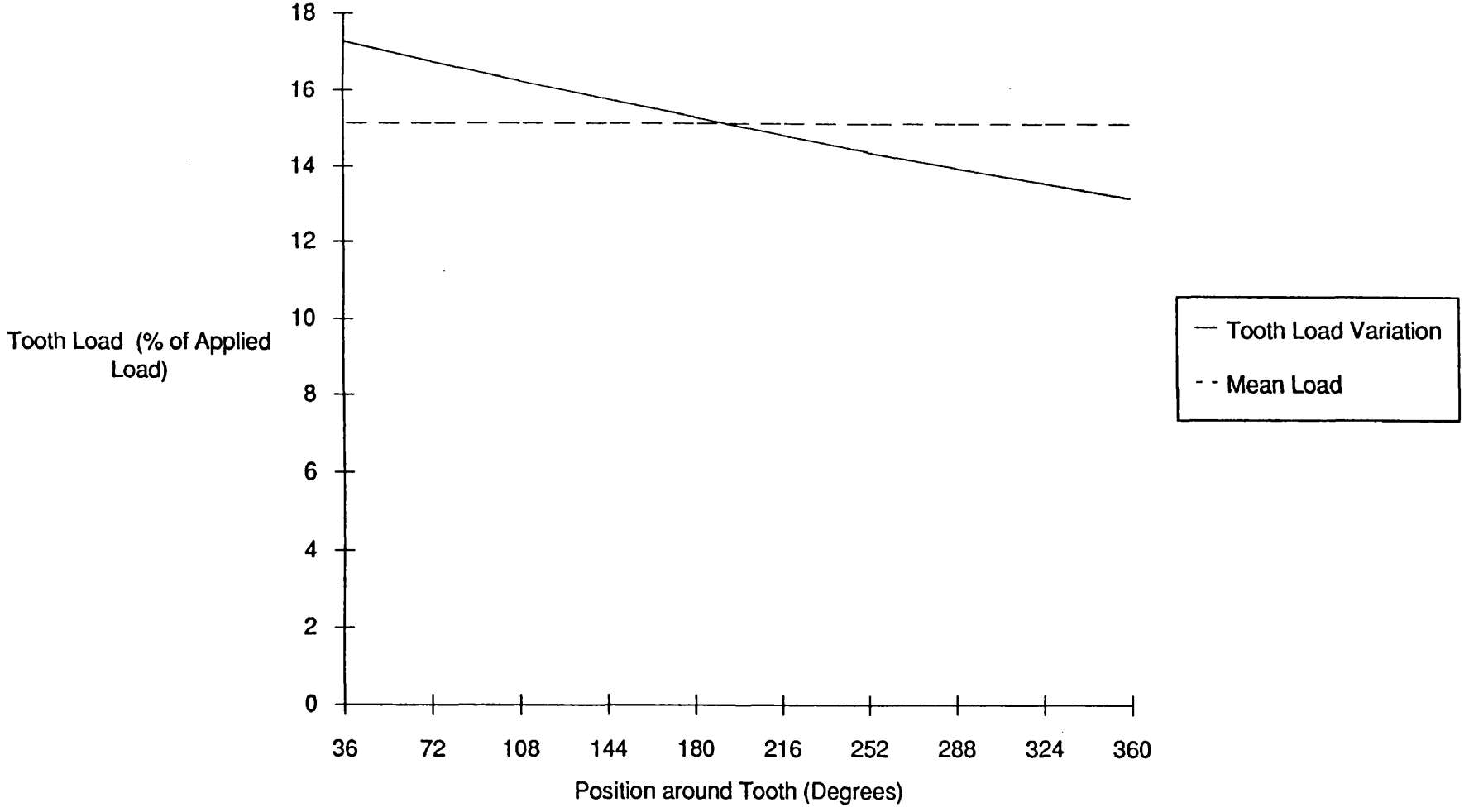

Figure A6 Distribution of tooth load around tooth No. 1

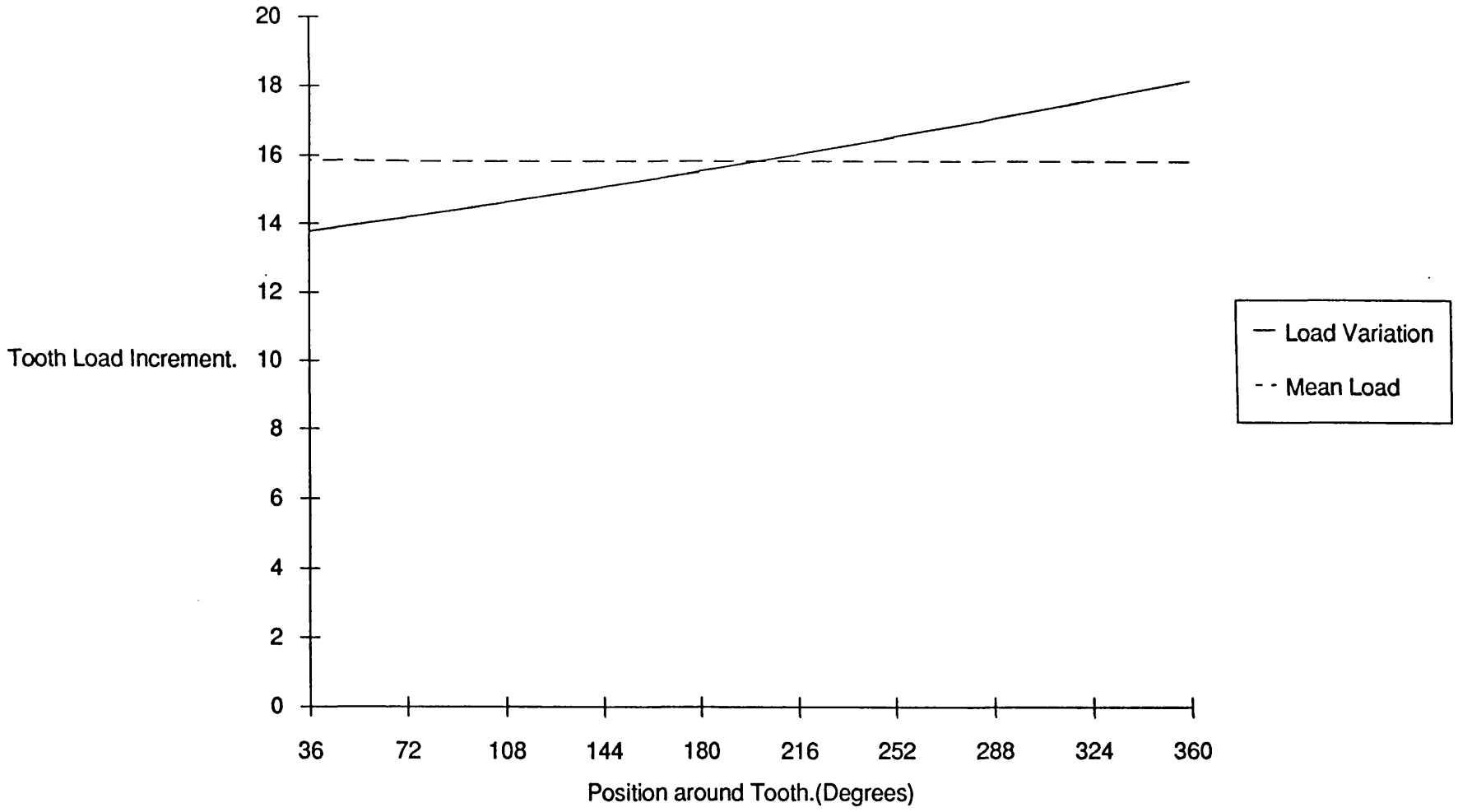

Figure A7.Variation in tooth load around tooth No.10

APPENDIX B

STRESS AND DEFLECTION OF A STUBBY CANTILEVER

1 INTRODUCTION

Engineering beam theory provides for the calculation of stresses and deflection for "simple" beams. The simplified equations which are based on bending theory are adequate for most structural applications but are not suitable in cases where the predominant loading does not result in bending deflections. For short deep beams, significant shear deformations can develop and these will not be accounted for in the simple theories. In addition, lateral restraint can lead to plain strain situation again not accounted for by simple beam theory.

When considering the deflection of thread teeth, beam theory is not appropriate and more rigourous approaches are necessary for correct modelling of the deflections and stresses.

One method of analysis involves the use of Airey stress functions [68].

2 BEAM ANALYSIS USING AIREY STRESS FUNCTIONS

The use of stress functions is well documented in the solution of stress analysis problems. This method depends on the choice of a suitable stress function ψ which can then be used to define the basic stress state of that structure in terms of the chosen function. The stress and strain state can then be used to predict deflection from the unloaded state.

Basic Principles

The stress in any direction can be defined using the stress function ψ as follows:-

$$\sigma_x = \frac{\delta^2\psi}{\delta y^2} \qquad \sigma_y = \frac{\delta^2\psi}{\delta x^2} \qquad \tau_{xy} = \frac{-\delta^2\psi}{\delta x \delta y}$$

Consider now the "stubby beam as shown in Figure B1. This could represent a section of buttress thread of rectangular cross section. The analysis of such a component is a plain strain problem and the strain relationships are:-

$$\varepsilon_x = \frac{1+\nu}{\varepsilon}[(1-\nu)\sigma_x - \nu\sigma_y]$$

$$\varepsilon_y = \frac{1+\nu}{\varepsilon}[(1-\nu)\sigma_y - \nu\sigma_x]$$

$$\gamma_{xy} = 2\frac{(1+\nu)}{\varepsilon}\tau_{xy}$$

This assumes $\varepsilon_z = 0$

For such a problem, a suitable stress function could be:-

$$\psi = -px^2\left(\frac{y^3}{d^3}-\frac{3y}{4d}+\frac{1}{4}\right) + \frac{pd^2}{5}\left(\frac{y^5}{d^5}-\frac{y^3}{2d^3}\right) + c_1x+c_2y+c_3 \qquad (1)$$

Such a function will be used to assess the problem of a stubby cantilever
Differentiating equation 1 twice:-

$$\frac{\delta^2\psi}{\delta y^2} = \sigma_x = -px^2\left(\frac{6y}{d^3}\right) + pd^5\left(\frac{20y^3}{d^5} - \frac{6y}{2d^3}\right) \qquad (2)$$

$$\frac{\delta^2\psi}{\delta x^2} = \sigma_y = -2p\left(\frac{y^3}{d^3} - \frac{3y}{4d} + \frac{1}{4}\right) \qquad (3)$$

$$\frac{\delta^2\psi}{\delta x\delta y} = \tau_{xy} = -\frac{\delta}{\delta x}\left(-px^2\left[\frac{3y^2}{d^3} - \frac{3}{4d}\right] + f(y) + c_2\right)$$

$$\tau_{xy} = 2px\left(\frac{3y^2}{d^3} - \frac{3}{4d}\right) \qquad (4)$$

Now $\varepsilon_x = \frac{1+\nu}{E}[(1-\nu)\sigma_x-\nu\sigma_y]$

Also $\varepsilon_x = \frac{\delta u}{\delta x}$

Hence $u = \int \varepsilon_x \delta x$

$$u = \frac{1+\nu}{E}\left[(1-\nu)\int\sigma_x\delta x - \nu\int\sigma_y\delta x\right] \qquad (5)$$

Integrating equation 2 and 3 gives

$$\int\sigma_x\delta x = -\frac{px^3}{3}\left(\frac{6y}{d^3}\right) + \frac{pd^2x}{5}\left(\frac{20y^3}{d^5} - \frac{6y}{2d^3}\right)+g_1(y)+k_1 \qquad (6)$$

$$\int\sigma_y\delta x = -2px\left(\frac{y^3}{d^3} - \frac{3y}{4d} + \frac{1}{4}\right) + g_2(y) + k_2 \qquad (7)$$

Substituting into equation 5 gives

$$u=\frac{1+\nu}{E}\left[(1-\nu)\left(-px^3\left(\frac{2y}{d^3}\right)+\frac{pd^2x}{5}\left(\frac{20y^3}{d^5}-\frac{6y}{2d^3}\right)\right)+2px\nu\left(\frac{y^3}{d^3}-\frac{3y}{4d}+\frac{1}{4}\right)\right]+F_1(y)+K_1 \tag{8}$$

Differentiating equation 8 with respect to y gives

$$\frac{du}{dy}=\frac{1+\nu}{E}\left[(1-\nu)\left(-\frac{2px^3}{d^3}+\frac{pd^2x}{5}\left(\frac{60y^2}{d^5}-\frac{6}{2d^3}\right)\right)+2px\nu\left(\frac{3y^2}{d^3}-\frac{3}{4d}\right)\right]+\frac{dF_1(y)}{dy} \tag{9}$$

Similarly for v:-

$$\varepsilon_y=\frac{1+\nu}{E}[(1-\nu)\sigma_y-\nu\sigma_x]=\frac{\delta v}{\delta y}$$

$$v=\frac{1+\nu}{E}\left[(1-\nu)\left[-2p\left(\frac{y^4}{4d^3}-\frac{3y^2}{8d}+\frac{y}{4}\right)\right]-\nu\left[-px^2\left(\frac{6y^2}{2d^3}\right)+\frac{pd^2}{5}\left(\frac{5y^4}{d^5}-\frac{6y^2}{4d^3}\right)\right]\right]+F_2(x)+K_2 \tag{10}$$

Differentiate with respect to x gives

$$\frac{dv}{dx} = \frac{1+\nu}{E}\left[2p\nu x\left(\frac{3y^2}{d^3}\right)\right] + \frac{dF_2(x)}{dx} \tag{11}$$

Considering now the shear strains,

$$\gamma_{xy} = 2\left(\frac{1+\nu}{E}\right)\tau_{xy}$$

Also $\gamma_{xy} = \frac{du}{dy}+\frac{dv}{dx}$

From equations 9 and 11 we get

$$\frac{du}{dy}+\frac{dv}{dx}=\left(\frac{1+\nu}{E}\right)\left[-\frac{2px^3}{d^3}+\frac{pd^2x}{5}\left(\frac{60y^3}{d^5}-\frac{3}{d^3}\right)+\nu\left[\frac{2px^3}{d^3}-\frac{9px}{10d}\right]\right]+\frac{dF_1(y)}{dy}+\frac{dF_2(x)}{dx} \tag{12}$$

$$\text{Also}\quad 2\left(\frac{1+\nu}{E}\right)\tau_{xy} \;=\; \left(\frac{1+\nu}{E}\right)\left[4px\left(\frac{3y^2}{d^3}\;-\;\frac{3}{4d}\right)\right] \tag{13}$$

Equating equations 12 and 13 gives

$$\frac{dF_1(y)}{dy} \;=\; \left(\frac{1+\nu}{E}\right)\left[(1+\nu)\left(\frac{2px^3}{d^3}-\frac{9px}{10d}\right)-\frac{3px}{2d}\right]-\frac{dF_2(x)}{dx}$$

or:- $f(y) \;=\; f(x)$

Note:

A differential of a function of x $f(x)$ is still a function of x or a constant. In the above expression we have $f(x) = f(y)$ for all values of x and y. For this to be true, both $f(x)$ and $f(y)$ must be equal and constant.

Hence $f(x)=f(y)=\alpha$ where α is a constant

where

$$\alpha \;=\; \frac{1+\nu}{E}\left[(1-\nu)\left(\frac{2px^3}{d^3}\;-\;\frac{9px}{10d}\right)\;-\;\frac{3px}{2d}\right]\;-\;\frac{dF_2(x)}{dx} \tag{14}$$

Integrating equation 14 with respect to x gives

$$\alpha x+\beta=\frac{1+\nu}{E}\left[(1-\nu)\left(\frac{2px^4}{4d^3}-\frac{9px^2}{20d}\right)-\frac{3px^2}{4d}\right]-F_2(x)$$

$$F_2(x)=\frac{1+\nu}{E}\left[(1-\nu)\left(\frac{2px^4}{4d^3}-\frac{9px^2}{20d}\right)-\frac{3px^2}{4d}\right]-(\alpha x+\beta) \tag{15}$$

Substituting for $F_2(x)$ in equation 10 gives

$$v=\frac{1+\nu}{E}\left[(1-\nu)\left[-2p\left(\frac{y^4}{4d^3}-\frac{3y^2}{8d}+\frac{y}{4}\right)\right]-\nu\left[-px^2\left(\frac{6y^2}{2d^3}\right)+\frac{pd^2}{5}\left(\frac{5y^4}{d^5}-\frac{6y^2}{4d^3}\right)\right]+(1-\nu)\left(\frac{2px^4}{4d^3}-\frac{9px^2}{20d}\right)\frac{3px^2}{4d}\right]-(\alpha x+\beta_1) \tag{16}$$

Noting that when $x = l$ and $y = 0$, $v = 0$

Substituting equation 15 into equation 10 and considering the above boundary condition gives

$$v_0 = \frac{1+\nu}{E}\left[(1-\nu)\left(\frac{2pl^4}{4d^3} - \frac{9pl^2}{20d}\right) - \frac{3pl^2}{4d}\right] - (\alpha l + \beta_1) = 0 \qquad (17)$$

A second boundary condition exists where

$$\frac{du}{dy} = 0 \quad \text{when} \quad x = l, \quad y = 0$$

Hence

$$\frac{dF_1(y)}{dy} = \frac{1+\nu}{E}\left[(1-\nu)\left(\frac{2pl^3}{d^3} + \frac{3pl}{5d}\right) + \frac{3\nu pl}{2d}\right] = \alpha \qquad (18)$$

Substituting for α in equation 16 gives

$$\beta_1 = \frac{1+\nu}{E}\left[(1-\nu)\left(\frac{2pl}{4d^3} - \frac{9pl^2}{20d} - \frac{2pl^4}{d^3} - \frac{3pl^2}{5d}\right) - \frac{3pl^2}{4d} - \frac{3\nu pl^2}{2d}\right] \qquad (19)$$

Substituting for α and β_1 in equation 16 gives

$$v = p\frac{(1-\nu)}{E}\left[(1-\nu)\left[\left(\frac{-y^4}{2d^3}+\frac{3y^2}{4d}-\frac{y}{2}\right)+\frac{x^4-l^4}{2d^3}-\frac{9(x^2-l^2)}{20d}-\frac{2l^3(x-1)}{d^3}-\frac{3l}{5d}(x-l)\right]+\nu\left[\frac{3x^2y^2}{d^3}-\frac{y^4}{d^3}+\frac{3y^2}{10d}-\frac{3lx}{2d}+\frac{3l^2}{2d}\right]-\frac{3}{4d}(x^2-l^2)\right] \qquad (20)$$

Where v is the vertical deflection of the beam.

Comparisons can now be made with beam theory

Equation 3 gave

$$\sigma y = -2p\left(\frac{y^3}{d^3} - \frac{3y}{4d} + \frac{1}{4}\right)$$

At $y = \frac{-d}{2}$ $\sigma_y = -p$ (Top surface)

At $y = \frac{d}{2}$ $\sigma_y = 0$ (Bottom surface)

These are consistent with what would be expected

Equation 2 gave

$$\sigma_x = -px^2\left(\frac{6y}{d^3}\right) + pd^5\left(\frac{20y^3}{d^5} - \frac{6y}{2d^3}\right)$$

For $\frac{x}{d} \gg \frac{y}{d}$

$$\sigma_x \approx -px^2\left(\frac{6y}{d^3}\right)$$

For a simple beam of unit width,

$$M = \frac{px^2}{2}, \quad Z = \frac{d^3}{12y}$$

$$\sigma_x = \frac{6pyx^2}{d^3}$$

This shows good agreement

Tip Deflection

Putting $x = 0, y = 0$ into equation gives

$$v = p\left(\frac{1+\nu}{E}\right)\left\{(1-\nu)\left(\frac{3l^4}{2d^3} + \frac{21l^2}{20d}\right) + \nu\left(\frac{3l^2}{2d}\right) + \frac{3l^2}{4d}\right\}$$

For large $\frac{l}{d}$ $\left(\text{i.e}\left(\frac{l}{d}\right)^3 \gg \frac{l}{d}\right)$

$$v = \frac{p}{E}(1-\nu^2)\frac{3l^4}{2d^3}$$

For a cantilever, (unit width)

$$\delta = \frac{wl^4}{8EI}, \quad I = \frac{d^3}{12}$$

$$\delta = \frac{3wl^4}{2Ed^3}$$

Again this shows good agreement.

This analysis is general and shows that for long beams, the solutions agree with those for beam theory. The solutions for tip deflection have been used in Chapter 4 to calculate theoretical tooth stiffness for input into the mathematical model.

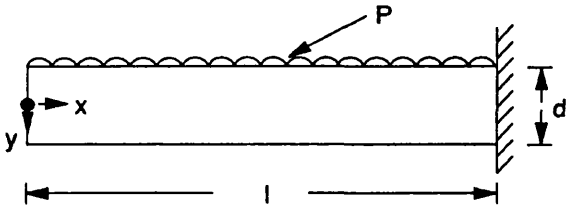

Fig.B1 General arrangement of beam model.

Special notation used in this Appendix.

d	Depth of beam
p	uniform pressure
u	Horizontal deflection
v	Vertical deflection
w	Force per unit length.

APPENDIX C

USE OF INSPECTION TRIALS FOR THE EVALUATION OF INSPECTION PERFORMANCE

1 INTRODUCTION TO PROBABILITY OF DETECTION

Any form of inspection will have associated with it an uncertainty regarding whether it will be successful. For crack detection using NDT this had led to the development of the concept of a Probability of Detection (POD) which can be defined, depending on the nature of the validation undertaken, with a certain confidence level.

NDT for cracks generally involves some form of sensor that can detect defective regions in an otherwise perfect or acceptable structure. The sensor could for instance measure a magnetic or electrical field perturbation around a defect but it could equally be simply monitoring emissions from the defect or changes in the behaviour of the whole component or specimen due to the presence of a defect. In many cases this means that the inspection task gets easier as the relative size of the flaw to the component, or the absolute size, gets larger. Under these circumstances it is customary to consider that the Probability of Detection varies as a function of flaw size and is expressed as the POD curve.

The nature of this curve is quite important for inspection reliability and in general the most desirable feature would be a rapid rise at the minimum detectable size from a POD of 0% to one of 100% (Figure C1). Looking at conventional NDT methods one can see that techniques such as MPI, dye penetrant and ACPD all would have a strong dependence on crack size but acoustic emission might not. Ultrasonics, radiography and eddy currents may be expected to have a lower dependence.

For a given NDT technique and application one could expect behaviour to conform to a POD curve peculiar to the given combination of influencing factors. It is obviously desirable to know the nature of this 'true' POD curve so that decisions can be made on component integrity on the basis of inspection results. In practice it is only possible to set up trials which will provide a measured POD curve. It is then necessary to establish the relationship between the measured and true POD curves, this can only be done with a specific confidence level.

A measured POD curve is obtained by grouping flawed components in terms of crack size (say N cracks in each group) and then conducting inspections to determine how successful one is in each group (say S successes in each group). The values of S/N would be point estimates of POD for each group and if plotted as a function of crack size would give a measured POD curve. Two key features in such a trial are the definition of success

and the relationship between this measured POD and the true POD. In statistical terms, each group is termed a sample where the sample inspected is deemed to be representative of the total population of defects (i.e. all those that could be found in service).

The steps in the procedure for measuring POD involve:-

a) Inspection of component; measurement of defect
b) Comparison with 'known' true size
c) Decision on success/failure (hit/miss)
d) Repeat of (a), (b) and (c) across whole sample
e) Point estimates of POD for each sample of a certain defect size
f) Link sample POD to true or 'population' POD with specified confidence limits.

The data from an inspection trial will be in the form of predictions of crack length, crack location and in some cases, crack depth. The scatter in such measurements often comes close to the 'Normal' distribution; in fact the same is derived from the description 'the normal curve of errors'.

These measurements need to be interpreted in terms of success, or failure, to detect or size the defect. To do this some inspection criterion has to be established for a particular application. For the case of a threaded connection one could anticipate that length and depth are critical dimensions but that the location is less important. A success criteria would therefore be based on the scatter in measured lengths (or depths) and one could choose to have either a specified portion of the total measurements (X standard deviations) or a specified accuracy. The criterion adopted depends on the use that will be made of the information. For example if successful detection and sizing is for a fracture mechanics analysis of fatigue crack growth, and the inspection intervals is 0.5 mm for a crack of depth 2.5 mm, then something better than ±10% is required. Alternatively if tether rejection is based on detection of any damage then the success criterion would embrace all values of crack size. In both cases the prediction of defects being present when none exist must be assessed as well, as this factor influences the economic benefits to be gained from the 'fitness for purpose' approach. These suggestions for success criteria are merely a first guess at what is needed. Decisions of this sort would need to be confirmed allowing discussions with designers and operators of critical threaded components. They need to be related to the use to which the data is eventually to be put and it is conceivable that the Inspection Reliability data produced will be evaluated for a number of different purposes.

Whichever criterion is adopted one eventually obtains a certain number of successful inspections (S) out of a total number of attempts N (= S + F) where F is failure. Thus the point estimate of the probability of detection for the sample, P, would be P = S/N. Reducing the data in this manner, to an outcome which is simply failure or success, allows one to make the point estimate for P but it is still necessary to relate P to the true probability of detection of the population, p. A binomial distribution can be used to describe the results from such trials [69] and it can be seen that this method of analysis is similar to say a coin/tossing experiment where discrete events give a (yes/no, success/fail) answer. Strictly speaking a binomial distribution describes the situation where a certain number of successes (S) occur in N independent inspections, each inspection having the same probability of success, P. For binomial statistics to be used, the following conditions must apply.

1) There are only two possible outcomes for each inspection (success/failure).
2) The probability of success/failure is the same for each defect in a particular group.
3) There are N inspections (N is a constant).
4) Each of the inspections is independent of the others.

For (1), in the case of crack detection, this is true but the outcome will depend on the definition of success.

For (2), this is only approximately true as some flaws may be inherently more difficult to detect than others.

For (3) and (4), this would seem to exclude the possibility of repeat testing to increase sample size. Increasing sample size improves the confidence one has in the outcome of each inspection.

To date, most inspection trials have been analysed using binomial statistics and this approach will be discussed.

2 THE USE OF BINOMIAL STATISTICS TO ANALYSE INSPECTION TRIALS RESULTS

It should be noted that any inspection trial, conducted on a representative sample, will only give a point estimate of the true POD. The use of binomial statistics enables one to estimate the probability that the measured POD is, within certain limits, representative of the population (true) POD.

If the size of the sample is N, it is theoretically possible to keep taking different samples of size N, randomly from the population and conduct trials on them. If the true probability of detection is p, then for all the above combinations of sampling, the probability of obtaining exactly S successes from a group of N defective samples, P(S), is given by:

$$P(S) = {}_NC_S\, p^S\, (1 - p)^{(N-S)} \quad (1)$$

where

$${}_NC_S = \frac{N!}{S!(N-S)!}$$

This is a binomial distribution and the mean μ and variance σ^2 are as follows:

$$\mu = Np \quad (2)$$

$$\sigma^2 = Np(1-p) \quad (3)$$

The shape of the distribution given by equation 1, varies with p and Figure C3 shows the effect of high, medium and low values of p. The negatively skewed distribution is of most interest since in general, one is attempting to establish the size of defect that can be detected with high probability (p).

For inspection trials the data is expressed in terms of proportions (= S/N) rather than individual successes and equations 1, 2 and 3 become:

$$F(P) = {}_NC_{NP}\, P^{NP}\, (1-p)^{N(1-P)} \quad (4)$$

$$\mu_p = p \quad (5)$$

$$\sigma_p^2 = \frac{p(1-p)}{N} \quad (6)$$

Figure C2 shows the effect of increasing sample size on the distribution for p = 90%. It can be seen that the mean does not vary but that the variance reduces with increasing N. This shows that the measured value of P is an unbiased indicator of the population mean μ.

For an inspection trial, a single sample is used and a single point estimate obtained. As an example, assume 30 defective components were inspected and defects were identified in only 24. Then S/N = 80% is the point estimate. The true POD is not known but it is

known that a series of measured POD values can be described by the binomial distribution. The problem one is faced with is the need to predict the mean value of the distribution (p) from a knowledge of only one of these values of P. Reasonable caution is applied to this prediction and one usually takes P to be a gross over-estimate of p. An example would be to assume that P is always within the top 5% of values one could get from repeated trials all using the same sample size. This type of assumption gives an estimate of p, based on P, where all other possible values within the range $p \rightarrow P$ form a predetermined confidence interval.

It can be seen from this that the variance is a key factor governing the interval P - p. Figure C2 shows that the variance is related to sample size and increases as N decreases. Thus, given only one measured value of P the interval P - p (for a given confidence level) will increase as the sample size decreases. Thus for a very small sample size one could have the situation where the measured value of P is 100% but the estimate of p is very low. Put another way the measured value P could always be 100% but the estimate of p will always be less than 100%. Achieving a prescribed level for p (given P = 100%) can be done for a given confidence limit by specifying a sample size.

In many engineering applications it has proved to be necessary to trade off between what it ultimately desirable and what is currently possible. Thus the choice of p = 0.9 associated with a confidence level of 95% has emerged as a possible target and trials based on this 90/95% POD have been conducted for some industries. It should be noted that this target governs the choice of sample size but, given that this sample will be repeated for several defect sizes, there is the opportunity to use different combinations to produce alternative target figures. The use of 90/95% POD might be the lower limit for TLP threaded connections and this aspect should be discussed with Industry before being adopted for inspection reliability trials.

Given these requirements and noting that the probability distribution for a binomial distribution is given by equation 1, an estimate of the sample size, N, required for an inspection trial can be obtained. Assuming that all defects in the sample are detected, (P = 100%) the following expression results:-

Equation 1 gave

$$P(S) = {}_{N}C_{S}\, p^{s}\, (1 - p)^{(N-S)}$$

Putting S = N gives

$$P(N) = p^N \quad (7)$$

For a true POD of p, if the probability of obtaining N successes in N trials is P(N), then the confidence, C, that the point estimate of P is representative of p is given by:

$$C = 1\text{-}P(N) \quad (8)$$

Thus, if a 90/95% POD is required, the minimum sample size is obtained as:

$$0.95 = 1 - 0.9^N$$
$$N = 28.4$$

Now N must be an integer, thus the minimum sample size for 90/95% POD is N = 29. In this situation, the trial would have to produce a 100% measured POD. Note that in such situations, the confidence level is defined as the single sided confidence level. In some applications, a confidence interval is defined. For a symmetrical distribution, a 95% confidence level gives 90% confidence interval.

The above calculation shows that a 90/95% POD can be achieved for a sample size of 29 although this requires a 100% success in the trial. Consider now a trial conducted at six crack size levels where the sample size at each crack size interval is 29. The measured POD curve could take the form shown in Figure C4.

It is seen that at large crack sizes, where the population POD could be expected to be high, the 100% measured POD could be achieved. However, as the crack size reduces, the measured POD would become less than 100%, as defects become missed, resulting in the 90/95% POD not being achieved. If one defect were to be missed in a sample of 29, the measured POD of 96.5% would represent an 84/95% POD. This indicates one problem with using the minimum size of sample, the effect of missing one defect in the sample could have a major effect on the estimated POD for a given confidence.

One way of minimising this effect to increase the sample size at each crack size. This is an extremely costly approach since for a 90/95% POD, missing one defect requires a sample size of 46. An alternative approach is that of sample grouping. For example, assume that the measured POD at crack sizes a_5 and a_6 were both 100% for a sample size of 29 at each group. Taking each size individually results in a best prediction of

90/95% POD. However, by grouping the samples, and presenting the result at the a_6 point (to be conservative) improves the predicted POD to 90/99.8% (which could alternatively be expressed as the 95/95% POD).

The foregoing section discusses the way that the confidence limit requirement dictates the size of sample (at each defect size) for a given value of true POD, p. If all samples at each crack size were grouped to form a sample containing 174 defects (6 sets of 29), the results of a trial on this sample would provide a single value of measured POD (P) but the confidence level would be high due to the high sample size. However, this single value would not be considered adequate for design purposes and instead a trend line for say six size intervals would be preferable. This would allow different grouping schemes and alternative prediction methods to be adopted, if required, and also the possibility of alternative choices of confidence levels. However despite these alternatives there is a minimum level to which trials should be directed and a sample size of twenty nine over a range of crack size intervals (for example six), which could give the 90/95% POD, would seem to be an appropriate minimum level.

In some cases, it may be possible to reduce the range of crack size intervals and this would be based on the actual shape of the POD curve (which of course can only be predicted during the trial). If the inspection system is near ideal and has a very rapid cut off between detected and not detected, the only part of the curve of interest is that at which the transition occurs.

3 APPLICATION TO THREADED CONNECTION

The above discussions indicate that in order to determine inspection reliability a large number of samples containing representative defects of known sizes need to be available. For large threaded tether connections, the production of a large number of real defects could be impractical. In such situations it is necessary to consider the requirements of defect detection from the fracture mechanics standpoint and to define the maximum allowable defect for a particular inspection regime. Any inspection reliability trials would need to initially address, as a minimum requirement, the capability of any inspection system to reliably detect/reject a defect of that size. This would provide a point estimate of inspection reliability in the critical size range for the component rather than identifying a complete inspection reliability trend. Given the practical limitations of producing representative defects in large connection, this may be a reasonable approach.

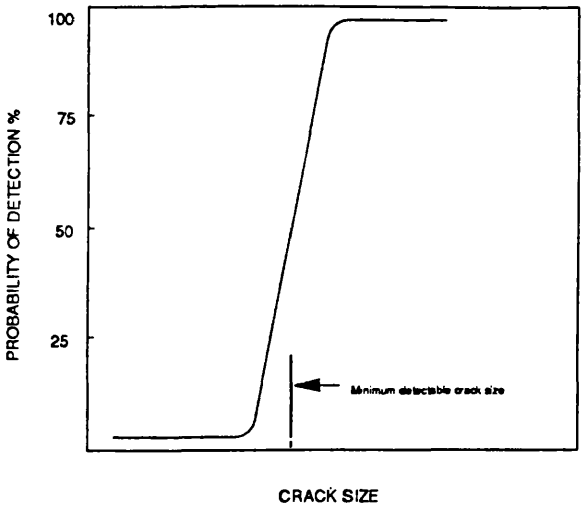

Fig. C1 Idealised POD Curve

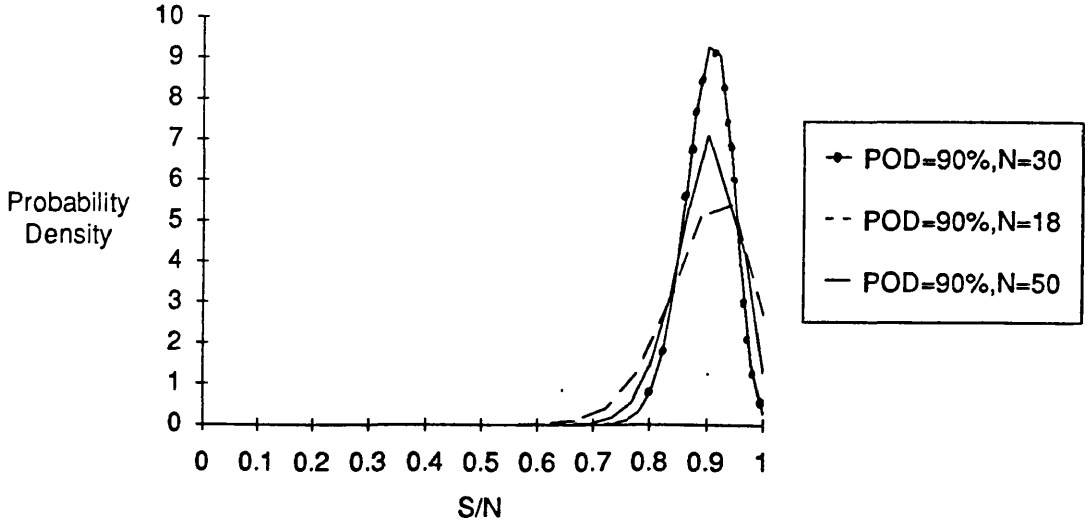

Fig C2 Effect of sample size on the distribution of all possible measured POD values.

Fig. C3a Binomial distribution for low probability of detection.

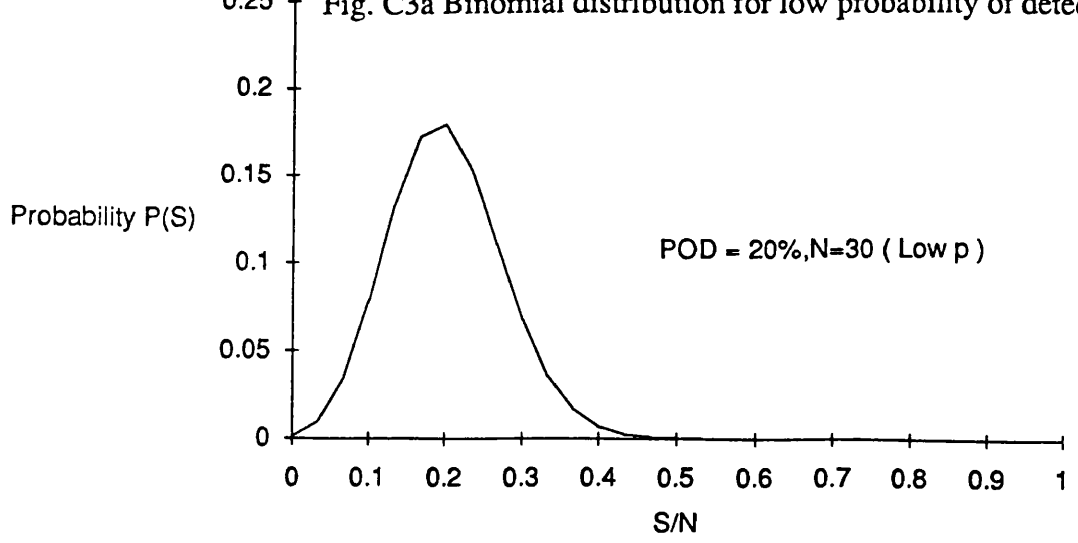

Fig. C3b Binomial distribution for medium probability of detection.

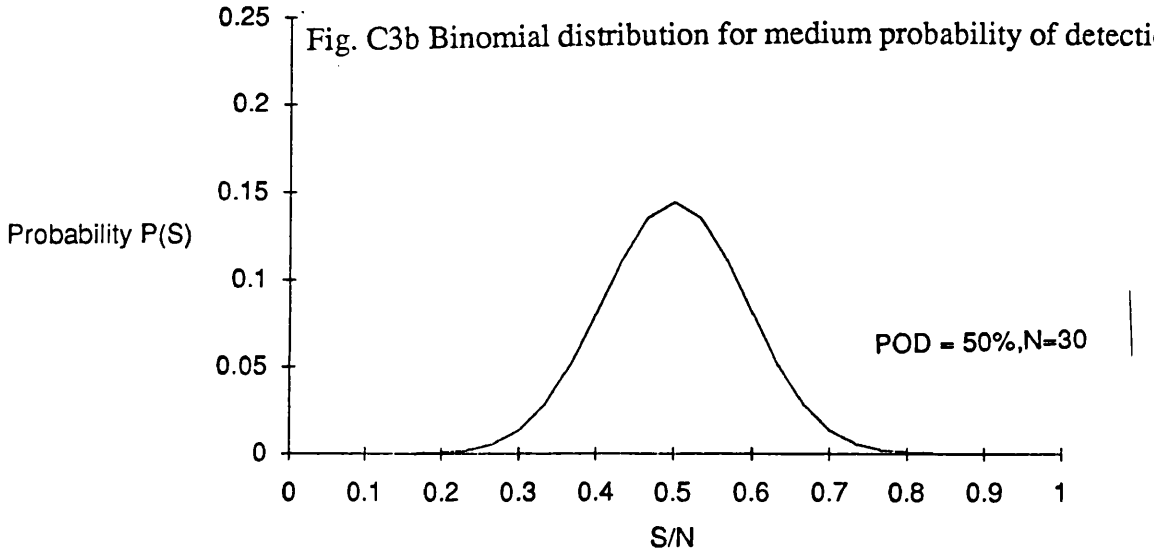

Fig. C3c Binomial distribution for high probability of detection.

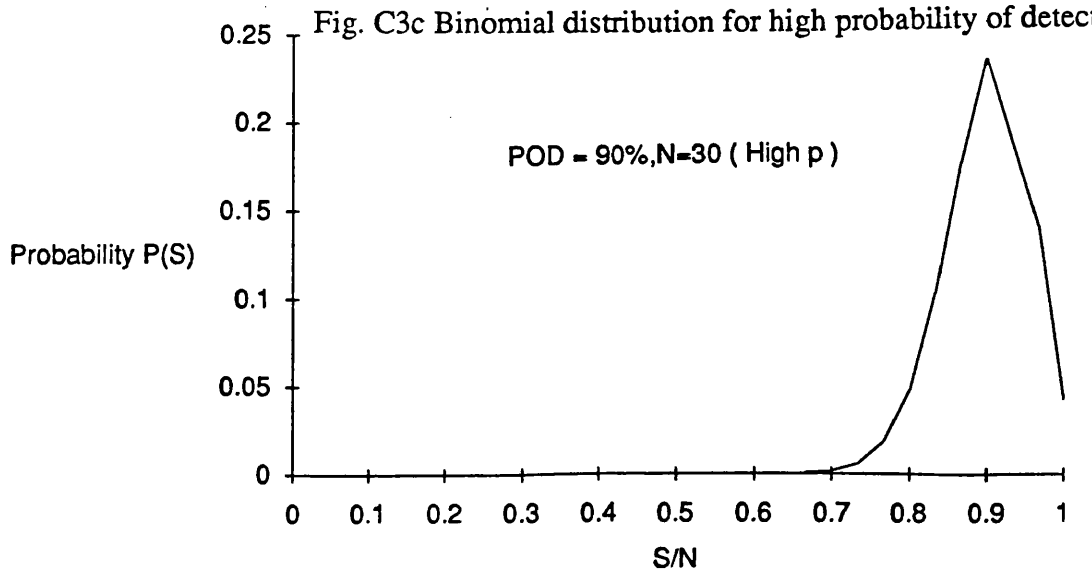

Fig. C3 Binomial distributions for varying degrees of POD.

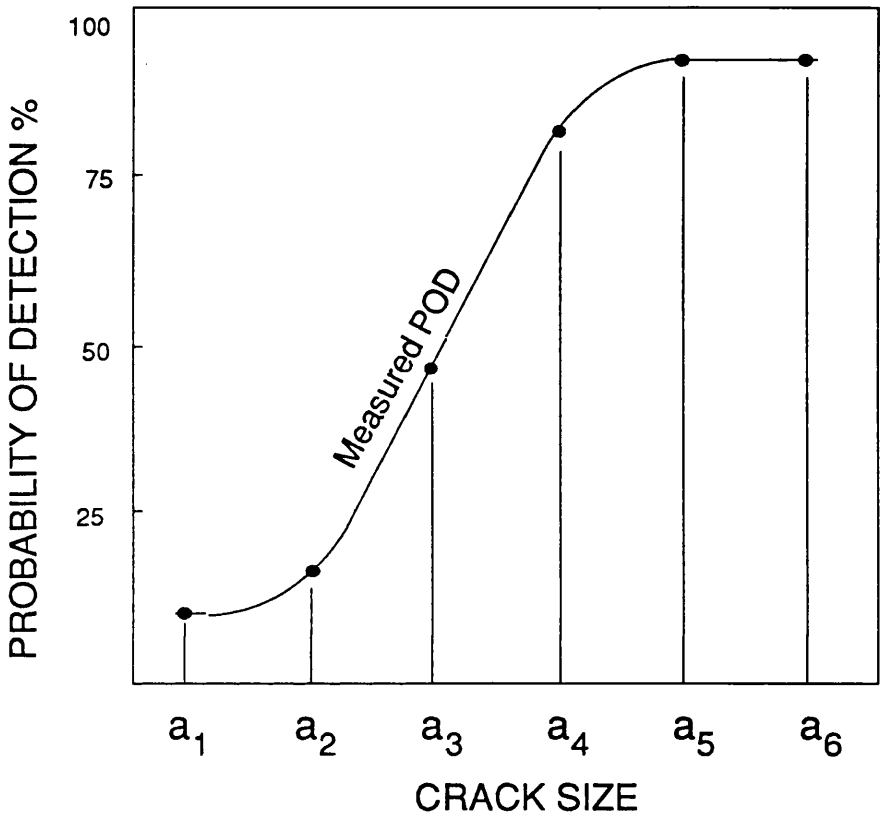

Fig.C4 Measured POD curve predicted from point estimates

APPENDIX D

FORTRAN PROGRAMME FOR

TOOTH LOAD DISTRIBUTION

```
C
C     ANALOG.FOR
C
      DIMENSION PPT(3)
      COMMON/COM1/ THET(30),ALPH(30),PREL(30,3),R1(30),R2(30),R3(30)
      COMMON/COM2/ RI1(30),RI2(30),RI3(30)
      COMMON/COM3/ A(4,4,30),AKT(4,4),AK2(4,4),AKTMP(4,4),AMT(4,4)
      COMMON/COM4/ AB(30),AP(30),TAU(30),RKB(30)
      COMMON/COM5/ P(30),FIN(4,4),TOP(4,4),AI(4,4),CON(4,4),RES(4,4)
      COMMON/COM6/ Q(4,4),TEMP(4,4),OUT(4,30),B(4,4)
      COMMON/COM7/ AB1(4,4),C(4,4),PTOO(30)
      COMMON/COM8/ PIT,DEP,V,NT,IPP,IPC,PP(2),PRELO(2),RKP(2),RKC(2)
C     ************************************************************
C     ************************************************************
C
C     THIS PROGRAM CALCULATES THE LOAD IN THREADS ON A PIN/BOX
C     WRITE CONNECTION. TAPERED SECTIONS ARE ACCOUNTED FOR IN THE
C     ANALYSIS. THE ANALYSIS IS BASED ON THE ELECTRICAL NETWORK
C     MODEL. ALL LOADS ARE EXPRESSED AS RATIOS OF THE LOAD ON THE
C     FIRST TOOTH. THE FIRST TOOTH IN THIS MODEL IS THE TOOTH
C     NEAREST TO THE FREE END OF THE PIN.
C
C     DAVE TOPP      JUNE 1983
C
C     W. HAMILTON    23rd APRIL 1985
C     Modified to include for terminal input of tooth stiffness
C
C     ************************************************************
C     ************************************************************
      PIE=3.142
      IZ=0
      II=0
C     ************************************************************
C     INITIALISE ALL ARRAYS
C     ************************************************************
      CALL INIT
      WRITE(*,9)
9     FORMAT(1X,'WRITE THE APPLIED LOAD')
      READ(*,*) PAPP
      WRITE(*,5)
5     FORMAT(1X,'THIS PROGRAM ALLOWS ONE CHANGE OF SECTION IN THE PIN
     1',/1X,'WHEN YOU TAKE UP THIS OPTION THE PROGRAM ASSUMES THE BORE
     2',/1X,'OF THE PIN AFTER THE CHANGE OF SECTION IS PARALLEL')
      WRITE(*,4)
4     FORMAT(1X,'DO YOU WANT TO USE THIS OPTION ?')
      WRITE(*,127)
      READ(*,*) ISECT
      IF(ISECT.EQ.0)GO TO 8
      WRITE(*,3)
3     FORMAT(1X,'WRITE TOOTH NUMBER AT WHICH SECTION CHANGES')
      READ(*,*) ITS
      WRITE(*,2)
2     FORMAT(1X,'THE FOLLOWING VALUES OF ID FOR THE PIN REFER TO
     1'/,'THE ID AT THE FREE END AND THE CHANGE OF SECTION')
8     CONTINUE
99    WRITE(*,10)
10    FORMAT(1X,'WRITE PIN ID AND OD AT LAST TOOTH (THIN END)')
      READ(*,*) PID1,POD1
      WRITE(*,20)
20    FORMAT(1X,'WRITE BOX ID AND OD AT THAT POINT TOOTH')
      READ(*,*) BID1,BOD1
      WRITE(*,30)
30    FORMAT(1X,'WRITE PIN ID AND OD AT FIRST TOOTH (THICK END) ')
      READ(*,*) PID2,POD2
      WRITE(*,40)
40    FORMAT(1X,'WRITE BOX ID AND OD AT THAT TOOTH ')
      READ(*,*) BID2,BOD2
C     CHECK THESE VALUES ARE OK
      DIFF1=BID1-POD1
      DIFF2=BID2-POD2
      DEP=DIFF1/2
      IF(DIFF1.NE.DIFF2)GO TO 60
90    WRITE(*,50) DEP
50    FORMAT(1X,'THE TOOTH DEPTH IS ',F8.4,'MM',///)
      WRITE (*,70)
      READ (*,*) KANS
      IF(KANS.EQ.99)GO TO 999
      WRITE (*,80) POD1,BID1,POD2,BID2
70    FORMAT(1X,'IF THIS IS NOT CORRECT GET OUT OF THIS PROGRAM
     1BY TYPING 99.',/,' IF IT IS OK WRITE ANY OTHER NUMBER ')
80    FORMAT(1X,'PIN OD =',F8.4,'BOX ID =',F8.4,/
     1'PIN OD=',F8.4,'BOX ID=',F8.4)
      GO TO 100
60    DI=ABS(DIFF1-DIFF2)
      IF(DI.LT.0.2)GO TO 90
```

```
      WRITE(*,61)
61    FORMAT(1X,'THE VALUES INPUT MEAN THE DEPTH OF THREAD IS NOT CONS
     1TANT')
      GO TO 99
100   CONTINUE
      WRITE (*,110)
110   FORMAT(1X,'INPUT NUMBER OF TEETH')
      READ (*,*) NT
      WRITE (*,120)
120   FORMAT(1X,'INPUT THE PITCH')
      READ (*,*) PIT
      POTAP=POD2-POD1
      PITAP=PID1-PID2
      BOTAP=BOD1-BOD2
      BITAP=BID2-BID1
C     ******************************************************
C     CALCULATE THE AREA AT EACH TOOTH SECTION AND CONVERT
C     TO A STIFFNESS. THE FIRST TOOTH IS NUMBERED AS TOOTH 1
C     'B' INDICATES BOX  'P' INDICATES PIN
C     ******************************************************
C     OPTION HERE TO CONSIDER PRELOAD ON THE END OF THE PIN
C     IF THIS OPTION IS TAKEN UP, TAU(1) IS MODIFIED BY
C     CONSIDERING THE STIFFNESS OF THE PRELOADING STUB
C     ******************************************************
127   FORMAT(1X,'WRITE 1 FOR YES, 0 FOR NO')
      WRITE (*,111)
111   FORMAT(1X,'DO YOU WANT PRELOAD AT THE PIN ?')
      WRITE (*,127)
      READ (*,*) IPP
      WRITE (*,112)
112   FORMAT(1X,'DO YOU WANT PRELOAD AT THE COUPLING ?')
      WRITE (*,127)
      READ (*,*) IPC
      IF(IPP.EQ.0)GO TO 114
      WRITE (*,113)
113   FORMAT(1X,'PIN PRELOAD DATA')
      II=1
119   CONTINUE
      WRITE (*,121)
121   FORMAT(1X,'WRITE THE VALUE OF PRELOAD APPLIED')
      READ (*,*) PRELO(II)
      WRITE (*,122)
122   FORMAT(1X,'WRITE PIN AREA, BOX AREA AND STUB LENGTH')
      READ(*,*) PAR,BAR,RLEN
      RKP(II)=PAR/RLEN
      RKC(II)=BAR/RLEN
      IF(II.EQ.2)GO TO 128
114   CONTINUE
      IF(IPC.EQ.0)GO TO 128
      WRITE (*,115)
115   FORMAT(1X,'COUPLING PRELOAD DATA')
      II=2
      GO TO 119

C     ************************************************************
C     OPTION TO CALCULATE OR INPUT TOOTH STIFFNESS HERE
C     ************************************************************
128   CONTINUE
      WRITE (*,600)
      READ (*,*) NOPT
600   FORMAT(//1X,'WRITE "1" FOR TERMINAL INPUT OF TOOTH STIFFNESS
     1',/1X,'WRITE "2" FOR CALCULATED TOOTH STIFFNESS  >')
      DO 130 I=1,NT
      BO=BOD2+(NT-I)*BOTAP/(NT-1)
      BI=BID1+(I-1)*BITAP/(NT-1)
      AB(I)=PIE*(BO**2-BI**2)/4
      PO=POD1+((I-1)*POTAP/(NT-1))
      IF(ISECT.EQ.0)GO TO 135
      IF(I.LE.ITS)PI=PID1-((I-1)*PITAP/(ITS-1))
      IF(I.GT.ITS)PI=PID1-PITAP
      GO TO 136
135   PI=PID1-((I-1)*PITAP/(NT-1))
136   AP(I)=PIE*(PO**2-PI**2)/4
      IF(NOPT.EQ.1)GOTO 610
C     ************************************************************
C     CALCULATE THE TOOTH STIFFNESS BASED ON PIN OD AT Ith TOOTH
C     TOOTH STIFFNESS IS BASED ON AN ANALYSIS USING STRESS FUNCTIONS
      CALL STIFF
      RKB(I)=PIE*PO*DEP/(1.8*V)
C     WRITE (*,129) RKB(I)
129   FORMAT(1X,'TOOTH STIFFNESS =',F10.5)
      GOTO 130
610   IF(I.NE.1)GOTO 650
      WRITE (*,620)
      WRITE (*,630)
```

```
620   FORMAT(//1X,'TOOTH STIFFNESS READED IN FREE-FORMAT')
630   FORMAT(/1X,'TOOTH NO. 1 IS THE TOOTH NEAREST THE FREE END',//)
650   NOTH=I
      WRITE (*,640) NOTH
      READ(*,*) RKB(I)
640   FORMAT(/1X,'TOOTH NO. ',I3,5X,'STIFFNESS > ')
130   CONTINUE
      DO 131 I=1,NT-1
      THET(I)=RKB(I+1)*PIT/AP(I)
      ALPH(I)=RKB(I+1)*PIT/AB(I)
      TAU(I)=RKB(I+1)/RKB(I)
C     WRITE (*,140) I,THET(I),I,ALPH(I),I,TAU(I)
      WRITE (*,*) 'area of box',AB(I),'area of pin',AP(I),RKB(I)
131   CONTINUE
      IF(IPP.EQ.1)GO TO 132
      RKP(1)=0.000001
      RKC(1)=AB(1)
132   IF(IPC.EQ.1)GO TO 133
      RKP(2)=AP(NT)
      RKC(2)=0.000001
133   CONTINUE
140   FORMAT(1X,'THETA(',I3,')=',F12.9,5X,'ALPHA(',I3,')=',F12.9,5X,'
     1TAU(',I3,')=',F12.4)
C145  FORMAT(1X,'AREA OF BOX =',F10.4,10X,'AREA OF PIN =',F10.4,10X,'
C     1RKB=',F10.4)
C     FOR EACH TOOTH ASSEMBLE THE 'A' MATRIX.
      DO 150 N=1,NT-1
      A(1,1,N)=1+THET(N)
      A(1,2,N)=-1*ALPH(N)
      A(1,3,N)=TAU(N)
      A(2,1,N)=-1*THET(N)
      A(2,2,N)=1+ALPH(N)
      A(2,3,N)=-1*TAU(N)
      A(3,1,N)=THET(N)
      A(3,2,N)=-1*ALPH(N)
      A(3,3,N)=TAU(N)
150   CONTINUE
C     THE TRANSFER FUNCTION MATRICES ARE NOW SET UP
C     THESE SHOULD NOW BE MULTIPLIED TOGETHER TO GIVE THE FINAL
C     TRANSFER FUNCTION
C     THE MULTIPLICATION ROUTINE FOLLOWS
      DO 210 I=1,3
      DO 210 J=1,3
      AK2(I,J)=A(I,J,1)
210   CONTINUE
      DO 190 K=2,NT-1
      DO 230 I=1,3
      DO 230 J=1,3
      AKT(I,J)=A(I,J,K)
230   CONTINUE
C     WRITE(*,*) ' AKTMP:', AKTMP
C     WRITE(*,*) ' AKT:',AKT
C     WRITE(*,*) 'AK2:',AK2
      CALL MULT(AKTMP,AKT,AK2,3,3,3)
      DO 240 I=1,3
      DO 240 J=1,3
      AK2(I,J)=AKTMP(I,J)
240   CONTINUE
190   CONTINUE
C     DO 250 I=1,3
C     DO 250 J=1,3
C     WRITE (*,260) AK2(I,J)
C250  CONTINUE
C260  FORMAT(1X,F15.9)
C     ***************************************************************
C     AK2 IS THE TRANSFER FUNCTION EXPRESSING I1(NT),I2(NT),I3(NT)
C     IN TERMS OF I1(1),I2(1),I3(1)
C     I IS THE ROW NUMBER J IS THE COLUMN
C     THE INITIAL AND FINAL CONDITIONS MUST NOW BE USED TO FORMULATE
C     THE SOLUTION. THE THE INITIAL FUNCTION IS AI( )
C     ***************************************************************
      AI(1,1)=1+RKB(1)/RKP(1)
      AI(1,2)=-1*RKB(1)/RKC(1)
      AI(2,1)=-1*RKB(1)/RKP(1)
      AI(2,2)=1+RKB(1)/RKC(1)
      AI(3,1)=RKB(1)/RKP(1)
      AI(3,2)=-1*RKB(1)/RKC(1)
C     NOW MULTIPLY AK2 BY AI AND PUT THE RESULT IN FIN
      CALL MULT(FIN,AK2,AI,3,3,2)
      DO 280 I=1,3
      DO 280 J=1,2
C     WRITE (*,290) FIN(I,J)
280   CONTINUE
290   FORMAT(1X,F10.4)
C     NOW CREATE A SIMILAR FUNCTION FROM THE FINAL LOOP
```

```
      CON(1,1)=-1*RKB(NT)/RKP(2)
      CON(1,2)=RKB(NT)/RKC(2)
C     WRITE (*,295) CON(1,1),CON(1,2)
295   FORMAT(1X,'CON 11 =',F10.5,'CON12 = ',F10.5)
C     TAKE UP THE FUNCTION EXPRESSING I1(NT-1) AND I2(NT-1)
C     IN TERMS OF I1(1) AND I2(1)
      DO 300 I=1,2
      DO 300 J=1,2
      TOP(I,J)=FIN(I,J)
300   CONTINUE
C     NOW MULTIPLY CON WITH TOP
      CALL MULT(RES,CON,TOP,1,2,2)
C     THERE ARE NOW TWO SOLUTIONS IN TERMS OF I1 AND I2 ONLY
      DO 310 J=1,2
      P(J)=FIN(3,J)-RES(1,J)
C     WRITE (*,311) P(J)
311   FORMAT(1X,'PJ=',F12.4)
310   CONTINUE
      RAT=-1*P(2)/P(1)
      TAPL=1+RAT
C     TAPL IS THE TOTAL APPLIED LOAD
      WRITE (*,320) RAT
320   FORMAT(1X,'RATIO OF P2 TO P1 IS',F10.3)
C     ***************************************************************
C     THE PROGRAM IS CHECKED UP TO HERE
C     ***************************************************************
C     BACK SUBSTITUTE TO GIVE THE LOADS IN EACH BRANCH
      Q(1,1)=RAT
      Q(2,1)=1
      CALL MULT(TEMP,AI,Q,3,2,1)
      DO 330 I=1,3
      OUT(I,1)=TEMP(I,1)
      B(I,1)=TEMP(I,1)
330   CONTINUE
      DO 500 K=1,NT-1
      DO 501 I=1,3
      DO 501 J=1,3
      AB1(I,J)=A(I,J,K)
501   CONTINUE
      CALL MULT(C,AB1,B,3,3,1)
      DO 500 I=1,3
      OUT(I,K+1)=C(I,1)
      B(I,1)=C(I,1)
500   CONTINUE
C     ************************************
C     THE RESULT IS NOW IN OUT
      DO 360 K=1,NT
C     WRITE (*,370) K
      DO 360 I=1,3
C     WRITE (*,380) I,OUT(I,K)
360   CONTINUE
370   FORMAT(1X,'LEVEL =',I3)
380   FORMAT(1X,'I',I2,' = ',F8.4)
C     ********************************************************************
C     THE SOLUTION IS NOW COMPLETE. PRINT OUT THE LOADS ON THE
C     INDIVIDUAL TEETH.
C     ***************************************************************
      IF(IPP.EQ.1)GO TO 384
      IF(IPC.EQ.1)GO TO 384
      GO TO 383
384   CALL PRELOA
      IF(IPC.EQ.0)GO TO 391
      PB=OUT(2,NT)*PAPP/TAPL
      WRITE (*,385) PB
391   IF(IPP.EQ.0)GO TO 383
      PA=RAT*PAPP/TAPL
      WRITE (*,382) PA
383   CONTINUE
382   FORMAT(1X,'LOSS OF PIN PRELOAD =',F8.4)
      DO 390 I=1,NT
      P(I)=OUT(3,I)
390   CONTINUE
385   FORMAT(1X,'LOSS OF COUPLING PRELOAD =',F8.4)
      PT=0
      DO 400 I=1,NT
C     WRITE (*,410) I,P(I)
      PT=PT+P(I)
400   CONTINUE
C     WRITE (*,411)
411   FORMAT(1X,'TOOTH NO.  LOAD  %OF TOTAL TOOTH LOAD  %OF TOTAL AP
     1PLIED LOAD')
      DO 401 I=1,NT
      PRAT1=100.*P(I)/PT
      PRAT2=100.*P(I)/TAPL
C     WRITE (*,410) I,P(I),PRAT1,PRAT2
```

```
401   CONTINUE
410   FORMAT(4X,I4,8X,F8.3,8X,F5.2,8X,F5.2)
C     ***************************************************
C     FINAL OUTPUT OF RESULTS
C     ***************************************************
450   CONTINUE
      WRITE (*,491)
491   FORMAT(6X,'TOOTH',6X,'APPL. LOAD',4X,'PIN PLOAD',4X,'BOX PLOAD
     1  TOTAL')
C     TOT=ABSOLUTE VALUE OF TOTAL APPLIED LOAD
C     PP=ABSOLUTE VALUE OF PRELOAD APPLIED
C     PPT=ABSOLUTE PRELOAD TOTAL
C     TOTA=ABSOLUTE SUM OF TOOTH LOADS
      TOTA=0
      TOT=0
      PPT(1)=0
      PPT(2)=0
      PTOT=0
      DO 470 I=1,NT
      PA=P(I)*PAPP/TAPL
      TOT=TOT+PA
      DO 471 II=1,2
      PP(II)=PREL(I,II)*PRELO(II)
      PPT(II)=PPT(II)+PP(II)
471   CONTINUE
      PTOT=PA+PP(1)+PP(2)
      TOTA=TOTA+PTOT
      WRITE (*,490) I,PA,PP(1),PP(2),PTOT
470   CONTINUE
480   FORMAT(1X,'TOOTH NO',I4,'LOAD=',F10.3)
490   FORMAT(4X,I4,4F16.2)
C410  FORMAT(1X,'LOAD ON TOOTH NO',I3,'=',F8.4)
C     WRITE (*,420) PT
420   FORMAT(1X,'SUM OF TOOTH LOADS =',F8.4)
      WRITE (*,550)
      WRITE (*,560) TOT,PPT(1),PPT(2),TOTA
      WRITE (*,550)
560   FORMAT(1X,'TOTALS',1X,4F16.2)
550   FORMAT(19X,5('-'),10X,6('-'),10X,6('-'),9X,7('-'))
      WRITE (*,570)
570   FORMAT(1X,/,/,'DO YOU WANT TO RERUN WITH THIS DATA ?')
      WRITE (*,127)
      READ (*,*) IRUN
      IF(IRUN.EQ.0)GO TO 999
      CALL INIT
      IPC=0
      IPP=0
998   CONTINUE
999   STOP
      END
C     SUBROUTINE MULT MULTIPLIES BB(L,M)*CC(M*N) WITH THE RESULT IS AA(L,N)
      SUBROUTINE MULT(AA,BB,CC,L,M,N)
      DIMENSION AA(4,4),BB(4,4),CC(4,4)
      DO 1 I=1,L
      DO 1 J=1,N
      E=0.
      DO 2 K=1,M
2     E=E+BB(I,K)*CC(K,J)
1     AA(I,J)=E
      RETURN
      END

C     SUBROUTINE INIT INITIALISES ALL ARRAYS
      SUBROUTINE INIT
      COMMON/COM1/ THET(30),ALPH(30),PREL(30,3),R1(30),R2(30),R3(30)
      COMMON/COM2/ RI1(30),RI2(30),RI3(30)
      COMMON/COM3/ A(4,4,30),AKT(4,4),AK2(4,4),AKTMP(4,4),AMT(4,4)
      COMMON/COM4/ AB(30),AP(30),TAU(30),RKB(30)
      COMMON/COM5/ P(30),FIN(4,4),TOP(4,4),AI(4,4),CON(4,4),RES(4,4)
      COMMON/COM6/ Q(4,4),TEMP(4,4),OUT(4,30),B(4,4)
      COMMON/COM7/ AB1(4,4),C(4,4),PTOO(30)
      COMMON/COM8/ PIT,DEP,V,NT,IPP,IPC,PP(2),PRELO(2),RKP(2),RKC(2)
C     INITIALISE ALL ARRAYS
      DO 5 I=1,29
      THET(I)=0
      PTOO(I)=0
      ALPH(I)=0
      R1(I)=0
      R2(I)=0
      R3(I)=0
      RI1(I)=0
      RI2(I)=0
      RI3(I)=0
      AB(I)=0
      AP(I)=0
```

```
      P(I)=0
      TAU(I)=0
      RKB(I)=0
      DO 5 J=1,3
      DO 5 K=1,3
      A(J,K,I)=0
5     CONTINUE

      DO 7 I=1,3
      DO 7 J=1,3
      AKT(I,J)=0
      AB1(I,J)=0
      AK2(I,J)=0
      AKTMP(I,J)=0
      AMT(I,J)=0
      FIN(I,J)=0
      TOP(I,J)=0
      AI(I,J)=0
      CON(I,J)=0
      RES(I,J)=0
      C(I,J)=0
      Q(I,J)=0
      TEMP(I,J)=0
      B(I,J)=0
7     CONTINUE
      DO 8 I=1,3
      DO 8 J=1,29
      OUT(I,J)=0
      PREL(J,I)=0
8     CONTINUE
      DO 9 I=1,2
      RKC(I)=0
      RKP(I)=0
      PP(I)=0
      PRELO(I)=0
9     CONTINUE
      RETURN
      END
      SUBROUTINE STIFF
C     ********************************************************
C     THIS SUBROUTINE CALCULATES THE STIFFNESS OF THE TOOTH
C     USING AN ANALYSIS BASED ON STRESS FUNCTIONS. THE FULL
C     SOLUTION IS A PROGRAM CALLED STUB.FOR
C     ********************************************************
      COMMON/COM8/ PIT,DEP,V,NT,IPP,IPC,PP(2),PRELO(2),RKP(2)
      REAL MEW,L,L2,L3,L4
      D=PIT/2.
      MEW=0.3
      Y=D/2.0
      L=DEP
      X=0.
      Y4=Y**4.
      Y2=Y**2.
      X4=X**4.
      X2=X**2.
      L4=L**4.
      L3=L**3.
      L2=L**2.
      D3=D**3.
C     THE VALUE OF Y/2 IS INPUT AS PLUS SINCE Y = -D/2 NOT D/2
      F1=(3*Y2/(4*D))-(Y4/(2*D3))+(Y/2)
      F2=(X4-L4)/(2*D3)
      F3=(L2-X2)*9/(20*D)
      F4=(L-X)*((2*L3/D3)+(0.6*L/D))
      F5=(3*X2*Y2/D3)+(0.3*Y2/D)-(Y4/D3)
      F6=1.5*L*(L-X)/D
      F7=(L2-X2)*3/(4*D)
      FUNC1=(1-MEW)*(F1+F2+F3+F4)
      FUNC2=MEW*(F5+F6)
      V=(1+MEW)*(FUNC1+FUNC2+F7)
      RETURN
      END

      SUBROUTINE PRELOA
C     ************************************************************
C     THIS SUBROUTINE CALCULATES THE INDIVIDUAL TOOTH LOADS
C     DUE SOLELY TO THE INITIAL APPLIED PRELOAD
C     IE. WITH NO EXTERNALLY APPLIED LOAD
C     ********************************************************
      COMMON/COM1/ THET(30),ALPH(30),PREL(30,3),R1(30),R2(30),R3(30)
      COMMON/COM2/ RI1(30),RI2(30)
      COMMON/COM4/ AB(30),AP(30),TAU(30),RKB(30)
      COMMON/COM8/ PIT,DEP,V,NT,IPP,IPC,PP(2)
      IZ=0
      DO 1 I=1,3
```

```
      DO 1 J=1,29
      PREL(J,I)=0
1     CONTINUE
      IF(IPP.EQ.0)GO TO 71
C     ****************************************************
C     FIRST SECTION IS FOR PRELOAD AT THE PIN
C     ****************************************************
      II=1
      DO 10 I=1,NT-1
      R1(I)=RKB(I)*PIT/AP(I)
      R2(I)=RKB(I)/RKB(I+1)
      R3(I)=RKB(I)*PIT/AB(I)
10    CONTINUE
C     FINAL TOOTH FIRST
      RI1(NT-1)=1
      RI2(NT)=RI1(NT-1)
      RI2(NT-1)=R1(NT-1)+R2(NT-1)+R3(NT-1)
      DO 20 I=1,NT-2
      J=NT-1-I
      RI1(J)=RI1(J+1)+RI2(J+1)
      RI2(J)=RI1(J)*(R1(J)+R3(J))+(RI2(J+1)*R2(J))
20    CONTINUE
21    CONTINUE

      TOT=0
      DO 50 I=1,NT
      TOT=TOT+RI2(I)
50    CONTINUE
      DO 70 I=1,NT
      PREL(I,II)=RI2(I)/TOT
C     PREL( )=RATIO OF TOTAL PRELOAD ON EACH TOOTH
70    CONTINUE
71    CONTINUE
      IF(IPC.EQ.0)GO TO 99
      IF(IZ.EQ.1)GO TO 99
      RI1(1)=1
      RI2(1)=1
      RI2(2)=RI1(1)*(THET(1)+ALPH(1)+TAU(1))
      RI1(2)=RI1(1)+RI2(2)
      DO 90 I=2,NT-1
      RI2(I+1)=(RI2(I)*TAU(I))+RI1(I)*(ALPH(I)+THET(I))
      RI1(I+1)=RI1(I)+RI2(I+1)
90    CONTINUE
      IZ=1
      II=2
      GO TO 21
99    RETURN
      END
```

REFERENCES

1. Van Nisselroy J.M., 't Hooft N., Whillas R.
Mechanised Ultrasonic Underwater Inspection of Girth Welds in Platform Legs. Shell Reasearch, Holland.

2. Sopwith D.G.
The Distribution of Load in Screw Threads. Proc. Inst. Mech. Eng. 1948, vol.159 p.373.

3. Stromeyer C.E.
Stress Distribution in Bolts and Nuts. Transactions of Institute Naval Architects 1918, Vol.160 p.112.

4. Haviland G.S.
Designing with Threaded Fasteners. Mechanical Engineering, October 1983 pp.17-31.

5. The Fox Connector.
Hunting Oilfield Services, Blackness Road, Altens Industrial Estate, Aberdeen AB9 8SY

6. Chen L.Y., Williams M.R., on the Fatigue Analysis of a differential thread connector. (Presented at an Aberdeen Conference in November 1983)

7. API Standard 5B Specification for threading, gauging and thread inspection of casing, tubing and line pipe threads. America Petroleum Institute, Department of Production, 300 Corrigan Tower, Dallas, Texas 75201.

8. Bickford J.H.
That Initial Preload - What happens to it? Mechanical Engineering pp.57-61 October 1983.

9. Heywood R.B.
Designing by Photoelasticity. Chapman and Hall, London 1952.

10. Coker E.G. and Filon, L.N.
Treatise on Photo Elasticity. Cambridge University Press, London 1931.

11. Solakian A.G.
Why Threaded Parts Fail. Product Engineering Vol.4 No.7 July 1933.

12. Goodier J.N.
"The Distribution of Load on the Threads of Screws". Journal of Applied Mechanics, Trans ASME Vol.62 1940.

13. Hetenyi M.
A Photoelastic Study of Bolt and Nut Fastening. Trans. ASME 1943 Vo.65.

14. Gray R.M., Pick R.J.,
Fatigue of Threaded End Closures of High Pressure Vessels. Proc. I. Mech. 1977 p.353.

15. Broadbent T.P. and Fessler H.
Stress analysis of screwed tubular connections. Paper C132/86. Proc. of International Conference on Fatigue and Crack Growth in Offshore Structures, I.Mech.E. London 1986.

16. Marino R.L. and Riley W.F.
Optimising Thread-root contours using Photoelastic Methods. Experimental Mechanics January 1964 pp 1-10.

17. Heywood R.V.
Tensile Fillet stresses in Loaded Projections. Proc. I.Mech.E. 1949, vol.160, p.124.

18. Fessler H. and Jobson P.K.
Stresses in a bottoming stud assembly with chamfers at the ends of the threads. Journal of Strain Analysis Vol.18 No.1.

19. Fessler H., Wang Jiong-Hua.
"Stress analysis of some unsummetric screwed connections". Journal of Strain analysis Vol.19 No.1 pp 111-119.

20. Crose J.G., Mack T.E., Wooley G.R., Smith R.E.
"Nonlinear Finite Element Analysis of Buttress Threaded Casing Connections". ASME paper No.76-Pet-82 present at Meeting Sept.19-24 1976.

21. Wooley G.R., Christman S.A., Crose J.G.
"Strain Limit Design of 13 3/8ths in. N-80 Buttress Casing". Journal Petroleum Technology Vo.29 April 1977 p.355-359.

22. Coker E.G.
Trans Inst. Naval Architects, 1911 Vol.53 Part 1 p.265.

23. Harris D.O.
Stress Intensity Factors for Hollow Circumferentially Notched Round Bars. Trans ASME Journal of Basic Engineering March 1967 pp 49-54.

24. Cohesive Programme of Research and Development into the Fatigue of Offshore Structures 1983-85 - Final Report issued by Dept. Mech. Eng. University College London.

25. Marston R.E.
An automatic micropolariscope: its design, development and use for tubular joint stress analysis. PhD Thesis, Nottingham University 1985.

26. Allison I.M.
Photoelastic Analysis of Buttress Threads in a tension coupling. 7th Congress on Materials Testing, Budapest, October 1978.

27. Dally J.W. and Riley W.F.
Experimental Stress Analysis, 2nd Edition Publ. McGraw Hill Kogakusha.

28. Pick R.J. and Burns D.J.
Finite element analysis of threaded end closures of thick walled vessels. Report No.71, January 1971. Solid Mechanics Division, University of Waterloo, Ontario, Canada.

29. Warnke E.G.
Design and Fatigue Life of Openable High Pressure vessels. Proc. Inst. Mech. Engrs. 1967-68 Vol.182 Part 3c.

30. Gray M.G., Pick R.J.
Fatigue of threaded end closures of high pressure vessels. Proc. I. Mech. 1977 p.353.

31. Brown A.P.C. and Hickson C.W.
A Photoelastic Study of Stresses in Screw Threads, Proc. I. Mech. E., 1952, IB, p605.

32. Gray R.M.
Preliminary investigation of load distribution in threaded connections. Report No. WAL 730/562-47 1954, Purdue Research Foundation, Contract DA-11-022-ORD-17.

33. Yoshimoto I., Maruyama K.
An idea to predict the fatigue failure of the high strength bolt. Bull. Japan Soc. of Prec. Eng. Vol.15 No.4 December 1981.

34. Bluhm J.I., Flanagan J.H.
A procedure for the elastic stress analysis of threaded connections including the use of an electrical analogue. Experimental Stress Analysis 1957, XV, p 85.

35. Neuber H
Theory of notch stresses: Principles for exact stress calculation.
(Kerbspannungslehre: Grundlagen fur Genaue Spannungsrechnung, Berlin 1937)
Translated by F A Raven,Navy Dept, David Taylor Model Basin, Washington D.C., Translation 74, Nov 1945.

36. Irwin, GR.
"Fracture Mechanics", Structural mechanics ed Goodier and Hoff, Pergaman Press, New York 1960 pp 567-591.

37. Griffiths A.A.
The Phenomena of Rupture and Flaw in metals. Philosophical Trans. Royal Soc. V0I221, 1920.pp 163-198.

38. Newman J.C., Raju, I.S.
An Empirical Stress Intensity Factor Equation for the Surface Crack, Engineering Fracture Mechanics, Vol.15 No.1 1981 pp 185-192.

39. Newport A., Topp D., Glinka G.
The Analysis of Elastic Stress Distribution in Threaded Tether Connections. Journal of Strain Analysis for Engineering Design, Vol.22 1987.

40. Private communication with Prof. Dover regarding confidential Final Report on project entitled "Fatigue Analysis of Drillstrings" prepared by NDE Centre, Dept. Mechanical Engineering,University College London. April 1990.

41. Newport A.,
PhD Thesis London University 1989.

42. British Steel Confidential Report. Report No.550/78/11/D.

43. Study of Calibration Procedures for accurately quantifying crack sizes in Welded Tubular Joints. HMSO Doc.OTH 255, 1966.

44. Webster S.E., Rudd J., Cook NT.,
Review of Information on the Fatigue of Tethering Systems for Tethered Buoyant Platforms - Report OT-R-8241, HMSO, London.

45. Neuber H.K.
Theory of Stress Concentration for Shear Strained Prismatical Bodies with Arbitrary Non-linear Stress-strain Law. ASME Journal of Applied Mechanics Vol.28 No.4 1961 pp 544-550.

46. Timoshenko S.P., Goodier J.N.
Theory of Elasticity, 2nd Edition, McGraw Hill Book Company, New York 1951.

47. Collins R., Dover W.D. and Michael D.H. (1985). The use of ac field measurements for non-destructive testing. Research Techniques in NDT, Vol.VIII, Chapter 5, ed. R.S. Sharpe, Academic Press, page 211-267.

48. Michael D.H., Collins R., Dover W.D.
"Detection and Measurement of Cracks in Threaded Bolts with an AC Potential Difference Method". Proc. Roy. Soc. London A385 145-168 (1983).

49. Available through Technical Software Consultants Ltd., 34 Linford Forum, Rockingham Drive, Linford Wood, Milton Keynes, MK14 6LY.

50. Topp D.A., McGugan J.D., and Dover W.D.
Automated Inspection System for Drillstring Threaded Connections using AC Field Measurement (ACFM) Techniques, to be presented at the 4th Annual 2 Day Offshore Drilling Technology Conference in Aberdeen, Nov.1990.

51. Private Communication with Drilling Dept., BP Exploration.

52. Paris P.C., Erdogan F.
A Critical Analysis of Crack Propagation Law. Journal of Basic Engineering Vol.85 pp 528, 1963.

53. Schijve J.
The Practical and Theoretical Significance of Small Cracks. An Evaluation. Proc. Fatigue 1984 Conference, 2nd Int. Conf. on Fatigue and Fatigue Thresholds, 3-7 Sept. 1984.

54. Kitagawa H., Yuuki R., Nakasone Y., Kawamura K., Iida M.
"Some Control Factors of Small Fatigue Cracks' Behaviour". Proc. Fatigue 1984 Conference, 2nd Int. Conf. on Fatigue and Fatigue Thresholds, 3-7 Sept. 1984.

55. Background to New Fatigue Guidance notes for Steel Welded Joints in Offshore Structures. DEn HMSO 1984.

56. Dover W.D., Wilson T.J.
Fatigue Fracture Mechanics Assessment of Tubular Welded T Joints. Cohesive Programme of Research and Development into the Fatigue of Offshore Structures, Final Report 1983-85. Editors Dover & Topp.

57. Holdbrook S.J., Dover W.D.
The Stress Intensity Factors for a Deep Surface Crack in a Finite Plate. Engineering Fracture Mechanics Vol.12 1979.

58. BS 5447 1977
Methods of Test for Plane Strain Fracture Toughness (K_{TC}) of Metallic Materials.

59. Thielen and Fine
"Fatigue Crack Propagation in 4140 Steel". Metallurgical Transaction, Vol.6A (1975) p 2133.

59. Chen W.C. and Lawrence F.V.
A model for joining the Fatigue Crack Initiation and Propogation Analysis - College of Engineering, University of Illinois.

60. Paris PC and Sih GC.
"Stress Analysis of Cracks" Fracture Toughness Testing and its applications, ASTM STP No 381, Philadelphia, Pa, 1965 pp30-81.

61. Glinka G.
"Relations Between the Strain Energy Density Distribution and Elastic-Plastic Stress-Strain Fields Near Cracks and Notches and Fatigue Life Calculation", ASTM STP 942, H.D. Solomon, G.R. Halford, L.R. Kaisand and B.N. Leis (eds) - Low Cycle Fatigue, American Society for Testing and Materials, Philadelphia, 1987.

62. Glinka G.
"Energy Density Approach to Calculation of inelastic strain-stress near notches and cracks", Engineering Fracture Mechanics, Vol.22 No.3 1985 pp 485-508.

63. Miner, M.A.
"Cumulative Damage in Fatigue", J. of Applied Mechanics, ASME, Vol.12, 1945, pp A-159-164.

64. Lugg M.C., Lewis A.M. Micheal D.H., Collins R.
The Non-contacting ACFM Technique, Electromagnetic Testing, Inst. of Physics Short Meeting 12, Bristol UK, pp 41-48 1988. Inst. of Phys. Publish.

65. Lugg M.C., Topp D.A.
Advances in Non-contacting ACFM Poster Session, 28th Annual British Conference on NDT, Sheffield, 18-21 Sept. 1989.

66. McPherson B., Dutton P., Dale B.A., Chiltern T.S.
A New Automated Tool Joint Inspection System to Reduce Drillstring Failures. Paper No.IADC/SPE 1962, presented at Inst. Ass. of Drilling Contractors/Soc. Petr. Engs. Drilling Conference, Houston, Texas Feb. 27 - March 2, 1990.

67. Niu X, and Glinka G.
"Theoretical and Experimental Analyses of Surface Fatigue Cracks in Weldments", Proceedings - The Symposium on Surface Crack Growth: Model, Experiments and Structures; ASTM, Reno, Nevada, USA, 25 April 1988.

68. WASH W.A.
Theory and Problems of Strength of Materials 2nd Ed, Schaum's Outline Series, McGraw-Hill, 1977.

69. Probability and Statistics for Engineers. 3rd Edition, Prentice Hall Int. Edition, Irwin Miller and John E. Freund.

A_B	Cross sectional area of box at section of interest
A_P	Cross sectional area of pin at section of interest
A_i	Local cross section area at section of tooth i
a	Crack depth
a′	Distance from surface to root of notch (or crack at root)
b	Fatigue strength exponent
C_1	Constant used by Neuber (= 0.8 Ref.[35])
C	Paris Constant
c	Diameter of hollow member
D	Mean diameter of tooth
d	Tooth depth
$\frac{da}{dn}$	Crack growth rate
d_c	Diameter at root of critical tooth
E	Modulus of elasticity
e	Nominal strain
e_t	Nominal elastic strain due to a nominal stress of S_t
I	Electrical representation of load in section
I_n	Electrical representation of load in branch No. n.
i	Generalised tooth number
ID	Inside diameter
j	Fatigue ductility coefficient
K	Stress intensity factor (General)
K_1	Stress Intensity Factor (Mode 1)
K_B	Tooth stiffness
K_{BB}	Bulk stiffness of box
K_{Bo}	Axial bolt stiffness
K_c	Box stiffness at preloaded section
K_P	Axial box stiffness
K_M	Axial pin stiffness
K_p	Pin stiffness at preloaded section
K_{PB}	Bulk stiffness of pin
K_{Pl}	Plate stiffness
K′	Cyclic strength coefficient
K″	Stiffness coefficient for a tooth
K_t	Elastic SCF
K_{ti}	Elastic SCF at tooth i
K_ε	Strain concentration factor
K_σ	Stress concentration factor
ΔK	Stress intensity factor range
l	Length of beam
M	Applied bending moment
m	Paris constant
N_f	Number of cycles to failure
n′	Strain hardening exponent
OD	Outside diameter
P	General symbol for load
ΔP	Transmitted load
ΔP_{bolt}	Change in bolt load due to applied load P
ΔP_{plate}	Change in plate load due to applied load P
P_p	Increase in pin load for a preloaded joint
P_n	Load in section n
P_r	Preload force
P_B'	Effective load in box
P_P'	Effective load in pin
P_i	Load on tooth i

p'	Pressure loading on tooth flank
p	Tooth pitch
ΣP	Sum of tooth loads
ΣP_i	Sum of tooth loads up to tooth i
R_B	Electrical representation of tooth stiffness
R_F	Electrical representation of box stiffness
R_M	Electrical representation of pin stiffness
r	Remaining uncracked ligament
S_i	Local nominal stress at section of tooth i
S_i	Elastic nominal notch stress
T_o	Applied torque
T	External tensile load
δT	Change in load (General case)
T_o'	Torsion in pin member
t	Wall thickness
W_e	Elastic strain energy density
W_s	Strain energy density
W_p	Elastic-plastic strain energy density
α	$=\frac{K_B}{K_M}=\frac{R_M}{R_B}$
α_1	SCF function used by Neuber [35]
α_2	SCF function used by Neuber [35]
α_3	SCF function used by Neuber [35]
α_K	SCF function used by Neuber [35]
α_{tk}	SCF function used by Neuber [35]
α_{fk}	SCF function used by Neuber [35]
α_{tb}	SCF function used by Neuber [35]
α_{1o}	Value for α_1 for small values of ρ
α_{2o}	Value for α_2 for small values of ρ
α_{3o}	Value for α_3 for small values of ρ
δ	General symbol for deflection
ε	Strain
$\Delta\varepsilon$	Cyclic strain range
ε_f	Fatigue ductility coefficient
ν	Poisson's ratio
Ψ	Stress Function
σ	Stress
$\Delta\sigma$	Stress range
σ_f	Fatigue strength coefficient
σ_m	Mean stress
σ_{max}	Maximum stress
σ_{nom}	Nominal stress
σ_x,σ_y	Orthogonal stress components
τ_i	$=\frac{K_{B_{i+1}}}{K_{B_i}}=\frac{R_{B_i}}{R_{B_{i+1}}}$
τ_{crit}	Torsional stress at critical section
τ_{xy}	Shear stress
θ	$=\frac{K_B}{K_M}=\frac{R_M}{R_B}$
ρ	Notch root radius

Also see appendices for special notations.